STEADY STATE THERMAL PERFORMANCE

OF A

HIGH TEMPERATURE REACTOR
FUEL ELEMENT

by

Terence Dennis Ballard

THESIS SUBMITTED FOR DEGREE OF

DOCTOR OF PHILOSOPHY

UNIVERSITY OF ASTON IN BIRMINGHAM

OCTOBER 1973

SUMMARY

The safe and economic operation of a nuclear reactor is highly dependent upon the detailed knowledge of the steady state thermal and hydraulic characteristics of the fuel.

Various designs of HTR fuel element are discussed and the Tubular Interacting concept is described in more detail. This design, the one adopted for the Oldbury 'B' tender, was the one on which the analytical methods, described in this thesis, were based.

The spatial and time distributions of heat generation, and fast neutron dose, are discussed and methods described which have been developed to determine spatial and time distributions of channel mass flow rate and coolant outlet temperature.

With these distributions as boundary conditions, methods (involving the use of computer programs) are described which analyse the thermal performance of a fuel element. Particular emphasis has been given to three important aspects of fuel behaviour. The heat transfer and pressure drop characteristics of the coolant passages are investigated analytically. Dimensional change caused by thermal and irradition effects has a marked effect upon fuel element temperatures and this phenomenon is studied in some depth. Methods have also been developed which postulate the form and development of corrosive attack of the fuel channel and determine the thermal and hydraulic effects of such corrosion.

Using all these methods detailed spatial and time dependent temperature distributions are determined for a single fuel element. Spatial distributions of peak fuel channel temperatures at a particular moment in the reactor core life (Snapshot) are also determined and, by making certain statistical observations, expected frequency distributions are found.

TO

JUDY

CONTENTS

Page

PREFACE

This research was carried out in the Thermal Performance Group of Systems Department of The Nuclear Power Group, and formed part of High Temperature Reactor design studies instigated by TNPG and the Central Electricity Generating Board.

I would like to express my gratitude to TNPG, in particular Mr. R. Rutherford and Mr. P.R.J. French, for allowing me to pursue this research. I would also like to thank Dr. P.N. Cooper of the University of Aston in Birmingham and Dr. E.C. Cobb of TNPG for their encouragement and helpful criticism. My thanks are also due to the Editorial Staff of TNPG, especially Mrs. E.J. Eyes, for the production of this thesis.

CHAPTER 1

INTRODUCTION

1 The High Temperature Reactor

The High Temperature Reactor is the logical development of the United Kingdom gas cooled reactor programme. The HTR (Mk III) system follows on from the Magnox (Mk I) and Advanced Gas Cooled Reactor (Mk II) systems.

The AGR has stainless steel clad UO_2 fuel, cooled by CO_2, achieving core power densities of about 2.8 MW/m^3. Fuel ratings and boiler inlet coolant temperatures are limited by fission product release from the UO_2 fuel, contained within the can, and by temperature limitations of the can itself.

The graphite moderator is resident in the core for the full thirty years' life of the reactor and must therefore be maintained below about $400^{o}C$ to avoid excessive corrosion and irradiation induced distortion. This is achieved by means of a steel baffle allowing the CO_2 to cool the moderator before the fuel. This baffle presents many design and operational problems.

The HTR has been designed to overcome the restrictions of the AGR system and to provide further development potential. The main characteristics of the HTR that contribute to the desirability of the system can be summarised as follows:

(i) Coated UO_2 particles which act as efficient fission product retention spheres are embedded and clad in graphite. Inert helium is the coolant with its high thermal conductivity and specific heat. A high core power density (e.g. 8.4 MW/m^3) is the result.

(ii) The whole active core is replaceable allowing the moderator to be run at higher temperatures.

(iii) Higher operating fuel, moderator and coolant temperatures resulting in greater heat transfer and overall plant efficiencies.

(iv) Large negative fuel temperature reactivity coefficient.

(v) Uranium ore and separative costs are lower because of the higher power densities.

(vi) As a result of the high plant efficiencies (41%) there are reduced requirements for cooling water allowing stations to be located inland, close to load centres.

(vii) In the longer term, the high coolant temperatures facilitate process heating (e.g. aluminium smelting) and direct cycle conversion (e.g. gas turbines).

Fig 1/1 shows the main features of a typical HTR.

2 Fuel element thermal performance calculations

As with all reactor systems 'safety' and 'economics' are opposing considerations. In order to make a desirable compromise a detailed knowledge of the contributory factors must be obtained.

For an HTR core the most important 'safety' factors are fission product release and core structural integrity. The opposing economic considerations would be high core power densities and operating temperatures (efficiencies).

Fission product release from the fuel and the structural behaviour of the core components are chiefly dependent upon their thermal and irradiation histories. Thermal performance calculations on the fuel and moderator are therefore required as one important step in achieving the lowest capital and operating costs of a 'safe' reactor system.

This thesis describes the steps taken to determine the steady state thermal performance of an HTR fuel element; from basic station parameters to complete temperature and coolant distributions required for 'safety' calculations. It should be noted that the steady state performance must be backed up by studies of the transient and fault conditions of the reactor.

CHAPTER 2

DESIGN OF HTR FUEL ELEMENTS

The fundamental temperature dependent component of the HTR system is the fuel particle. The composition of the particle, its incorporation in the fuel bed and particle failure modes are described in section 1 of this chapter. In section 2 the various fuel element design concepts are discussed which have been considered over the last few years. Finally, in section 3, the design concept adopted for the Oldbury 'B' tender is described in rather more detail and the optimisation of its geometry briefly discussed.

1 Fuel particle and matrix

1.1 Composition of the fuel particle and matrix

The coated particle concept was devised to perform as its own fission product retaining vessel; such a system allowing higher irradiations than pellet (AGR) type fuel. These particles, of approximately 1100 µm in diameter, are shown in Fig 2/1, made available by VOICE (1).

The fission product retention is achieved by a series of 'shells' surrounding the UO_2 kernel. Fig 2/1 shows a section through a typical particle. The UO_2 kernel (800 µm diameter) has immediately adjacent a coating of porous pyrocarbon (100 µm diameter). This buffer layer, as well as providing additional fission product accomodation space, also acts as a sacrificial layer for arresting fission fragments. A high density isotropic (HDI) pyrocarbon pressure retaining layer is then deposited (110 µm) followed by a metallic fission product retention layer of SiC. The 'pre-stressing' of the inner HDI pyrocarbon and SiC layers is achieved by another coating of (HDI) pyrocarbon (50 µm) which also provides protection against external chemical attack. The thickness of the coatings has been chosen to give a compromise between high heavy metal densities and particle integrity.

There are two methods by which the particles are bonded together:

(i) 'Loose-bonding'

The particles are bound together by a resin-graphite 'glue' producing high heavy metal densities. Under irradiation, however, the bonding has a tendency to break down allowing particles to become free.

(ii) 'Compacting'

Here the particles are placed in a die with graphite and compacted at high temperatures. The heavy metal densities achieved (1g/ cc) are not as high as with the loose bonding method because of the risk of particle fracturing but the compacts so formed are highly stable under irradiation.

A more detailed description of irradiation experience, types of graphite etc. can be found in BISHOP (2). The bonding method finally adopted for the Oldbury 'B' tender design (partly as a result of the BISHOP committee work) was the compacting process; high integrity being preferred to low cost - at least for the first HTR.

1.2 Failure modes of the fuel particle

There have been two failure modes recognised from the limited irradiation experience available and they will now be briefly described. Further details can be obtained from BISHOP (2) who has attempted to quantify these failure phenomena so as to provide limiting criteria in design studies.

(i) Amoeba attack

This is believed to be a chemically induced failure where the creation of free oxygen from the fission of the uranium allows oxidation of the buffer layer. It is a reversible process and the oxidation of carbon on one side of the kernel is accompanied by carbon deposition on the other side; the cross-kernel temperature difference (ΔT) causing this effect. Kernel rating (Q), absolute temperature (T) and irradiation (t) are also believed to be important variables; the amoeba attack building up in a cumulative way throughout the fuel dwell. After a certain degree of attack the particle becomes sufficiently weakened for the internal pressure to cause failure and the emmission of fission products. BISHOP (2) has quantified this effect in the following way.

Since it is not possible to state a specific limit on amoeba attack which, once exceeded, will cause the particle to fail, BISHOP has defined a limit after which the particle is said to be 'at risk' i.e. the amoeba life, F, is equal to 1.0 when this limit has been reached. F is given by (see GREEN (3)):

$$F = 0.072t\,(Q\,\Delta T)^{\frac{1}{2}} \exp\left[\,6.7 - \frac{21200}{T + \Delta T}\,\right] \qquad \text{.....1}$$

where t is in days, Q in W/cm^3, ΔT and T in ^{o}K.

(ii) Pressure failure

During irradiation of the fuel the PyC will shrink giving a compressive stress in the stable SiC layer. Shrinkage of the inner PyC layer will give further compressive stress in the SiC before, possibly, becoming detached. As the fission gas pressure builds up, the compressive stress in the SiC reduces until it finally goes into tension where upon it is assumed to fail, so allowing metallic fission products to escape. The fission gas pressure is dependent upon burn-up and instantaneous temperature and unlike amoeba failure is independent of temperature history. WALTHER (4) has provided a mathematical model of the stresses within the particle and CONWAY-JONES (5) describes how this model can be used to supply the limiting criteria on particle temperature and burn-up.

2 Fuel element and moderator block designs

As described above one of the essential features of the HTR is the integration of fuel and moderator such that, on refuelling, moderator is also replaced. A common feature of most designs considered to date is a hexagonal brick between 350 and 500 mm A/F which is the basic refuelling unit. Columns of these bricks contain the fuel and control channels and it is with the type and distribution of fuel within the brick where conceptual variations have been applied. These designs can be divided into two categories arising from independent experimental experience of the USA and the UK:

(i) fuel pin concepts (UK)

(ii) integral brick (USA)

(The Pebble Bed reactor, studied in West Germany, will not be considered here.)

The fuel pin concepts are those design where the brick has a number of channels containing fuel encased in graphite and cooled by helium passing over the pin. The integral brick designs are of a more homogeneous type where the fuel and moderator are closely integrated by having a large number of small channels; some containing fuel compacts and some passing coolant.

2.1 Fuel pin designs

The most important of the various designs considered in the UK are the Hollow-rod, Teledial and Tubular (non-interacting and interacting) designs. These are shown schematically in Fig 2/2 reproduced from SMITH (6)

(i) Hollow-rod

This is a cylindrical compact in a cylindrical graphite can with three longitudinal anti-bowing ribs. Coolant passes through the annular channel between can and channel wall. This design has the advantage of simplicity of thermal and hydraulic analysis, (e.g. the position of peak fuel temperature is fixed at the inner compact surface). With limited heat transfer surface, however, thermal ratings are low. The compact is unrestrained providing low compact stresses and therefore large (up to 1.0 mm) interface gaps can develope with irradiation producing high fuel temperatures at the end-of-life when the burn-up is at a maximum. From particle 'pressure' failure considerations this is undesirable.

(ii) Teledial

This is a cylindrical graphite tube with three anti-bowing ribs. Within the wall of the tube are contained a number of small cylindrical compacts. Coolant passes either side of the graphite annulus. With this design there are the advantages of a large wetted perimeter, low fuel shrinkage and small gaps. It is however a complex design with high stresses within the graphite. There are also increased costs arising from the larger number of compacts. Higher enrichments are also required because of the more homogeneous nature of the fuel and moderator.

(iii) Tubular (Non-interacting and interacting)

With these designs annular compacts are contained between graphite sleeves and coolant can pass within the inner sleeve and in the annular passage formed by the outer sleeve and channel wall. In the non-interacting case the clearance between compact inner surface and the outer surface of the inner can is chosen so as to ensure no interaction throughout the fuel dwell. This gives low compact stresses but leads to higher fuel temperatures owing to large gaps forming. In the interacting design the initial clearance is chosen so as to give interaction early in the fuel dwell producing smaller gaps at the cost of higher compact stresses. The tubular designs although more complex than the Hollow rod has the advantage of a larger wetted surface producing lower temperatures and higher power densities. These tubular designs are formed by trepanning a graphite rod to form the two sleeves which are connected at one end. There are therefore limitations on inner-outer sleeve temperature differences caused by unacceptable stresses in this end region.

Two major disadvantages are common to all these designs:

(i) high manufacturing costs of fuel pins

(ii) heterogeneous nature of the fuel which leads to high fuel temperatures.

Both these faults can be overcome (with the inevitable introduction of others) by the adoption of an Integral Brick.

2.2 Integral Brick

This design, developed by Gulf General Atomic, has a lattice, usually triangular, of a large number (200 - 400) of holes containing fuel or coolant. The GGA design has 252 compacts and 126 coolant passages so that one coolant channel accepts heat from two compacts, assuming symmetry.

With such a large number of compacts and coolant channels temperature drops are lower than with pin designs resulting in lower fuel temperatures. This is further enhanced by the reduced fuel shrinkage and interface gaps. In general, apart from its analytical complexity, the IB is, thermally, a highly desirable design as it goes a long way towards the ideal heat transfer system where the fuel and coolant are intimately mixed (e.g.

as in a fluidised bed). There are however three major disadvantages:

(i) high compact manufacturing costs arising from the large numbers

(ii) high stresses within the brick

(iii) higher enrichments resulting from worsening resonance integrals in this homogeneous design.

In an attempt to lessen these problems compromise designs have been proposed - the Semi-Integral Bricks. Instead of solid fuel compacts they are made annular with an inner protective graphite sleeve and coolant is allowed to pass within. There are also a similar number of compacts as in the pin designs (seventeen approximately). The Semi-Integral design overcomes the compact manufacturing cost problem but suffers from inferior heat transfer and probably higher graphite stresses. More detail of this design together with the I.B. can be found in a comparative exercise carried out by the Author: BALLARD (7).

3 The tubular interacting design

At the time of the Oldbury 'B' Enquiry Specification (September 1970) it was believed that the T.I. design was the most satisfactory as a fuel element for the first HTR. The advantages of the I.B. although highly attractive could not be substantiated by irradiation experience in the UK. The T.I. design was probably the most attractive economically, of the pin type elements and the two major problems of compact and sleeve stressing were relieved in the former by further, more detailed, analysis and in the latter by optimisation of the pin geometry.

It should be noted, however, that at the time of writing this thesis the I.B. appears to be the favourite for the first HTR. This probably results from increased American influence over the last two years.

For the vast majority of the work described the methods have been applied to the T.I. element which will now be described in more detail.

3.1 Optimisation of fuel element geometry

Before the fuel pin and channel dimensions can be optimised there are certain overall design constraints which must be considered:

(i) active core height - decided by core size considerations

(ii) fuel compact thickness and diameter - manufacturing limitations

(iii) fuel area - derived from reactor physics considerations

(iv) sleeve thickness - manufacturing and stress limitations

With these limitations in mind the geometry is chosen so as to achieve, for the T.I. design, the maximum channel power and minimum pressure drop without exceeding the limits on fuel and graphite peak temperatures and inner-outer graphite sleeve temperature differences.

The optimisation of a T.I. element is a complex procedure and although the Author was intimately involved in choosing the final T.I.

dimensions the work is not believed relevant to the main object of the thesis and will therefore not be related here. (See BALLARD (8).)

3.2 The Tubular Interacting fuel element and moderator block geometry

The final fuel element dimensions chosen for the Oldbury 'B' tender are given in Table 5/1 and Fig 2/3 is a drawing of the pin. It will be observed that the compacts are retained within the sleeves by a screwed end-cap which is at the downstream or bottom end of the pin for fuel corrosion reasons. (See Chapter 4, section 4.)

The fuel block, containing seventeen fuel channels is shown in Fig 2/4 and Fig 2/5 shows a control brick where there are nine fuel and three control channels containing, typically, one grey rod, one black rod and one secondary shutdown device, respectively.

CHAPTER 3

THE REACTOR ENVIRONMENT

Before the performance of the fuel element can be examined in depth the conditions under which it will exist in the reactor must first be studied.

The aspects in which the reactor environment influences the performance of a single fuel element are as follows:

(i) heat generation distribution within the fuel element and associated moderator

(ii) distribution of fast neutron damage dose within the fuel and moderator

(iii) coolant mass flow rate through the fuel channel

(iv) thermal interaction between the fuel channel and its neighbours.

Items (i) and (ii) are dealt with only briefly in section 1 since the Author made only a small contribution to their derivation. Item (iii) in which the Author was intimately involved is discussed in more detail in sections 2 - 5.

In the case of the fuel pin type of elements (e.g. the hollow rod and tubular interacting elements) there is very little thermal interaction between fuel channels in a block and certainly as far as fuel element temperatures are concerned, fuel channels can be examined in isolation in this respect.

In summary, therefore, the object of this chapter is to provide the complete distributions of heat generation, channel flow and coolant outlet temperature in the HTR core which is the basic data required for the work described in Chapters 4 and 5.

1 Time and spatial distributions of heat generation and damage dose

1.1 Axial rating distribution

The method of calculations of the axial rating profile using the one dimensional two-neutron energy groups code BLAZE is described in OLDBURY 'B' TENDER (9).

Initially just one enrichment was specified axially and the conventional axial temperature profile was obtained where there is a large fuel temperature differential between channel inlet and outlet. In this HTR design the limiting criterion on fuel rating is fuel temperature and there are large incentives to reduce these temperatures without de-rating the core. It was realised that this could be done by having more than one enrichment axially, the higher enrichments towards inlet.

From studies carried out by the Author it was found that substantial fuel temperature reductions could be obtained with just two axial enrichments where the enrichment boundary is between the second and third brick from inlet.

The enrichments were initially chosen to give equal fuel temperatures at the 2m and 4m level. This 'equi-temperature' criterion, however, neglects the effect of rating on partical failure and the enrichments should be chosen to meet an 'equi-amoeba failure risk' criterion.

There are two major factors which need to be considered and which prevent the full benefits of a multi-axial enrichment scheme from being realised.

(i) Coolant leakage

As explained in section 5 of this chapter certain columns in the periphery of the core, with large thermal and fast neutron dose gradients, bow and by interaction with their neighbours form gaps at their brick ends. Coolant flow can therefore bypass the channels upstream of these gaps producing higher temperatures at these positions. A dual axial enrichment scheme which increases the rating in the top bricks could raise temperatures in this region above the design limits. Fortunately it is unlikely the highest rated column will be a leaking column.

(ii) Compact corrosion

As discussed in Chapter 4, section 4, the protection of the fuel compact depends upon the high temperature graphite reacting with the water as it permeates through the sleeves.

Towards inlet however, the graphite temperatures are lower and if the fuel temperatures are near the design limit resulting from the dual enrichment scheme the fuel could suffer appreciable chemical attack.

In conclusion, therefore, the dual axial enrichments were chosen (e.g. inner region, 4.74%, 5.88%) so that the fuel temperatures at the 2m peak were still well below the 4m temperatures (approximately 100°C, see Fig 5/1) and the design limit. Even with this safety margin fuel temperature reductions of approximately 60°C over the normal single enrichment scheme were obtained.

The axial rating shape is dependent on: the radial position in the core, the proximity of control rods and their degree of insertion. It will also depend upon fuel and moderator temperature and there is a certain amount of iteration between the reactor physics and thermal performance calculations to obtain the correct axial profile.

The axial rating profile for a particular channel will vary with the irradiation of that channel. As the irradiation proceeds the high rating peaks will burnup at a faster rate than the lower rated positions.

For the purposes of the work in this thesis the axial rating profiles which apply to the peak rated channel in an equilibrium core have been used. Fig 3/1 shows the profile for different times in the dwell.

1.2 Radial rating distribution

The channel power distribution for an equilibrium core has been calculated using a 2-group SNAP model with six triangular meshes per column. A more detailed description of the method can be found in the OLDBURY 'B' TENDER (9). Each column in the core has been represented and the program calculates life average rating values at the centroid of each of the six equilateral triangles making up the hexagonal bricks (Fig 3/2).

There are two radial enrichments chosen (5.2% mean inner, 6.7% mean outer) to give equal peak pin powers in the two regions of the core (Fig 3/3).

From this SNAP information both column and channel powers are determined. The column powers are found by taking the arithmetic mean of the six values which are themselves normalised to a core mean of 10^4. Channel powers are found by first calculating an effective column gradient.

By referring to Fig 3/2; if y_c is the distance of the centroid from the brick centre and y_p is the distance of the furthest fuel channel from the brick centre then the across column 'gradient' is defined as:

$$G = \frac{y_p}{y_c} \cdot \frac{\hat{r}}{\bar{r}} \qquad \ldots\ldots 1$$

Where $\hat{r}$ is the peak value of the centroid rating values and $\bar{r}$ is the arithmetic mean.

From Fig 3/2 $y_p = 178$ mm and therefore $y_p/y_c = 1.33$

NB It is believed that across column gradients will burn down over life. However, no firm data on the magnitude of the effect is as yet, available.

The column power is proportional to $\bar{r}$ and it is now necessary to find the constant of proportionality.

W_F = total fuel channel flow

$\bar{T}_{2C}$ = mixed core outlet temperature of coolant

$\bar{T}_{1C}$ = inlet temperature of coolant

N_F = number of fuel channels

C_p = coolant specific heat

mean channel power, $\bar{Q}_{CH} = C_p\ (\bar{T}_{2C} - T_{1C})$ 2

and $\bar{Q}_{CH} = 10^4$ on the SNAP power map.

If Nc is the number of fuel channels within a column then:

$$\text{column power} = \frac{\bar{Q}_{CH} Nc}{10^4}\ \bar{r} \qquad ......3$$

From OLDBURY 'B' TENDER (9) and core data given in Table 3/1 the value of $\bar{Q}_{CH}$ is 397 kW.

Fig 3/3 shows the spatial distribution of column average powers ($\bar{r}$) and across column gradients for a 1/6 sector of the core.

The peak rated channel power (life mean), 514 kW, has been determined from this power map but also includes a margin for fuel management.

1.3 Time evolution of channel power

Owing to the burn-up of fissile atoms there is a reduction in the rating as the irradiation of a fuel element proceeds. This is offset to some extent by the creation of further fissile atoms in the form of ^{239}Pu. The fuel is left in the core until a particular burn-up (MWd/Te) has been achieved and since different columns have different ratings there is consequently a whole spectrum of fuel residence times.

The residence time assumed for the peak rated channel is 770 days at 75% load factor. This dwell is consistent with a burn-up of 72000 MWd/Te. The age factor is defined as the ratio of the start of life channel rating to the life average value. The program BLAZE has been used to calculate the age factors for different regions of the core. The results are reported in OLDBURY 'B' TENDER (9). The peak rated channel is assumed to lie in the inner region of the core and therefore, according to this data, has an age factor of 1.18.

It is a good approximation to assume that the channel power falls linearly with time and Fig 3/4 shows the evolution of peak rated channel power with dwell. (OLDBURY 'B' TENDER (9)).

1.4 Fine structure effects

(i) Axial effects

These arise from the presence of burnable poisons which are only present in the initial loadings. At equilibrium there will be no appreciable axial perturbations.

(ii) Across pin gradients

These gradients are only important for channels at the edge of the core or close to control rods. A peak rated channel is not likely to occupy either of these positions.

(iii) Flux depression effect

There is negligible flux depression within the fuel compact of the Tubular Interacting element according to TNPG studies.

1.5 Damage dose distributions

The axial fast neutron flux profile follows very closely the rating shape and, for the purposes of the calculations in this thesis, the fast neutron dose at axial position z, will be given by:

$$D(z) = \frac{R(z)\,\bar{D}}{\bar{R}}$$

where $R(z)$ = the axial rating factor at position z

$\bar{R}$ = channel mean rating factor (normally equal to 1)

$\bar{D}$ = channel mean dose.

The units of damage dose are usually given as neutrons/cm^2 EDN (equivalent neutron flux in the DIDO reactor).

From Table 3/1 the channel mean dose assumed for the peak rated channel was 2.0×10^{21} n/cm^2 EDN.

The dose at any particular moment in time must of course be determined by the integration of the axial profile with time up to the moment of interest since, as can be seen from Fig 3/1, the axial rating shape varies with burn-up.

1.6 Refuelling scheme

Up to the time at which this work was carried out there was no refuelling pattern available for an equilibrium core. The Author has therefore devised a scheme which should be typical of a realistic pattern. The method for deriving this scheme was simple. Ten age groups were chosen: one at fuel loading, one at each gag change and one at the mid-point of each gag interval (Fig 3/4). (These ages were chosen to be of most use in the corrosion calculations described in Chapter 4 section 4).

The columns in the sextant of the core considered were then allocated an age such that the following conditions were satisfied:

(i) The total power in the sextant at this snapshot time is the same as that given by the sum of the life average SNAP rating. This was achieved to within 1%.

(ii) There were equal numbers of columns in all age groups. With 51 columns in the sextant age group 10 was allocated the extra column. (See Table 5/3).

Fig 3/3 shows the distribution of ages in the sextant of the core considered.

1.7 Moderator heat generation

Heat is generated within the moderator as a result of neutron and γ irradiations. The axial and time distributions of this heat generation is assumed to follow the fuel heat generation.

The fraction of the total channel heat generated within the moderator is small (8%) and the entire component is assumed to be within the fuel block; the graphite sleeves being only a small fraction of the total graphite volume.

2 An introduction to the optimisation of core flow distribution

The Oldbury 'B' design of HTR for which this study was made has 301 columns; containing either seventeen (fuel column) or nine (control rod column) fuel channels (Figs 2/4, 2/5) totalling 4533 fuel channels in all.

As explained in the previous section the power variations between these channels at any particular time can be divided into two components:

(i) Irradiation

(ii) Spatial.

The major limiting phenomena in this design of HTR are fission product release and graphite corrosion both of which are highly sensitive to fuel element temperatures. In order to maintain these limits in a peak channel, without the adjustment of channel flow to offset the power variations, it would be necessary to reduce the core rating or coolant gas outlet temperature, grossly overcooling the rest of the channels. Whereas, with the only major cost arising from higher pumping powers, significantly higher ratings and cycle efficiences can be obtained by judicious adjustment of the core flow distribution.

This section describes the methods developed in a detailed study made on the Oldbury 'B' equilibrium core and gives the thermal and fuel performance repercussions for a range of flow gagging assumptions.

The gagging scheme chosen for the Oldbury 'B' design is described in detail and using the radial power distribution and age factor data presented in section 1 the time and spatial distributions of channel gas outlet temperature are derived.

3 Time gagging

3.1 General considerations

The reduction in channel power with burn-up, described in section 1 would, with a constant gag setting, produce a corresponding reduction in channel gas outlet temperature and whilst maintaining the desired life average gas outlet temperature, large swings in temperature would occur. An alternative is to periodically adjust the gag so as to progressively reduce the mass flow rate in step with the channel power. In the limit the gag would be continuously changed so as to achieve the minimum (zero) deviation from the desired life mean gas outlet temperature.

Appendix I derives the relationship between the peak gas outlet temperature and the life mean value assuming N gag changes at equal intervals throughout the fuel dwell.

For the peak rated channel case (Table 5/1) the gas and fuel element temperature effects of different numbers of gag changes are given in Fig 3/6 and Tables 3/2, 3/3 derived using the AZIMUSTAP 5 program.

The ideal scheme, with remotely controlled continuous gag changing, as employed in the AGR, has special design problems in the HTR. In the TNPG Oldbury 'B' design the gags are changed by the refuelling machine and because of this time consuming method it is desirable to have as few a number of gag changes as possible.

The following sub-section gives the fuel endurance repercussions of such reductions.

3.2 Fuel element endurance considerations

The incentive to reduce the number of gag changes depends upon the limiting criteria, namely fission product release and graphite corrosion.

In order to remain within the limits on fission product release it is necessary not to exceed a particular failed particle fraction. The two recognised modes of particle failure during reactor operation, 'amoeba' and 'pressure', are both highly temperature sensitive.

As described in Chapter 2 'amoeba' attack is a corrosion phenomenon of the inner PyC layer and is cumulative over life. 'Pressure' failure is due to gaseous fission products causing the SiC layer to come under tension and is dependent upon the instantaneous particle temperature and burn-up.

It is therefore important, in order to escape 'pressure' failure, to have a sufficiently low fuel temperature at the end of life, when the burn-up is at a maximum. For 'amoeba' failure, however, the integrated fuel temperature over life is the important factor.

To restrict the number of gag changes will result in higher temperatures at the start-of-life, lower at the end-of-life but with approximately the same life average values (Fig 3/6). From the above 'pressure' failure considerations this form of life evolution of fuel temperature would appear beneficial and the fact that the life average temperature is unaffected by reducing the number of gag changes, suggests that 'amoeba' attack would not be increased. There is however some increase, as 'amoeba' attack is an exponential function of fuel temperature, although a linear function of time (days).

Table 3/3, derived using the AZIMUSTAP 5 - PARTICLE FAILURE link applied to the peak rated channel (Table 5/1) shows fuel element temperatures and fuel endurance for the reference four gag change scheme and a scheme where the gag is not changed throughout the dwell.

As a measure of the integrated 'amoeba' attack the factor F is given such that the particle is said to be at risk if $F > 1$. The extent of the 'failure' is also given in terms of the failed particle fraction in the channel.

From the table it is clear that for this, the most limiting channel, the 'amoeba' failure is increased by reducing the number of gag changes to zero, whereas the possibility of pressure failure is removed.

Although the peak fuel temperature for the no-gag case is 65°C above the reference case it can also be seen from this table that by a reduction of only 20°C on the mean gas outlet temperature 'amoeba' failure can be reduced to below the four-gag change value.

As far as the corrosion of graphite components is concerned there is no well defined limiting criterion on temperature. If, however, the number of gag changes are reduced, increasing the overall peak graphite temperatures, this is known to significantly increase the graphite removal rates and such factors as a smaller allowable water ingress and the possible replacement of corroded graphite components have to be offset against the advantages of a smaller number of gag changes.

For the Oldbury 'B' tender work and for this thesis a four gag change scheme has been adopted (Fig 3/4, 3/5).

Fig 5/2 shows the life evolution of peak fuel and graphite temperatures for the reference peak rated channel for this scheme.

In this section it has been assumed that in each gagging interval the mean gas temperature is maintained at the life mean value. If there is a large variation in fuel and graphite temperatures over life there is obviously some incentive to gag such that, although the overall mean gas temperature is maintained, the distribution with life of gas temperature provides a more propitious distribution of fuel element temperatures. However, since the variation of fuel temperature with life is small and the two graphite sleeve temperature distributions are opposite in form (Fig 5/2) there appears to be little incentive to shape gas temperature distribution with this fuel element design.

4 Spatial gagging

4.1 General spatial gagging philosophy

Spatial gagging can be regarded as providing an 'optimum' distribution of channel gas outlet temperature within certain design limitations.

The radial power variations between channels across the core, which are to be gagged out, are made up of two components:

(i) column to column variations

(ii) across column power gradients.

For the Oldbury 'B' design, however, there is one gag per column and therefore only column to column power variations can be gagged out. This design limitation implies that uniform peak channel temperatures cannot be realised. Therefore, the criterion for a successful spatial gagging scheme within these limits would be if all columns, or group of columns, gagged to their own gas outlet temperature, had the same peak temperature; the temperatures assumed in this study being peak channel gas outlet, graphite and fuel temperatures. Ultimately instead of temperatures, fission product release or corrosion could be considered.

In order to realise equal peak channel temperatures between columns it is necessary to gag each column to its own gas outlet temperature because of differing column average powers and gradients (e.g. the higher the gradient the lower the $\overline{T}_2$).

By applying the 'grouping' principle, following AGR practice, the columns can be arranged into groups of similar gradient, gagging all the columns within a group to the same $\overline{T}_2$. This reduces, to some extent, operational complexities at some cost in performance.

For example, if $\hat{G}$ is the maximum gradient and N groups are chosen these groups would contain channels of gradient $0 - \hat{G}/N$, $\hat{G}/N - 2\hat{G}/N$, ...$(N-1)\ \hat{G}/N - \hat{G}$.

The following section itemises the calculation route from obtaining core power maps to the final temperature distributions and gives the resulting thermal performance for different spatial gagging schemes and optimisation criteria. Finally, for the chosen gagging scheme, the core flow - T_2 distribution is determined.

In order to compare different gagging options it has been assumed that there is constant flow axially through all columns i.e. there is no inter-brick leakage of flow.

In reality there will be significant leakage in particular areas of the core and this is discussed, giving the resulting flow distributions in section 5.

4.2 General theory of group gagging

Although it is possible to equalise peak fuel and graphite temperatures between groups only the equalisation of peak channel gas outlet temperature will be considered here.

Let $\bar{R}$ be a column mean channel heat generation and let G be the column 'gradient' where $G = \frac{\hat{R}}{\bar{R}}$ and $\hat{R}$ = maximum channel heat generation. Rc_{ij} is the heat generation (life mean) of the jth column in the ith group. Assuming N gag groups then:

> $\hat{G}_1, \hat{G}_2, \hat{G}_3 \ldots\ldots \hat{G}_N$ are the maximum gradients in each group where the columns are grouped according to gradient i.e. group 1 contains those columns with the lowest gradient and group N those with the largest.

If there are M_1 columns in group 1, M_2 columns in group 2 etc. then the combined heat generation of all columns in the groups is given by:

$$\Sigma R_1 = Rc_{11} + Rc_{12} + Rc_{13} \ldots\ldots Rc_{1M_1}$$

$$\Sigma R_2 = Rc_{21} + Rc_{22} + Rc_{23} \cdots\cdots Rc_{2M_2}$$
$$\vdots$$
$$\Sigma R_N = Rc_{N1} + Rc_{N2} + Rc_{N3} \cdots\cdots Rc_{NM_N}$$

The heat balance from the core shows:

$$C_p W_F(\overline{T}_{2c} - T_{1c}) = \Sigma R_1 + \Sigma R_2 + \cdots\cdots \Sigma R_N$$

where W_F = total core flow through fuel channels

$\overline{T}_{2c}$ = mixed gas outlet temperature from all fuel channels

T_{1c} = inlet gas temperature

If $\overline{T}_{21}$, $\overline{T}_{22}$ - - - are the column mean gas outlet temperatures from each group:

$$\frac{\Sigma R_1 + \Sigma R_2 + \Sigma R_3 - - - \Sigma R_N}{(\overline{T}_{2c} - T_{1c})} = \frac{\Sigma R_1}{(\overline{T}_{21} - T_{1c})} + \frac{\Sigma R_2}{(\overline{T}_{22} - T_{1c})} + \frac{\Sigma R_N}{(\overline{T}_{2N} - T_{1c})} \quad \cdots\cdots 4$$

The gagging criterion is that the peak channel gas outlet temperatures from each group are equalised i.e.

$$(\overline{T}_{21} - T_{1c})\,\hat{G}_1\,F'_1 = (\overline{T}_{22} - T_{1c})\,\hat{G}_2\,F'_2 = \cdots\cdots (\overline{T}_{2N} - T_{1c})\,G_N F'_N$$

where F'_1, F'_2, - - - F'_N is the factor which allows for across-block flow variations. ($F \simeq G^{0.4}$ derived in Appendix II).

Therefore:

$$\left.\begin{aligned} (\overline{T}_{22} - T_{1c}) &= (\overline{T}_{21} - T_{1c})\,\hat{G}_1\,F'_1/\hat{G}_2\,F'_2 \\ (\overline{T}_{2N} - T_{1c}) &= (\overline{T}_{21} - T_{1c})\,\hat{G}_1\,F'_1/\hat{G}_N\,F'_N \end{aligned}\right\} \quad \cdots\cdots 5$$

Substituting equations 5 in 4 we have:

$$(\overline{T}_{21} - T_{1c}) = \frac{(T_{2c} - T_{1c})}{(\Sigma R_1 + \Sigma R_2 + \cdots \Sigma R_N)} \left(\Sigma R_1 + \frac{\hat{G}_2 F'_2}{\hat{G}_1 F'_1}\,\Sigma R_2 + \cdots \frac{\hat{G}_N F'_N}{G_1 F'_1}\,\Sigma R_N \right) \quad \cdots\cdots 6$$

Having found $\overline{T}'_1$ from equation 6 $\overline{T}_2$ - - $\overline{T}_N$ can be found from equations 5.

The maximum reduction in peak channel gas outlet temperature is obtained, when the number of groups equals the number of columns in the core when individual column $\overline{T}_2$ gagging is achieved.

4.3 Thermal performance effects of various gagging schemes

Group gagging to the gas outlet temperature criterion can be done explicitly without the need for iteration to ensure conservation of mass flow. Gagging to other criteria such as peak fuel or graphite temperature is, however, a complex iterative calculation requiring computing techniques.

A program, FOIL, has been written, specified by WILLIAMS(10) which incorporates the $\overline{T}_2$ gagging criterion method developed by the Author as well as the peak fuel and graphite temperature criteria. The program derives the resulting temperature histograms, using the method of deducing channel peak temperature from integral AZIMUSTAP 5 data developed by the Author and described in Chapter 5.

FOIL has been used to investigate the performance repercussions of different gagging schemes and the Author acknowledges the assistance of Mr. L.G. Williams in making this study.

4.3.1 Channel gas outlet temperature criterion

Using the case where all the columns in the core are gagged to the same gas outlet temperature as the datum, Fig 3/7 shows that for the maximum gas outlet temperature the greatest saving occurs when changing from one to two groups and for further increases in the number of groups, the saving diminishes until the limiting value is obtained at around twelve groups. The relationship between the number of groups and the gas outlet temperature appears to follow an exponential curve, but the relationships relating the fuel and surface temperatures are more complex.

The results for fuel and surface temperatures shown in Fig 3/7 indicate that savings in fuel are less than gas temperature savings while savings in surface temperatures are greater. The grouping of columns on cross-column gradient, neglects the effect of rating and columns having high gradients do not necessarily have high ratings. This means that peak fuel temperatures can occur in columns which are not necessarily the peak gradient columns in a group. It is this phenomenon that causes the saving in fuel temperature to fall below the saving in gas temperature; the fluctuation of location of peak temperatures from one column to another also causes the discontinuous nature of the curves.

The surface temperature results all show reductions that are greater than the gas temperature reductions as these peak temperatures occur in columns more closely related to the peak channel gas temperature columns. The minimum saving appears to occur for the inner sleeve; the maximum occurring for the channel wall. These savings are consistent with the characteristics of the Tubular Interacting element where the peak inner sleeve temperature occurs further from outlet than the peak outer sleeve and channel wall temperatures and therefore does not benefit to such a great extent from flow increases. An increase in the number of groups results in an increase of flow in the channels having the peak temperatures and this produces a slight modification in the heat and flow splits which also contributes to the effect of the saving in temperature on the inner sleeve surface being less than that on the outer sleeve surface. The channel wall has the greatest reduction in temperature because there is an additional reduction owing to a smaller radiation component heat flux, resulting from the lower outer sleeve temperatures.

The core distribution of life peak fuel and graphite surface temperatures are shown in Figs 3/8-3/11. These results show that the effect of increasing the number of groups on the temperature distributions, is to produce a more weighted histogram at the higher temperature end; at the same time, however, reducing the overall peak value.

N.B. These are results produced at the early stages of the research programme and do not include all the work described in Chapter 4 (e.g. corrosion). They are, therefore, only to be used to compare different gagging schemes and cannot be expected to be consistent with the final results presented in Chapter 5.

4.3.2 Fuel and graphite surface temperature criteria

The significant reductions in fuel and graphite temperature by gagging to equalise peak channel gas outlet temperature can be further improved if the fuel and graphite temperatures themselves are equalised.

The gas outlet temperature of each column is chosen so that the peak fuel or particular graphite surface temperature is equal in all columns. The distribution of column $\overline{T}_2$ values will depend on which temperature is being optimised and so it would not be possible to simultaneously optimise fuel and all graphite surface temperatures. If, however, on-line computing facilities were available a combined fuel and graphite temperature optimisation scheme may be devised.

In order to determine the possible performance advantages of a more complex optimisation procedure the program FOIL has been employed where it is possible to optimise the flow distribution to satisfy the following options:

Option 1 - Equalisation of life peak fuel temperature in all columns

Option 2 - Equalisation of life peak inner graphite surface temperature in all columns

Option 3 - Equalisation of life peak outer graphite surface temperature in all columns

Table 3/4 gives the corresponding life peak temperatures for the three options together with, for comparison, a 12 group equalised channel gas outlet temperature scheme.

N.B. Once again these temperatures are presented only for comparison and are not consistent with the Chapter 5 figures.

The distribution changes to which these temperature reductions correspond are similar to those experienced by increasing the number of groups given in the previous sub-section i.e. the high temperature 'tail' is forced into the lower temperature bands.

The 20°C to 30°C temperature reduction found by optimising the flow distribution in this way is quite significant particularly for the graphite surfaces. As explained in Chapter 5 it is the changes of distribution where the high temperature tail is removed that has the most beneficial effect on graphite corrosion.

It is conceivable to advance one stage further and optimise to 'equal risk of particle failure' which would provide the maximum performance savings. The lack of understanding on particle failure modes and the uncertainty on local rating and temperature perturbations, however, make such a scheme unjustifiable.

4.4 <u>The reference three group peak channel gas outlet temperature scheme</u>

For the Oldbury 'B' tender a relatively simple scheme was devised so as not to deviate from previous (AGR) experience. Operation of the reactor is certainly simplified if only three life mean gas outlet temperatures need to be considered at, of course, some cost in reactor performance.

The object therefore was to determine three values of column overall mean gas outlet temperature ($\bar{T}_2$) which, given the radial power distribution, minimises peak channel gas outlet temperature.

The quantities which need to be known are:

(i) column average power for each column,

(ii) power gradient for each column,

(iii) number of channels in each column.

Sextant symmetry has been assumed and the above data for $^1/6$ th of the core is given in section 1 (Fig 3/3).

The across column flow variation factors (F') also need to be known and these can be found from Appendix II.

Using the theory developed in section 4.2 the three values of $\bar{T}_2$ can be derived (Appendix III) i.e.

$819^\circ C$, $782^\circ C$, $754^\circ C$.

The overall peak value of channel gas outlet temperature found in the largest gradient column of each group is $850^\circ C$.

The resultant distributions of column flow, $\bar{T}_2$ and channel peak gas outlet temperature are shown in Fig 3/12.

The peak rated channel in the core which has been used for the studies of single channel performance in the following chapter is not shown on either the power map (Fig 3/3) or flow map (Fig 3/12) since it includes additional margins. It has been assumed, however, that it has an across column gradient of 7.5% and can therefore be allocated to group 2 (Appendix III) giving its column a $\bar{T}_2$ of $782^\circ C$ and a channel gas outlet temperature (life mean) of $833^\circ C$.

So far inter-column flow leakage has been neglected. As will be explained it is not possible to gag spatially allowing for leaking columns and the final flow distribution will be off optimum to some degree. The effect on channel flows and temperatures of leakage is given in section 5 below.

4.5 Gagging sensitivity to the radial power distribution

Variations in column average rating will not affect a peak gas outlet temperature gagging scheme although there will be some effect on fuel element temperatures. Gagging and temperature distributions are, however, most sensitive to across-column gradients - the higher the gradient, the higher the peak temperatures for the same number of gag groups.

A comparison has been made between two radial power maps where, for one case, the maximum gradient was 17% (maximum/average) and for the other 11%.

The results are shown in the table below:

Power map (Max. gradient)	T_2 (^{o}C)	
	3 groups	12 groups
11%	842	826
17%	858	842

It can also be seen from this table that in order to achieve the same peak gas outlet temperature a greater number of groups need be taken for the map with the higher gradients.

It is possible to compensate for the effect of high gradient columns by reducing the rating of those columns by radial enrichment zoning i.e. from equation 6, if ΣR_N is the rating of columns with a peak gradient of G_N, then by reducing ΣR_N and increasing ΣR_1 by δR, the total core power is unchanged and because $\frac{\hat{G}_N F'_N}{\hat{G}_1 F'_1} > 1$, $\hat{\hat{T}}_{21}$ and $\hat{T}_2$ are reduced.

There is obviously a limit to this radial power shaping as, although peak channel gas outlet temperatures are reduced there will begin to be a net increase in the rating dependent fuel and graphite temperatures.

5 Inter-brick leakage

N.B. The information given below in sub-sections 5.1 and 5.2 was obtained from general TNPG design work in which the Author made no significant contribution.

5.1 Cause of leakage

The gaps between adjacent columns are sealed to coolant flow at the bottom of the core and, therefore, provided there are no gaps between bricks in a stack the flow entering a column at the top of the core is equal to that leaving the column at the bottom.

For a cold unirradiated array of columns this non-leaking situation prevails. Under hot, irradiated conditions however, temperature and fast neutron dose gradients exist across all columns causing them to bow, owing to differential expansion and shrinkage.

This bow causes, through the interaction of the column with its neighbours, gaps to open up between the brick (Fig 3/13). The gradients across some columns can be sufficiently large to produce gaps of such a size as to present a relatively easy flow path to the coolant.

In this way a fraction of the normal column flow by-passes the bricks up-stream of the gaps and flows down the interstitial space, flowing back into column at the gap-opening.

5.2 Nature of leakage

5.2.1 Distribution of flow within a column

From the wedge shaped nature of the gap it is clear that the channels within a column leak to varying degrees and in fact some channels at the apex will have virtually the design flow. Fig 3/14 shows a typical axial variation of flow for the column and the worst affected channel, given as fraction of the normal non-leaking flow.

5.2.2 Leakage as a function of time

(a) Thermal gradient bowing

High thermal flux gradients across columns, predominant in the outer region of the core, produce, through the resulting power gradient, a gas and moderator temperature differential across the column.

This temperature gradient will occur immediately the column is loaded but owing to creep effects the thermal gap will reduce to effectively zero during the life of the column.

(b) Fast neutron dose gradient bowing

As with thermal flux gradient, dose gradients are also a maximum towards the outer region of the core.

The resulting irradiation shrinkage is a time integrated effect which implies a zero gap at the start of a column life and maximum gaps at discharge.

With the combination of these two gap opening effects a situation exists at some time in the dwell of the column that the gaps, and therefore the leakage are a minimum. Fig 3/15 shows a typical time evolution of leaking column flow.

5.2.3 Distribution of leaking columns

As stated above the high thermal and fast neutron dose gradients required for significant bow to occur exist in the outer region of the core and in general it is only the peripheral fuel columns which are affected. Fig 3/16 shows these columns together with their modified $\bar{T}_2$ values, the derivation of which is given in the following sub-section.

5.3 Thermal performance repercussions of inter-brick leakage

5.3.1 Whole core effects

Although only 20% of the columns have appreciable gaps and suffer a flow surplus the surplus is such (approximately 20%) that the non-leaking columns in the core experience a significant flow deficit (3.5%).

This result follows from the basic assumption that the core is gagged ignoring leakage and core flow is fixed rather than the core pressure drop. This latter assumption is valid as the core heat generation and boiler inlet temperature are design limitations. The former assumption, that the core is gagged neglecting leakage, results from within column considerations.

5.3.2 Within column effects

As mentioned above there will be some channels in a leaking column which will have the design flow. In addition the bricks up stream of the first gap will suffer flow starvation as can be seen from Fig 3/14.

If, however, effort is made to gag out the effects of leakage by restricting the flow in the column then the non-leaking channels and starved bricks in the leaking column will have even lower cooling flows resulting in higher than design temperatures.

For this reason, in order to maintain the limiting temperatures, leakage can not be compensated for when deciding the core flow distribution and over-cooling must be tolerated.

The core temperature distributions, however, should be calculated taking into account the true core flow distribution.

5.3.3 Temperature distribution effects

Models are not sufficiently refined to calculate the fuel element temperature effects of an axially varying flow rate although HEATAX, described in Chapter 5 and Appendix VII could be easily modified to make an initial assessment. It is unjustified at present, therefore, to develop the sophisticated method required to determine the distribution of channel gas outlet temperature within a leaking column.

For the present work it will be pessimistically assumed that leaking columns have the design gas outlet temperatures and the non-leaking column $\bar{T}_2$ values will be based on an overall flow deficit of 3.5%.

Fig 3/16 shows the column and peak channel gas outlet temperatures for this hypothetical leaking core.

The effect on the peak rated channel, referring to sub-section 4.4 above, is to increase the life average channel gas outlet temperature to 852°C.

CHAPTER 4

THE FUEL ELEMENT

In the previous chapter the reactor environment was dealt with and the derivation of the axial, radial and time evolutions of heat generation were discussed. Methods were also described for obtaining the coolant mass flow rate and outlet temperature for any fuel channel in the core.

With channel power distribution and flow as the basic starting points, the major part of the work - to develop methods which can evaluate the thermal and hydraulic characteristics of the fuel element - can now be described. The objective of this work was to develop methods which would derive:

(i) important temperatures within the fuel channel, e.g. fuel and graphite, at a number of axial positions and times throughout the fuel dwell

(ii) flow distribution and pressure drop within the channel.

As a starting point to this work the program MUSTAP, briefly discussed in Appendix VI, has been utilized. This program has the following limitations:

(i) thermal and fast neutron irradiation effects on dimensions are neglected (The calculation is made for one instant in time and the interface gap conductance is assumed invariant with temperature and axial position.)

(ii) material properties are assumed independent of fast neutron dose

(iii) corrosion induced roughening and changes of dimension have been neglected.

Firstly in this chapter in section 1, there is a critical discussion of the model used in MUSTAP to obtain temperatures within the fuel element, given the element surface temperatures.

In section 2 the heat transfer from the fuel element is subject to an original examination.

In section 3 the modifications to MUSTAP (AZIMUSTAP-5) specified by the Author to allow for effects (i) and (ii) above, are described.

Section 4 details the model developed by the Author to cover effect (iii), above, which is incorporated in the HEATAX code.

1 Heat transfer through the fuel element

Presented in this section are the basic equations that are used in the programs MUSTAP and HEATAX for calculating the heat transfer through the fuel, across the interface gaps and through the graphite sleeves. For completeness, the equations used will be derived here, together with a discussion of other effects not included in the equations.

1.1 The fuel matrix

As described in Chapter 2 the fuel bed is made up of coated particles, approximately 1 mm in diameter, set in a matrix of graphite. There are two temperature distributions within the compact which can be considered:

macroscopic distribution derived from smeared values of thermal conductivity, heat generation, etc.

fine structure distribution, superimposed on the macroscopic distribution, arising from the presence of the particles, where the heat transfer through the particle must be considered.

1.1.1 Macroscopic temperature distribution within the fuel compact

Firstly the macroscopic distribution is derived, assuming a mean thermal conductivity k_f (see Chapter 5) and a mean volumetric heat generation q_f'''. In fact, q_f''' is not constant throughout the fuel for the following reasons.

(i) The neutron flux depression effect

The fuel at the centre of the compact is shielded from the thermal neutron flux by the fuel towards the outside of the compact. As already explained in Chapter 3 this effect is negligible in the case of the tubular interacting elements.

(ii) Across-pin flux gradients

As described in Chapter 3 this effect is small for peak rated channels and will be neglected since, in order to allow for them, we would depart from axial symmetry thus making an analytical method intractable.

For cylindrical fuel, with conduction in the radial direction only, the Fourier heat conduction equation can be applied across an element dr i.e.

$$q''(r) = -k_f \frac{dT}{dr} \qquad .....1$$

Where $q''(r)$ is the heat flux across the element and is given by

$$q_f''(r) = q_f''' \; (r^2 - r_i^2)/2r$$

r_i is the radius of peak fuel temperature and is termed the 'heat split radius'.

Substituting into Eq. 1 and separating variables we have

$$\frac{q_f'''}{2} \left(r - \frac{r_i^2}{r}\right) dr = -k_f dT \qquad .....2$$

If k_f is assumed constant radially, integration gives

$$T = \frac{-q_f'''}{4k_f} \; (r^2 - 2r_i^2 \ln r) + \text{constant} \qquad .....3$$

The boundary conditions are:

$$r = r_{f1}, \quad T = T_{F1}$$

$$r = r_{f2}, \quad T = T_{F2}$$

By substituting these conditions and eliminating the constant of integration and r_i we obtain

$$T = T_{F1} - \frac{q_f'''}{4k_f} \left[r^2 - r_{f1}^2 + \frac{\ln r/r_{f1}}{\ln r_{f2}/r_{f1}} \; (r_{f2}^2 - r_{f1}^2 - \frac{4k_f}{q_f'''}(T_{F2} - T_{F1})) \right] ....4$$

This distribution has been evaluated for the conditions given in Table 4/1 and is shown in Fig 4/1.

The peak fuel temperature T_{FP} is given by

$$T_{FP} = T_{F1} - \frac{q_f'''}{4k_f} \left(r_i^2 - r_{f1}^2 - 2r_i^2 \ln \frac{r_i}{r_{f1}}\right) \qquad .....5$$

where
$$r_i^2 = \frac{1}{2 \ln {r_{f2}}/{r_{f1}}} \left[\frac{4k_f}{q_f'''} \left(T_{F2} - T_{F1}\right) + \left(r_{f2}^2 - r_{f1}^2\right)\right] \qquad .....6$$

1.1.2 Local temperature variations within a compact

In order to ascertain how the smeared peak fuel temperature derived above relates to the peak UO_2 kernel temperature the heat transfer properties of the kernel, buffer, pyrolytic carbon and silicon carbide shells (Chapter 2) must be examined. This has been done by ROSSITER (11) and RAPIER (12).

As described in Chapter 2 the important temperature values, as far as particle failure is concerned, are the kernel temperature and across-kernel temperature difference. ROSSITER has shown that the mean kernel temperature is only a fraction above the 'smeared' compact temperature ($3^{\circ}C$ for the conditions taken). The across-kernel temperature difference can be calculated from the macroscopic temperature gradient (Eq. 2). This gradient for the Table 4/1 conditions has been plotted in Fig 4/1. Across-kernel temperature differences of up to $18^{\circ}C$ for a kernel diameter of 0.8 mm are seen to occur. RAPIER has shown, however, that an important factor to be considered is the anisotropy of the shell thermal conductivity which can be 100 times greater in the circumferential direction than in the radial direction. This has the effect, according to RAPIER, of shielding the kernel from the macroscopic gradient producing across-kernel temperature difference of nearer $2^{\circ}C$.

The effects described above depend heavily upon two factors:

(i) the size and degree of eccentricity of the interface gap between kernel and shells

(ii) the thermal conductivity of the kernel and shells in the radial and circumferential directions.

Information, both analytical and experimental, relating to these two factors is severely lacking and we will assume for the benefit of this study that the kernel temperature and across-kernel temperature difference can be given by the macroscopic relations derived above.

1.2 The fuel/sleeve interface gaps

The heat transfer conductance of narrow gas filled gaps, where there are stagnant gas conditions, consists of three components:

(i) conductance through the gas

(ii) radiation across the gap

(iii) in the case of a nominally zero gap, when the surfaces are in the contact, we have solid conductance.

Let us define an effective gap conductance k_j, i.e.

$$k_j = \frac{q''}{T_F - T_I}$$

where q" is the heat flux across the relevant interface gap, which has fuel side and sleeve side temperatures of T_F and T_I respectively.

q" can be derived from q_f''' and r_i (Eq. 6) i.e.

$$\left.\begin{aligned} q_1'' &= q_f''' \, (r_i^2 - r_{f1}^2)/2r_{f1} \\ q_2'' &= q_f''' \, (r_{f2}^2 - r_i^2)/2r_{f2} \end{aligned}\right\} \quad .....7$$

1.2.1 Heat conduction through the filling gas

The gas conductance can be defined as

$$h_G = \frac{k_G}{g_{eff}} \qquad .....8$$

where k_G is the gas conductivity evaluated at $(T_F + T_I)/2$ and g_{eff} is the effective gap width. MAIN (13) defines g_{eff} as

$$g_{eff} = g + g_1' + g_2' + g_1'' + g_2'' \qquad .....9$$

The components of g_{eff} are:

(i) the nominal gap clearance g

(ii) an allowance for the gas lying between the peaks of the surface asperities - g_1', g_2'

(iii) the 'temperature jump distance' - g_1'', g_2'' - an additional thermal resistance caused by the imperfections in the transference of kinetic and vibrational energy between the solid and gas molecules.

The calculation of g, which depends upon the irradiation and temperature history of the fuel, is described in section 3 and we will consider items (ii) and (iii) above.

(a) Surface roughness

The equivalent increase in gap width is proportional to the roughness height:

$$g' = C.R$$

where R is the roughness height in CLA. The constant C, the subject of a literature survey by MAIN (13) has been shown to have a value of approximately 2.5, when the surfaces are not in contact. R is more difficult to quantify as there is no known measurement of surface roughness of extruded graphite tubes or pressed compacts. WARBURTON (14) has investigated the surface roughness of machined graphite and has shown a wide variation (4 - 15 μm CLA). The effective increase in gap width ($g_1' + g_2'$) using C = 2.5 and an average value of R (10 μm CLA) is 50 μm. One would expect, however, that a smoother finish would be possible by extrusion and pressing producing a smaller effect on the HTR fuel gaps.

In the work described here no increase in the effective gap has been allowed and in this respect the interface gaps have been probably underestimated by between 0 and 50 μm. The effect is sufficiently significant, therefore, to warrant experimental measurements to be made of compact and tube roughness.

(b) Temperature jump distance

As reported by MAIN (13) g" is a function of the thermal accommodation coefficient α_t, which itself depends on the molecular weight of the gas and solid surface, and on the mean free path L of the gas molecules. For any particular gas L is dependent upon the gas temperature and pressure, i.e.

$$L \propto \sqrt{T}/P \qquad \text{(from MAIN (13))}$$

where T is in $^{\circ}K$

and $$g'' \propto \frac{2 - \alpha_t}{\alpha_t} . L$$

MAIN has calculated g" (g''_{ref}) for helium assuming T = 500°C, P = 1 atmosphere and α_t = 0.4. This value of g" (4.4 μm) can be used to obtain g" for the HTR fuel interface gap.

As reported by MAIN Jeans suggested the following relation for α_t:

$$\alpha_t = 1 - \left(\frac{M - m}{M + m}\right)^2$$

where M and m are the gas and solid molecular weights respectively. For helium and graphite:

$$\alpha_t = 0.75$$

Also $\quad P \simeq 50$ atmospheres

and $\quad T \simeq 1000^{\circ}C$

and since $$g''/g''_{ref} = \frac{\frac{2-\alpha_t}{\alpha_t}\sqrt{T} \quad P_{ref}}{\left(\frac{2-\alpha_t}{\alpha_t}\right)_{ref} \quad P.\sqrt{T_{ref}}}$$

then $\quad g''/g''_{ref} = 0.01$

Therefore $g'' \simeq 0.04\ \mu m$

Although there is considerable uncertainty on α_t the high pressures in the HTR fuel gaps ensure small mean free paths and a negligible temperature jump distance.

1.2.2 Radiation across the gap

The radiative component of the gap conductance is given by the standard relation

$$h_r = \frac{\varepsilon_f \varepsilon_g \sigma_s}{\varepsilon_f + \varepsilon_g - \varepsilon_f \varepsilon_g} \frac{(T_F^4 - T_I^4)}{(T_F - T_I)} \qquad .....10$$

where T_F, T_I – interface temperatures in $^{\circ}K$

If we define the mean interface temperature as

$$\bar{T}_I = (T_F + T_I)/2$$

and $$\varepsilon_{eff} = \varepsilon_f \varepsilon_g / (\varepsilon_f + \varepsilon_g - \varepsilon_f \varepsilon_g)$$

then $$h_r = \varepsilon_{eff}\, \sigma_s .\, 2\, \bar{T}_I\, [4\, \bar{T}_I^{\,2} - 2\, T_F T_I\,]$$

For moderate gap temperature differences we can assume

$$T_F T_I \simeq \bar{T}_I^{\,2}$$

(e.g. for $T_F = 1150^{\circ}C$, $T_I = 1000^{\circ}C$, $\bar{T}_I = 1075^{\circ}C$, $\sqrt{T_F T_I} = 1073^{\circ}C$)

Therefore

$$h_r = 4\varepsilon_{eff}\, \sigma_s\, \bar{T}_I^{\,3} \qquad .....11$$

1.2.3 Effective gap conductance

The effective gap conductance, k_j, is given by a combination of the fluid conductance (h_G, Eq. 8) and the radiative conductance (h_r, Eq. 10) i.e.

$$k_j = \frac{k_G}{g_{eff}} + \varepsilon_{eff}\ \sigma_s\ (T_F+T_I)(T_F^2+T_I^2) \qquad .....12$$

The simplified form of the equation for h_r (Eq.11) will be used to demonstrate how k_j varies with gap width (g_{eff}). The values of ε_{eff} and the variation of k_G with temperature are given in Chapter 5. Fig 4/2 shows how k_j varies with g_{eff} for different mean temperatures ($\bar{T}_I$). From the log-log scale on which the curves are plotted, it is clear that thermal radiation contributes only 5% to the heat transfer process with gaps of less than approximately 50μ m. In addition, of course, the higher the mean interface temperature the more significant the radiation component for any particular gap size.

1.2.4 Effective interface conductance for nominally zero gap

When the compact and tube are in contact the interface conductance will depend upon the interface pressure. In this work, however, an effective maximum value of k_j - k_{jm} is assumed - which will apply regardless of how small the gap becomes below a value g_{min}. This approach is necessary if one wishes to use Eq. 12 to evaluate k_j, since, from Eq. 12:-

as $g_{eff} \rightarrow 0$, $k_j \rightarrow \infty$

The value of k_{jm} is derived from contact resistance experiments noted in Chapter 5, and has been taken to be 2×10^4 W/m^2 ^{o}C. The corresponding value of g_{min} can be seen from Fig 4/2 to be approximately 20 μm.

1.3 Conduction through the fuel sleeves

Again using the Fourier equation:

$$q'/2\pi r = -\ kg\ dT/dr \qquad \text{.....13}$$

Where q' is the linear heat rating across a sleeve given by Eq. 7 i.e.

$$q'_1 = q''_1\ 2\pi r_{f1}$$

$$q'_2 = q''_2\ 2\pi r_{f2}$$

It is assumed here that a negligible part of the total heat generation is from within the sleeves. This is supported by information given in Chapter 2. The assumption is also made that the thermal conductivity is uniform across the sleeve. Conductivity values used in the work are given in Chapter 5 and section 4 discusses the corrosion effect on sleeve conductivity. Integration of Eq. 13 for the two sleeves gives:

Inner sleeve:

$$T = T_{W1} + q''_1 \frac{r_{f1}}{kg} \ \ln r/r_{s1}$$

Outer sleeve: 14

$$T = T_{W2} + q''_2 \frac{r_{f2}}{kg} \ \ln r_{s2}/r$$

These temperature distributions are plotted in Fig 4/1 for the conditions given in Table 4/1. The interface temperatures T_{I1} and T_{I2} are given by:

$$\left.\begin{aligned} T_{I1} &= T_{W1} + \frac{q''_1\ r_{f1}}{kg}\ \ln r_{f1}/r_{s1} \\ T_{I2} &= T_{W2} + \frac{q''_2\ r_{f2}}{kg}\ \ln r_{s2}/r_{f2} \end{aligned}\right\} \qquad \text{.....15}$$

2 Heat transfer to the coolant and coolant pressure drop

In the previous section relations were derived providing temperatures within the fuel element which required the tube surface temperatures as boundary conditions.

In the case of the tubular element, the graphite surface heat fluxes are also dependent upon the heat transfer from the surfaces as well as on heat transfer within the element.

In this section this surface heat transfer is studied and convective heat transfer coefficients are defined in terms of the surface heat fluxes q''_s . q''_s can be derived from Eq. 7 i.e.

$$q''_{s1} = q''_1 \, r_{f1}/r_{s1}$$
$$q''_{s2} = q''_2 \, r_{f2}/r_{s2} \qquad \ldots\ldots 16$$

For the inner surface, the total of q''_s is removed by convection. From the outer surface, only a proportion of q''_s is removed by convection; the remaining fraction being the net thermal radiation to the channel wall (q''_{Rs2}). The heat flux from the channel wall q''_{s3}, therefore, is given by:

$$q''_{s3} = q''_{Rs2} \frac{r_{s2}}{r_{s3}} + q'_B/2\pi r_{s3} \qquad \ldots\ldots 17$$

where q'_B is the liner heat rating of the moderator block.

The three surface convective heat transfer coefficients are therefore defined:

$$h_{s1} = q''_{s1}/(T_{W1} - T_{g1})$$
$$h_{s2} = (q''_{s2} - q''_{Rs2})/T_{W2} - T_{g2}) \qquad \ldots\ldots 18$$
$$h_{s3} = q''_{s3}/(T_{W3} - T_{g2})$$

In order to determine the bore and annulus pressure drop it is also necessary to have expressions for friction factor f which is defined

(Fanning) as

$$f = \frac{De}{2\rho\bar{u}^2} \cdot \frac{dp}{dx} \qquad .....19$$

where dp/dx - channel pressure gradient (friction).

In the HTR design studies carried out by TNPG it is a requirement for particular sources of certain data, e.g. heat transfer and pressure drop data, to be used.

Those engaged on HTR thermal performance design are kept up to date on recommended heat transfer and friction factor correlations by the Heat Transfer Study Group of the collaborative Reactor Policy Committee. These correlations come, in fact, from experiments and literature survey work carried out by the UKAEA at the Windscale Laboratory under the directorship of Dr. D. Wilkie.

It is these Wilkie correlations which have been used for certain of the convective heat transfer and pressure drop calculations described in this thesis.

It was believed necessary, for this thesis, to justify fully the use of these correlations and to this end an original analytical derivation of heat transfer coefficients and friction factors, applicable to a helium coolant has been made, and then compared with the Wilkie correlations actually used.

2.1 Heat transfer and friction factors in smooth tubes

2.1.1 Dimensional analysis

The heat transfer coefficient can be assumed to be dependent upon the fluid velocity $\bar{u}$, density ρ, viscosity μ, specific heat Cp, thermal conductivity k_G and a linear dimension D which, for confined flows, would be the equivalent diameter De, i.e.

$$h = C.\, u^{\alpha}\, Cp^{\beta} \rho^{\gamma}\, \mu^{\varepsilon} k_G^{\varepsilon} De^{\psi}$$

These variables can be reduced into their basic units of mass, length, time and temperature. By comparing indices, four simultaneous equations containing the six unknown exponents can be obtained. Thus defining γ, δ, ε and ψ in terms of α and β we obtain

$$h = C\left(\frac{\bar{u}\rho}{\mu De}\right)^{\alpha}\left(\frac{\mu Cp}{k_G}\right)^{\beta}\frac{k_G}{De}$$

$$\therefore \quad \frac{hDe}{k_G} = C\left(\frac{\bar{u}\rho}{\mu De}\right)^{\alpha}\left(\frac{\mu Cp}{k_G}\right)^{\beta}$$

Thus the heat transfer coefficient can be defined in terms of a dimensionless group $\frac{hDe}{k_G}$ - the Nusselt number (Nu) as a function of the dimensionless groups $\left(\frac{\bar{u}\rho}{\mu De}\right)$ Reynolds number (Re) and $\left(\frac{\mu Cp}{k_G}\right)$ the Prandtl number (Pr) i.e.

$$Nu = C\,Re^{\alpha}\,Pr^{\beta} \qquad \text{.....20}$$

The Reynolds number clearly defines the hydrodynamic conditions (fluid velocity, degree of turbulence, geometry, etc.), whereas the Prandtl number appears to be merely a property of the fluid. Although the form given above is how heat transfer coefficients are normally expressed, in order to obtain some idea of C, α and β it is necessary to look further into the physical processes involved.

2.1.2 Velocity distribution in a tube

The velocity profile of developed turbulent flow in a tube can be divided conveniently into three regions where different physical laws are involved in the momentum transfer process (see Fig 4/3).

(i) Close to the wall - laminar sub-layer

Momentum exchange is by molecular interaction and there is little or no macroscopic movement across the stream of fluid particles. The velocity gradient in this region is high, the velocity at the wall being zero.

(ii) Centre region - turbulent core

Here momentum exchange is predominently achieved by the macroscopic movement of fluid across the stream. The velocity gradient in this region is comparatively low.

(iii) Transition region - buffer layer

This region lies between the above two and obviously there is a mixture of the two momentum exchange processes.

If a fully developed velocity profile is assumed, the velocity can be expected to depend only upon cross-stream distance (y), shear stress at the wall (τ_o), fluid kinematic viscosity (ν), and density (ρ) i.e.

$$u = f(y, \tau_o, \nu, \rho) \quad \text{where } y \ll r_o$$

applying dimensional analysis

$$\frac{u}{\sqrt{\tau_o/\rho}} = f\left(\frac{y\sqrt{\tau_o/\rho}}{\nu}\right) \quad .....21$$

$\sqrt{\tau_o/\rho}$ and $\sqrt{\tau_o/\rho}/\nu$ have dimensions of velocity and distance respectively and therefore we can write Eq. 21 in terms of dimensionless quantities u^*, y^*,

$$\text{where } u^* = \frac{u}{\sqrt{\tau_o/\rho}}$$

$$\text{and } y^* = \frac{y\sqrt{\tau_o/\rho}}{\nu}$$

$$\text{therefore } u^* = f(y^*)$$

implying a constant relationship between u^*, y^* for all cases.

We will now try to determine $f(y^*)$ for the three regions described above.

(a) Laminar sub-layer

In this very confined region close to a wall the shear stress can be defined simply as

$$\tau/\rho = \nu\frac{du}{dy} \quad .....22$$

$$\text{therefore} \int\frac{\tau}{\rho}\,dy = \int\nu\,du$$

assuming constant ρ , ν and assuming τ is constant at the wall value τ_o

$$\frac{\tau_o}{\rho} y = \nu u + c$$

$u = 0$ at $y = 0$ therefore $C = 0$

Introducing u^*, y^*

$$\underline{u^* = y^*} \qquad .....23$$

(b) Turbulent core

One would expect an apparent shear stress to be governed by a similar equation Eq. 22 in the turbulent core. Although in this case μ in Eq. 22 would be replaced by a more complicated expression.

To provide this expression the Prandtl Mixing Length theory will be employed giving a clear, if somewhat crude, explanation of the physical process of turbulence.

Consider a particle of fluid of mass δm moving in the x direction with velocity u. If now, due to turbulence, the particle moves in the y direction into a stream of velocity $u + \delta u$, the two streams being a distance L_m apart, a similar particle of fluid must pass from the $u + \delta u$ stream to the u stream in order for mass to be conserved. Thus there is a fluctuating velocity v' in the cross-stream direction.

If δm does not lose or gain momentum in moving distance L_m, then L_m is defined as the mixing length.

The net exchange of momentum is $\delta m \delta u$ which if occurring in a time δt the apparent shear force is given by

$$F = \frac{\delta m \delta u}{\delta t}$$

If A is the area over which the force acts, the apparent shear stress τ is

$$\tau = \frac{1}{A} \frac{\delta m \delta u}{\delta t} \qquad .....24$$

If L_m is small $\delta u = L_m$ (du/dy)

$$\frac{\delta m/\delta t}{A} = \bar{v}'\rho$$ where $\bar{v}'$ is a statistically averaged fluctuating velocity in the y direction.

Eq. 24 becomes, therefore,

$$\frac{\tau}{\rho} = (L_m \bar{v}') \frac{du}{dy} \qquad .....25$$

The similarity between equations 22 and 25 is obvious and $(L_m \bar{v}')$ is the turbulent exchange equivalent of the molecular exchange kinemetic viscosity and is termed the 'momentum eddy diffusivity' ε_m. Equations 22 and 25 now describe the exchange mechanism in the laminar sub-layer and the turbulent core.

In the buffer layer where both mechanisms play a part, the apparent shear stress will be given by

$$\frac{\tau}{\rho} = (\nu + \varepsilon_m) \frac{du}{dy} \qquad .....26$$

However, returning to the turbulent core Eq. 25, we can say:

$$\bar{v}' = \bar{u}' \times \text{CONST.}$$

and $\quad \bar{u}' = \text{CONST.} \times \delta u$

and, from above,

$$\delta u = L_m \frac{du}{dy}$$

Absorbing the constants in L_m we have, by substitution,

$$\frac{\tau}{\rho} = L_m^2 \left(\frac{du}{dy}\right)^2$$

In Prandtl's argument he also assumed the mixing length was proportional to y. Therefore $L_m = Ky$

and $\quad \frac{\tau}{\rho} = K^2 y^2 \left(\frac{du}{dy}\right)^2$

Away from the centre of the tube it is a fair approximation to say

$$\tau = \tau_o$$

the wall value, therefore, in terms of u* and y* the equation becomes

$$\frac{du^*}{dy^*} = \frac{1}{Ky^*}$$

Integrating

$$\underline{u^* = \frac{1}{K} \ln y^* + C} \qquad .....27$$

(c) Buffer layer

Returning to Eq. 26 it can now be implemented in deriving the velocity profile within the transition region.

Again we will use the mixing length theory in deriving an expression for ε_m i.e.

$$\varepsilon_m = K^2 y^2 \frac{du}{dy} \qquad .....28$$

Substituting in Eq. 27

$$\tau/_\rho = (\nu + K^2 y^2 \frac{du}{dy}) \frac{du}{dy} \qquad .....29$$

Once again we will assume $\tau = \tau_o$ and that K is constant within the region of interest.

Eq. 29 becomes, using u^* and y^*

$$du^*/_{dy^*} = (-1 + \sqrt{(1 + 4K^2 y^{*2})})/2K^2 y^{*2} \qquad .....30$$

This differential equation has been solved with the help of GREEN (15) and gives the following profile:

$$u^* = \frac{1}{2K^2 y^*} + \frac{1}{K}\left[\ln\left(2Ky^* + \sqrt{2Ky^* + 1}\right) - \frac{\sqrt{1 + 4K^2 y^{*2}}}{2Ky^*}\right] + C$$

Substituting $x^* = 2Ky^*$

$$u^* = \frac{1}{K}\left[\frac{1 - \sqrt{1 + x^{*2}}}{x^*} + \ln\left(x^* + \sqrt{1 + x^{*2}}\right)\right] + C \qquad .....31$$

This equation tends to Eq. 27 as $X^* \rightarrow \infty$. This would be expected because, as y^* increases, ε_m becomes dominant over ν.

As x^* tends to zero, $u^* \rightarrow C$ which implies that Eq. 31 does not apply very close to the wall.

(d) Velocity profile - Comparison with other work

The experimental work carried out by NIKURADSE (16) has had curves fitted to it for the three regions of the boundary layer by MARTINELLI (17).

From this experimental work the three regions can be defined approximately by:

Laminar sub-layer	$0 < y^* < 5$
Buffer layer	$5 < y^* < 30$
Turbulent core	$y^* > 30$

and the three equations are:

$$\left.\begin{array}{lll} 0 < y^* < 5 & u^* = y^* & \text{(Eq. 23)} \\ 5 < y^* < 30 & u^* = -3.05 + 5.00 \ln y^* & \\ y^* > 30 & u^* = 5.5 + 2.5 \ln y^* & \text{(Eq. 27)} \end{array}\right\} .32$$

These three profiles are shown in Fig 4/3.

Eq. 31 derived above is also plotted. With a K value of 0.15 this expression is in good agreement with the NIKURADSE/MARTINELLI data over the range $1 < y < 40$ and can therefore be regarded as an adequate description of a large proportion of the laminar sub-layer as well as the buffer layer.

Fig 4/4 shows the variation of velocity gradient (non-dimensional du^*/dy^*) with y^* derived from Eq. 30. As expected, the velocity gradient reduces with y^* the further one moves into the turbulent stream whereas $\frac{du^*}{dy^*}$ tends to the laminar value of 1 as the wall is approached.

The velocity gradient close to the wall given by Eq. 30 obviously has the correct form and also overcomes the problem of the discontinuity at $y^* = 5$. This equation has, therefore, an important advantage over the Martinelli representation in deriving the heat transfer properties of the system where it is the velocity gradient only that is used.

It can be seen from Fig 4/3 that above $y^* = 30$ i.e. in the turbulent core, that Eq. 31 ceases to apply with K = 0.15.

This is entirely due to the constant value of K that has been taken. K should, of course, be made a function of y. VAN DRIEST (<u>18</u>) suggests a $(1 - \exp(y^*/A^*))$ variation derived from a study of Stokes, oscillating plate experiments. Van Driest's relation simplifies, as does Eq. 31 to the form of the universal velocity profile at large y^*, namely Eq. 27.

For the purposes of deriving the heat transfer characteristics of turbulent flow in a smooth tube, we will accept one discontinuity for the sake of mathematical simplicity and use Eq. 31 for $0 \leq y^* \leq 30$ and Eq. 27 for $y^* > 30$ where K = 0.4 and C = 5.5.

2.1.3 Friction factor

As a major proportion of the flow is confined between the centre of the pipe and $y^* = 30$ it is possible to derive the bulk mean velocity using Eq. 27 and the expression

$$\bar{u} = \frac{2}{r_o^2} \int_o^r rudr$$

The shear stress at the wall can be put in terms of the friction factor f from

$$\tau_o = \frac{f \rho \bar{u}^2}{2}$$

also, introducing the Reynolds number $(\frac{2 \rho \bar{u} r_o}{\mu})$

Kármán - Nikuradse derived the following expression:

$$\frac{1}{\sqrt{4f}} = -0.8 + 0.87 \ln (Re \sqrt{4f})$$

(reported by KAYS (19))

where the constants - 0.8 and 0.87 have been adjusted to fit experimental data.

This equation can be simplified to

$$f = 0.046 \ Re^{-0.2} \qquad .....33$$

and is valid for $3 \times 10^4 < Re < 10^6$

The wholly experimental BLASIUS equation gives

$$f = 0.079 \ Re^{-0.25} \qquad .....34$$

which gives better agreement than Eq. 33 for the HTR channel bore according to WILKIE (20).

It is interesting to note from KAYS (19), that Eq. 34 can be reasonably approximated to the following relationship between u* and y*

$$u^* = 8.7\ (y^*)^{1/7} \qquad .....35$$

2.1.4 Temperature distribution and heat transfer coefficient

In the derivation of heat transfer coefficients in smooth tubes for developed turbulent flow, the similarity between momentum and heat turbulent exchange is often used.

As a starting point in this present analysis we will use the Kármán-Boelter-Martinelli analogy as described by KAYS (19).

The description of turbulent momentum transfer is by

$$\tau/\rho = (\varepsilon_m + \nu)\ du/dy \qquad .....36$$

By analogy, the turbulent heat transfer can also be defined by a modified Fourier law:

$$\frac{Q''}{\rho C_p} = (\varepsilon_H + \alpha_h)\frac{dT}{dy} \qquad .....37$$

where ε_H is eddy diffusivity of heat and is the turbulent equivalent of the laminar α_h (or $\dfrac{k_G}{\rho\, C_p}$).

For a cylindrical geometry, with just molecular heat diffusion in the radial direction we have

$$\frac{1}{r}\frac{\partial}{\partial r}\left(r\, k_G \frac{\partial T}{\partial r}\right) = u\rho\, C_p \frac{\partial T}{\partial x}$$

By analogy, we can replace k_G by the combined turbulent and molecular equivalent:

$$\rho\, Cp\ (\varepsilon_H + \alpha_h)$$

i.e.

$$\frac{1}{r}\frac{\partial}{\partial r}\left(\rho r Cp\ (\varepsilon_H + \alpha_h)\frac{\partial T}{\partial r}\right) = u\rho\, Cp \frac{\partial T}{\partial x} \qquad .....38$$

transforming, such that

$$y = r_o - r$$

$$dy = -dr$$

and assuming

$$\frac{\partial T}{\partial x} \simeq \frac{\partial Tg}{\partial x}$$

also

$$u = \bar{u}$$

$$T_W - T = \frac{Q''}{\rho C_p} \int_o^y \frac{1 - y/r_o}{(\varepsilon_H + \alpha_h)} \, dy \qquad .....39$$

where

$$Q'' = \frac{\rho}{2} r_o \bar{u} \, Cp \frac{dTg}{dx}$$

In order to solve Eq. 39 it remains to obtain a relationship between ε_H and y.

Again, by the similarity between momentum diffusion and heat diffusion we will assume

$$\varepsilon_H = \varepsilon_m$$

This is a good approximation for fluids of Prandtl number close to unity which is the case for gases.

From Eq. 36 and the fact that τ is linear with radius and also introducing the non-dimensional velocity gradient du*/dy* we obtain

$$\varepsilon_m/_\nu = \frac{1 - (y/r_o)}{du^*/dy^*} - 1$$

and therefore

$$\varepsilon_H/_\nu = \frac{1 - (y/r_o)}{du^*/dy^*} - 1 \qquad .....40$$

By using the expressions derived above for du*/dy* the temperature profile can be derived.

As already stated the channel can be divided into two regions: one close to the wall ($y^* < 30$) described by Eq. 31 and the turbulent core where the universal velocity profile is said to apply (Eq. 27).

(a) $y^* < 30$

Eq. 39 becomes

$$T_W - T_{30} = \frac{Q''}{\rho C_p} \int_0^{y^*=30} \frac{1 - y/r_o}{(\varepsilon_H + \alpha_h)} \, dy \qquad \text{.....41}$$

close to wall

$$y \ll r_o \qquad \therefore \; y/r_o \to 0$$

$$\therefore \; \frac{\varepsilon_H}{\nu} \to \frac{1}{du^*/dy^*} - 1 \qquad \text{.....42}$$

Introducing y^* we have

$$T_W - T_{30} = \frac{Q''}{\rho C_p} \frac{1}{\sqrt{\tau_o/\rho}} \int_0^{y^*=30} \frac{dy^*}{\varepsilon_H/\nu + \alpha_h/\nu} \qquad \text{.....43}$$

$$\alpha_h/\nu = 1/Pr \qquad \text{.....44}$$

and from Eq. 42 and Eq. 30 we have

$$\frac{\varepsilon_H}{\nu} = \frac{2K^2y^{*2}}{\sqrt{1+4K^2y^{*2}} - 1} - 1 \qquad \text{.....45}$$

Combining equations 45 and 44 in Eq. 43 we obtain

$$T_W - T_{30} = \frac{Q''}{\rho C_p \sqrt{\tau_o/\rho}} \int_0^{30} \frac{dy^*}{\frac{2K^2y^{*2}}{\sqrt{1+4K^2y^{*2}} - 1} + (\frac{1}{P_r} - 1)} \qquad \text{.....46}$$

Eq. 46 has been solved with the help of GREEN (<u>15</u>) to give

$$T_W - T_{30} = \frac{Q''}{K\rho C_p} \frac{1}{\sqrt{\tau_o/\rho}} \Bigg|_0^{30} \ln(2Ky^* + \sqrt{4K^2y^{*2} + 1}) - \frac{a^*}{b^*}\left[\frac{2Ky^* + \sqrt{4K^2y^{*2}+1} + a^* - b^*}{2Ky^* + \sqrt{4K^2y^{*2}+1} + a^* + b^*}\right]$$

where

$$a^* = \frac{2}{P_r} - 1 \quad ; \quad b^* = 2\sqrt{(\frac{1}{P_r} - 1)^2 + (\frac{1}{P_r} - 1)}$$

$$\text{Let } Z^*_{30} = 2K.30 + \sqrt{4K^2 30^2 + 1}$$

Therefore

$$T_W - T_{30} = \frac{Q''}{K\rho C_p} \frac{1}{\sqrt{\tau_o/\rho}} \left\{ \ln Z^*_{30} - \frac{a^*}{b^*} \ln \left[\frac{(Z^*_{30} + a^* - b^*)(1 + a^* + b^*)}{(Z^*_{30} + a^* + b^*)(1 + a^* - b^*)}\right]\right\} \qquad \text{.....47}$$

(b) $y^* > 30$

The velocity gradient for the turbulent core is given by

$$\frac{du^*}{dy^*} = \frac{1}{K_T y^*} \qquad (K_T \text{ refers to the turbulent core})$$

Substituting in Eq. 40 we obtain

$$\frac{\varepsilon_H}{\nu} = (1 - y/r_o)\, K_T y^* - 1$$

Substituting into Eq. 39

$$T_{30} - T_C = \frac{Q''}{\rho C_p \sqrt{\tau_o/\rho}} \int_{30}^{y=r_o} \frac{(1 - y/r_o)}{(1 - y/r_o) K_T y^* - 1 + \frac{1}{Pr}}\, dy^*$$

For the turbulent core $\varepsilon_H/\nu >> 1$

and for gases where the Prandtl number is close to unity

$$(1 - y/r_o)\, K_T y^* - 1 + \frac{1}{P_r} \simeq (1 - y/r_o)\, K_T y^*$$

(The approximation made by KAYS (19))

Thus we obtain

$$T_{30} - T_C = \frac{Q''}{\rho C_p \sqrt{\tau_o/\rho}} \int_{30}^{y_c^*} \frac{dy^*}{K_T y^*}$$

Thus

$$T_{30} - T_C = \frac{Q''}{K_T\, \rho C_p} \sqrt{\frac{\rho}{\tau_o}}\; \ln \frac{y_c^*}{30} \qquad \text{.....48}$$

Combining equations 47 and 48 we have

$$T_W - T_C = \frac{Q''}{\rho C_p} \sqrt{\frac{\rho}{\tau_o}} \left\{ \frac{1}{K_T} \ln \frac{r_o}{30\nu} \sqrt{\frac{\tau_o}{\rho}} + \frac{1}{K} \left[\ln Z_{30}^* - \frac{a^*}{b^*} \ln \left[\frac{(Z_{30}^* + a^* - b^*)(1 + a^* + b^*)}{(Z_{30}^* + a^* + b^*)(1 + a^* - b^*)} \right] \right] \right\} \qquad \text{..49}$$

Introducing the friction factor which is defined as

$$f = \frac{2}{\bar{u}^2} \frac{\tau_o}{\rho}$$

also the Reynolds number is defined as

$$Re = \frac{2\bar{u}\, r_o}{\nu} \qquad \therefore \sqrt{\frac{\tau_o}{\rho}} = \sqrt{\frac{f}{2}} \left(\frac{\nu Re}{2r_o}\right)$$

Eq. 49 becomes

$$T_W-T_C = \frac{Q''}{\bar{u}\rho C_p\sqrt{f/2}} \left\{\frac{1}{K_T} \ln \frac{(Re\sqrt{f/2})}{60} + \frac{1}{K}\left[\ln Z^*_{30} - \frac{a^*}{b^*} \ln \left[\frac{(Z^*_{30}+a^*-b^*)(1+a^*+b^*)}{(Z^*_{30}+a^*+b^*)(1+a^*-b^*)}\right]\right]\right\} \quad ..50$$

In order to define a heat transfer coefficient in terms of the bulk mean fluid temperature we must obtain a relationship between T_C and T_g

Following KAYS (19) we use the 1/7 power law given by Eq. 35 and assume a similar variation over the bulk of the fluid for temperature.

Thus

$$\frac{T - T_W}{T_C - T_W} = (y/r_o)^{1/7}$$

hence

$$\frac{T_g-T_W}{T_C-T_W} = 0.833 \quad .....51$$

The Stanton number is given by

$$St. = \frac{h}{\bar{u}\rho C_p} \quad .....52$$

and

$$h = \frac{Q''}{T_W-T_g} \quad .....53$$

Using equations 51, 52, 53 and the relation

$$Nu = St.Re.Pr$$

Eq. 50 becomes

$$N_u = \frac{Re\ Pr\sqrt{f/2}}{0.833\left\{\frac{1}{K_T} \ln(\frac{Re\sqrt{f/2}}{60}) + \frac{1}{K}\left[\ln Z^*_{30} - \frac{a^*}{b^*} \ln \left[\frac{(Z^*_{30}+a^*-b^*)(1+a^*+b^*)}{(Z^*_{30}+a^*+b^*)(1+a^*-b^*)}\right]\right]\right\}} \quad .....54$$

Using Eq. 34 to provide an expression for the friction factor (which, of course, is dependent chiefly on the turbulent core velocity profile) we can obtain an expression for the Nusselt number as a function of the Reynolds number. Fig 4/5 shows this variation for Pr = 0.7, a typical value for helium under HTR conditions. The Reynold number range has been chosen to cover the variation between channels in an HTR at full power.

2.1.5 Comparison of derived Nusselt number correlation with other data

Shown in Fig 4/5 is that data derived from KAYS (21) which is a theoretical approach including a more refined eddy diffusivity relationship close to the wall (Diessler) and the 'Jenkins' momentum/thermal diffusivity ratio. The resulting equations have been solved numerically on a digital computer. They can be seen to agree very well with the present analysis over this Reynolds number range, the maximum error being 5% at a Reynolds number of 3×10^4.

Also shown in Fig 4/5 is that data recommended by WILKIE (20) with the term allowing for the temperature dependence of coolant properties ignored, since that is the assumption made in this analysis. The 'simplified' WILKIE recommendation is

$$Nu = 0.023 \, Re^{0.8} \, Pr^{0.4} \qquad .....55$$

This is essentially the Dittus - Boelter equation and can be shown in Fig 4/5 to give reasonably good agreement with Eq. 54, the maximum difference being about 11% at a Reynolds number of 3×10^5.

It is believed that this justifies fully the use of the basic WILKIE correlation for developed turbulent flow in the smooth bore of the HTR fuel channel.

It now remains to discuss the necessary modifications to Eq. 55 to allow for temperature dependent properties and to justify (not so rigorously) the correlation used for heat transfer calculations in a smooth HTR channel annulus.

2.1.6 Temperature dependence of coolant properties correction

In the previous analysis it has been assumed that the fluid properties are invariant with temperature. In fact, for helium, the density varies inversely with temperature and viscosity and thermal conductivity to approximately a 0.8 power law (Chapter 5). Specific heat and Prandtl number are essentially constant.

The normal way of allowing for this effect is to evaluate the properties at the axially local bulk mean coolant temperature and apply a correction to the Nusselt number and friction factor calculated from, say, equations 34 and 55.

This correction takes the form of $\left(\frac{T_W(^oK)}{T_g(^oK)}\right)^M$ where M is evaluated from experiments.

There is considerable uncertainty associated with the value of M as it depends upon the temperature range, the value of T_W/T_g and the properties of the particular gas.

BARNES (22) has investigated the effect on Nusselt number for helium and proposes M = -0.185. Whereas Deissler, reported by KAYS (19) suggests M = -0.34. In this work a value of M = -0.15 is taken, as this is the value recommended by WILKIE (20).

It is interesting to note that with a value of -0.34 for M as opposed to -0.15 and with the maximum surface-to-bulk ratio encountered in the HTR channel (1.5) this reduces the Nusselt number by 8%, giving some indication of the uncertainty in heat transfer coefficient arising from possible errors in this correction factor.

The effect is much less significant on friction factor and WILKIE (20) suggests M = -0.05.

2.1.7 Thermal entry effects

The assumption of a fully developed turbulent boundary layer does not apply just after entry to the bore or annulus where the thermal boundary layer, at least, is still developing. The Nusselt number in this region is, in general, higher than the developed value, and KAYS (19) suggests that for a tube it would take approximately 30 equivalent diameters before the Nusselt number is within 1% of the developed value, which for the HTR fuel channel bore is 1m (one brick length). For the annulus, development can be expected to be much sooner. As, in general, it is peak temperatures which govern thermal performance, one can feel justified in neglecting these entry effects and for the purposes of this thesis fully developed conditions are assumed throughout.

The velocity and temperature profiles are once again disturbed at discontinuities in the channel and once again these effects will be ignored.

2.2 Annulus heat transfer and pressure drop

The presence of two walls, at first sight, would seem to complicate significantly the derivation of the velocity and temperature profiles and consequently the friction factors and heat transfer coefficients in the annulus. However, a number of simple observations can be made. If r_1, r_2 are the inner and outer radii respectively of an annulus:

(i) there is a position of zero velocity gradient at some radial position between the two walls - radius of no-shear (r_s) - which generally coincides with the position of maximum velocity. (This only applies for high values of radius ratio $\bar{r}$ ($^{r_1}/r_2$) according to LAWN (23)).

(ii) it is possible to find the radius of no-shear by assuming dp/dz is constant with r and also that the mean velocity within this radius is equal to that outside it

(iii) by considering the flow area inside and outside the radius of no-shear separately (i.e. reducing to one relevant surface) data already derived for tubes can be applied to an annulus. (This 'transformation' was first proposed by HALL (24), who developed the method so that data for passages with different geometries, friction and heat transfer characteristics could be compared.)

2.2.1 Friction factor

The pressure gradient, assumed uniform across the channel, can be defined in the inner and outer flow regions by

$$\frac{dp}{dz} = \frac{2f_1}{De_1} \rho \bar{u}_1^2 = \frac{2f_2}{De_2} \rho \bar{u}_2^2$$

where f_1, $\bar{u}_1$, De_1 and f_2, $\bar{u}_2$, De_2 refer to the inner and outer regions, respectively. With common peak velocities and with smooth surfaces it is reasonable to assume

$$\bar{u}_1 = \bar{u}_2$$

therefore $f_1/f_2 = De_1/De_2$ 56

If we now assume

$$f_1 = 0.079\ Re_1^{-0.25}$$

$$f_2 = 0.079\ Re_2^{-0.25} \qquad \text{(Eq. 34)}$$

$$f_1/f_2 = \left(\frac{de_1}{de_2}\right)^{-0.25} \qquad .....56(a)$$

Therefore, for equations 56(a) and 56 to hold simultaneously

$$de_1 = de_2$$

Defining the hydraulic diameter as (4xflow area)/wetted perimeter then

$$De_1 = 2(r_s^2 - r_1^2)/r_1$$

$$De_2 = 2(r_2^2 - r_s^2)/r_2$$

$$\therefore\ r_s^2 = \frac{r_1 De_1}{2} + r_1^2 \qquad .....57$$

Since $De_1 = De_2$

$$De_1 = 2(r_2 - r_1)$$

which is equal to the hydraulic diameter of the whole channel as would be expected.

Substituting for De_1 into Eq. 57 we have

$$r_s^2 = r_1 r_2$$

and if $\bar{r}_s = r_s / r_2$

$$\bar{r}_s = \sqrt{\bar{r}} \qquad .....58$$

KAYS (21) quotes an experimentally derived relationship between the radius of no-shear and the radius ratio. The equation is:

$$\bar{r}_s = \frac{\bar{r}^{0.343} + \bar{r}}{1 + \bar{r}^{0.343}} \qquad .....59$$

This is plotted in Fig 4/6 together with Eq. 58. As can be seen they are virtually identical at high radius ratios. (Difference at $\bar{r} = 0.9$ is less than 0.1%.)

From the above analysis it is clear that the tube friction factor correlation should apply equally to the annulus for high radius ratios.

The experimental results given by LAWN (23) certainly shows that as the radius ratio approaches unity the tube friction factor correlation is also approached. From the limited number of results quoted in this reference, however, the conclusion drawn is that even for parallel plates ($\bar{r} = 1$), the friction factor is 5% above that of the tube. This would indicate limitations in the hydraulic diameter concept used in Hall's method.

The correlation recommended by WILKIE (20) for the HTR fuel channel ($\bar{r} = 0.866$) annulus gives a value of friction factor 10% above the tube value, i.e.

$$f = 0.087\ Re^{-0.25} \qquad .....60$$

2.2.2 Heat transfer coefficient

The heat transfer coefficient for both surfaces of a smooth annulus can also be expected to be similar to the tube value providing the position of peak temperature in the fluid coincides with the position of no-shear and the bulk mean gas temperature within the radius of no shear is equal to that outside it. This condition can be met if the heat fluxes from the two surfaces are equal.

In the HTR annulus, however, there is a much higher heat flux from the inner surface than from the outer, and clearly the heat transfer correlation for the two surfaces should include a heat flux ratio function (ψ).

WILKIE (20) suggests for the two surfaces:

$$\psi = 1/1+0.25(1-q''_o/q''_i) \qquad \text{for the inner surface}$$

$$\psi = 1/1+0.125(1-q''_i/q''_o) \qquad \text{for the outer surface}$$

As expected, if $q''_i = q''_o$, ψ becomes unity and the tube value is obtained.

The work by KAYS (21) is again used to give a comparison with the WILKIE correlation.

The results quoted by KAYS are for two cases:

(i) inner tube heated only

(ii) outer tube heated only.

A range of radius ratio values were considered. Fig 4/7 shows Nusselt number versus $\bar{r}$ for Reynold numbers of 10^4, 10^5 and 10^6 for Pr = 0.7. The interpolated Nusselt numbers for $\bar{r}$ = 0.866 are plotted against Reynold number in Fig 4/8.

The WILKIE correlation for HTR annulus inner surface is:

$$Nu = \frac{0.023\ Re^{0.8} Pr^{0.4}}{1+0.25(1-q''_o/q''_i)} \left(\frac{T_W}{T_B}\right)^{-0.15} \qquad .....61$$

For the HTR annulus $q''_o \ll q''_i$ and for the purposes of comparison we assume $q''_o/q''_i = 0$ and compare with (i) above.

In addition, the T_W/T_g term is ignored since KAYS assumes constant fluid properties.

Eq. 61 becomes:

$$Nu = 0.0184\ Re^{0.8}\quad Pr^{0.4} \qquad .....62$$

For Pr = 0.7 Eq. 62 is plotted in Fig 4/8. There is good agreement with KAYS over this Reynolds number range, the error being generally less than 5%.

2.2.3 Annulus hydraulic diameter

The equivalent diameter for the annulus is calculated from the basic relationship

$$De = \frac{4 \text{ x flow area}}{\text{wetted perimeter}}$$

The calculation of the flow area and wetted perimeter must make full allowance for the presence of the ribs i.e.

$$\text{flow area} = \pi\,(r_o^{\,2} - r_i^{\,2}) - Ndl$$

Since $l \approx r_o - r_i$ the wetted perimeter on the rib end is neglected as well as the adjacent perimeter in the channel wall, as recommended by WILKIE (20)

$$\text{Wetted perimeter} = 2\pi\,(r_o + r_i) + 2Nl - 2Nd$$

$$De = \frac{2\left[\pi\,(r_o^{\,2} - r_i^{\,2}) - Ndl\right]}{\pi(r_o + r_i) + N(l-d)} \qquad .....63$$

2.3 Summary of convective heat transfer and pressure drop in a HTR fuel channel

2.3.1 Convective heat transfer

The standard correlations used in the bulk of the work described in the thesis are based on three major assumptions:

(i) fully developed turbulent flow

(ii) azimuthal symmetry

(iii) smooth channels.

(The effects of roughness will be discussed in section 4.)

The correlations (WILKIE (20)) used are as follows:

Channel bore:

$$Nu = 0.023\, Re^{0.8}\, Pr^{0.4}\ (T_{W1}/T_{g1})^{-0.15} \qquad .....64$$

Annulus inner surface:

$$Nu = \frac{0.023\, Re^{0.8}\, Pr^{0.4}}{1 + 0.25(1-q''_o/q''_i)}\ (T_{W2}/T_{g2})^{-0.15} \qquad .....65$$

Annulus outer surface:

$$Nu = \frac{0.023\, Re^{0.8}\, Pr^{0.4}}{1+0.125\ (1-q''_i/q''_o)}\ (T_{W3}/T_{g2})^{-0.15} \qquad .....66$$

2.3.2 Pressure drop

The Guggenheim equation is the basic relation giving the axial pressure distribution within a channel. The equation, derived from force balance and mass conservation considerations is:

$$\Delta P = \frac{\rho}{2}\bar{u}^2\left[\frac{4f\,\Delta z}{De} + \frac{2\Delta T}{Tg} + \frac{2\Delta P}{\bar{P}} + K_D\right] \qquad .....67$$

Buoyancy effects are small compared with the other terms.

ΔP is the pressure drop over axial element Δz

ΔT is the temperature rise over axial element Δz

Tg is the mean gas temperature in axial element Δz

$\bar{P}$ is the mean pressure in axial element Δz

K_D is the pressure loss due to discontinuities (e.g. brick joints).

This equation can be further simplified by noting that for the HTR under operating pressure $\Delta P \ll \bar{P}$ $\therefore$ $\frac{2\,\Delta P}{\bar{P}} \simeq 0$

The friction factors used (WILKIE (20)) are given by:

Bore:

$$f = 0.079\, Re^{-0.25}\ (T_{W1}/T_{g1})^{-0.05} \qquad .....68$$

Annulus:

$$f = 0.087\, Re^{-0.25}\ (T_{W2}/T_{g2})^{-0.05} \qquad .....69$$

2.4 Radiative heat transfer in the HTR channel annulus

If one assumes the annulus to be represented by two infinitely long concentric cylinders, both being 'grey bodies' i.e. they emit and absorb all wavelengths to the same degree, then the net heat flux emitted by the inner surface is given by (JACOB (25)):

$$q''_{Rs2} = \frac{\sigma_s \left(T^4_{W2} - T^4_{W3}\right)}{\frac{1}{\varepsilon_1} + \frac{r_{s2}}{r_{s3}}\left(\frac{1}{\varepsilon_2} - 1\right)} \qquad \ldots\ldots.70$$

where ε_1 and ε_2 are the emmissivities of the inner and outer surfaces respectively and σ_s is Stefans constant $(5.67 \times 10^{-8} W/m^{2o}C)$.

The radiative heat flux removed by convection from the channel wall is given by:

$$q''_{RW} = q''_{Rs2} \frac{r_{s2}}{r_{s3}} \qquad \ldots\ldots71$$

The small effect of the ribs has been neglected.

3 Thermal and irradiation induced dimensional change

3.1 Description of the phenomena

The fuel pin, as described in Chapter 2, consists of a number of compacts placed one on top of another, between a pair of nominally concentric graphite tubes. From the point-of-view of heat transfer, it would be desirable to have zero clearance between the compacts and the sleeves. However, the manufacturing tolerances on the dimensions of the pin components immediately introduce interface gaps which, from a thermal resistance standpoint, are highly significant. These gaps, of about 100 μm and filled with helium under stagnant conditions, present a resistance to heat transfer of the same order as the convective heat transfer resistance at the pin surface. Thus any change in the size of the gaps, although dimensionally small, needs to be predicted with some accuracy.

The precise size of the gaps before the fuel enters the reactor is immediately subject to uncertainty. By matching compact size with tube size it is believed possible to reduce the radial gap to between zero and 80 μm for a concentric system. With a fully eccentric compact the maximum gap is 160 μm.

For the purposes of the analysis below a concentric system will be assumed.

As soon as the fuel is loaded into the core the temperatures of compact and tube are increased, perhaps by 1200°C and 1000°C respectively. This difference in temperature rise - combined with the inherently large difference in thermal expansion coefficient CTE - produces, by differential thermal expansion, large changes in the gap sizes. The net effect produces an increase in the radial outer gap of about 100 μm and a similar decrease for the inner gap - there being only small strains in the fuel and large strains in the tubes.

As the irradiation proceeds, the effect of fast neutron damage produces significant changes in the CTE (Chapter 5). These changes, together with any temperature variation, again modify the interface gaps.

Fast neutron dislocation of atoms from the crystal lattice of the compact and sleeves also produces large dimensional changes which are negative until high fast neutron doses are reached (> 3×10^{21} n/cm^2 EDN). The graphite crystal structure consists of hexagonal arrays of carbon atoms lying in planes; of separation 3.35 A$^{\circ}$. The energy required to displace one carbon atom is 25 ev . Under elastic bombardment of neutrons in excess of this energy atoms are displaced from the arrays and, subsequently, are trapped in defects, crystallite edges or return to a vacancy. After some dose, lines of vacancies are formed which collapse producing the 'shrinkage' effect. When high doses are reached, porosity within the crystal becomes 'filled' and 'growth' occurs.

With the graphite form encountered in the compact these so-called 'Wigner' strains are highly significant, and can attain well over 0.5 mm radially, if unrestrained. Wigner shrinkage is highly temperature dependent (Chapter 5) and the radial temperature distribution through the fuel element produces not only thermal stresses, but stresses arising from the shrinkage effect. These stresses are relieved slightly by the third important phenomenon - creep.

So far we have assumed that the compact and tube are free to expand or shrink at will. This certainly applies in the non-interacting, or hollow-rod, designs of element (see Chapter 2). In the former, the interface gap between inner tube and compact is made sufficiently large to ensure there is no interaction. In the latter, there is no inner tube. (On present data it is not thought possible for the compact and outer tube to interact with the foreseeable fast neutron doses.) As mentioned above, this condition produces larger outer gaps and consequently worse heat transfer characteristics (see section 1 of this chapter.)

With the interacting 'tubular' design, the compact and inner tube are allowed to interfere and a nominal inner gap is chosen to give a satisfactory compromise between high stresses and low heat transfer. Interaction is not allowed to occur at the start of a fuel dwell as creep will have no time to relieve the high stresses produced. Thus a nominal radial gap is chosen (say, 150 μm) which ensures that interaction occurs only after some irradiation period.

The axial variation of interface gap is as highly significant as the time variation and arises from the axial distributions of temperature and fast neutron dose (see Chapters 3 and 5). The axial variation of interface gap is more important in the tubular design. This is because the temperatures at an axial position are affected by the upstream partition of heat between inner and outer coolant passages. This partition is greatly affected by the upstream interface gaps. Therefore, in order to assess the endurance of the fuel and graphite at a point in the channel, an accurate estimate of the axial and time variation of the interface gaps is essential.

The first attempts to allow for these effects were made by the Author (<u>26</u>, <u>27</u>); the final method, described below, is included in the AZIMUSTAP program and used these references as a starting point. This final version of AZIMUSTAP, AZIMUSTAP 5, has been used to provide the predictions of interface gap development described in sub-section 3.4.

3.2 <u>Basic theory</u>

3.2.1 <u>Unirradiated conditions - thermal expansions</u>

Consider an axial section of the fuel pin Δz. For any hollow cylinder of inner/outer radii r_1/r_2 with no end restraints and with a temperature distribution being a function of radius r only, the three stresses a point given in cylindrical co-ordinates (Pr, Pθ and Pz) are given by TIMOSHENKO (28):

$$
\left.
\begin{aligned}
Pr &= \frac{Y\alpha}{(1-\sigma)r^2}\left[\frac{r^2 - r_1^2}{r_2^2 - r_1^2}\int_{r_1}^{r_2} rT^*\,dr - \int_{r_1}^{r} rT^*\,dr\right] \\
P\theta &= \frac{Y\alpha}{(1-\sigma)r^2}\left[\frac{r^2 + r_1^2}{r_2^2 - r_1^2}\int_{r_1}^{r_2} rT^*\,dr + \int_{r_1}^{r} rT^*\,dr - r^2T^*\right] \\
Pz &= \frac{Y\alpha}{(1-\sigma)r^2}\left[\frac{2}{r_2^2 - r_1^2}\int_{r_1}^{r_2} rT^*\,dr - T^*\right]
\end{aligned}
\right\} \quad \ldots\ldots 72
$$

and Hooke's law gives:

$$Y\left(\frac{u}{r} - \alpha T^*\right) = P\theta - \sigma\,(Pr + Px) \quad \ldots\ldots 73$$

Young's modulus, Y. is assumed constant with radius.

These equations can be closely applied to the compact which is unrestrained. They apply less accurately to the tubes which are connected at one end.

For the fuel inner radius displacements, $r_1 = r_{f1}$, $r_2 = r_{f2}$, $r = r_{f1}$

Substituting for the radii in equations 72 and 73 we have

$$Pr = 0$$

$$
\left.
\begin{aligned}
P_\theta &= \frac{Y\alpha_f}{(1-\sigma)r_{f1}^2}\left[\frac{2r_{f1}^2}{r_{f2}^2 - r_{f1}^2}\int_{r_{f1}}^{r_{f2}} rT^*dr - r_{f1}^2\,T^*\right] \\
Pz &= \frac{Y\alpha_f}{(1-\sigma)}\left[\frac{2}{r_{f2}^2 - r_{f1}^2}\int_{r_{f1}}^{r_{f2}} rT^*\,dr - T^*\right]
\end{aligned}
\right\} \quad \ldots\ldots 74
$$

Substituting Eq. 74 in Eq. 73 we derive the expression for the fuel displacement given as:

$$u_{f1} = \frac{2\alpha_f\, r_{f1}}{r_{f2}^2 - r_{f1}^2}\int_{r_{f1}}^{r_{f2}} rT^*\,dr \quad \ldots\ldots 75$$

Similar expressions can be obtained for the other surfaces

$$u_{f2} = \frac{2\alpha_f r_{f2}}{r_{f2}^2 - r_{f1}^2} \int_{r_{f1}}^{r_{f2}} rT^* \, dr \qquad .....76$$

$$u'_{s1} = \frac{2\alpha_g r'_{s1}}{r'^2_{s1} - r^2_{s1}} \int_{r_{s1}}^{r'_{s1}} rT^* \, dr \qquad .....77$$

$$u'_{s2} = \frac{2\alpha_g r'_{s2}}{r^2_{s2} - r'^2_{s2}} \int_{r'_{s2}}^{r_{s2}} rT^* \, dr \qquad ......78$$

Now $T^* = T - T_o$ where T_o is room temperature ($\sim 20^{o}C$)

therefore $\frac{2}{r_2^2 - r_1^2} \int_{r_1}^{r_2} rT^* \, dr$ becomes

$$\frac{2}{r_2^2 - r_1^2} \int_{r_1}^{r_2} rT \, dr - \frac{2}{r_2^2 - r_1^2} \int_{r_1}^{r_2} rT_o dr$$

and $\frac{2}{r_2^2 - r_1^2} \int_{r_1}^{r_2} rTdr - T_o$

Now $\frac{2}{r_2^2 - r_1^2} \int_{r_1}^{r_2} rTdr$ is the volumetric mean temperature $\bar{T}$ and

equations 75 - 78 can be rewritten:

$$U_{f1} = \alpha_f r_{f1} [\bar{T}_f - T_o] \qquad .....79$$

$$U_{f2} = \alpha_f r_{f2} [\bar{T}_f - T_o] \qquad .....80$$

$$U_{s2} = \alpha_g r'_{s2} [\bar{T}_{s1} - T_o] \qquad .....81$$

$$U_{s1} = \alpha_g \, r'_{s1} \, [\bar{T}_{s2} - T_o] \qquad .....82$$

These displacements can be combined to give the net change in the inner and outer interface gaps. Also, if $g_1(o) << r_{f1}$ and $g_2(o) << r_{f2}$

$r'_{s1} \simeq r_{f1}$ and $r'_{s2} \simeq r_{f2}$

Thus

$$g_1(o) = g_{c1} + r_{f1} \, [\alpha_f \, (\bar{T}_f - T_o) - \alpha_g \, (\bar{T}_s - T_o)] \qquad .....83$$

$$g_2(o) = g_{c2} + r_{f2} \, [\alpha_g \, (\bar{T}'_s - T_o) - \alpha_f \, (\bar{T}_f - T_o)] \qquad .....84$$

The CTE, α, has been assumed constant. In fact both α_f and α_g vary with temperature, as can be seen in Chapter 5.

The temperature difference across the graphite sleeves can be as large as 100°C and the constant CTE assumption could produce significant errors in the thermal gap. Correctly, α should be included in the integral term of Eq.72, and a function of temperature substituted; whereas a more convenient method would be to use a value of α evaluated at $\bar{T}_{s1}$ or $\bar{T}_{s2}$. Appendix IV shows that, assuming α is a linear function of graphite temperature, which in turn is a linear function of radius r, the differences in approach lead to errors in the strain of less than 0.02%. Similar errors in fuel strain can be expected but, as these strains are very much less significant than the graphite displacements, the thermal gap is less affected.

Arising from this error study, therefore, good accuracy can be expected for the thermal gaps if α_f and α_g given in equations 83 and 84 are evaluated at $\bar{T}_f$, $\bar{T}_{s1}$ and $\bar{T}_{s2}$.

3.2.2 Conditions under irradiation

(a) Thermal strain

If $\bar{T}_f(d)$, $\bar{T}_{s1}(d)$ and $\bar{T}_{s2}(d)$ are the mean fuel and graphite temperatures which exist after a dose d, then the CTE values are given by $\alpha_f(d, \bar{T}_f(d))$,

$\alpha_g(d,\overline{T}_{s1}(d))$ and $\alpha_g(d,\overline{T}_{s2}(d))$ and the expressions for the thermal gaps at dose d are:

$$g_{1t}(d) = g_{c1} + r_{f1}[\alpha_f(d,\overline{T}_f(d))(\overline{T}_f(d) - T_o) - \alpha_g(d,\overline{T}_{s1}(d))(\overline{T}_{s1}(d)-T_o)] \quad ..85$$

$$g_{2t}(d) = g_{c2} + r_{f2}[\alpha_g(d,\overline{T}_{s2}(d))(\overline{T}_{s2}(d)-T_o)- \alpha_f(d,\overline{T}_f(d))(\overline{T}_f(d)-T_o)] \quad ..86$$

where $g_{1t}(d)$ and $g_{2t}(d)$ are the interface gaps at dose d due to thermal strains only.

(b) Wigner shrinkage

After a dose, d, it is assumed that there is a small additional dose Δd. If at d the rate of change of Wigner strain with dose is $\S(d)$ the strain at $d + \Delta d$ is $\S(d)\Delta d$. Now consider Eq. 75 written in a general form

$$Sr_1 = \frac{2}{r_2^2-r_1^2}\int_{r_1}^{r_2} r\,Sr\,dr$$

where Sr_1 is the strain at radius r_1 and Sr, is the strain at radius r.

This equation is valid regardless of the origin of the strain Sr if it obeys the same elastic laws. Therefore, assuming Wigner shrinkage can be treated in this way, Sr can be replaced by $\S(d)\Delta d$ i.e.

$$\Delta Wr_1(d) = \frac{2}{r_2^2-r_1^2}\int_{r_1}^{r_2} r\,\S(d)\,\Delta d\,dr \quad .....87$$

$\Delta Wr_1(d)$ is the increment of Wigner strain after a dose Δd at dose d at radius r_1.

For both the fuel and graphite it is a good approximation to assume that dose is independent of radius. However, as can be seen from Ref. (43) $\S(d)$ is dependent on temperature which is, of course, a function of radius. Fig 4/9 shows the variation of $\S(d)$ with temperature for the fuel and graphite where $d = 2.0 \times 10^{20} n/cm^2$ EDN. It can be seen that for the expected temperature variations (less than $100^\circ C$) linearity, is a reasonable approximation i.e.

$$\S\,(d) = M(d)T + N(d)$$

Thus, substituting in Eq. 87 we have:

$$\Delta Wr_1(d) = \frac{2\Delta d}{r_2^2 - r_1^2} \int_{r_1}^{r_2} r\,(M(d)T + N(d))\,dr$$

$$= \Delta d \left[\frac{2\,M(d) \int_{r_1}^{r_2} rTdr}{r_2^2 - r_1^2} + N(d) \right]$$

and $\quad \Delta Wr_1(d) = \Delta d(M(d)\overline{T} + N(d))$

$\therefore \quad \Delta Wr_1(d) = \Delta d\,\S\,(d,\overline{T})$ 88

Therefore, as with CTE, shrinkage is evaluated at mean fuel or graphite temperature conditions.

The Wigner shrinkage gaps can be written as follows

$$g_{1W}(d + \Delta d) = g_{1W}(d) + r_{f1}[\S_f(d, \overline{T}_f) - \S_g(d, \overline{T}_{g1})]\Delta d \quad .....89$$

$$g_{2W}(d + \Delta d) = g_{2W}(d) + r_{f2}[\S_g(d, \overline{T}_{g2}) - \S_f(d, \overline{T}_f)]\Delta d \quad .....90$$

Although in equations 89 and 90 no distinction is made between the doses in the three annuli, in principle there is no reason why different doses can not be assumed.

If Δd ceases to become small compared with d, it then becomes necessary to evaluate § at some mean dose, say $(d + \frac{\Delta d}{2})$.

A treatment by HAIG (29) which includes creep in the analysis shows that, providing the creep constant is invariant with radius r, similar expressions for the strain to those derived above are obtained.

N.B. It is also assumed that r_{f1}, r_{f2} are independent of temperature and dose i.e. thermal and Wigner strains are very much less than 1.

(c) An interacting fuel element

The equations given above only apply if tubes and compact are unrestrained as with the hollow rod element or tubular non-interacting designs. With the tubular interacting (T.I.) element, however, the inner gap is made sufficiently small so as to ensure interference between compact and inner tube after some accumulation of dose. The compact so restrained has a lower strain rate at its outer surface resulting in a smaller gap. The precise size of the gap at any dose is highly dependent upon the inner interface pressure and creep, involving highly specialised analysis. A series of equations were developed to deal with the interacting condition by a stress analysis specialist (ROBINSON (30)) and although the Author had no hand in their derivation they are given here for completeness.

In the use of the equations, however, some modifications were made by the Author, and these are described in sub-section 3.3.

The outer gap at dose d + Δd is given by

$$g_2(d + \Delta d) = g_2(d) + r_{f2} (V_g - V_f) - Rr_{f1}\Delta X \qquad .....91$$

where V_g and V_f are the combined Wigner and thermal strains derived in equations 86 and 90. The term $Rr_{f1}\Delta X$ is the reduction in displacement due to the interacting effect. Where

$$R = 2r_{f1}^2/[(1 - \sigma_f) r_{f1}^2 + (1 + \sigma_f)r_{f2}^2]$$

and ΔX is given by

$$\Delta X = -P(d)L\mu(1-\lambda)+(V_g - V_f)+ \frac{L}{\mu} (V_f - V_g) \left(Y_g K_g + \frac{\mu(1 - \lambda)}{\Delta d} \right) \qquad .....92$$

L, μ, λ, Y_g and K_g are evaluated at dose d + Δd.

The interface pressure P(d) is evaluated at dose d, and

$$P(d + \Delta d) = P(d) \lambda (d + \Delta d) - \frac{(1 - \lambda (d + \Delta d))}{\mu \Delta d} (V_f - V_g) \qquad .....93$$

$$\left.\begin{aligned}
&\lambda(d+\Delta d) = \exp[-\phi\ \Delta d)] \\
&L = \frac{1-\sigma g}{Y_g}\ , \quad \mu = 1 - \frac{Y_g K_g}{\phi} \\
&\phi = \mu/_\theta \quad , \quad \theta = \frac{m+\sigma f}{Y_f} + \frac{k-\sigma_g}{Y_g} \\
&m = \frac{r_{f2}^2 + r_{f1}^2}{r_{f2}^2 - r_{f1}^2}\ , \quad k = \frac{r_{f1}^2 + r_{s1}^2}{r_{f1}^2 - r_{s1}^2} \\
&u = K_f\ (m+\sigma_f) + K_g\ (k - \sigma_g)
\end{aligned}\right\} \quad .....94$$

In order to treat the unusual occurrance of interaction at zero irradiation owing to thermal effects only, the following simplified expression gives the resulting interface stress

$$\left.\begin{aligned}
&P = \frac{\Delta X}{\theta} \\
&\text{where} \quad \Delta X = (\overline{T}_{s1} - T_o)\ \alpha_g\ (\overline{T}_{s1}) - (\overline{T}_f - T_o)\ \alpha_f\ (\overline{T}_f) - g_{c1}/r_{f1}
\end{aligned}\right\} .....95$$

The outer gap is assumed unaffected by interaction and is given by Eq. 84.

3.3 Description of method as incorporated in AZIMUSTAP

3.3.1 General

Material properties and temperatures are complicated functions of axial position and dose, and it is therefore not feasable to determine analytically the interface gaps at any point in space and time. The program AZIMUSTAP was employed therefore, to carry out step-wise calculations both axially and with irradiation dose. The axial calculation method is described in Appendix VI and only one axial position, z, will be considered here.

The gaps at any dose are dependent upon the gaps at previous doses and hence on the whole preceding irradiation history. It is therefore necessary to start the calculation by analysing fresh fuel and, at discrete dose intervals, repeat the calculations, passing on calculated gaps and other necessary data to the next dose step. At each dose step the relevant operating conditions (channel power and gas outlet temperature) and material properties are used, having been derived from arrays input as data.

TRG 1000(R)(43) (Ch. 5) shows the fuel and graphite thermal conductivity as a function of temperature and fast neutron dose (EDN) and Fig 3/4 shows typical time evolutions of channel power and gas outlet temperature.

As described in Appendix VI there are two main iterative loops in the AZIMUSTAP calculation.

(i) Axial mesh point iteration

At each axial step the gas temperatures, calculated at the previous step are the boundary conditions for the calculation. The fuel and graphite temperatures are then derived by calculating the temperature dependent conductances and then iterating until consistancy is achieved.

(ii) Flow iteration

For the tubular designs where there are two flow passages there is an iteration on flow split in order to achieve an equal pressure at outlet, since flow resistances are temperature dependent.

Using the axial mesh point iteration as a framework, the temperature dependent interface gap can be incorporated as an additional dependent variable.

Let us now consider the axial mesh point calculation at the start of the fuel dwell where the interface gaps are influenced by thermal effects only.

3.3.2 Thermal gap at zero irradiation

For the first axial calculation step the first guess for the interface gap is taken as g_c, the cold unirradiated radial interface gap, assumed constant axially. Because the only temperatures known at this stage are the inlet gas temperatures, Eq. 12, which gives the gap conductances, is approximated to

$$k_j = \frac{k_G(T_1)}{g_c} \qquad .....96$$

where $k_G(T_1)$ is helium conductivity evaluated at T_1. The thermal radiation term can, in any case, be assumed small since at the inlet temperatures are low. For example k_j would typically have a value at outlet of ~ 0.26 W/cm^2 ^{o}C where the radiation term contributes only 3.6%. The conductance given by Eq. 96 is therefore included in the calculation of the temperatures for that axial position. The bulk mean temperatures are calculated(SINCLAIR (51)) and gaps calculated from equations 83 and 84. New gap conductances are calculated from Eq. 12 and the procedure repeated until fuel temperatures have converged to a specific criterion.

α_f and α_g are input as arrays of α versus temperature. The value of α required for a particular temperature is then found by linear interpolation.

For subsequent axial steps the procedure is identical, except that as a first guess the previous axial step converged gap conductances are taken.

The maximum value of k_j, k_{jm}, is derived experimentally (see sub-section 1.2.4) and is prescribed in the program so that k_j is set equal to it should its value be greater when derived from Eq. 12.

If, from Eq. 83, $g_1(o)$ is found to be negative, interaction is said to have occurred and as well as setting k_{j1} equal to k_{jm} and $g_1(o)$ equal to zero, the interface pressure is calculated from Eq. 95. Young's modulus is given as an array with temperature which is interpolated linearly. Poisson's ratio for the fuel and graphite are taken as constant with temperature.

3.3.3 Gap calculation under irradiation

The irradiation calculation is carried out in step-wise fashion through the irradiation period of the fuel channel. At each step the full axial calculation is carried out, together with the flow iteration, after which interface gaps and other necessary information are passed onto the next step. The size of the step is chosen to give the desired accuracy.

The thermal conductivity, dimensional change and mechanical property data are given as functions of fast neutron dose (EDN) and it is therefore convenient to divide the irradiation period into dose steps and specify channel operating conditions, power, flow, also as functions of dose.

When calculating an interface gap at axial position z and dose d_n the new gap is dependent upon the previous gap at dose d_{n-1} at that axial position. It is therefore necessary to store the complete axial distribution of interface gaps for use in the next dose step. This also applies to other calculated quantities.

For the dose calculation it is necessary to be able to specify property data as two-dimensional arrays, dose as well as temperature, and the value of any property is found using the temperature and dose which apply to a particular axial position for a particular dose step.

The irradiation period of the channel is divided into steps of channel mean dose and the dose at any axial position is found from the relation:

$$\Delta\, d(z) \;=\; \frac{\bar{\Delta d}}{\bar{R}(z)} \quad R(z)$$

where $\Delta d(z)$ is the increment of dose accumulated by an axial position z; $\Delta\bar{d}$ is the specified channel mean dose; $\frac{R(z)}{\bar{R}(z)}$ is the normalised axial rating factor. The justification for using the axial rating shape as opposed to an axial dose shape is given in Chapter 3.

The axial rating shape is not a constant with irradiation and it is therefore necessary to pass on to the next dose step the accumulated dose. Therefore if $d(z)_{n-1}$ is the accumulated dose up to step n-1 for axial position z, the dose at step n for axial position z is

$$d(z)_n = d(z)_{n-1} + \Delta\bar{d}_n \left(\frac{R(z)}{\bar{R}(z)}\right)_n \qquad .....97$$

where $\Delta\bar{d}_n = \bar{d}_n - \bar{d}_{(n-1)}$ specified as data.

Consider dose step n and z = 0. As with the start-of-life calculation Eq. 96 is used for a first guess but now $g_{(z=0)(n-1)}$ is taken instead of the cold unirradiated gap. For other axial positions the converged interface conductances of the previous axial step is taken - as before.

Let us consider an axial position z at the start of the calculation at dose step n. A test is first made to find if, at n-1, interaction has occurred. If not, the non-interacting equations are used.

(a) <u>The non-interaction method</u>

The inner and outer gaps are given by:

$$g_{1n} = g_{1(n-1)} + r_{f1}\,(V_f(d_n,\bar{T}_{fn}) - V_g(d_n,\bar{T}_{s1n})) \qquad .....98$$

$$g_{2n} = g_{2(n-1)} + r_{f2}\,(V_g(d_n,\bar{T}_{s2n}) - V_f(d_n,\bar{T}_{fn})) \qquad .....99$$

V_g and V_f are combined thermal and Wigner strains and are derived from a combination of equations 85, 86, 89 and 90 thus:

$$V_f(d_n,\bar{T}_{fn}) = \S_f(d_n,\bar{T}_{fn})\,\Delta d_n + (\bar{T}_{fn} - T_o)\,\alpha_f(d_n,\bar{T}_{fn}) - \{(\bar{T}_f - T_o)\alpha_f\}_{n-1} \qquad ....100$$

$$V_g(d_n,\bar{T}_{s1n}) = \S_g(d_n,\bar{T}_{s1n})\,\Delta d_n + (\bar{T}_{s1n} - T_o)\,\alpha_g(d_n,\bar{T}_{s1n}) - \{(\bar{T}_{s1} - T_o)\alpha_g\}_{n-1} \qquad ....101$$

$$V_g(d_n,\bar{T}_{s2n}) = \S_g(d_n,\bar{T}_{s2n})\,\Delta d_n + (\bar{T}_{s2n} - T_o)\,\alpha_g(d_n,\bar{T}_{s2n}) - \{(\bar{T}_{s2} - T_o)\alpha_g\}_{n-1} \qquad ....102$$

The $\{\ \}_{n-1}$ terms are the thermal strains which apply to the previous dose step (n - 1).

$\S(d_n,\overline{T}_n)$ terms are mean gradients of shrinkage for the dose step and $\S(d_n\ \overline{T}_n)$ is taken as the difference between the shrinkage ordinate at dose d_n and dose d_{n-1} of the shrinkage versus dose curve applying at temperature $\overline{T}_n$. It would be more consistent if an average temperature between $\overline{T}_n$ and $\overline{T}_{n-1}$ were taken. However this would necessitate passing on large numbers of temperatures which would be cumbersome and, providing small enough dose steps are taken (which, in any case, is necessary for an average $\S\ (d_n\ \overline{T}_n)$ to apply) errors can be made acceptably small.

If it is found on convergence that Eq. 98 leads to a negative gap i.e. if the accumulated strain over an irradiation period is greater than $g_{1(n-1)}/r_{f1}$, then the axial step calculation is repeated using the interacting method.

(b) <u>Interacting method</u>

We now use the equations 91 - 95 for evaluating the outer gap and interface pressure at dose step n. The equations assume, however, that there has been interaction throughout Δ dn, whereas in general the onset of interaction would have occurred between steps n - 1 and n.

This discrepancy is not very significant in calculating the outer gap as only the correction term $Rr_{f1}\,\Delta X$, in equation 91, is in error and providing the dose steps are not too large the effects can be ignored.

With the interface pressure, however, its value at n - and therefore the accumulated peak value - is highly dependent upon the precise time at which interaction occurs. Therefore, in order to avoid uneconomically small dose steps a correction term is necessary to allow for this effect.

If $g_{1(n-1)}$ is the inner gap calculated at dose step n-1 and g_{1n} is negative, the problem is to find the dose increment $\Delta d'$ after dose step (n-1) when g_1 becomes zero and interaction is said to begin (see Fig 4/10).

We have

$$g_{1n} = g_{1(n-1)} + r_{f1}\ (V_f(d_n,\overline{T}_{fn}) - V_g(d_n,\overline{T}_{s1n}))$$

The mean strain rates over the dose increment $d_n - d_{(n-1)}$, $(\Delta\ d_n)$

for the fuel and graphite are given by

$$V_f(d_n,\overline{T}_{fn})/\ \Delta d_n = V_f'$$

$$V_g(d_n,\overline{T}_{s1n})/\ \Delta d_n = V_g'$$

Thus $\Delta d'$ is calculated from

$$g_1\ (\ d_{(n-1)} + \Delta d')\ = 0$$

and therefore

$$-g_1\ (n-1) = \Delta d' r_{f1}\ (V_f' - V_g')$$

and $$\Delta d' = \frac{-g_{1(n-1)}}{r_{f1}(V_f'-V_g')} \qquad .....103$$

Therefore the stress is applied for a dose increment given by $\Delta d_n - \Delta d'$ and since $P(n-1) = 0$

from Eq. 93

$$Pn = -\mu(1-\lambda n)(V_f' - V_g')$$

λ_n which gives the creep effect on pressure is an inverse function of Δd, the period over which the pressure is maintained.

i.e. $\lambda_n = \exp\left[-\phi_{(n-1)}\Delta d\right]$

where, in this case, $\Delta d = \Delta dn - \Delta d'$

Therefore substituting in for $\Delta d'$ from Eq. 103 we have

$$\lambda_n = \exp\left[-\phi_{(n-1)}\left(\Delta d_n + \frac{g_{1(n-1)}}{r_{f1}(V_f'-V_g')}\right)\right]$$

$$\lambda_n = \exp\left[-\phi_{(n-1)}\Delta d_n\left(1 + \frac{g_{1(n-1)}}{r_{f1}(V_f(d_n,\overline{T}_{fn})-V_g(d_n,\overline{T}_{sn}))}\right)\right] \qquad .....104$$

Thus the complete expression for the pressure is given by

$$P_n = P_{(n-1)}\lambda_n - \left(\frac{1-\lambda n}{\mu\Delta d_n}\right) \left(V_f(d_n,\overline{T}_{fn}) - V_g(d_n,\overline{T}_{sn})\right) \qquad \ldots\ldots 105$$

where λ_n is given by Eq. 104.

This expression now applies at any dose step, for if there is no interaction at n-1, then P(n-1) = 0. Conversely, if there were interaction at n-1, $g_{(n-1)} = 0$ and the equation reverts to Eq. 93.

The effect this correction has on interface pressure is shown schematically in Fig 4/10.

(c) <u>Correction for the termination of interaction between dose steps</u>

If the test which was made to find out if there was interaction at the previous dose step, is found to be positive then the interacting equations (equations 91 - 95) are used for the first round of iterations.

It is possible, however, particularly at high doses for the fuel and graphite strain rates to change such that $V'_f - V_g$ is no longer negative i.e. when $\S_f$ becomes less negative than $\S_g$. If $V'_f - V'_g$ is sufficiently positive, the interface pressure will be relieved (calculated to be negative) and the inner gap will begin to grow. This can be shown from Eq. 93 i.e.

$$P_n = P_{(n-1)}\ _n - (1 - \lambda_n)\ (V'_f - V'_g)/\mu$$

For $P_n = 0$

$$P_{(n-1)}\ \lambda_n = (1 - \lambda_n)\ (V'_f - V'_g)/\mu \qquad \ldots\ldots 106$$

From Eq. 94 $0 < \lambda_n < 1$

$\therefore\ V'_f - V'_g > 0$

In order to allow for the fact that interaction ceases between doses, the expression for the inner gap (Eq. 98), for use in the second round of iterations, must be modified so that accuracy as well as consistency are maintained.

Again the problem is to find the dose increment $\Delta d'$ necessary to achieve a zero interface pressure, i.e. from Eq. 106.

$$\lambda_n(\Delta d')\ (P_{(n-1)} + \frac{1}{\mu}\ (V'_f - V'_g)) = \frac{1}{\mu}\ (V'_f - V'_g)$$

$$\exp\left[-\phi_{(n-1)}\ \Delta_{d'}\right] = \frac{1}{\mu}\ (V'_f - V'_g)/(P_{(n-1)} + \frac{1}{\mu}\ (V'_f - V'_g))$$

$$\Delta d' = \frac{1}{\phi_{(n-1)}}\ \ln\ \left[\frac{P_{(n-1)} + \frac{1}{\mu}(V'_f - V'_g)}{\frac{1}{\mu}\ (V'_f - V'_g)}\right] \qquad .....107$$

Thus Eq. 98 can be rewritten

$$g_n = g_{(n-1)} + r_{f1}\ (V'_f - V'_g)(\Delta d_n - \Delta d')$$

where, in this case, $g_{(n-1)} = 0$, and $\Delta d_n - \Delta d'$ is the dose increment over which the strain rate differential is contributing to the inner gap. Therefore, in terms of calculated quantities:

$$g_n = r_{f1}\left[V_f(d_n,\bar{T}_{fn}) - V_g(d_n,\bar{T}_{Sn})\right](1 - \frac{\Delta d'}{\Delta d_n}) \qquad .....108$$

Consistency is achieved since, when $P = 0$ at d_n, $\Delta d' = \Delta d_n$ and therefore g_n, from Eq. 108, is also zero and if $P = 0$ at $d_{(n-1)}$, the equation for g_n reverts to Eq. 98.

3.4 Typical gap and stress evolution for a fuel channel

The mechanical and dimensional change and conductivity data given in Chapter 5 have been used in AZIMUSTAP-5 to produce the axial and time variations of interface gaps and pressures for a peak rated channel. The parameters and operating conditions of this channel are given in Tables 4/1 and 5/1.

3.4.1 Time evolution

The time variation of the interface gaps and pressures at the 2m (from top reflector) level are given in Fig 4/11.

On loading the column the inner gap is reduced by thermal effects on reaching the steady state operating temperatures.

(The dwell of the channel is divided into 20 equal dose steps, the end of life, channel average, dose being 2×10^{21} n/cm^2 EDN.)

At 1×10^{20} n/cm^2 EDN channel average dose the inner gap has decreased still further and at 2×10^{20} n/cm^2 EDN interaction has occurred. By extrapolating the straight line drawn between the zero and 1×10^{20} n/cm^2 EDN dose points it was found it passed through the 2×10^{20} n/cm^2 EDN/ zero gap point. However, interaction must have occurred slightly before this dose since a finite interface pressure has been calculated. Therefore in order to obtain the precise time of interaction, which is needed for compact stressing calculations, extrapolation should not be used for accuracy and more dose steps at these low doses should be taken.

At dose step 3×10^{20} n/cm^2 EDN the stress had increased markedly. The rapid increase being due to the large values of $\S_f$ at these doses.

As is noted in Chapter 3 (also see Fig 4/32) gags are changed at doses 4×10^{20}, 8×10^{20}, 12×10^{20} and 16×10^{20} n/cm^2 EDN. In order to represent the step change in temperatures which occur at each gag change extra dose steps have been introduced into the calculation at 3.9999×10^{20}, 7.9999×10^{20}, 11.9999×10^{20} and 15.9999×10^{20} n/cm^2 EDN.

Therefore the next dose step after 3.0×10^{20} n/cm^2 EDN is 3.9999×10^{20} n/cm^2 EDN. Here it is found that the stress has reduced since creep and reduced thermal effects have begun to counteract the shrinkage part.

Once the gag is changed there is an abrupt increase in fuel and graphite temperatures. It is found therefore at dose step 4×10^{20} n/cm^2 EDN that there is an increase in interface pressure owing to the increased thermal contribution. There is clearly a transient effect of changing the gag which has not been allowed for.

Beyond 4×10^{20} n/cm^2 EDN the interface pressure generally decreases owing to the reduction of δ_f.

This reduction proceeds until, at 1.9×10^{21} n/cm^2 EDN, an inner gap has formed again. At the next dose step, 2×10^{20} n/cm^2 EDN the channel has come to the end of its dwell and is discharged.

The outer gap varies monotonically as it is unaffected by gag changes, the thermal strain making only a small contribution to the total strain.

It can be seen from the figure that the rate of change of gap size is greater at low doses than at high doses and is therefore consistent with the fuel shrinkage/dose curve.

3.4.2 Axial distribution

Fig 4/12 shows the axial variation of interface gaps and pressures for a channel average dose of 2.0×10^{20} n/cm^2 EDN.

The fuel region in the column is 5m in length and has been divided into twenty axial slabs. Therefore each slab is $\frac{1}{4}$ of a brick and $\frac{1}{2}$ of a pin, there being two pins per brick.

At the top of the first pin where the fuel is at inlet conditions the temperatures and doses are low (see Chapters 3 and 5). The thermal and Wigner strains are, therefore, small and gaps have changed little from their cold unirradiated values. Further down the stack the inner and outer gaps are decreasing and increasing respectively resulting from the increased temperatures (thermal strains) and doses (Wigner strains).

At the 2m level it is found that interaction has occurred, initially at approximately 1.9m (found by extrapolation).

From the top of the third brick downwards the enrichment is lower.

Therefore, just below the 2m level, the doses and temperatures are also lower and it is found that there is no interaction and the outer gap has reduced.

Further down the column, temperatures and doses are increasing again until at 2.88m interaction has occurred, causing the corresponding outer gap to be smaller. With the increasing doses and temperatures both the outer gap and interface pressure increase until 4.44m where, with a reduced dose, there is no interaction.

3.5 Thermal expansion and irradiation effects on channel dimensions

In the calculations described so far the core and annulus dimensions have been assumed invariant. The thermal expansion and Wigner shrinkage effects, however, cause the dimensions of the flow passages to have an axial and time distribution.

3.5.1 Thermal effects

Let us first consider the start-of-life where only thermal expansion effects are relevant. There are three radial dimensions which need to be considered: r_{s1}, r_{s2}, r_{s3}. It is assumed that the expansion of the channel wall dimension is controlled by the channel wall temperature. In fact, the whole temperature and stress field within the block decides the channel dimensions.

From equations similar to Eq. 79 the displacements of the three surfaces at an axial position z are given by:

$$\begin{aligned}
\Delta r_{s1}(z) &= \alpha_g(\bar{T}_{s1}(z)) \,.\, r_{s1} \,.(\bar{T}_{s1}(z) - T_o) \\
\Delta r_{s2}(z) &= \alpha_g(\bar{T}_{s2}(z)) \,.\, r_{s2} \,.(\bar{T}_{s2}(z) - T_o) \qquad \ldots\ldots 109 \\
\Delta r_{s3}(z) &= \alpha_g(T_{W3}(z) \,.\, r_W \,.(\bar{T}_{W3}(z) - T_o)
\end{aligned}$$

The varying temperature axially ensures an axial variation of passage geometry. The change in dimension, however, is sufficiently small to cause minimal effects on boundary layer development.

The changes in passage geometry do have an effect on heat transfer and pressure drop. The latter effect in turn changes the flow division between the bore and annulus. To allow for all these factors the HEATAX program has been modified (HEATAX-II). Appendix VII includes a description of the HEATAX series of codes.

Fig 5/1, derived from HEATAX, shows the axial variation of graphite surface temperature for the channel operating conditions given in Table 5/1.

The corresponding axial distribution of dimensional change (Δr) for the three surfaces is shown in Fig 4/13. This has also been derived from HEATAX which has used Eq. 109.

As can be seen from Fig 4/13 the bore dimension experiences a maximum expansion of 140 µm. In the annulus, at the inlet region, the pin surface has a larger value of Δr than the wall since the temperature difference offsets the differences in radius. As the wall temperature increases Δr_{s3} increases until outlet is reached; at which point Δr_{s3} is greater than Δr_{s2}. The result of this axial distribution is an increase in annulus pressure drop down to about 3.5m from inlet and a reduction from there to outlet. The net result, as shown by HEATAX, is only a slight increase in annulus pressure drop (less than 0.5%). There is, of course, a reduction in bore pressure drop and the program shows this to be 1.5%.

The heat transfer effect on surface temperature is small and HEATAX shows maximum changes of 1 or 2°C for the same flow split. The change in flow split arising from the resulting imbalance in outlet pressure has the following effect on the axial peak surface temperatures:

$$\Delta\hat{T}_{W1} = -2^{\circ}C$$

$$\Delta\hat{T}_{W2} = +6^{\circ}C$$

$$\Delta\hat{T}_{W3} = +8^{\circ}C$$

3.5.2 Irradiation effects

The small temperature changes arising from the thermal effects tend to be reduced by Wigner shrinkage as this is an opposite effect. As the maximum shrinkage that can occur, for the maximum dose, is about 0.5%, the changes in graphite dimensions are not more than about 150 μm. Wigner shrinkage has not, however, been included in HEATAX since this would be a difficult development and the thermal calculations, already described, suggest a small effect.

4 Corrosion within the HTR fuel channel

One of the main reasons helium was chosen as a coolant is its inability, unlike CO_2, to react with the core components and so reduce core integrity. It is particularly important in the HTR to have an inert coolant because of the high temperatures that will be experienced.

Steam which can leak into the core from, say, a faulty boiler tube weld can cause significant damage to core components because of these high operating temperatures.

The form this corrosion can take and its effect on fuel performance and endurance is highly important as it is these factors which will determine the limits on water ingress. It is the aim of this section to describe the models that have been developed by the Author to analyse the phenomenon. Using these models the effects of corrosion are predicted. The first work published on this subject was by the Author in September 1969 (31) which, in an analytical way, dealt with the removal of graphite from the pin surface assuming a smooth Hollow-rod element. In November 1970, the Author studied a smooth tubular interacting element (32).

The present work is a further extension on the references above so as to include:

(i) a model to describe the form and development of corrosion induced roughness

(ii) a study of the heat transfer and fluid flow effects of roughness

(iii) specially written computer codes to analyse the problem.

This present work is a new step forward in analysing the corrosion phenomenon since, by one method, the degree and form of corrosion is determined, the heat transfer and fluid flow effects of the change of geometry and degree of roughness are found (making allowance for the temperature feed-back effect), and the resulting fuel channel performance is determined for the whole channel and throughout the fuel dwell.

4.1 The corrosion phenomenon

4.1.1 Corrosion mechanism

There are three corrosion regimes which apply to the case of chemical attack by a gaseous medium (water vapour) of a porous solid (graphite). These three regimes operate over three temperature ranges (Fig 4/14). Reactor pressures (approximately 53 bars) are assumed.

(i) The chemical regime

Below temperatures of about 800°C the water vapour diffuses through the medium and because of the low temperatures an even concentration occurs, equal to that of the gaseous environment. The corrosion rate K1 is given by the Arrhenius relation:

$$K1 = K_o^{-\frac{E}{RT}} \qquad .....110$$

where E is the activation energy and R is the gas constant.

(ii) The in-pore diffusion regime (between approximately 800 and 1200°C)

At these higher temperatures a water vapour concentration gradient exists where, at equilibrium, the rate of depletion of corrodant is balanced by the rate of diffusion.

The corrosion rate K2 is given by

$$K2 = \sqrt{K1\ D_{eff}} \qquad .....111$$

Where D_{eff} is the effective diffusion coefficient and is itself dependent upon the level of corrosion.

(iii) The mass transfer regime (above about 1200°C)

The corrosion is a surface effect – the rate determined by diffusion through the gaseous boundary layer δ.

$$K3 = Kc\ (Co - Cs)$$

where

Kc = mass transfer coefficient

Co = concentration of reactant in main gas stream

Cs = concentration of reactant at graphite surface

In order to determine the effects of changes in geometry and for realistic graphite temperatures, the in-pore diffusion regime is of interest and is now investigated further.

As stated above, the in-pore diffusion mechanism is controlled by diffusion through the graphite pores. As the graphite becomes corroded, the pores widen, increasing the diffusion coefficient and thus the corrosion rate.

As described by BIRCH (33) the concentration, γ, of corrodant within the porous solid is given by

$$\gamma = \exp \left[-\phi_o \, \S_t \right] \qquad .....112$$

where γ is the mole fraction of corrodant relative to the gaseous environment.

and $$\S_t = \frac{\text{distance from surface}}{\text{wall thickness } (d_t)}$$

and ϕ_o, the catalyst number is given by

$$\phi_o = d_t \sqrt{\frac{k_{mo}\,\rho_g}{D_{eff}}}$$

where

ρ_g = density of graphite

k_{mo} = chemical reaction rate at T^oK

and $$D_{eff} = Do\lambda \left(\frac{T}{273.2}\right)^{1.75} \left(\frac{1}{p}\right) \qquad .....113$$

where

Do = free gas diffusion coefficient at 0^oC and 1 atm

T = temperature of graphite

P = total gas pressure

λ = a variable defining pore shape and size.

Therefore, since the pore size is burn-off dependent the diffusion coefficient and the corrodant concentration are also burn-off dependent.

If equations 110 and 111 are now combined, we obtain

$$k_{eff}(T) = Ae^{-\frac{B}{T}} \qquad \text{.....114}$$

where $k_{eff(T)}$ is defined as the effective burn-off rate at surface temperature T, B is assumed constant and A, which includes the diffusion coefficient, is dependent upon burn-off.

4.1.2 Data used

(a) Burn-off rate - temperature correlation

Effective burn-off $k_{eff(T)}$, at one atmosphere pressure, is shown as a function of temperature in Fig 4/15 derived from HELSBY (34) where he has assumed that the Arrhenius form (Eq. 114) applies and a burn-off of 50 mg/cm^2.

From Fig 4/15

$$A = 1.563 \times 10^4 \text{ mg.cm}^{-2}\text{h}^{-1}\,\mu\text{ at.}H_2O$$

$$B = 2.0174 \times 10^4$$

The experimental work of HELSBY shows that $k_{eff(T)}$ at 100 mg/cm^2 burn-off is approximately eight times that at zero burn-off. It is assumed, in this work, that $k_{eff(T)}$ at 50 mg/cm^2 represents a mean burn-off rate. (N.B. Beyond about 100 mg/cm^2 $k_{eff(T)}$ is constant.)

Assuming an average value of $k_{eff(T)}$ given by the 50 mg/cm^2 burn-off value, is reasonable because:

(i) at the temperatures and pressures of interest, 1000°C and 53 bars respectively, corrosion is chiefly concentrated at or near the graphite surface and therefore k_{eff} will tend to be less dependent on burn-off

(ii) there is sufficient doubt on corrosion data to make factors of two or three on k_{eff}, unfortunately, the level of irreducible error.

(b) Pressure effects

HELSBY (34) recommends a factor of $\sqrt{P_2/P_1}$ (equations 111 and 113) to convert k_{eff} at pressure P_1 to a pressure of P_2, however, BIRCH (33) suggests this is only true at zero burn-off or when the steady-state has been reached (i.e. when k_{eff} becomes constant with burn-off). Fig 4/16 derived from BIRCH (33), shows how the factor Cp ($=k_{eff}(P_2)/k_{eff}(P_1)$) varies with burn-off and graphite temperature.

For the work described in sub-section 4.2, on the Hollow-rod element, some allowance is made for the variation of Cp with burn-off and temperature and for the temperatures 1000°C, 1050°C and 1100°C Cp is taken as 0.2, 0.154 and 0.143 respectively. (Reactor pressure is assumed to be 53 atm.)

In later work, (sub-section 4.6), where burn-offs are less, a constant value of C_p of 0.25 has been taken since a variation is not justified when considering basic data uncertainties.

(c) Moderator block data

The data derived above can be applied to the pin graphtie. There is evidence quoted by MERRETT (35) that the moderator block, being made of different graphite, has a much higher chemical reactivity, the level of which is very uncertain. It is assumed, for the purposes of this work, that

$$k_{eff}\ (\text{block}) = 10 \times k_{eff}\ (\text{Pin})$$

$$\therefore \quad k_{eff}\ (\text{block}) = 1.563 \times 10^5 \exp\left(\frac{-2.0174\times 10^4}{T^oK}\right) \text{mgcm}^{-2}\text{h}^{-1}\,\mu\,\text{atm}\ H_2O$$

where k_{eff} (block) applies at one atmosphere pressure.

(d) Water vapour concentration

The concentration of water vapour present basically depends upon:

(i) the amount of leakage from the boilers

(ii) the net reactivity of the core.

In fact, there is a maximum continuous tolerable concentration (MCTC) which is defined by considering the corrosion to the most limiting reactor component. That is, a study is made of the corrosion effect (thermal, mechanical etc) of a range of concentration levels on certain key reactor components and the MCTC is chosen that just meets the severest limit. The work described below on the channel performance effects would be one important factor that is considered in setting the MCTC.

The lowest MCTC that can be measured is approximately 0.1 vpm and for the purpose of obtaining realistic answers to the thermal performance questions this concentration is assumed in the work to follow.

0.1 vpm water concentration for a reactor at 53 atm gas pressure is equivalent to 5.3 μ atm H_2O concentration.

(e) Summary of corrosion data

Combining the above factors together, the following expressions are obtained for the effective burn-off rates (k_{eff}) for the pin and block:

Pin:

$$k_{eff} = 8.282 \times 10^4 . \ Cp.e \ \frac{-2.0174 \times 10^4}{T^oK} \ mgcm^{-2}h^{-1}$$

Block:

$$k_{eff} = 8.282 \times 10^5 . \ Cp.e \ \frac{-2.0174 \times 10^4}{T^oK} \ mgcm^{-2}h^{-1}$$

At the temperatures of interest it is reasonable to assume that all the graphite is removed at the surface.

N.B. from corrosion profiles shown by BIRCH (33), at 1030°C, less than 1% of the graphite is removed below a depth of 250μ m - half the grist particle diameter (see sub-section 4.3)

The rate of removal in mm (k_d) is obtained, therefore, by dividing the equations above by the density (1800 mg/cm^3) i.e.

Pin:

$$k_d = 460.1\ C_p\ e^{\frac{-2.0174 \times 10^4}{T^\circ K}}\ \text{mm/h} \qquad .....115$$

Block:

$$k_d = 4601\ C_p\ e^{\frac{2.0174 \times 10^4}{T^\circ K}}\ \text{mm/h} \qquad .....116$$

4.2 Planar removal

The early work in this field, by the Author (31, 32), deals with the effect on thermal performance of corrosion induced changes of graphite section.

4.2.1 Hollow-rod element

The Hollow-rod element, described in Chapter 2 is the subject of the 1969 work (31). Below is shown, diagrammatically, a section through the element.

The increased reactivity of the block graphite was not known when this work was done, and with the lower temperatures of the hollow rod moderator block (850°C maximum) it was assumed that the block would remain unscathed. The outer surface of the graphite sheath, however, was attacked and it was the effect on the temperatures of removal of that surface which was considered. This work is now related here.

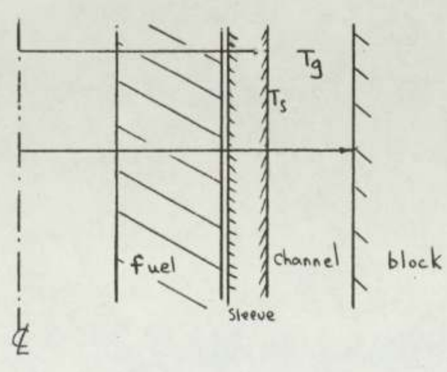

Table 4/2 lists the operating conditions assumed for the analysis. To determine the effect of different surface temperatures three bulk gas temperatures have been assumed (Table 4/2). One axial position has been taken.

As described in Chapter 2 the Hollow-rod, with a continuous gagging scheme experiences approximately constant surface temperatures - in the absence of corrosion. If, therefore, the surface temperature at any time is given by

$$T_S = T_g + \frac{q'_c}{2\pi rh} \qquad \text{.....117}$$

then the ratio of convection linear heat rating q'_c to heat transfer coefficient(h) is approximately a constant. This is because the channel flow (W) is reduced at the same rate as q'_c to maintain T_g constant and $h \propto W^{0.8}$.

The equation for h assumed is

$$h = \frac{0.019k}{de}c \left(\frac{W}{A}\frac{De}{\mu}\right)^{0.8} P_r^{\;0.4} \left(\frac{T_S}{T_g}\right)^{-0.3} \qquad \text{.....118}$$

If $(^T S/T_g)^{-0.3}$ is assumed to remain constant then

$$T = T_g + \frac{G}{r}\left(r_c^2 - r^2\right)^{0.8} (r_c - r)^{0.2} \qquad \text{.....119}$$

Since $De = 2(r_c - r)$ and $A = \pi\,(r_c^2 - r^2)$

and $G = q'_c\;(^T S/T_g)^{-0.3}/0.0416\; k_c P_r^{\;0.4}(^W/_\mu)^{0.8}$

where $q'_C = q'_T - q'_R$ and q'_R, the radiative linear heat rating, is assumed constant. q'_T is the total linear heat rating.

If $r = r_o - \Delta r(t)$ where r_o is the uncorroded dimension and $\Delta r(t)$ the removal up to time t, then if one assumed $\frac{\Delta r}{r_o} \ll 1$ Eq. 119 can be reduced to

$$T_S = T_g + \frac{GCO}{r_o}\left(1 + C_1\, \Delta r(t)\right) \qquad \text{.....120}$$

where $C_o = (r_c^2 - r_o^2)^{0.8} (r_c - r_o)^{0.2}$

and $C_1 = \frac{1.6 r_o}{r_c^2 - r_c^2} + \frac{0.2}{r_c - r_o} + \frac{1}{r_o}$

From Eq. 115

$$\frac{d}{dr}(\Delta r) = 460.1 . Cp . e^{\frac{-2.0174 \times 10^4}{T_S (^\circ K)}} \quad \text{.....121}$$

and set a = 460.1, b = 2.0174 x 10^4

Differentiating Eq. 120 w.r.t. time t we have

$$\frac{dT_S}{d(\Delta r)} = \frac{GC_o C_1}{r_o} \quad \text{.....122}$$

Combining equations 121 and 122

$$\frac{dT_S}{dt} = \frac{aGC_o C_1 C_p}{r_o} e^{-\frac{b}{T_S}} \quad \text{.....123}$$

Let $H = \frac{aGC_o C_1 C_p}{r_o}$ then, separating variables and integrating:

$$Ht = \int_{T_o}^{T_S} e^{\,b/T_S} \, dT_S$$

where T_o is the surface temperature at start-of-life (t-0).

We can substitute $y = \frac{-b}{t}$:

$$\int_{T_o}^{T_S} e^{\,b/T_S} \, dT_S = b \int_{-\frac{b}{T_o}}^{-\frac{b}{T_S}} e^{-y} \frac{d}{dy}\left(-\frac{1}{y}\right) dy$$

Integrating by parts:

$$\text{Integral} = \left[-\frac{b}{y} e^{-y} \right]_{-\frac{b}{T_o}}^{-\frac{b}{T_S}} - b \int_{-\frac{b}{T_o}}^{-\frac{b}{T_S}} \frac{1}{y} e^{-y} \, dy$$

$$\int_{-\frac{b}{T_o}}^{-\frac{b}{T_S}} \frac{1}{y} e^{-y} \, dy = \int_{-\frac{b}{T_o}}^{\infty} \frac{1}{y} e^{-y} \, dy - \int_{-\frac{b}{T_S}}^{\infty} \frac{1}{y} e^{-y} \, dy$$

The integrals on the R.H.S. are E functions of the first kind and can be evaluated using tables calculated by SINCLAIR (36)

and $\int_x^\infty \frac{1}{y} e^{-y}\, dy = E_1(-x) = \bar{E}_1(x)$

Thus: $Ht = T_S\, e^{b/T_S} - T_o\, e^{b/T_o} - b\bar{E}_1\left(\frac{b}{T_S}\right) + b\,\bar{E}_1\left(\frac{b}{T_o}\right)$ 124

Eq. 124 is evaluated by substituting increasing values of T_S, starting with T_o, until a value of t is reached that exceeds the dwell of the fuel. Table 4/3 shows values of $\bar{E}_1\,(^b/T_S)$, $T_S\, e^{b/T_S}$ and t over a range of T_S. Three starting temperatures (T_o) were assumed to investigate the effect of temperature level. These temperatures were chosen to cover the range of interest for the Hollow-rod design considered, but the precise values were chosen for convenience in reading the tables of $\bar{E}_1(^b/T_S)$ i.e. the three values of T_o chosen were: 1099°C, 1054°C and 989°C. Other data used (e.g. C_p values) are given in sub-section 4.1.2.

The removal Δ r associated with each temperature T_S is found from Eq. 120.

Figs 4/17 and 4/18 show surface temperature T_S and removal respectively, versus fuel dwell. With the long life times of the Hollow-rod fuel (2000 days) quite large removals are experienced. At normal operating peak surface temperatures of say 1050°C, more than 1 mm of the 5 mm thick sleeve is removed, producing increases in surface temperatures of about 40°C. At hot spots, say 1100°C, even larger effects are noticed. In this early work no allowance had been made for roughening, which would tend to offset these increases in temperature. This serious problem, however, was eventually alleviated by changing the design to the tubular interacting element which, because of its shorter dwell times (800 days), experienced much less, although still significant, corrosion attack.

The special corrosion analysis problems introduced by the T.I. element are now discussed.

4.2.2 Tubular interacting element

The T.I. element, as described previously, has cooling gas passing both inside and outside the pin and because of interface gap growth the surface temperatures, heat fluxes, etc., cannot be assumed constant with irradiation. The method of calculation derived for the hollow rod element is, therefore, no longer applicable.

The method developed by the Author (32), to deal with the T.I. element, was to divide the dwell into finite steps and, assuming constant conditions over that step, calculate the removal Δr and change of temperatures according to the above equations. Once again this work does not consider removal from the channel wall, nor the effect of roughness. It assumes also no change in the flow division between bore and annulus. With these limitations, which have now all been overcome, it is not proposed to describe that early work here, but to begin the description, immediately, of the final method that has been developed for analysing corrosion in the T.I. element and incorporated in the HEATAX program.

4.3 The form and hydrodynamic definition of roughness

4.3.1 A model to describe roughness development

So far in the analysis of the thermal performance repercussions of graphite corrosion, only changes in geometry have been considered - the planar removal effects. Throughout smooth channel heat transfer coefficients and friction factors have been assumed - which is reasonable if the corrosion is uniform over the graphite surface. Owing to the lack of homogeneity of the graphite tubes and moderator, however, this assumption is far from valid.

Arising from the manufacturing process the graphite consists of 'grist' particles set in a matrix of pitch binder and from experiments by HELSBY (34) it is clear that the binder has a much higher chemical reactivity than the particles. This leads to preferential attack, pitting, and a generally rough surface.

The longer the dwell in the corrosive environment the deeper the pitting and more pronounced the roughness until a grist particle is exposed to such an extent it can be eroded away, resulting in the planar removal already described.

This roughening of the graphite surfaces leads to a general improvement in heat transfer and a corresponding increase in frictional drag.

There is very little experimental information on the form and degree of corrosion induced roughening, although it is known to be highly dependent on the type of graphite and the presence of small quantities of impurity. Even one sample of graphite is corroded unevenly owing to property variations within the sample. Any model developed, therefore, to describe the form of the roughness and which determines the characteristic roughness height can only be highly speculative. The following is such an attempt to relate measured bulk graphite removal rates to a characteristic roughness height.

Fig 4/19 shows an idealised section through a graphite sample where the average 'grist' particle diameter is 'd'.

If k_{eff} is the measured effective corrosion rate of the sample this will include graphite removal from the particles and binder. If k_p and k_B are the respective components of k_{eff} after a dwell δt with a water concentration H the corrosion depths of binder and particle are respectively,

$$\delta h_B = \frac{k_B H \delta t}{\bar{\rho}}$$

$$\delta h_p = \frac{k_p H \delta t}{\bar{\rho}}$$

where $\bar{\rho}$ is the mean graphite density. (Assume equal areas of binder and particle exposed.)

The net roughness height after time δ t is

$$\varepsilon = \frac{1}{\bar{\rho}} (k_B - k_p) H \delta t$$

Let $K_p/k_B = x$

$$\varepsilon = \frac{k_B}{\bar{\rho}} (1 - x) H \delta t \qquad .....125$$

Now:

$$k_{eff} = \frac{k_B + k_p}{2} = \frac{k_B}{2} (1 + x)$$

Therefore we can substitute for k_B in Eq. 125

$$\varepsilon = \frac{2k_{eff}}{(1+x)\bar{\rho}} (1 - x) H \delta t \qquad .....126$$

From this equation it can be seen that if the grist particle did not corrode ($x = 0$) the roughness height would be that given by $2k_{eff}$ since k_{eff} is defined in terms of the total surface area when in fact only half is being corroded. The other extreme of ε is zero when the binder and particle corrode equally.

As the dwell (δt) increases, ε increases until sufficient of the particle is exposed so that it becomes dislodged. From this time on (t_{crit}) the roughness height will be assumed to remain constant. (Fig 4/19(a)).

One would expect the mean depth of particle still embedded before dislodgment to be $^d/2$, although with sticking the probability distribution of dislodgment could become skewed (Fig 4/19(b)). The amount of sticking is a complete unknown and the maximum roughness height is assumed to be $^d/2$.

The value of x is unknown and we will arbitarily assume that the roughness height ε is given by the effective burn-off k_{eff} i.e.

$$\varepsilon = \frac{k_{eff}\, H^{\delta}\, t}{\bar{\rho}} \qquad \text{.....127}$$

This is equivalent to assuming the binder reactivity is three times higher than the particles i.e. x = 0.333.

4.3.2 Hydrodynamic definition of roughness

As already described in section 2 the turbulent flow velocity profile has, adjacent to the wall, a laminar sub-layer in the region $0 < y^* < 5$

where $y^* = {}^{y}/_{\nu}\sqrt{\tau_o/\rho}$ 128

According to NIKURADSE (37) a surface is hydrodynamically rough when the protruberences extend beyond the laminar sub-layer. The limiting roughness height will depend upon the Reynolds number since, as has already been shown, the laminar sub-layer thickness decreases as the Reynolds number increases.

Let us first establish the limiting roughness height/Reynolds number range, applying to the current design of fuel element.

For a rough channel $\varepsilon > y_L$

where $y_L = \dfrac{5\nu}{\sqrt{\tau_o/\rho}}$

the wall shear stress can be defined in terms of the friction factor f, i.e.

$$\tau_o = \bar{\rho}\frac{\bar{u}^2 f}{2}$$

Therefore

$$y_L = {}^{5\nu}/_{\bar{u}}\sqrt{^f/_2}$$

Now

$$Re = \bar{u}D_e/\nu$$

Therefore

$$y_L = \frac{5D_e}{Re\sqrt{f/2}}$$

That is

$$\varepsilon/D_e > 5/Re\sqrt{f/2} \qquad .....129$$

As can be seen from Eq. 129 the critical value of the dimensionless roughness height ε is Reynolds number dependent - the larger the Reynolds number becomes, the smaller ε/D_e.

For a smooth tube:

$$f = 0.079\ Re^{-0.25}$$

Therefore

$$(\varepsilon/D_e) = 25.2\ Re^{-0.875} \qquad .....130$$

Fig 4/20 shows the critical values of ε/D_e, plotted against Reynolds number.

Under normal operation the Reynolds numbers for the fuel core and annulus are of the order 10^5 and 10^4 respectively, resulting in critical ε/D_e values of 10^{-3} and 8×10^{-3} respectively. For the bore and annulus this gives corresponding critical ε sizes of 30 and 80 μm. With graphite grain sizes of the order 500 μm it is clear there is every likelihood the coolant channels will behave as rough surfaces after some period in the core. In fact it has been shown by WARBURTON (14) that even the originally machined graphite surfaces can approach these critical roughness heights.

4.4 Friction in rough channels

4.4.1 Friction in rough tubes

Initially the data available are investigated which can be applied to the bore of the fuel element.

The majority of work carried out in this field can be divided into two classes:

(i) that applied to manufactured regular roughness - in connection with studies into the improvement of heat transfer from reactor fuel elements and heat exchangers

(ii) random roughness or sand grain roughness - more applicable to the natural state of surfaces and ducts.

The latter category would seem to apply to a corroded graphite surface since, as with sand grains, we have grist particles of nominally uniform size exposed in a somewhat random manner.

WARBURTON (14) has shown, by comparing friction factors; that naturally rough graphite surfaces have similar characteristics as sand grain roughness.

In the absence of experimental results specifically applicable to corroded graphite surfaces, it would therefore seem reasonable to use the results of sand grain roughness work.

The most authoratative work on velocity distributions and friction factors for sand grain roughened tubes is that published by NIKURADSE (37) in 1933 and forms the basis of the following treatment.

NIKURADSE used water as the working fluid and achieved a Reynolds number range of $10^3 - 10^6$ and a ε / D_e range of 0 - 0.03, which encompasses very well the range of interest in the present work.

NIKURADSE defines the roughness height ε as the average sand grain diameter which, because of the thinness of adhesive, is effectively the average 'peak to valley' height. As applied to this particular case, this is equivalent to the average depth of grist particle exposed, or ε as defined by Eq. 127. In the reference work D_e is defined as the diameter of the pipe and is therefore the roughness root diameter which, for this work, is the average binder diameter.

At low Reynolds numbers($<$ 2000) where the flow is laminar, the friction factor is independent of ε/D_e.

There is then a range of Reynolds number (transition range) where the friction factor increases with Reynolds number for a particular ε/D_e. In this region NIKURADSE suggests that the projections are of the same order as the laminar sub-layer and individual.projections extend beyond the layer causing vortices and a resulting loss of energy. As the Reynolds number increases an increasing number of projections extend through the layer producing larger energy losses.

In the third range (fully rough region) the sub-layer is sufficiently thin for all the projections to extend beyond it and the energy losses - and thus frictional drag - become independent of Reynolds number. These characteristics can be observed in Fig 4/23.

In the analysis of the smooth tube velocity distribution it was found that, except for radial positions close to the wall, the Universal Velocity Profile applied (see Fig 4/3).

$$u^* = A + B \ln y^* \qquad \text{.....131}$$

where $u^* = u\sqrt{\tau o/_{\rho}}$

and $y^* = \frac{y}{\nu}\sqrt{\tau o/_{\rho}}$

are dimensionless quantities

and $A = 5.5$ and $B = 2.5$.

NIKURADSE has shown that a similar equation to Eq. 131 can be applied to rough tubes and, in fact, B $(\delta u^*/\delta y^*)$ is unchanged. The value of A, however, is dependent upon the relative roughness ε/D_e and Reynolds number, i.e.

$$u^* = A(\varepsilon/D_e, Re) + 2.5 \ln y^* \qquad \text{.....132}$$

Fig 4/21, derived from NIKURADSE (37) shows by comparison with the smooth wall velocity profile the equivalent rough wall profiles for a range of $^{\varepsilon}/D_e$ and Reynolds numbers.

Let us define a dimensionless roughness height ε * such that

$$\varepsilon^* = \frac{\varepsilon}{\nu}\sqrt{\tau o/_\rho} \qquad .....133$$

Combining Eq. 133 with Eq. 132 and the definition of y*, we obtain

$$u^* = A(^{\varepsilon}/D_e, Re) + 2.5 \ln {}^{y}/_{\varepsilon} + 2.5 \ln \varepsilon^*$$

which becomes

$$u^* = A^* + 2.5 \ln {}^{y}/_{\varepsilon} \qquad .....134$$

where A* is still a function of $^{\varepsilon}/D_e$ and Reynolds number and, in fact, NIKURADSE found that A* was purely a function of ε*. Also:

$$\varepsilon^* = Re\sqrt{f}\,\frac{\varepsilon}{D_e} \qquad .....135$$

When NIKURADSE plotted u* -2.5 ln $^{y}/_{\varepsilon}$ versus ε* he found the experimental points could be represented by five straight lines over the ε* range covered (Fig 4/22).

The five lines are:

(i) Smooth region:

$0 \leqslant \varepsilon^* \leqslant 3.04 \qquad A^* = 5.5 + 2.5 \ln \varepsilon^*$

(ii) Transition region:

$$\left.\begin{array}{lll} (a) & 3.04 \leqslant \varepsilon^* \leqslant 7.2 & A^* = 6.59 + 1.52 \ln \varepsilon^* \\ (b) & 7.2 \leqslant \varepsilon^* \leqslant 15.0 & A^* = 9.59 \\ (c) & 15.0 \leqslant \varepsilon^* \leqslant 73.0 & A^* = 11.5 - 0.705 \ln \varepsilon^* \end{array}\right\} \qquad .....136$$

(iii) Fully rough region:

$\varepsilon^* \geqslant 73.0 \qquad A^* = 8.48$

By integration of the velocity profiles to obtain $\bar{u}$, the mean velocity, NIKURADSE obtained an expression for the peak velocity $\hat{u}$ in terms of $\bar{u}$, i.e.

$$\frac{\hat{u} - \bar{u}}{\sqrt{\tau o/_\rho}} = 3.75 \qquad .....137$$

also $\tau_o/_\rho = \frac{1}{2}\bar{u}^2 f$ 138

when $u^* = \dfrac{\hat{u}}{\sqrt{\tau o/_\rho}}$ $y = D_e/2$

and substituting into Eq. 134 we have

$$\frac{\hat{u}}{\sqrt{\tau o/_\rho}} = A^* + 2.5 \ln D_e/2\varepsilon$$

Substituting for $\hat{u}$, $\tau o/_\rho$ from equations 137 and 138 we have

$$\sqrt{2/_f} = A^* - 2.5 \ln 2\varepsilon/D_e - 3.75$$

and $f = \dfrac{2}{(A^* - 2.5 \ln \frac{2\varepsilon}{D_e} - 3.75)^2}$ 139

The friction factor, f, can now be found from equations 135, 136 and 139, although it is clear that an iterative method is required since ε^* is friction factor dependent.

The method of iteratively solving the equations is as follows:

(i) the smooth value of f is taken from the expression

$$f = 0.079\ Re^{-0.25}$$

(ii) ε^* is calculated from 135.

(iii) depending upon the value of ε^* the relevant equation from Eq. 136 is used to calculate A*. (N.B. If $\varepsilon^* \lesssim 3.04$ the initial smooth value of f is valid.)

(iv) f is calculated from Eq. 139

The procedure is then repeated from step (ii) until convergence.

Fig 4/23 shows friction factor as a function of Reynolds number for various values of ε/D_e derived from the above equations using a simple FORTRAN program. Typical relative positions of the HTR channel bore and annulus are shown. The ε value is 0.25 mm (the maximum roughness height for a grist particle diameter of 0.5 mm.)

4.4.2 Friction in a rough annulus

(a) The theoretical method

In sub-section 2.2 the Hall transformation method was applied to friction in a smooth annulus to show the validity of smooth tube correlations when applied to an annulus. We will use the same method to deal with an annulus with walls of varying degrees of roughness.

From force balance considerations the following relation has been derived:

$$\frac{f_1 \bar{\rho}_1 \bar{u}_1^2}{De_1} = \frac{f_2 \bar{\rho}_2 \bar{u}_2^2}{De_2} \qquad .....140$$

where the suffixes 1 and 2 apply to inside and outside the no-shear boundary, respectively.

In order to separate the heat transfer and momentum transfer phenomena it is assumed, for simplicity, that $\bar{\rho}_1 = \bar{\rho}_2$

As before:

$$De_1 = 2\,(r_s^2 - r_1^2)/r_1 \qquad .....141$$

$$De_2 = 2\,(r_2^2 - r_s^2)/r_2$$

Therefore

$$\frac{De_2}{De_1} = \frac{r_1\,(r_2^2 - r_s^2)}{r_2\,(r_s^2 - r_1^2)} \qquad .....142$$

Eq. 140 becomes:

$$\left(\frac{\bar{u}_2}{\bar{u}_1}\right)^2 \frac{f_2}{f_1} = \frac{r_1\,(r_2^2 - r_s^2)}{r_2\,(r_s^2 - r_1^2)} \qquad .....143$$

From Hall's work it is obviously reasonable to determine f_1 and f_2 from tube results using transformed values of Reynolds number and hydraulic diameter. If Re_1 and Re_2 are the transformed Reynolds numbers for inside and outside the plane of no shear then:

$$Re_1 = \bar{\rho}\,\bar{u}_1 De_1/\bar{\mu}$$
$$Re_2 = \bar{\rho}\,\bar{u}_2 De_2/\bar{\mu} \qquad .....144$$

Where, as before, we have assumed

$$\bar{\rho}_1 = \bar{\rho}_2 = \bar{\rho}$$

and $\bar{\mu}_1 = \bar{\mu}_2 = \bar{\mu}$

From NIKURADSE (37) for a tube: (Eq. 139)

$$f = \frac{2}{\left(A^*(\varepsilon^*) - 2.5 \ln \frac{2\varepsilon}{De} - 3.75\right)^2}$$

Now for the transformed annulus:

$$f_1 = \frac{2}{\left(A_1^*(\varepsilon_1^*) - 2.5 \ln \frac{2\varepsilon_1}{De_1} - 3.75\right)^2}$$
$$f_2 = \frac{2}{\left(A_2^*(\varepsilon_2^*) - 2.5 \ln \frac{2\varepsilon_2}{De_2} - 3.75\right)^2} \qquad .....145$$

where

$$\varepsilon_1^* = Re_1 \sqrt{f_1/2}\ \ \varepsilon_1/De_1$$
$$\varepsilon_2^* = Re_2 \sqrt{f_2/2}\ \ \varepsilon_2/De_2 \qquad .....146$$

From Eq. 143 and 145 it is possible by iteration to evaluate f_1 and f_2 providing $\bar{u}_2/\bar{u}_1$ the mean velocity ratio can be determined.

WHITE (38) who has also used NIKURADSE'S tube results for annuli implies $\bar{u}_2/\bar{u}_1$ should be made equal to unity. This only applies if the shear stress, and therefore the roughness at the two walls, is not very different.

The case that is investigated by WHITE is one where the inner surface is very rough, and the outer smooth. Such a case is bound to produce significant differences in mean velocity between the two regions.

This limitation can be avoided by deriving velocity profiles in roughened annuli from the transformation of NIKURADSE'S tube results.

These profiles can then be compared with some experimental results for rough annuli with the hope of justifying Hall's transformation theory as applied to this particular case. It will then be possible, using these profiles, to determine the mean velocity ratio and show how friction factors in rough annuli are modified by a consideration of velocity distribution.

In order to determine the mean velocity ratio NIKURADSE'S expression for the velocity profile in a rough or smooth tube is used:

$$u^* = A + 2.5 \ln y \qquad \ldots\ldots 147$$

where, for a rough tube, A is roughness dependent.

Substituting the expression for u* we have

$$\frac{u}{\sqrt{\tau_o/\rho}} = A + 2.5 \ln y \qquad \ldots\ldots 148$$

Eq. 148 should now be transformed to apply to an annulus and in the same way as we define a transformed hydraulic diameter for the annulus we must define a transformed y in Eq. 148:

(i) for a tube:

$y = R - r$

where r is the radial distance from the tube centreline and R is the tube radius.

(ii) for an annulus:

$y_T = R_T - r_T$

where $R_T = \frac{De_1}{2} = \frac{r_s^2 - r_1^2}{r_1}$ (or $\frac{De_2}{2} = \frac{r_2^2 - r_s^2}{r_2}$ for outer surface)

and therefore, as suggested by NICOL (39) it is reasonable to make the analogy:

$$r_T = \frac{r_s^2 - r^2}{r} \quad \left(\text{or } \frac{r^2 - r_s^2}{r} \quad \text{for outer surface}\right)$$

Therefore

$$\frac{u}{\sqrt{\tau o/\rho}} = A + 2.5 \ln (R_T - r_T) \qquad .....149$$

for the plane of no shear ($r_T = 0$)

$$\frac{\hat{u}}{\sqrt{\tau o/\rho}} = A + 2.5 \ln R_T \qquad .....150$$

where $\hat{u}$ is the peak velocity.

By combining Eq. 149 and Eq. 150 we have

$$\frac{u - \hat{u}}{\sqrt{\tau o/\rho}} = 2.5 \ln \left(\frac{R_T - r_T}{R_T}\right) \qquad .....151$$

The mean velocity within the plane of no shear $\bar{u}_1$ is given by:

$$\bar{u}_1 = \frac{2}{R_T^{\,2}} \int_{R_T}^{o} r_T \, u dr_T$$

and substituting Eq. 151 for within the plane of no shear we have

$$\bar{u}_1 = \frac{2}{R_T^{\,2}} \int_{R_T}^{o} r_T \left(2.5 \sqrt{\frac{\tau o}{\rho}}_1 \ln \left(\frac{R_T - r_T}{R_T}\right) + \hat{u}\right) dr_T$$

which gives

$$\bar{u}_1 = \hat{u} - 3.75 \sqrt{\frac{\tau o}{\rho}}_1 \qquad .....152$$

For the outer region:

$$\bar{u}_2 = \hat{u} - 3.75 \sqrt{\frac{\tau_o}{\rho}}_2 \qquad .....153$$

As expected similar expressions to those for a tube are obtained.

Now

$$\sqrt{\frac{\tau_o}{\rho}}_1 = \bar{u}_1 \sqrt{\frac{f_1}{2}}$$

and

$$\sqrt{\frac{\tau_o}{\rho}}_2 = \bar{u}_2 \sqrt{\frac{f_2}{2}}$$

Substituting in Eq. 152 and Eq. 153 we have

$$\bar{u}_1 \left(1 + 3.75\sqrt{f_1/2}\right) = \hat{u} \qquad .....154$$

$$\bar{u}_2 \left(1 + 3.75\sqrt{f_2/2}\right) = \hat{u} \qquad .....155$$

and therefore

$$\bar{u}_2/\bar{u}_1 = \frac{1 + 3.75\sqrt{f_{1/2}}}{1 + 3.75\sqrt{f_{2/2}}} \qquad .....156$$

a further relation between $\bar{u}_2$ and $\bar{u}_1$ can be derived.

If $\bar{u}$ is the mean velocity for the channel then

$$\bar{u} = \frac{2}{(r_2^2 - r_1^2)}\int_{r_1}^{r_2} rudr = \frac{W}{\rho(r_2^2 - r_1^2)}$$

Where W is the channel mass flow rate.

Therefore, since

$$\bar{u}_1 = \frac{2}{(r_s^2 - r_1^2)}\int_{r_1}^{r_s} rudr$$

and $$\bar{u}_2 = \frac{2}{(r_2^2 - r_s^2)}\int_{r_s}^{r_2} rudr$$

Also

$$\int_{r_s}^{r_2} rudr + \int_{r_1}^{r_s} rudr = \int_{r_1}^{r_2} rudr$$

Therefore

$$(r_s^2 - r_1^2)\bar{u}_1 + (r_2^2 - r_s^2)\bar{u}_2 = \frac{W}{\rho} \qquad .....157$$

By the simultaneous solution of equations 141, 142, 144, 145, 146, 156 and 157, it is possible to obtain mutually consistent mean velocity, Reynolds number, hydraulic diameter and friction factor for the two regions of the annulus. The solution of these equations, together with other dependent relations requires digital methods and a simple FORTRAN IV program RUSTAN (Appendix V) has been developed by the Author for this purpose.

(b) Velocity profile and friction factors in rough annuli - some observations

Table 4/4 shows a typical RUSTAN output for a range of annulus flow rates and for various degrees of roughness on the two surfaces. This case applies to the HTR channel annulus where the effects of the ribs have been ignored. The radius ratio is 0.866 and, therefore, one would expect the assumption made in the foregoing - that the peak velocity occurs at the radius of no-shear - to be valid.

As a check upon the programming, the transformed values of friction factor for the particular values of transformed ε/De and Re can be compared with the NIKURADSE results and, as one would expect, they agree within acceptable calculation approximation and convergence limits.

Fig 4/24 shows how the mean velocity within the surface of no-shear $\bar{u}_1$ varies with roughness height and channel Reynolds number. As can be seen, $\bar{u}_1$ increases above the channel mean value (and $\bar{u}_2$ decreases below it) as the roughness on the outer surface increases. The opposite effect is seen with a smooth outer surface and with the roughness on the inner surface increasing.

As one would expect, the greater the Reynolds number the greater the effective roughness and consequently the further $\bar{u}_1$ deviates from $\bar{u}$.

Since we have assumed similar velocity profiles in the two regions the mechanism by which $\bar{u}_1$ and $\bar{u}_2$ change is by a movement of the radius of no-shear.

From Eq. 140 it is clear that if the outer channel roughness increases and f_2/f_1 increases then this must be met by a corresponding change in De_1/De_2 and, or $\bar{u}_2/\bar{u}_1$.

A change in both these ratios is achieved by a movement of the radius of no-shear <u>away</u> from the surface of increasing relative shear stress.

Fig 4/25 demonstrates this phenomenon and also shows how this movement is not so great if the approximation of equal mean velocities is assumed .

To show the deviation from the situation of two smooth surfaces $\bar{r}_s$ has been plotted in Fig 4/25 where:

$$\bar{r}_s = \frac{r_s - r_1}{\sqrt{r_1 r_2} - r_1}$$

In Figs 4/26 and 4/27 the transformed friction factors for the two surfaces are plotted against channel Reynolds number for a smooth inner surface and varying degrees of roughness on the outer surface.

Once again the effect of assuming equal mean velocities inside and outside the surface of no-shear is indicated.

The transformed friction factors are normalised to the effective channel friction factor (F) where:

$$f_{1/F} = \frac{De_1 \, \bar{u}^2}{De \, \bar{u}_1^2} \qquad \text{.....158}$$

and $$f_{2/F} = \frac{De_2 \, \bar{u}^2}{De \, \bar{u}_2^2}$$

Although the approximation of assuming equal mean velocities introduces calculable errors in transformed friction factors (up to about 5%), the effect on F and therefore ΔP, the channel pressure drop, is virtually negligible. This is because the change in f_1 is almost entirely offset by the changes in De_1 and $\bar{u}_1$.

There is very little experimental work carried out on sand-grain type rough annuli, although the work of NICOL (39) can be applied to this case. It is clear from the results quoted in that work that the artificially formed rough surfaces described can be assumed to follow the sand-grain characteristics. They have also shown that transforming the data according to Hall results in a favourable comparison with NIKURADSE'S work .

As predicted by the present theory NICOL shows a movement of the radius of no-shear away from the surface of increasing roughness. However, he states that no appreciable change in r_s was seen with varying Reynolds number, contrary to the present theory and as shown in Fig 4/25.

As the Reynolds number increases the smooth surface friction factor decreases (Fig 4/23) and the effect on rough friction factor depends on the degree of roughness. For the surface of no-shear to remain unchanged it is necessary for f_1/f_2 to remain unchanged, and although this is conceivable over a limited range of Reynolds numbers and roughness heights, it cannot generally be true.

Alternatively it is possible that with varying Reynolds number the velocity profile could alter, compensating for the change of friction factor.

In conclusion one can say that the method described here, applying Hall's transformation theory, adequately predicts the trends and certainly provides, to a good approximation, friction factors in an annulus assuming sand-grain roughness. Any limitations which may be indicated from Nicol's work are probably overshadowed by the assumptions made on the actual form of the roughness.

The final method that calculates the fuel performance throughout life, allowing for corrosion, is considerably simplified if the channel mean velocity can be assumed to apply inside and outside the plane of no shear. It has been shown that the effects of this refinement are small and therefore this simplification has been incorporated in the complete performance code HEATAX III.

4.5 Heat transfer in rough channels

4.5.1 Heat transfer in rough tubes

It has been seen above how surface roughness tends to increase the frictional drag in tubes owing to a destruction of the laminar sub-layer. This increase in turbulence at the surface can also produce large increases in heat transfer. There is very little published data on heat transfer in rough tubes that can be applied to the sand-grain type and probably the most respected is that by DIPPREY and SABERSKY (40). WHITE (38) uses this source in his analysis of heat transfer coefficients in the roughened HTR channel and in the absence of specific experimental data we will follow the example of his limited case and extend to a more general case.

(a) The Dipprey and Sabersky results

DIPPREY (40) has used water as the working fluid and adjusted the bulk temperature to obtain a Prandtl number range of 1.2 to 5.94.

Because of the difficulty in defining the sand-grain roughness height and in order to achieve consistency with the respected NIKURADSE work, DIPPREY defines effective ε/D_e values. These were such that his measured friction factors were identical with the NIKURADSE results over the 'hydraulically fully rough region'. In this way the effective ε/D_e values were calculated to be 0.0488, 0.0138 and 0.0024 respectively.

This normalisation carried out by DIPPREY very conveniently ensures consistancy between the heat transfer coefficients and the ε/D_e relations already derived from NIKURADSE in the previous section.

DIPPREY then considers the similarity between momentum and heat diffusivities and using the Universal Velocity Profile derives a relationship between Stanton number ($h/\bar{\rho}\ \bar{u}\ C_p$) and friction factor:

$$\frac{(f/2St) - 1}{\sqrt{f/2}} + A = g(\varepsilon^*, Pr) \qquad .....159$$

where A is the fully rough value of A* (8.48) and g is dimensionless roughness height and Prandtl number dependent. The Prandtl number dependence was found to be $Pr^{0.44}$ in the fully rough region and Fig 4/28 shows how $gPr^{-0.44}$ (B*) varies with ε^* over the Prandtl number range covered. As the lwest Prandtl number in these results is 1.2 it is necessary to extrapolate to 0.64 the helium value at HTR temperatures.

DIPPREY does make an extrapolation of Prandtl number to 0.72 and it is this $B^*-\varepsilon^*$ relation used by WHITE (38) to deal with the HTR channel.

In following suit, however, it was found that if the limiting value of B* for Pr = 0.72, that is 6.66, was substituted into Eq. 159, then a value of Stanton number was found which was appreciably greater (4%) than the value calculated for some small values of ε^* (e.g. 3.9). Since one would expect the Stanton number to be always increased by roughening, the DIPPREY extrapolation becomes suspect.

This was checked by first plotting the smooth tube values of g derived from Fig 4/28 (see Fig 4/29) and plotting on the same curve the smooth tube value of NUNNER at Pr = 0.72 (air) quoted by DIPPREY. As can be seen, a smooth curve relates well the results of NUNNER and DIPPREY which suggests a value of B^*_{smooth} (Pr = 0.72) of 7.5 not 6.66.

With this smooth value of B* it was found that St (smooth) was always less than St(rough) for Pr = 0.72 and for ε^* greater than 3.5.

It only remained, therefore, to extrapolate further to Pr - 0.64. This was achieved by plotting $B^*_{(Pr=0.72)}$ versus ε^* (from DIPPREY) on a logarithmic scale (Fig 4/30). It was found that two straight lines could be fitted:

$\varepsilon^* > 60$ fully rough region $B^* = 5.58\ (\varepsilon^*)^{0.1865}$ 160

$3.5 \leq \varepsilon^* \leq 60$ transition region $B^* = 6.61\ (\varepsilon^*)^{0.1410}$ 161

From Fig 4/29 the smooth value of B^*, B^*_s, for Pr = 0.64 was found to be 6.64. Therefore:

$$B^*_s\ (Pr = 0.72) - B^*_s\ (Pr = 0.64) = 0.86$$

This difference was assumed to exist at $\varepsilon^* = 3.5$ and a corresponding line to Eq. 161 could be drawn (Fig 4/30). Therefore at Pr = 0.64 for the transition region $B^* = 5.54\ (\varepsilon^*)^{0.1885}$. 162

Eq. 160 and 162 are very similar and to a very close approximation (less than 1% error) Eq. 160 can be assumed to apply over the whole roughness range.

Fig 4/31 shows how Nusselt number varies with Reynolds number for different ε/De values for a Prandtl number of 0.64 derived using the program mentioned in sub-section 4.4.1 where the equations 159 and 160 have been incorporated..

It is clear that factors of two on the smooth Nusselt number can be easily obtained in roughened tubes.

(b) Variations in the coolant – property correction

As described in sub-section 2.1.6 for smooth surfaces, a correction must be applied to the heat transfer coefficient to allow for variations in the coolant properties with radial distance from the surface. This correction would be expected to be different for roughened surfaces.

There is little experimental evidence related to roughened surfaces, but WALKER (41) has carried out comparative studies between rough and smooth rods in smooth channels for CO_2 and N_2 coolants. The rod was roughened by transverse ribs where ε/De was 0.006.

Although the results quoted cannot be directly applied to a helium cooled corrosion induced rough surface any major effects can be determined.

WALKER shows, for N_2, that there is very little difference in the $(^{T}W/T_B)$ index. For CO_2, however, the rough index is a large factor down on the smooth case. By noting the standard deviations, that are also quoted for the CO_2 rough case the difference can be largely explained by the greater experimental error in the rough test.

For the purpose of this work we will assume an unchanged index from the smooth value i.e. -0.15.

4.5.2 Heat transfer in rough annuli

To obtain the heat transfer coefficient on the two surfaces of the annulus, the concept of transformation can again be implemented. The expression derived for a tube describing the effect of roughness on Stanton number (Eq. 159) can be used therefore, providing transformed values are taken.

For the pin surface:

$$St_1 = \frac{f_1}{2\left(\sqrt{\frac{f_1}{2}}\,(g_1 - A)\right)}$$

For the channel wall:

$$St_2 = \frac{f_2}{2\left(\sqrt{\frac{f_2}{2}}\,(g_2 - A)\right)} \qquad \ldots\ldots 163$$

f_1, f_2 are obtained from the equations given in sub-section 4.4.2(a) and g_1 and g_2 are given by

$$g_1 = 5.58\,(\varepsilon_1^*)^{0.1865}\,Pr^{0.44}$$

$$g_2 = 5.58\,(\varepsilon_2^*)^{0.1865}\,Pr^{0.44} \qquad \ldots\ldots 164$$

where ε_1^* and ε_2^* refer to the inner and outer annulus surfaces respectively.

In deriving consistent values of $f_1 \epsilon_1^*$, De_1 etc, as described in sub-section 4.4.2, it was necessary to consider the mean velocity ratio $\bar{u}_1/\bar{u}_2$. Having determined in sub-section 4.4.2(b), however, that this ratio has a small effect on channel pressure drop the effect on surface heat transfer must now be examined.

In Table 4/4 derived from RUSTAN one case is shown where there is a roughness height of 0.4 mm on the pin outer surface and a smooth channel wall. The annulus flow is 0.25 kg/s.

This case has been repeated also using RUSTAN where $\bar{u}_1/\bar{u}_2 = 1$. The table below gives the important parameters for the two cases

	r_s(mm)	$\bar{u}_1/\bar{u}_2$	ϵ_1^*	f_1	St_1
'real'	36.15	0.908	222.34	0.01376	0.005198
$\bar{u}_1/\bar{u}_2 = 1$	36.31	1.0	228.01	0.01350	0.005093

where equations 163 and 164 were used to derive the Stanton numbers.

Now $\quad St_1 = \dfrac{h_1}{\rho \bar{u}_1 C_p} \quad$ and $\quad St_1' = \dfrac{h_1'}{\rho \bar{u}_1' C_p}$

where St_1', h_1' and $\bar{u}_1'$ are derived for the $\bar{u}_1/\bar{u}_2 = 1$ case

Also $\bar{u}_1' = \bar{u}$ which can be derived from Eq. 157, i.e. $\bar{u}_1/\bar{u} = 0.966$.

We obtain therefore:

$$\frac{h_1}{h_1'} = \frac{St_1}{St_1'} \frac{\bar{u}_1}{\bar{u}}$$

and by substitution:

$$\frac{h_1}{h_1'} = 0.986$$

If one remembers that this 1.4% difference applies to a fairly extreme roughness difference across the annulus (0.4 mm/smooth) it is a reasonable approximation to neglect this velocity ratio correction in the determination of heat transfer coefficients in the HEATAX code as has been done in the derivation of friction factors.

So far it has been assumed that the no-heat transfer boundary corresponds to the no-momentum transfer (or no-shear) boundary which can only apply if there are equal heat fluxes from the two surfaces (as described in section 2). Ideally the temperature profile in the annulus should be considered and a radius chosen that gives $\frac{\delta T}{\delta r} = 0$. In the absence of any reliable information on temperature profiles in a rough annulus, for the purposes of this work the heat flux ratio correction term recommended by WILKIE (20) for a smooth annulus are employed here i.e.

$$\left.\begin{array}{l} \text{Outer pin surface:} \\ h_1 = \dfrac{St_1\ Re_1\ Pr\ k}{De_1(1 + 0.25(1 - q''_o/q''_i))} \left(\dfrac{T_{W2}}{T_{g2}}\right)^{-0.15} \\ \text{Channel wall:} \\ h_2 = \dfrac{St_2\ Re_2\ Pr\ k}{De_2(1 + 0.125(1 - q''_i/q''_o))} \left(\dfrac{T_{W3}}{T_{g2}}\right)^{-0.15} \end{array}\right\} \qquad 165$$

4.6 Graphite corrosion effects on channel performance

4.6.1 General approach

It will now be shown how the corrosion mechanisms described in the previous sub-sections affect temperatures, flow, pressure drop and general fuel element endurance.

As before, the method will be applied to the final concept of cylindrical element - the tubular interacting design.

In sub-section 4.1 the basic mechanisms and the corrosion data used were described. Sub-section 4.2 used this data to investigate the planar removal phenomenon and sub-section 4.3 proposed a model to investigate corrosion induced roughening. In 4.4 and 4.5 theory was developed to estimate roughening effects on friction and heat transfer. It now remains to combine the methods developed into a single routine so that the total effect on fuel element performance can be determined.

Corrosion is highly temperature dependent and in a tubular element the flow division between the two passages will, in addition, be corrosion dependent. It is clear therefore that a computer method is required where the effects of the interdependent variables of temperature, flow rate and corrosion can be allowed for simultaneously.

The program HEATAX - II, already used to calculate the effect of thermal expansion on channel performance (section 3), has been further developed (HEATAX - III) to include the relevant corrosion equations given in the sub-sections above. Appendix VII gives a detailed description of the HEATAX series of codes.

In order to assess the effect of corrosion on the peak temperatures in the core, the model will be applied to a peak rated channel. The operating conditions of this channel are given in Table 5/1. The gas conditions are based upon the gagging scheme described in Chapter 3.

As described in Appendix VII HEATAX calculates only the thermal expansion component of the fuel/can interface gap and therefore it is necessary to determine the shrinkage component using AZIMUSTAP (see section 3) for the peak rated channel at each dose step to be considered, and then to assume that this shrinkage component will remain unchanged. As only small changes in fuel temperatures are envisaged within the HEATAX calculation this assumption causes negligible errors.

The fuel channel flow rate is gagged down four times during the fuel dwell after equal intervals of time. The saw-toothed evolution of gas outlet temperature that results is shown in Fig 4/32. In order to determine the precise corrosion effect throughout the dwell it would be necessary to have a large number of steps (24) in the HEATAX calculation, as in the AZIMUSTAP calculation, to describe this evolution. As demonstrated in Appendix VIII, however, HEATAX requires a large amount of data, e.g. shrinkage gaps, fuel and graphite conductivity, to be input at each calculation dose step and it is therefore impractical to have 24 dose steps. To keep the data preparation within reason, seven time steps are taken: one at the start-of-life, one to represent the mean conditions within each gag interval i.e. at the mean temperature point and one at the end-of-life (Fig 4/32).

4.6.2 Data input

The data input to the AZIMUSTAP run is described in Chapter 5 since it is common to more than this section.

The data input to HEATAX-III is shown in Appendix VIII . The origins of the property data used both in the AZIMUSTAP and HEATAX runs are also described in Chapter 5.

For the case studied here, as described above, a calculation is made at the end-of-life. Data at this time is very little different from that at the previous step ($^9/10$ life) and the same data has been assumed to apply.

As described in Chapter 3 the dwell for the peak rated channel for this design is 770 days. Table 4/5 shows how this dwell has been sub-divided into seven steps and gives the equivalent fast neutron doses and the associated operating conditions.

4.6.3 Peak rated channel graphite corrosion - Results

(a) Previous work

There are only two pieces of work known to the author that have been applied to channel performance effects of corrosion, and both of these studies are highly limited. WHITE (38), already quoted in connection with the roughness effects on heat transfer and friction factor, goes on to estimate the approximate effects on channel pressure drop and graphite temperatures. However, no attempt is made to allow for the following effects:

(i) corrosion does occur as a progressive phenomenon over the fuel dwell and it is extremely unlikely that the entire quota of water ingress occurs at the start-of-life, as assumed by WHITE.

(ii) planar removal is a parallel and inter-related phenomenon

(iii) there is a redistribution of heat flow within the fuel element

(iv) the channel wall does corrode at probably a faster rate than the sleeve surfaces and cannot, therefore, be assumed to be smooth

HOUGH (42) allows for items (i) and (iii) but neglects items (ii) and (iv). In addition HOUGH, who uses friction factor and heat transfer data derived from WHITE (38), assumes St(rough)/St(smooth) and f(rough)/f(smooth) relations are dependent upon temperature only, for particular roughness heights. In fact, they will also be dependent upon Reynolds number and hydraulic diameter which change because of roughening. Changes in flow division between bore and annulus have also been neglected by HOUGH.

With such fundamental differences between the present and previous work comparison is difficult, particularly as HOUGH does not quote the channel operating conditions which have been assumed.

(b) Present work

As described in sub-section 4.1, the allowable water ingress is assumed to occur evenly throughout the fuel dwell so that there is a constant 0.1 vpm. In addition, the abrupt changes in temperature caused by gagging are neglected. The resulting fuel element roughnesses, planar removal and temperatures are, therefore, smooth functions of time. In order to estimate the effect on a realistic, gagged, fuel channel these results are adjusted.

So as to obtain the time effect of corrosion two sets of HEATAX runs have been carried out on a peak rated channel:

(i) data as shown in Appendix VIII

(ii) data as shown in Appendix VIII but the time intervals Δt set of zero.

Case (ii) simulates an uncorroded channel.

The HEATAX results for cases (i) and (ii) are shown in Appendix IX. Figs 4/33-4/37 summarise the tabulated results.

(c) Discussions of results

Fig 4/33(a) and (b)

These figures show how planar removal and roughness height vary with axial position and dwell. The high block graphite reactivity explains the 1mm peak removal from the channel wall and it can be seen that the maximum roughness height (0.25 mm) only occurs on the channel wall. The axial distribution of planar removal follows the axial temperature distributions (Fig 4/36) and it is the peak in the inner surface temperature at the 20% height position (enrichment boundary), that is responsible for the small peak in the planar removal.

Fig 4/34 (a)

This figure shows the effect on channel pressure drop. Here we have two compensating effects:

(i) increasing roughness - increasing pressure drop

(ii) increasing planar removal - decreasing pressure drop.

This results in the almost constant increase (approximately 4%) on pressure drop over a large proportion of the dwell.

N.B. On this basis there would be no increase in pumping power, owing to corrosion, as that depends upon peak or start-of-life pressure drop. An increase in pumping power could only occur if a boiler tube started to leak badly just as a peak rated channel was being loaded.

Fig 4/34 (b)

The growth in the outer fuel/can interface gaps relative to the inner gaps (Fig 4/11) results in progressively more heat being forced into the bore. This leads to higher temperatures, lower densities and therefore a higher bore flow resistance. The flow split ratio W(bore)/W(annulus) can be expected to decrease with dwell. This is demonstrated by Fig 4/34(b).

With corrosion there is a general increase of resistance owing to roughening and a decrease arising from planar removal. However, with the significantly larger removals from the channel wall (Fig 4/33) the net effect is a relative increase in bore resistance and at the end of life the flow split ratio has been reduced by 10.0%. This reduction is made up of a 4.5% reduction in bore flow and a 5.5% increase in annulus flow.

Fig 4/35 (a)

In order to determine the corrosion effect, only, on friction factor the initial pressure loop results of cases (i) and (ii) have been compared i.e. the values of W(bore)/W(annulus) are the same for the corroded and uncorroded cases. There are, of course, two friction factors to consider for the annulus in the corroded case - arrived at by the transformation - and Fig 4/35(a) shows a maximum of 37% increase in pin surface friction factor and 54% for the channel wall.

N.B. The maximum friction factor for the channel wall does not occur at the peak corroded position owing to the influence of the outer pin surface.

Fig 4/35 (b)

As with the friction factors, flow split changes are not included in the heat transfer coefficient effects shown. The effect on channel wall heat transfer coefficient is interesting.

At axial heights of about 60% the roughness heights are small enough (30 μm) to have a negligible effect. However, the combined planar removal in the annulus (60 μm) produces a 2% reduction in the coefficient. As the roughness increases the coefficient increases until the maximum roughness is attained at 80% axial position. At this level the maximum increase in coefficient is obtained (20%). Above this level the roughness height remains constant but the planar removal increases sharply (Fig 4/33(a)) decreasing the coefficient until the 100% position is reached when it is 3% below the uncorroded value. A similar effect is noticed on the pin outer surface heat transfer coefficient, although the reduction in coefficient at the 100% position is due to the large amount of planar removal from the channel wall.

Fig 4/36 (a)

As one would expect there is a general decrease in graphite surface temperature due to corrosion. The decrease in annulus temperatures is due to flow split changes as well as heat transfer coefficient increases. It is the flow split effect that causes the increase in inner pin surface temperature at the low axial position levels (less than 55%).

Fig 4/36 (b)

There is an expected decrease in fuel temperatures above the 55% axial position.

Fig 4/37

The temperature effects with life are shown for the peak temperature axial position(%). The maximum temperature reductions occur at the end of life and are as follows:

peak fuel (80%)	31°C
peak pin inner surface (90%)	35°C
peak pin outer surface (90%)	28°C
peak channel wall (100%)	29°C

(d) Application of results

It is now necessary to convert these results, derived from a seven step calculation, to a gagged channel. The starting point is an AZIMUSTAP calculation of the peak rated channel (Chapter 5) which will be termed the reference case.

Table 4/6 gives the temperature reductions, for the peak temperature positions, applying to each of the seven time steps. These results are now interpolated to find the intermediate points. For instance, in the peak inner pin surface temperature case, there is a 14°C reduction at 30% dwell and a 24°C reduction at 50% dwell. It is assumed, therefore, a 19°C reduction at 40% dwell at the second gag change. In such a way Figs 4/38(a), (b) and (c) have been drawn showing the corrosion effect on the gagged peak rated channel graphite surface temperatures and Fig 4/39, similarly, for the peak fuel temperature.

(e) Fuel element endurance

With the assumptions made it is clear that substantial reductions in temperatures can be expected from corrosion, without any penalty on pumping power. This would be encouraging were it not for the uncertainty surrounding the form and development of roughness and planar removal. It has been assumed that the binder has a reactivity three times that of the particle. If the difference is not so large the roughness is reduced, together with the temperature savings. With smooth surfaces the effect of panar removal would produce only small increases in temperature and, as some roughness is inevitable, it is most probable that there will be a net temperature reduction.

With the temperature distributions calculated the effect on endurance can be summarised as follows.

There is a mean reduction in fuel temperature of 19°C over life, which would reduce the likelihood of both 'Amoeba' and 'Pressure' failure of the particle. According to the rules set out in Chapter 2 a 19°C reduction in fuel temperature would lengthen the life of the peak temperature particle by approximately 19%.

A 1 mm removal from the channel wall has a number of effects:

(i) reducing the integrity of the block (There is a 9 mm ligament and therefore a 1 mm loss could have an effect on the mechanical strength.)

(ii) widening the channel by 1 mm increases the amplitude of vibrations of the fuel element

(iii) the pin can bow to a greater extent leading to higher assymetry and higher peak temperatures.

Quantitative answers to (i), (ii) and (iii) will not be given in this work.

4.7 Additional corrosion effects

So far, we have only considered the effect of corrosion on heat transfer from the graphite surfaces. There are two further corrosion phenomena which need consideration:

(i) reduction in graphite conductivity arising from corrosion induced density changes

(ii) changes to the interface gap conductance owing to compact corrosion.

We will consider each of these effects in turn.

4.7.1 Graphite thermal conductivity effects

At the temperatures which are important from a fuel endurance view-point, i.e. the peak or near peak graphite temperatures (1030°C), corrosion takes place very close to the surface. BIRCH (33) shows a corrosion profile for a graphite temperature of 1050°C and 53 atmospheres total pressure and it is observed that less than 1% of corrosion takes place below 250 μm. It can be assumed therefore that weight losses are sufficiently small for this effect to be neglected.

4.7.2 Compact corrosion

Water vapour can gain access to the compact by two routes:

(i) diffusion through the sleeves. (This mechanism only applies if the sleeve temperatures are low enough for the water to escape reaction (less than about 800°C).)

(ii) access through the pin end. (By design, the open pin end is at the downstream or low pressure end of the pin and, therefore in this configuration no water can enter.)

In conclusion, therefore, for the purposes of peak temperature and fuel endurance calculations the compact corrosion effect can be neglected.

CHAPTER 5

TIME AND SPATIAL DISTRIBUTIONS OF FUEL ELEMENT TEMPERATURES

The methods derived in Chapters 3 and 4 can now be employed to derive complete time and spatial distributions of fuel channel temperatures. From Chapter 3 the channel power, axial rating profile and channel gas outlet temperature of each and every channel in the core can be obtained. Chapter 4 using this basic information, presents methods that can be used to obtain the axial and time distributions of fuel channel temperatures for any desired channel.

In this chapter we will first summarise the basic data that has been used in all this work (section 1). In section 2 the computer codes which have been developed to, collectively, include the analytical methods derived in Chapter 4 will be presented together with axial and time evolutions of fuel channel temperatures for a typical channel. Section 3 discusses further systematic effects previously not considered. A method, developed by the Author, to determine whole core temperature distributions from a limited number of single channel calculations will then be described in section 4.

So far we have only considered Best Estimate property, heat transfer, corrosion data etc., and because of the statistical variation of these values precise distributions cannot be evaluated and the final results must be expressed in terms of an Expected Frequency Distribution of Temperature. These aspects will be discussed in section 5.

In conclusion section 6 gives an indication of what these temperatures actually mean in terms of fuel element endurance.

1 A summary of data used

Most of the material property data used has been taken from TRG 1000 (R) (43) i.e. 'Data and Conventions for Mk. III calculation' compiled by the UKAEA from recommendations made by the relevant collaborative working party. Where property data has not been taken from this reference, for example in the corrosion work, this has been referenced separately in the relevant section. Fuel element data; geometry, particle failure criteria etc., are given in Chapter 2 and operating conditions, e.g. channel powers and gas outlet temperatures are given in Chapter 3. Heat transfer and friction factor data can be found in Chapter 4 section 2. A summary of data assumed for the peak rated channel is given in Table 5/1 and includes additional items (e.g. brick and pressure drop losses) not mentioned elsewhere.

As revised data becomes available, from in-pile experiments for example, the relevant section of TRG 1000 (R) (43) becomes re-issued. Table 5/2 lists all these properties together with the issue number at the time of use. Errors associated with this data are discussed in section 5.

2 Axial and time evolutions of fuel channel temperatures

The two programs employed in determining single channel temperatures are AZIMUSTAP 5 and HEATAX III. The former code calculates axial temperature distributions at discrete times in the fuel dwell. The time dependent calculation is described in Chapter 4 sub-section 3.3 and the axial calculation is given in Appendix VI. This final version of AZIMUSTAP, as already noted in Chapter 4, does not include the thermal expansion effect on channel dimensions or the corrosion phenomenon which are discussed in Chapter 4. HEATAX II and III have been written to take account of these two effects respectively. Appendix VII describes the HEATAX series of codes and also gives a listing as programed by the Author.

As HEATAX III only calculates the thermal expansion component of the fuel/can interface gap AZIMUSTAP is needed to produce shrinkage gaps at each axial position and time in life required by the HEATAX run.

In addition, HEATAX only makes a limited number of calculations with time and therefore AZIMUSTAP is also required to describe the saw toothed time evolution caused by gagging.

Chapter 4 sub-section 4.6 describes the general approach.

As an example of axial and time temperature distributions the peak rated channel will be taken, the operating conditions of which are given in Tables 4/1, 5/1.

The axial rating distributions for this channel are shown in Chapter 3. The data input to HEATAX is given in Appendix VIII.

2.1 Axial distributions of temperature

Fig 5/1 shows plots of the important fuel channel temperatures for the start of life of a peak rated channel and have been taken from the HEATAX III output listed in Appendix IX. The reader is referred to the nomenclature (Appendix VII).

The heat split radius (r_i) versus axial position is also shown in Fig 5/1. The initial value of r_i at channel inlet is 23.8 mm indicating 54% of fuel heat generation is passing into the bore of the channel. This percentage increases down the channel since the annulus gas temperature rises at a faster rate than the gas temperature in the bore resulting from the mass flow deficiency in the annulus (Fig 4/34). After the 2m level, the enrichment boundary, $-\partial r_i/\partial_z$ increases sharply, the reason for which is obvious from Chapter 4 equation 6. From this equation it can be seen that r_i^2 is inversely proportional to the heat generation rate q_f''' which of course, decreases immediately below the enrichment boundary. The increase of $\partial r_i/\partial_z$ towards channel outlet is explained by the reduction in rating resulting from thermal neutron flux shape effects (Chapter 3).

The partition of heat in favour of the bore shows itself in the resulting temperature distributions. Those temperatures within the radius of peak fuel temperature follow more closely the axial flux shape than those outside this radius. Consequently the inner tube graphite temperatures (T_{W1}, T_{I1}) exhibit the 'twin peak' effect at the 2m and 4m positions more strongly than the outer tube temperature (T_{W2}, T_{I2}).

Only ten axial slabs were represented in the HEATAX run and consequently in the sharply changing areas between the 2m and 2.5m levels the shape has been drawn by interpolation. There is, however, little justification for decreasing the step length since axial conduction effects at this position will play a significant part.

2.2 Time evolutions of temperature

The distributions of temperature with time were generated in a similar way to that described in Chapter 4 sub-section 4.6 i.e. differences between the HEATAX and AZIMUSTAP temperatures were found for each HEATAX time step, and differences at the intermediate AZIMUSTAP dose step obtained by linear interpolation. In this way a complete time evolution of temperature was obtained which was consistent with the HEATAX method.

Fig 5/2 shows the time evolutions for peak fuel and graphite wetted surface temperature. The relevant axial positions were chosen so that the peak temperature overall was represented. It is interesting to note that the peak temperature occurs at different axial positions at different times i.e. the overall peak values of $\hat{T}_{FP}$ and $\hat{T}_{W1}$ occur just after the first gag change (154 days) at the 4m and 4.5m positions respectively, whereas the peak values of $\hat{T}_{W2}$ and $\hat{T}_{W3}$ occur immediately after loading at the 4.5m and 5.0m positions respectively.

The time evolutions of temperature shown in Fig 5/2 follow in quite a predictable fashion the evolution of channel gas outlet temperature controlled by a four change gag scheme (Chapter 3). The corrosion effect, as already explained in Chapter 4, depresses the distribution towards the end-of-life. (This will have a beneficial effect on particle failure.) The distributions are rather more complicated over the period 0-154 days. As described in Chapter 4 section 3 this period is one of rapid development of the interface gaps. Between 0 and 77 days the inner gap decreases and the outer gap increases forcing more heat into the bore of the channel. This explains the high level of $\hat{T}_{W1}$ and the steep fall of $\hat{T}_{W2}$ and $\hat{T}_{W3}$. Interaction between inner sleeve and fuel occurs towards the end of this period, ($1\text{-}2 \times 10^{20}$ n/cm^2 EDN) slowing down the rate of outer gap growth and hence heat re-distribution. This explains the fall in $\hat{T}_{W1}$ between 77 and 154 days. The minimum (39 days) and maximum (80 days) in the $\hat{T}_{FP}$ distribution can also be explained by the gap development. Initially the growth of the outer gap is offset by the reduction in the inner gap producing a net decrease in $\hat{T}_{FP}$. Once interaction has occurred the outer gap growth begins to take effect by increasing $\hat{T}_{FP}$ until the rate of gap growth reduces and corrosion starts to play a part towards the end of the first gag interval.

3 'Best Estimate' temperatures and other systematic effects

As part of the analysis of the fuel element described in this thesis certain assumptions have been made. The major assumptions are:

(i) One dimensional (radial) heat conduction within the fuel and graphite

(ii) Axial development and symmetry of velocity and temperature profiles in the coolant

Strictly, therefore, in order to obtain the so called 'Best Estimate' temperature allowance should be made for any effects which lay outside these basic assumptions. The most important of these factors are now discussed.

3.1 Fuel pin bowing

Arising from damage dose gradients across the fuel pin differential shrinkage occurs which causes pin bow. The bow is limited by the anti-bowing ribs which interact with the channel wall. The bow causes the annulus flow passage and compact/tube gaps to become eccentric resulting in azimuthal temperature variations within the element and a three dimensional velocity temperature field within the coolant. The calculations of the fuel performance under such conditions becomes highly complex and for the purpose of thesis we will use the results of a simplified case investigated by CONWAY-JONES (44).

This work showed a 25°C increase in overall peak fuel temperature and although there will be a corresponding reduction elsewhere in the pin and the net effect on particle failure will be less than an overall 25°C increase implies we will assume a full 25°C increment.

As far as graphite temperatures are concerned we will assume no net increase due to bowing which is approximately equivalent to taking the azimuthal mean values.

3.2 Across-pin rating gradients

Across-pin gradients are caused by two factors:

(a) Macroscopic radial neutron flux gradient

(b) Fine structure effects of control rods.

The former effect is only really significant towards the edge of the core (Chapter 3) where, in any case, the rating tends to be lower. Close to control rods gradients can be large but again channel ratings will be low.

It is a fair approximation to say that peak rated channels will have low gradients and for the purposes of this work the effect will be neglected.

3.3 Heavy metal density variations

Owing to systematic manufacturing defects the HMD varies axially within a compact by, as quoted by GUILD (45), ± 3%. The resulting perturbations to the axial rating shape cause peaks in temperature which are smoothed to some extent by axial conduction. The net effect on fuel and graphite temperatures is as follows:

$\hat{T}_{FP}$ - $7^{\circ}C$

$\hat{T}_{W1}$ - $9^{\circ}C$

$\hat{T}_{W2}$ - $3^{\circ}C$

3.4 Total systematic increments

The net systematic increments on the peak temperatures are therefore:

$\hat{T}_{FP}$ - $32^{\circ}C$

$\hat{T}_{W1}$ - $9^{\circ}C$

$\hat{T}_{W2}$ - $3^{\circ}C$

$\hat{T}_{W3}$ - $0^{\circ}C$

3.5 Peak 'Best Estimate' temperatures

The 'Best Estimate' peak temperatures for the peak rated channel are therefore defined as the HEATAX III/AZIMUSTAP 5 values (Fig 5/2) plus the increments given above i.e. the peak 'Best Estimate' temperatures over life are:

$$\hat{T}_{FP}(BE) = 1237^{\circ}C$$

$$\hat{T}_{W1}(BE) = 1014^{\circ}C$$

$$\hat{T}_{W2}(BE) = 1048^{\circ}C$$

$$\hat{T}_{W3}(BE) = 1008^{\circ}C$$

4 Channel to channel distributions of temperature

Having obtained complete distributions, both axially and with time, of temperatures for one channel and also determined how the axial peak temperatures must be modified to allow for other systematic effects, the spatial distribution of channel peak temperature will now be evaluated.

We will concern ourselves only with the spatial distribution at one moment in time ('snapshot') of axial peak 'Best Estimate' fuel ($\hat{T}_{FP}$) inner sleeve surface ($\hat{T}_{W1}$), outer sleeve surface ($\hat{T}_{W2}$) and channel wall ($\hat{T}_{W3}$).

The method that has been developed by the Author to evaluate these spatial distributions from single channel calculations will now be described.

4.1 Integral data method

From Chapter 3 the methods for obtaining channel power and gas outlet temperature distributions are discussed and in theory, at least, it is now possible to run single channel temperature calculation programs (e.g. AZIMUSTAP) for each channel to obtain whole core distributions. The expense, however, in terms of computer running times would be prodigious.

The object, therefore, was to derive a correlation between the important fuel element temperatures and channel power and gas outlet temperature. This correlation could then be applied to each channel in turn given its operating conditions.

In order to derive this correlation a number of AZIMUSTAP cases were run covering the range of start-of-life channel power (Q_{CHS}) and channel life mean gas outlet temperature ($\bar{T}_{c2}$) values experienced in an HTR core. From the results, for any desired dose step the values of $\hat{T}_{FP}$, $\hat{T}_{W1}$, $\hat{T}_{W2}$ and $\hat{T}_{W3}$ can be plotted against Q_{CHS} for each value of $\overline{T}_{c2}$ in turn. Fig 5/3 (a) is such a plot for $\hat{T}_{FP}$ at the start-of-life and end-of-life times.

As can be seen the curves are linear to within $5^{\circ}C$. Fig 5/3 (b) shows plots of $\hat{T}_{FP}$ (500 kW) and $\partial \hat{T}_{FP}/\partial Q_{CHS}$ versus $\overline{T}_{c2}$. Linearity is again evident in the former case, whereas in the latter a stright line drawn between the two extreme points results in an accpetable error of 1-1.5% in $\partial \hat{T}_{FP}/\partial Q_{CHS}$ at a $\overline{T}_{c2}$ of $775^{\circ}C$. This analysis suggests the following correlation between $\hat{T}_{FP}$ and Q_{CHS} and $\overline{T}_{c2}$:

$$\hat{T}_{FP} = (A\overline{T}_{c2} + B)Q_{CHS} + C\overline{T}_{c2} + D \qquad .....1$$

In the case of the graphite surface temperatures these are only weakly dependent on channel power. Fig 5/4 illustrates this point where the grahite surface temperatures are plotted against $\overline{T}_{c2}$ for different values of Q_{CHS} i.e.

$$\hat{T}_{W} = C\overline{T}_{c2} + D + f(Q_{CHS})$$

$f(Q_{CHS})$ will be small but to make some allowance for this the relationship given in equation 1 will be assumed, i.e. if $\hat{T}$ is any desired fuel channel temperature then:

$$\hat{T} = (A\overline{T}_{c2} + B) Q_{CHS} + C\overline{T}_{c2} + D \qquad .....2$$

Where the constants A, B, C and D will depend upon the temperature and time considered.

In order to evaluate the constant A, B, C and D only four AZIMUSTAP cases need to be run. For each time step the four peak values of the desired temperature can be plotted against Q_{CHS} for the two values of $\overline{T}_{c2}$ (Fig 5/5). The expression for the constants are therefore seen to be:

$$A = (T_4 - T_3 - T_2 + T_1)/(Q''_{CHS} - Q'_{CHS})(\overline{T}''_{c2} - \overline{T}'_{c2})$$

$$\left.\begin{aligned} B &= (T_2 - T_1)/(Q''_{CHS} - Q'_{CHS}) - A\overline{T}'_2 \\ C &= (T_2 - T_1)/(\overline{T}''_{c2} - \overline{T}'_{c2}) - AQ'_{CHS} \\ D &= T_1 - (A\overline{T}'_{c2} + B)Q'_{CHS} - C\overline{T}'_{c2} \end{aligned}\right\} \quad \ldots\ldots 3$$

A computer program - BATTLEAXE - was written which evaluated the equations, given T_1, T_2, T_3, T_4, $\overline{T}'_{c2}$, $\overline{T}''_{c2}$, Q'_{CHS} and Q''_{CHS}. The constants A, B, C and D so determined are then used by BATTLEAXE to evaluate equation 2 given the values of Q_{CHS} and $\overline{T}_{c2}$ for each channel.

Having determined the relevant peak temperatures for each channel the numbers of channels within a 10° interval are summed and the resulting histogram printed out.

BATTLEAXE was programmed in Functional Language to the Author's specifications by LUXMOORE (46).

4.2 BATTLEAXE input data

The information required is as follows:

(a) Spatial channel power (start-of-life) distribution

(b) Refuelling pattern

(c) Distribution of leaking columns

(d) Gagging pattern

(e) Integral temperature data.

Items (a) → (d) can be obtained from Chapter 3 and are summarised in Table 5/3. We will now discuss the derivation of the integral temperature data.

A set of AZIMUSTAP runs was available which could be applied to the fuel element under consideration. However, owing to data and program changes there were differences between these runs and the current AZIMUSTAP 5/HEATAX III results and although the differences were small it was felt necessary to correct them so as to remain consistent with the rest of the work in this thesis. The four runs covered the channel power range: 300 - 600 kW and the channel $\bar{T}_{c2}$ range 700 - 850°C. Table 5/4 shows these 'nominal' temperatures for each of the ten age groups together with the derived 'Best Estimate' temperatures which, as well as being normalised to the HEATAX III/ AZIMUSTAP results also include the additional systematic mentioned in section 4 above. Two assumptions have been made in normalising the integral data:

(i) The deviations from the 'Best Estimate' can be divided into two categories - power dependent, flow dependent - the correction factors scaled accordingly.

(ii) Corrosion is negligible in all the four AZIMUSTAP cases except 600 kW/850°C when it is as given in Chapter 4 and varies linearly between these two extremes. (This is a major approximation and given more time it would have been desirable to have applied the HEATAX III/AZIMUSTAP 5 model to channels operating over a range of conditions).

4.3 Snapshot temperature histograms

Figs 5/6 - 5/9 show the snapshot distributions of $\hat{T}_{FP}$, $\hat{T}_{W1}$, $\hat{T}_{W2}$ and $\hat{T}_{W3}$. It will be noticed that the peak 'Beat Estimate' fuel temperature over life of 1237°C (sub-section 4.5) is not achieved. This is because the peak channel power of 607 kW includes margins to cover the effects of fuel management.

The histograms of peak outer pin surface and channel wall temperature (Figs 5/8, 5/9) show that there are channels with higher temperatures than the peak rated channel temperatures (sub-section 4.5).

This is because $\hat{T}_{W2}$ and $\hat{T}_{W3}$ are more dependent upon T_2 than channel rating and there are of course channels with higher gas outlet temperatures than that in the peak rated channel.

It will be noticed that the high temperature 'tail' of the histograms is shorter than the tail at the low temperature range. This phenomenon results from a gagging scheme where those columns with high across column gradients are gagged to lower temperatures than those with low gradients. It follows, therefore, that since the lowest, as well as the highest, temperatures occur in the high gradient columns there will be a larger number of low temperature channels.

5 Statistical aspects

5.1 Variations in data input parameters

So far in the analysis only the Best Estimte values of parameters have been considered. In practice, around the most probable value there will be a statistical distribution which will be decided by, for example, manufacturing tolerances or experimental error.

The object of this section is to assess the probability of a temperature occurring in the reactor to replace the 'rigid' histograms presented in the foregoing.

A distinction must be made, initially, between 'within core' and 'whole core' statistical variations.

The 'within core' variations will be termed 'randoms' and originate from statistical variations between points in the reactor. An example would be manufacturing tolerances of the fuel element.

In the 'whole core' case we are thinking in terms of variations which affect the whole core equally. Such variations are defined as 'uncertainties' and would include reactor operating variations.

The purpose of this distinction is so that the 'randoms' can be combined statistically to obtain a modified histogram of temperature within the core, the Expected Frequency Distribution, whereas the 'uncertainties' provide maximum and minimum envelopes to this histogram.

It is not always straightforward, to allocate a factor to one category or the other. Material property variations are an example. They arise from:

(i) the property measurement errors of a material sample

(ii) sample-to-sample differences within the core.

The latter is clearly a 'random' factor and is usually the dominant component. A certain experimental measurement error, however, is constant over the whole core i.e. suggesting it to be an 'uncertainty' factor. This uncertainty will, of course, lead to different increments of temperature within the core arising from, say local rating differences.

Data variations quoted by references (e.g. TRG 1000(R)) are not usually divided into components in this way and only recently have the relevant working parties of the RPC begun to think in these terms.

For material property variations we will use TRG 1000 (R) (43) and assume the whole of the quoted standard deviations to be allocated to the 'random' category.

Variations also occur in channel power and point rating but these can be quite easily defined as 'random' since an overestimation of rating at one point in the core must, necessarily, be associated with a corresponding underestimation elsewhere. This argument equally applies to the estimation of coolant flow rate in various parts of the core for, as with reactor thermal power, total core flow is a design constant. There will, of course, be fluctuations in these constants owing to perturbations in the reactor operation but these will come under the category of 'uncertainty' as mentioned above. The study here will be confined to obtaining the Expected Frequency Distribution of channel peak temperature in an equilibrium core at a particular moment in time ('snapshot') and Table 5/5 lists all the random factors assumed. The standard deviations have been taken from:

(i) GRUNDY (47)

(ii) TRG 1000 (R) (43)

(iii) general TNPG design work (unreported)

The noteworthy omission from Table 5/5 is the variation in corrosion data. According to MERRETT (35) chemical reactivities of gilsocarbon graphite can vary by as much as a factor 10 from sample to sample owing to, for example, the presence of differing quantities of impurity. Such a large variation would dominate other variations to such an extent as to make the statistical analysis highly speculative. The random variations in corrosion rate will therefore be excluded from the temperature standard deviation calculations.

Once the Expected Frequency Distribution has been evaluated, neglecting corrosion randoms, the effect of this distribution on the corrosion of critical components, for the range of graphite reactivities, can be found.

5.2 Combination of 'randoms'

ABERNATHY (48) has shown that if σ_T is the standard deviation on temperature T arising from random deviations in variables u_1, u_2 ....u_n then if the variables are independent:

$$\sigma_T^2 = a_1^2 \sigma_{u_1}^2 + a_2^2 \sigma_{u_2}^2 + - - - a_n^2 \sigma_{u_n}^2$$

where $a_1 = \overline{\partial_T / \partial_{u_1}}$ etc.

We can define $\sigma_T(u_1)$ which is the contribution to σ_T from variable u_1 and :

$$\sigma_T(u_1) = a_1 \sigma u_1$$

$$\therefore \quad \sigma_T = \sqrt{\sigma_T(u_1)^2 + \sigma_T(u_2)^2 + - - - \sigma_T(u_n)^2} \quad .....4$$

As well as knowing the standard deviation of temperature T it is equally important to know the form of its probability distribution. The distributions of the component variables will not all be the same; some will be rectangular, e.g. pin dimensions, whereas others will be closer to a Gaussian distribution e.g. channel power. The only precise way of determining the temperature T probability distribution is to perform a 'Monte-Carlo' calculation. This is where values of each variable are chosen from its distribution in a random fashion and the temperature T calculated. If this is done many thousands of times the distribution of T and its standard deviation can be found accurately.

If one considers, however, the number of variables on which T is dependent and the complexity of the basic calculations this Monte-Carlo method is seen to be a difficult proposition. It has been applied in a limited way by GRUNDY (49) who has determined the probability distribution of various fuel element temperatures resulting from the rectangular distributions of pin dimensions. These temperature distributions are similar to the Gaussian form with, of course, upper and lower cut-offs. These calculations were for just one axial position and if the probability distribution of a temperature T were required which included a combination of all the variables given in Table 5/5 then a whole channel temperature calculation would be necessary. GRUNDY (49) suggests that, assuming 1000 runs, the routine for choosing the values of the variables and performing once the channel temperature calculation should take no longer than 10 secs; the 3 hours total running time being acceptable for a generic study. HEATAX III takes 2.4 secs per time step and therefore lends itself for use in the Monte-Carlo method. Future development of the work in this thesis could, therefore, usefully include such a study.

N.B. By using a Monte-Carlo method which incorporates HEATAX III the large variation in corrosion data could be allowed for correctly.

For the purposes of this work the standard deviation of temperature T will be obtained from equation 4 and its distribution from the Central Limit Theorem described by ABERNATHY (48). This theorem states: The distribution of the sum of n independent random variables asymptotically approaches the normal distribution as n approaches infinity. (It also assumes that no one factor is dominant over the others and if, therefore, the highly dominant corrosion factor were to be included this theorem would not apply). If f_T (T) is the frequency function for temperature T then from the theorem it can be assumed:

$$f_T(T) = \frac{1}{\sigma_T \; 2\pi} \quad \exp\left[-\frac{(T - \bar{T})^2}{2\ \sigma_T^2}\right] \qquad .....5$$

where $\bar{T}$ is the mean value of T. The probability of a temperature oocurring between T_1 and T_2 is given by:

$$P(T_1 \leqslant T \leqslant T_2) = \frac{1}{\sigma_T\sqrt{2\pi}} \int_{T_1}^{T_2} e - \left[\frac{(T - \bar{T})^2}{2\ \sigma_T^2}\right] dT \qquad .....6$$

If in a reactor there are N fuel pins with identical frequency functions $f_T(T)$ as given by equation 5 then the expected number of fuel pins with a temperature between T_1 and T_2 is given by NP $(T_1 \leqslant T \leqslant T_2)$.

In general there will be different values of $\bar{T}$ and σ_T for each fuel pin and the Expected Frequency Distribution of temperature within the reactor can be found by the summation of the probability function (equation 6) for each pin.

Let $\bar{T}_i$ be the mean temperature of Pin i and σ_{T_i} the standard deviation then the expected number of fuel pins within the temperature range $T_1 - T_2$ is:

$$n_{(T_1 - T_2)} = \frac{1}{2\pi} \sum_{i=1}^{i=N} \frac{1}{\sigma_{T_i}} \int_{T_1}^{T_2} e - \frac{(T - \bar{T}_i)^2}{2\,\sigma_{T_i}^{\;2}} \quad dT \qquad .....7$$

5.3 <u>Expected Frequency Distributions of fuel channel temperatures</u>

In order to obtain the component variances $(\sigma_T(u_i)^2)$ of the temperature T variance $(\sigma_T^{\;2})$ the derivatives, a_i, must be derived. Take for example the standard deviation on column power (σ_{QS}).

If the column power is different from design the gag will be adjusted and the only major effect on the fuel temperature will arise from the local rating changing the fuel - gas temperature difference. If Z is the axial position of peak fuel temperature then to a close approximation:

$$a_{QS} = \hat{T}_{FP} - \tfrac{1}{2}\left(T_{W1}(Z) + T_{W2}(Z)\right)$$

since the film drops ($T_{W1} - T_{g1}$, $T_{W2} - T_{g2}$) are only slightly affected if the column gas outlet temperature is maintained by gagging. (From Chapter 4 equations 64, 65, 66, $T_W - T_g \propto \text{flow}^{0.2}$).

Therefore:

$$\sigma_{\hat{T}_{FP}}(u_{QS}) = \sigma_{QS}\left(\hat{T}_{FP} - \tfrac{1}{2}\left(T_{W1}(Z) + T_{W2}(Z)\right)\right)$$

Similarly, values of a_i can be determined for the other random factors and for the other temperatures of interest (i.e. T_{W1}, T_{W2} and T_{W3}). The values of a_i will of course change for a different axial position, irradiation and fuel pin. The component values of $\sigma_T(u_i)$ quoted in Table 5/5 have been derived assuming the peak temperature axial positions and peak temperature times in life for a peak rated channel (Table 5/1). Also given in Table 5/5 are the standard deviations for $\hat{T}_{FP}$, $\hat{T}_{W1}$, $\hat{T}_{W2}$, $\hat{T}_{W3}$ calculated using Eq. 4.

To demonstrate the dependence of σ_T on axial position and irradiation values of standard deviations for the peak fuel temperature in a peak rated channel have been derived for different axial positions (Fig 5/10) and irradiation times (Fig 5/11). As would be expected the value of sigma (σ_T) follows closely the axial rating profile (see Chapter 3). There is little variation of sigma with time as would be predicted by observing the time evolution of peak fuel temperature shown in Fig 5/2.

The Expected Frequency Distribution of channel peak temperatures at one moment in time will be considered and, for simplicity, a value of sigma will be assumed for each of the temperatures (the Table 5/5 values) and assumed constant for all the fuel channels. A program, HISTRAND, has been written by VANDER STEEN (50) which accepts histograms together with the standard deviations and calculates the expected frequency distributions according to the theory given in the previous sub-section. This program has been used, together with the Best Estimate histograms given in Figs 5/6 - 5/9 and the values of sigma given in Table 5/5, to derive Expected Frequency Distributions of fuel channel temperatures in an equilibrium HTR core at one moment in time. These distributions are shown in Figs 5/12 - 5/15 in the form of a number of channels having a peak temperature between T and T + 10^{o}C.

In all these distributions, there has been a shift of 10^{o}C in the 'most common' temperature when compared with the Best Estimate distributions. This shift downwards is caused by the skewed nature of the Best Estimate histograms where, as already pointed out, there are a greater number of channels at temperatures below the 'most common' than there are above it.

The length of the high temperature 'tails' of the Expected Frequency Distributions are highly important in assessing core integrity and safety and this will be discussed in the following section. So as to determine accurately the number of channels within the 'tail' it will be necessary to refer to the tabulated distribution given by the program HISTRAND and listed in Appendix X.

6 Fuel element endurance and integrity

6.1 Temperature limiting criteria

Traditionally, in reactor design calculations the '2σ peak temperature' has been taken as the limiting criterion. This criterion is the peak 'Best Estimate' temperature plus two standard deviations and has been chosen in a more or less arbitrary fashion. Normally, the statistical distributions of temperature have been assumed Gaussian in form and the 2σ limit corresponds to 2.3% of the number exceeding this limit.

For the AGR the limiting temperature is on the stainless steel fuel can gas swept surface, where 825°C is taken as the 2σ temperature criterion. If 2.3% of all channels in the core experience peak temperatures above this temperature the actual proportion of total can surface above the limit is, of course, less since only approximately 1½ pins out of 288 within the cluster are at, or near, the peak value. The 2σ criterion, applied in this way, corresponds therefore to 1 in 10^4 pins at risk which is regarded as acceptable.

It should be noted that an acceptable risk is a purely subjective concept and is merely a compromise between reactor safety and conflicting economic factors.

6.1.1 2σ random temperature limits in the HTR

The 2σ concept is still in use in HTR design work e.g. the specification for the Oldbury B tender requires that, given the most limiting channel from 'amoeba' failure considerations, its peak 2σ random fuel temperature should be such that at the end of its dwell the maximum 'amoeba' failure factor is 1.0 i.e. 'failure' to have just occurred.

Frequency Distribution of temperature which would just meet, with, of course, the necessary uncertainty margins, the activity release and corrosion criteria.

This procedure requires iteration between the temperature calculation and the calculation of the dependent phenomena. The first step in this iteration loop would be to determine the Expected Frequency Distributions of temperature similar to those given in Figs 5/12 - 5/15. From these distributions and other necessary information important parameters could be determined e.g. failed fuel particle fraction and water concentration. The final step would be to calculated the limiting parameters such as rate of release of fission products, local graphite removal etc. Reactor design, or operation, changes can then be made, revising the temperature distributions, so as to approach more closely the limiting criteria.

CHAPTER 6

CONCLUSION

Methods were developed which optimised the core coolant flow distributions. Using these techniques the flow and channel gas outlet temperature distributions were found for the reference core design for the two cases of leaking and non-leaking columns. The channel flow rate and gas outlet temperature evolutions with time were also determined for the peak rated channel.

A single channel was then considered and the temperature distributions were determined within the fuel, can and interface gap.

Derivations of the temperature and velocity profiles were then made within the bore and annulus of the channel and the heat transfer coefficients were determined for developed turbulent flow. These coefficients were then compared with other theoretical and experimental work; in particular with the WILKIE correlations which were used in the thermal performance assessments.

Thermal and irradiation effects on the fuel and can geometry were then dealt with and the mathematical model incorporated in the AZIMUSTAP program. This model made it possible to determine the fuel/sleeve interface gaps at any axial position and at a finite number of time steps throughout the fuel dwell. This method also allowed for the effects of changing channel operating conditions (e.g. gagging) and material properties. Typical results were presented.

The other important phenomenon considered was graphite corrosion which necessitated the specification and writing of a major new computer code, HEATAX. Models were derived to describe the form and development of corrosion attack. The effects on local heat transfer and friction factor within the bore and annulus were assessed chiefly using the experimental results of NIKURADSE (37) and DIPPREY (40). Finally, these models were incorporated within a single channel performance code so that the interplay between corrosion and temperature could be properly determined. The resulting AZIMUSTAP/HEATAX model calculated the complete axial and time dependence of corrosion and temperature within a fuel channel.

Methods were also developed which applied single channel temperature calculations to the whole core. As a result complete spatial distributions of channel peak temperatures at a 'snapshot' time were determined and presented in histogram form. These histograms were further modified to allow for statistical variations in the contributory factors, and Expected Frequency Distributions of peak temperatures were the final result.

NOMENCLATURE

The diversity of subjects tackled in this thesis has necessitated the repetition of certain symbols. In general, the symbols have been defined where they occur, but, in those cases where they have not, their definition will be given here.

d	rib width
De	hydraulic diameter
F	channel friction factor
f_1, f_2	transformed inner, outer annulus friction factor
fa	failed particle volume fraction from 'Amoeba'
f_P	failed particle volume fraction from 'Pressure'
f_T	total failed particle volume fraction
g_{c1}, g_{c2}	cold inner, outer radial interface gaps
k_c	can thermal conductivity (Hollow-rod work)
k_f	fuel thermal conductivity
k_g	graphite thermal conductivity
k_j	interface gap thermal conductance
l	rib height
N	number of ribs
P	gas pressure
q''_1, q''_o	annulus inner, outer surface heat fluxes
R	gas constant
r_i	heat split radius
r_{f1}, r_{f2}, r_{s1}, r_{s2}, r_{s3}	See Fig AVI-1
r_{s1}'	outer radius of inner can
r_{s2}'	inner radius of outer can
T_C	gas temperature at centre of tube

T_{W1}, T_{W2}, T_{W3}) T_{F1}, T_{F2})	See Fig AVI-1
T_{FP}	radial peak fuel temperature
$\hat{T}_{W1}, \hat{T}_{FP}$, etc	axial peak temperatures
T_2	channel, column gas outlet temperature
T_{c2}	channel gas outlet temperature
T^*	temperature rise; $(T - T_o)$
T_o	ambient or 'room' temperature
Z	axial distance from channel inlet
α_f, α_g	fuel, graphite coefficients of thermal expansion

Subscript

c	channel value

TABLES

TABLE 3/1

REACTOR CORE DATA AND OPERATING PARAMETERS

Station electrical output, gross	MW	765
net	MW	734
Reactor thermal output	MW	1803
Fuel channel coolant inlet temperature	^{o}C	300
Fuel channel coolant outlet temperature (core mean)	^{o}C	800
Core power density	MW/m^3	8.43
Diameter over active core	m	7.378
Diameter overall across flats	m	9.315
Length of active core	m	5.00
Across flats dimension of fuel brick	mm	400
Lattice pitch of hexagonal bricks	mm	405
Number of fuel channels		4533
Number of columns containing 17 fuel channels		228
Number of columns containing 9 fuel and 3 absorber channels		73
Total number of: black rods		91
grey rods		91
SSD units		48
Control rod diameter (both types)	mm	87
Uranium density in compact	gm/cc	0.8
Peak channel average dose	n/cm^2 EDN	$2x10^{21}$
Peak channel residence time (75% load factor)	days	770

TABLE 3/2

CHANNEL GAS OUTLET AND FUEL TEMPERATURE
DEPENDENCE ON THE NUMBER OF GAG CHANGES

Peak rated channel life mean gas outlet temperature 852°C.

Number of gag changes	Peak gas outlet temperature (°C)	Peak (AZIMUSTAP) fuel temperature (°C)
0	951	1269
1	898	1230
2	882	1216
3	874	1207
4	869	1204

TABLE 3/3

PEAK FUEL ELEMENT TEMPERATURES AND PARTICLE FAILURE FACTORS FOR FOUR AND NO GAG CHANGE SCHEMES (PEAK RATED CHANNEL)

No. of gag changes	$\bar{T}_g$ ^oC	$\hat{T}_{FP}$ ^oC	$\hat{T}_{W1}$ ^oC	$\hat{T}_{W2}$ ^oC	$\hat{T}_{W3}$ ^oC	F	f_a (%)	f_p (%)	f_T (%)
4	852	1204	1009	1035	995	1.011	0.031	1.289	1.320
0	852	1269	1093	1130	1095	1.184	5.016	0	5.016
0	832	1249	1070	1107	1070	0.997	0	0	0

(see Nomenclature)

TABLE 3/4

PEAK FUEL AND GRAPHITE TEMPERATURE EFFECTS OF VARIOUS SPATIAL GAGGING OPTIONS

Gagging option	$\hat{T}_{FP}$ ^oC	$\hat{T}_{W1}$ ^oC	$\hat{T}_{W2}$ ^oC	$\hat{T}_{W3}$ ^oC
12 group	1189	1010	1035	998
1	1151	1017	1044	1017
2	1171	992	1019	990
3	1172	994	1017	988

(See Nomenclature)

TABLE 4/1

FUEL ELEMENT PARAMETERS AND BOUNDARY CONDITIONS
TUBULAR INTERACTING ELEMENT

Peak rated channel (start-of-life) Peak rated position
(2 m from inlet)

Operating conditions:			
Channel power	Q_{CHS}	607	kW
Mixed gas outlet temperature	T_{C2}	869	°C
Active core height	L	5.0	m
Volumetric rating	q'''_f	0.1396	W/mm^3
Dimensions:			
Bore radius	r_{s1}	15.05	mm
Fuel inner radius	r_{f1}	20.15	mm
Fuel outer radius	r_{f2}	27.50	mm
Annulus inner radius	r_{s2}	32.60	mm
Channel radius	r_W	37.90	mm
Thermal conductivities:			
Fuel	k_f	28.5	W/m°C
Inner graphite sleeve	kg	41.0	W/m°C
Outer graphite sleeve	kg	43.1	W/m°C
Typical AZIMUSTAP results:			
Heat split radius	r_i	24.46	mm
Temperatures:			
Inner gas	T_{g1}	485	°C
Outer gas	T_{g2}	605	°C
Inner sleeve surface	T_{W1}	855	°C
Outer sleeve surface	T_{W2}	835	°C
Inner interface surface	T_{I1}	945	°C
Outer interface surface	T_{I2}	882	°C
Inner fuel surface	T_{F1}	1041	°C
Outer fuel surface	T_{F2}	1060	°C
Peak fuel	T_{FP}	1085	°C
Interface gaps:			
Inner radial gap	$g_1(o)$	68.8	μm
Outer radial gap	$g_2(o)$	202.5	μm

TABLE 4/2

'HOLLOW ROD' DATA FOR PLANAR REMOVAL ASSESSMENT

Reactor pressure		53	bars
Linear rating	q''_T	805.5	W/cm
Channel flow rate	W	0.159	kg/s
Channel radius	r_C	66.5	mm
Fuel sleeve outer radius	r_o	52.0	mm
Bulk gas temperature (T_o = 1099°C)	T_g	866	°C
Bulk gas temperature (T_o = 1054°C)	T_g	815	°C
Bulk gas temperature (T_o = 988°C)	T_g	744	°C

TABLE 4/3

VALUES IN THE EVALUATION OF PLANAR REMOVAL EFFECTS

T_o = 1054°C

$^b/_T$	T (°C)	$\bar{E}_1(^b/_T)$ x 10^{-5}	$e^{\,b/T}$ x 10^{-6}	t (days)
15.2	1054	2.829	3.993	0
15.1	1063	2.578	3.613	533
15.0	1072	2.350	3.269	1021
14.9	1081	2.142	2.958	1471
14.8	1090	1.952	2.676	1885
14.7	1099	1.779	2.422	2257

(See Chapter 4 sub-section 4.2.1 for nomenclature)

TABLE 4/4

RUSTAN RESULTS

RUSTAN RESULTS

RC1 RC2 (M)
0.0326 0.0379

FLOW	EH1	EH2	RE1	RE2	RE	DE1	DE2	RM	UR	E*1	E*2	F1	F2
0.0500	0.0010	0.0010	14707	14706	14707	10.60	10.60	35.15	1.000	0.08	0.08	0.00654	0.00654
0.0500	0.0010	0.1000	14022	15295	14707	10.04	11.08	35.02	1.011	0.08	8.69	0.00703	0.00753
0.0500	0.0010	0.2000	12877	16280	14707	9.10	11.89	34.80	1.033	0.08	19.37	0.00718	0.01001
0.0500	0.0010	0.4000	11435	17521	14707	7.90	12.92	34.52	1.068	0.09	45.11	0.00741	0.01384
0.0500	0.1000	0.2000	13590	15666	14707	9.68	11.39	34.94	1.021	9.04	19.61	0.00829	0.01016
0.0500	0.1000	0.4000	12160	16897	14707	8.48	12.43	34.65	1.055	9.43	45.66	0.00864	0.01410
0.2500	0.0010	0.0010	73533	73532	73535	10.60	10.60	35.15	1.000	0.34	0.34	0.00475	0.00475
0.2500	0.0010	0.1000	58783	86219	73535	8.23	12.64	34.60	1.047	0.36	44.18	0.00498	0.00839
0.2500	0.0010	0.2000	52825	91344	73535	7.26	13.48	34.37	1.074	0.37	100.25	0.00511	0.01094
0.2500	0.0010	0.4000	47727	95729	73535	6.42	14.20	34.17	1.103	0.38	226.22	0.00523	0.01407
0.2500	0.1000	0.2000	67453	78762	73535	9.59	11.47	34.91	1.025	47.86	104.69	0.00926	0.01162
0.2500	0.1000	0.4000	62091	83374	73535	8.68	12.25	34.70	1.051	49.59	235.68	0.00961	0.01459
1.2000	0.0010	0.0010	352956	352956	352967	10.60	10.60	35.15	1.000	1.28	1.38	0.00345	0.00345
1.2000	0.0010	0.1000	240938	449310	352967	6.90	13.78	34.28	1.072	1.51	212.89	0.00372	0.00853
1.2000	0.0010	0.2000	218530	468583	352967	6.15	14.43	34.10	1.095	1.55	474.29	0.00379	0.01067
1.2000	0.0010	0.4000	196093	487883	352967	5.39	15.08	33.92	1.125	1.60	1071.77	0.00387	0.01372
1.2000	0.1000	0.2000	328049	374380	352967	9.73	11.34	34.95	1.021	233.42	503.96	0.00960	0.01166
1.2000	0.1000	0.4000	301672	397069	352967	8.80	12.15	34.73	1.048	241.42	1134.37	0.00992	0.01505
0.2500	0.1000	0.0010	88610	60564	73535	13.03	8.51	35.71	0.956	43.81	0.35	0.00830	0.00455
0.2500	0.2000	0.0010	94997	55070	73535	14.08	7.61	35.95	0.932	99.02	0.36	0.01077	0.00505
0.2500	0.4000	0.0010	100472	50360	73535	14.99	6.82	36.15	0.908	222.34	0.38	0.01376	0.00516
0.2500	0.2000	0.1000	79687	68239	73535	11.63	9.72	35.39	0.976	104.24	47.65	0.01156	0.00921
0.2500	0.4000	0.1000	85224	63476	73535	12.57	8.91	35.60	0.951	233.57	49.15	0.01483	0.00951

(See Appendix V for nomenclature)

TABLE 4/5

TIME DEPENDENT DATA USED IN CORROSION ASSESSMENT

% dwell	Dose n/cm^2 x 10^{-20}	Q_{CH} (kW)	T_2 (°C)	W_1 g/s	W_2 g/s	Δt days
0	0	607	869	117.0	88.58	0
10	2.0	589	852	115.7	89.66	77
30	6.0	551	852	107.9	84.62	154
50	10.0	514	852	100.4	79.15	154
70	14.0	477	852	93.03	73.59	154
90	18.0	440	852	85.79	67.91	154
100	20.0	422	835	84.73	67.18	77

Q_{CH} Channel power

T_2 Mean channel gas outlet temperature

W_1 Bore flow rate

W_2 Annulus flow rate

Δt Time increments

TABLE 4/6

CORROSION EFFECTS ON PEAK TEMPERATURES

% dwell	Corrosion temperature reductions °C			
	$\Delta \hat{T}_{FP}$	$\Delta \hat{T}_{W1}$	$\Delta \hat{T}_{W2}$	$\Delta \hat{T}_{W3}$
0	0	0	0	0
10	0	0	0	2
30	14	14	8	9
50	22	24	18	18
70	28	31	23	24
90	30	35	28	27
100	31	35	28	29

TABLE 5/1

A SUMMARY OF DATA RELATING TO THE PEAK RATED CHANNEL
(also see TABLE 4/1)

Channel flow: life mean/life peak	kg/s	0.180/0.205
Channel gas outlet temperature: life mean/life peak	^{o}C	852/869
Fraction of active core height containing fuel		0.94
Cold inirradiated radial fuel sleeve interface gaps inner/outer	μm	150/100
Coolant inlet pressure	bars	55.2
Fraction of channel power generated in moderator		0.08
Velocity head losses owing to discontinuities etc: bore/annulus		1.4/4.5
Fuel/sleeve interface conductance (nominal zero gap) (TRG 1000(R) (43))	$W/m^{2o}C$	2×10^4

TABLE 5/2

MATERIAL PROPERTY DATA (DERIVED FROM TRG 1000(R) (43))

Property		Issue
Coefficient of thermal expansion:	compact	2
	graphite	2
Creep constant:	compact	1
	graphite	1
Thermal conductivity:	compact	3
	graphite	1
Wigner shrinkage:	compact	3
	graphite	1
Young's modulus:	compact	1
	graphite	1
Helium thermodynamic properties:		
Density		1
Specific heat (constant pressure)		1
Thermal conductivity		1
Viscosity (dynamic)		1

TABLE 5/3

COLUMN RATING AND COOLANT TEMPERATURE DATA REQUIRED FOR BATTLEAXE

(See Chapter 3-4.2 for nomenclature)

Age group	Column No.	$\bar{R}$	G	L	F	$\bar{T}_2$	Age group	Column No.	$\bar{R}$	G	L	F	$\bar{T}_2$
1	41	909	1.0932	1	2	782		45	936	1.0689	1.035	2	782
	75	994	1.0248	1.035	1	819	6	132	1104	1.0153	1.035	1	819
	94	1059	1.0125	1.035	1	819		46	1028	1.0162	1.035	1	819
	77	1022	1.0223	1.035	1	819		8	1069	1.1019	1	1	754
	30	926	1.0357	1.035	1	819		80	1100	1.0101	1.035	2	819
2	114	1033	1.0638	1.035	2	782		48	1022	1.0294	1.035	1	819
	31	983	1.028	1.035	1	819	7	42	1009	1.055	1.035	1	782
	115	1124	1.012	1.035	1	819		59	993	1.023	1.035	1	819
	63	1074	1.0126	1.035	1	819		44	945	1.0306	1.035	1	819
	33	989	1.0375	1.035	1	819		6	936	1.0662	1	1	782
3	3	1034	1.0937	1	1	782		78	991	1.0655	1.035	2	782
	57	991	1.0627	1.035	1	782	8	7	1047	1.1327	1	1	754
	28	1048	1.0993	1	1	782		79	1083	1.0142	1.035	1	819
	16	1005	1.1433	1	1	754		32	1008	1.0224	1.035	1	819
	95	1048	1.0265	1.035	1	819		9	1009	1.0626	1.035	1	782
4	61	1015	1.0191	1.035	1	819		10	1021	1.042	1	1	819
	151	1064	1.0552	1.035	3	782	9	58	937	1.0404	1.035	1	819
	62	1057	1.0139	1.035	1	819		76	1032	1.0107	1.035	2	819
	19	1118	1.0414	1.035	2	819		60	994	1.028	1.035	1	819
	1	1020	1.119	1	1	754		17	934	1.0889	1.035	2	782
5	2	947	1.1474	1	2	754		96	1065	1.0176	1.035	1	819
	27	1015	1.1042	1	1	754	10	18	1073	1.05	1.035	1	782
	43	1099	1.0422	1.035	2	819		97	1105	1.0126	1.035	1	819
	29	1037	1.0598	1.035	1	782		47	1048	1.0136	1.035	2	819
	113	1069	1.0209	1.035	1	819		20	933	1.05	1.035	1	782
								21	895	1.0648	1.035	2	782

L = Leakage flow deficit
F = 1, 17 fuel channels
F = 2, 9 fuel channels
F = 3, 3 fuel channels (centre channel in sextant representation)

TABLE 5/4

INTEGRAL FUEL ELEMENT TEMPERATURES REQUIRED FOR BATTLEAXE

Age group	Channel power kW	Channel $\bar{T}_2$ ^oC	$\hat{T}_{FP}(^oC)$		$\hat{T}_{W1}(^oC)$		$\hat{T}_{W2}(^oC)$		$\hat{T}_{W3}(^oC)$	
			Nominal	Normalised	Nominal	Normalised	Nominal	Normalised	Nominal	Normalised
1	600	850	1180	1213	1003	1004	1032	1039	991	996
	600	700	1014	1048	823	822	850	856	804	808
	300	850	1063	1080	977	977	1006	1014	985	991
	300	700	899	916	799	798	827	833	800	804
2	600	850	1168	1202	998	1001	994	995	950	945
	600	700	1004	1039	821	821	824	826	776	774
	300	850	1044	1061	962	964	982	984	958	956
	300	700	889	906	786	786	811	813	784	782
3	600	850	1199	1231	1014	1014	1015	1006	971	957
	600	700	1027	1067	841	843	833	830	785	779
	300	850	1070	1090	980	986	1002	998	977	968
	300	700	908	928	802	804	825	822	797	791
4	600	850	1183	1212	993	987	995	978	950	926
	600	700	1019	1063	825	827	815	809	768	758
	300	850	1053	1075	959	966	982	974	956	942
	300	700	893	915	789	791	808	802	779	769
5	600	850	1201	1230	1008	1002	1019	993	974	941
	600	700	1036	1084	837	844	832	823	785	771
	300	850	1069	1093	980	992	1004	992	979	960
	300	700	906	930	805	812	823	814	794	780
6	600	850	1183	1210	987	979	1000	967	953	913
	600	700	1023	1073	819	828	816	806	768	753
	300	850	1049	1064	960	975	985	971	958	937
	300	700	891	916	792	801	806	796	775	760
7	600	850	1195	1220	1005	997	1023	986	975	930
	600	700	1034	1085	832	843	833	821	783	766
	300	850	1068	1093	978	996	1007	991	978	955
	300	700	902	927	807	818	822	810	788	771
8	600	850	1174	1194	987	976	1004	962	954	904
	600	700	1018	1067	820	832	817	804	767	749
	300	850	1053	1078	960	979	987	969	959	934
	300	700	888	913	795	807	805	792	773	755
9	600	850	1186	1203	1006	995	1026	982	975	931
	600	700	1028	1075	835	843	834	822	781	769
	300	850	1074	1098	979	999	1009	992	979	962
	300	700	903	927	809	822	821	809	787	775
10	600	850	1164	1179	989	975	1006	959	953	901
	600	700	1008	1054	824	837	817	804	764	747
	300	850	1054	1077	962	982	989	971	958	934
	300	700	889	912	797	810	805	792	770	753

TABLE 5/5

LIFE PEAK VALUES OF STANDARD DEVIATION FOR THE PEAK FUEL AND GRAPHITE TEMPERATURES

Prime mover	σ	$\sigma_T(u)$ °C			
		$\hat{T}_{FP}$	$\hat{T}_{W1}$	$\hat{T}_{W2}$	$\hat{T}_{W3}$
Physics uncertainties:					
(i) Column power	0.045	9	2	2	0
(ii) Across column rating gradient	0.02	18	14	15	14
(iii) Axial power distribution	0.04	17	11	3	1
(iv) Fraction of heat generated in moderator	0.01	4	3	1	0
(v) Control rod position	(47)	10	7	7	2
(vi) Across pin rating gradient	0.01	4	3	1	0
(vii) Fast neutron dose	0.19	8	7	7	0
Flow uncertainties					
(i) Flow division between channels	0.02	14	14	15	14
(ii) Flow division between sub channels	0.02	14	14	15	14
(iii) Flow leakage	0.01	7	11	11	10
Material property uncertainties:					
(i) Compact CTE	0.10	2	2	2	0
(ii) Tube CTE	0.10	3	2	2	0
(iii) Compact shrinkage	0.13	6	5	5	0
(iv) Tube shrinkage	0.15	1	1	1	0
(v) Compact conductivity	0.19	10	0	0	0
(vi) Tube conductivity	0.10	7	0	0	0
(vii) Compact emmissivity	0.04	2	1	1	0
(viii) Tube emmissivity	0.04	2	1	1	0
Additional uncertainties:					
Heat leakage	0.005	1	0	0	0
Column mean T_2	(47)	10	10	10	10
Pin end effects	(47)	5	5	5	0
Column mean T_1	(47)	2	2	2	2
Bowing	(47)	10	10	10	0
Anti-bowing ribs	(47)	3	3	3	0
Fuel/sleeve interface resistance	0.3	2	0	0	0
Dimension tolerances	(49)	10	7	7	0
Fuel enrichment	0.01	4	3	1	1
Fuel heavy metal density	0.02	9	6	2	1
	σ_T	44.5	36.3	35.2	28.3

Note: Where σ components not given see given references

FIGURES

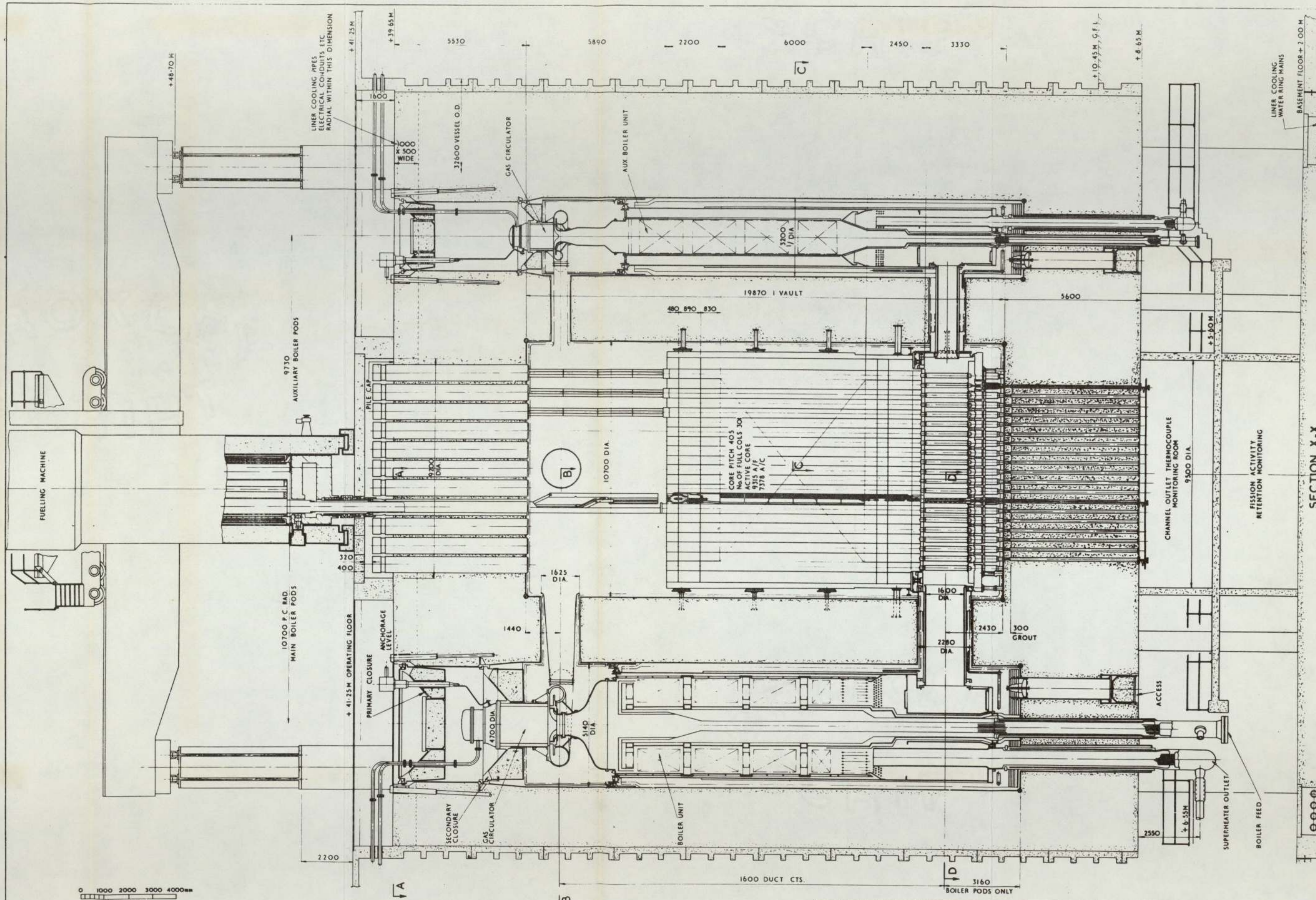

GENERAL ARRANGEMENT OF HTR CORE

FIG 1/1

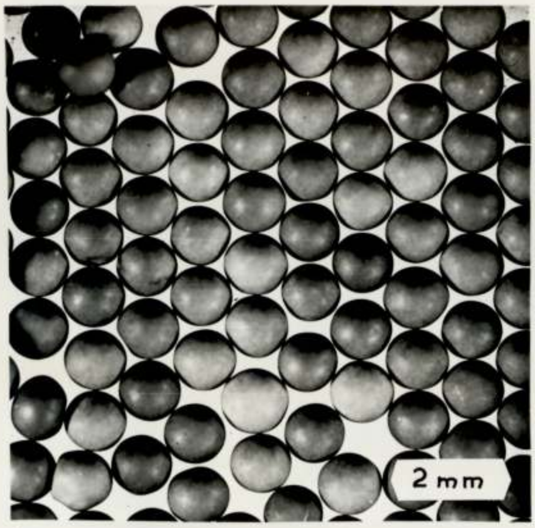

A THE SUPERFICIAL APPEARANCE

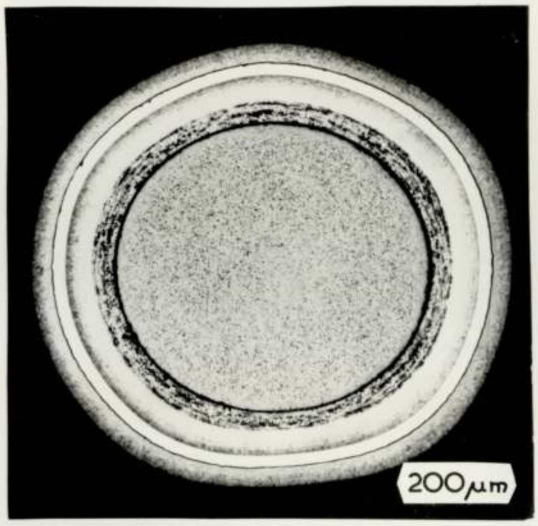

B A POLISHED SECTION

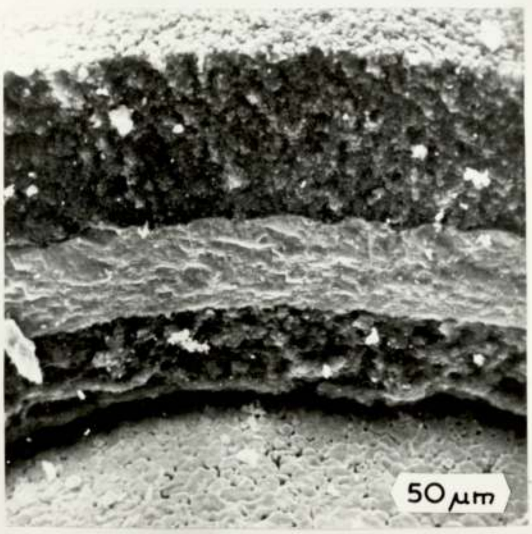

C THE FRACTURE SECTION OF A COATING BY "STEREOSCAN"

THE COATINGS ON A DRAGON FUEL PARTICLE

THE COATED PARTICLE	FIG 2/1

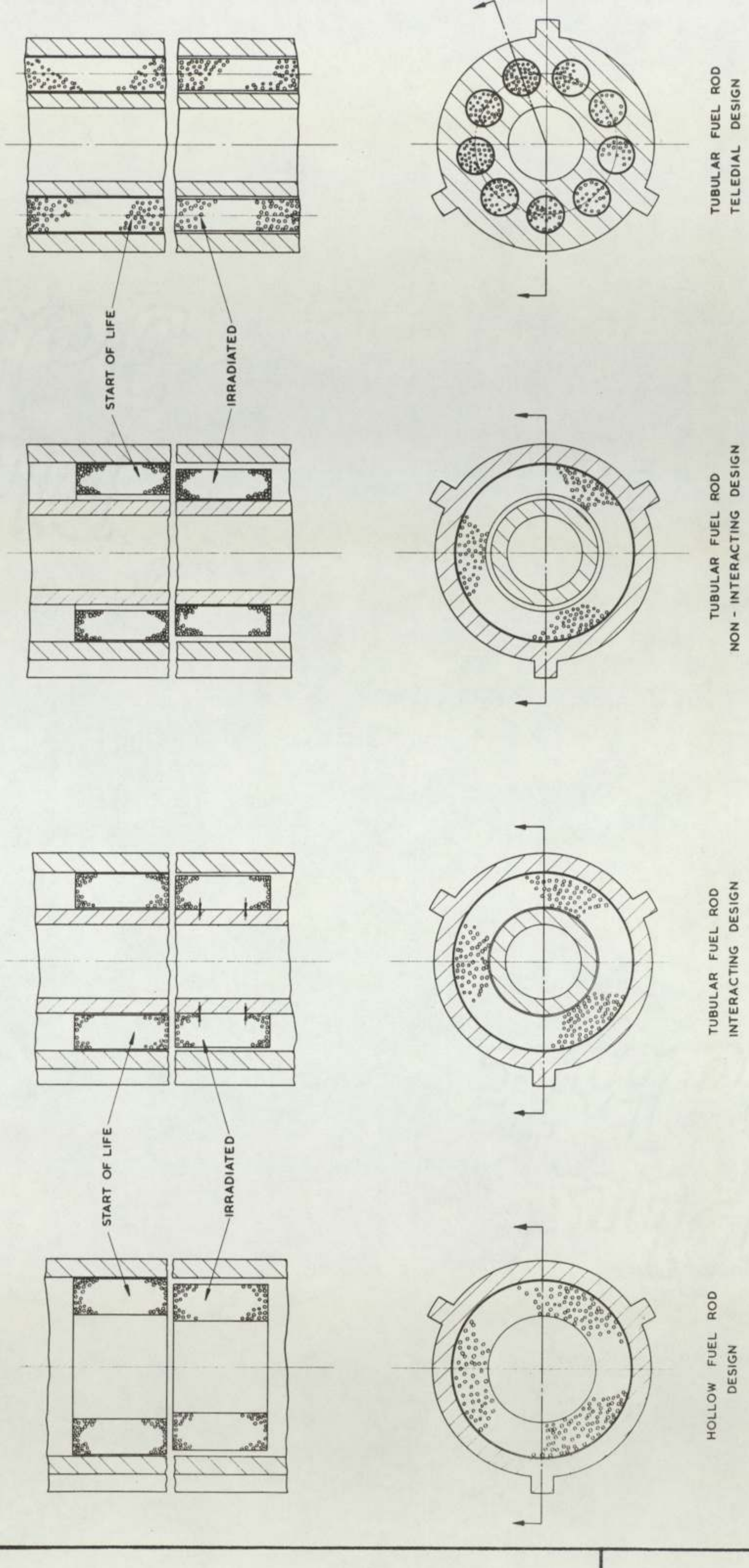

FUEL PIN DESIGN CONCEPTS	FIG 2/2

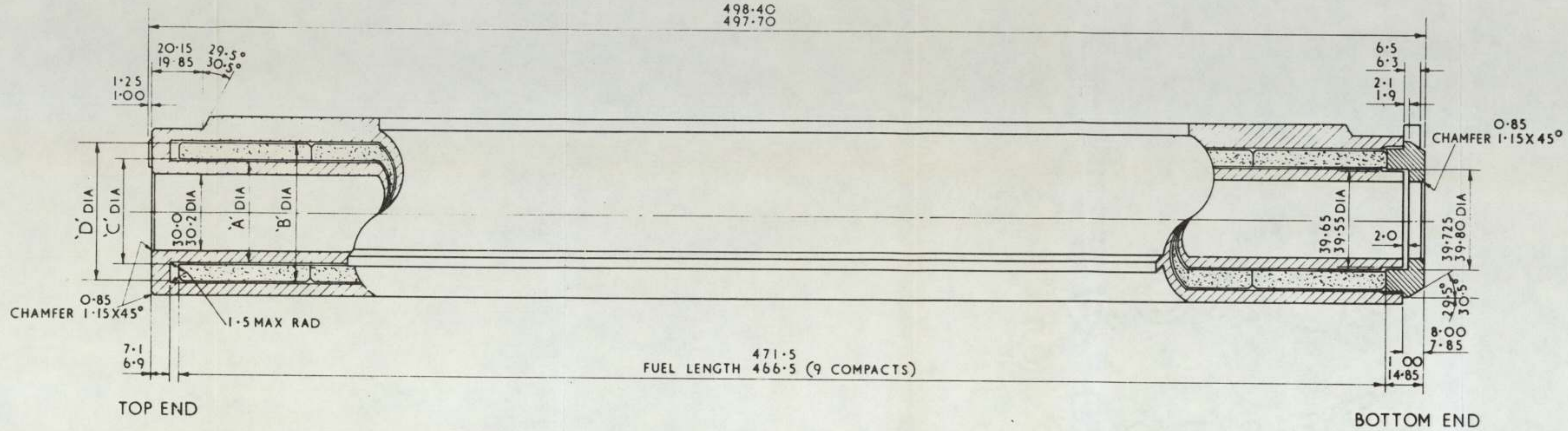

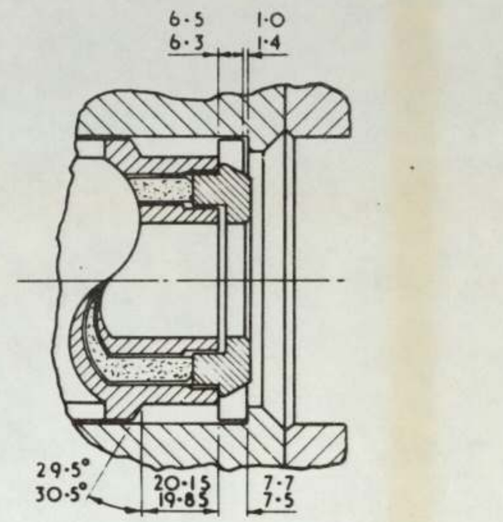

SECTION 'X-Y' SHOWING FUEL PIN IN CHANNEL

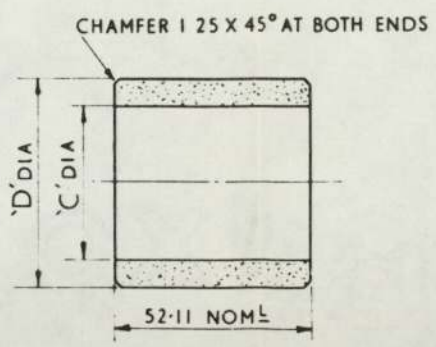

FUEL COMPACT

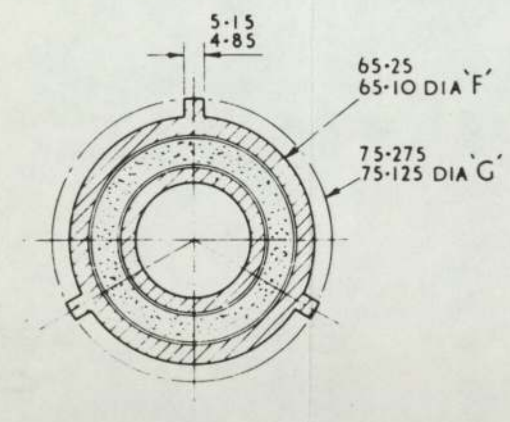

TYPICAL SECTION THROUGH FUEL PIN

THE TUBULAR INTERACTING FUEL ELEMENT	FIG 2/3

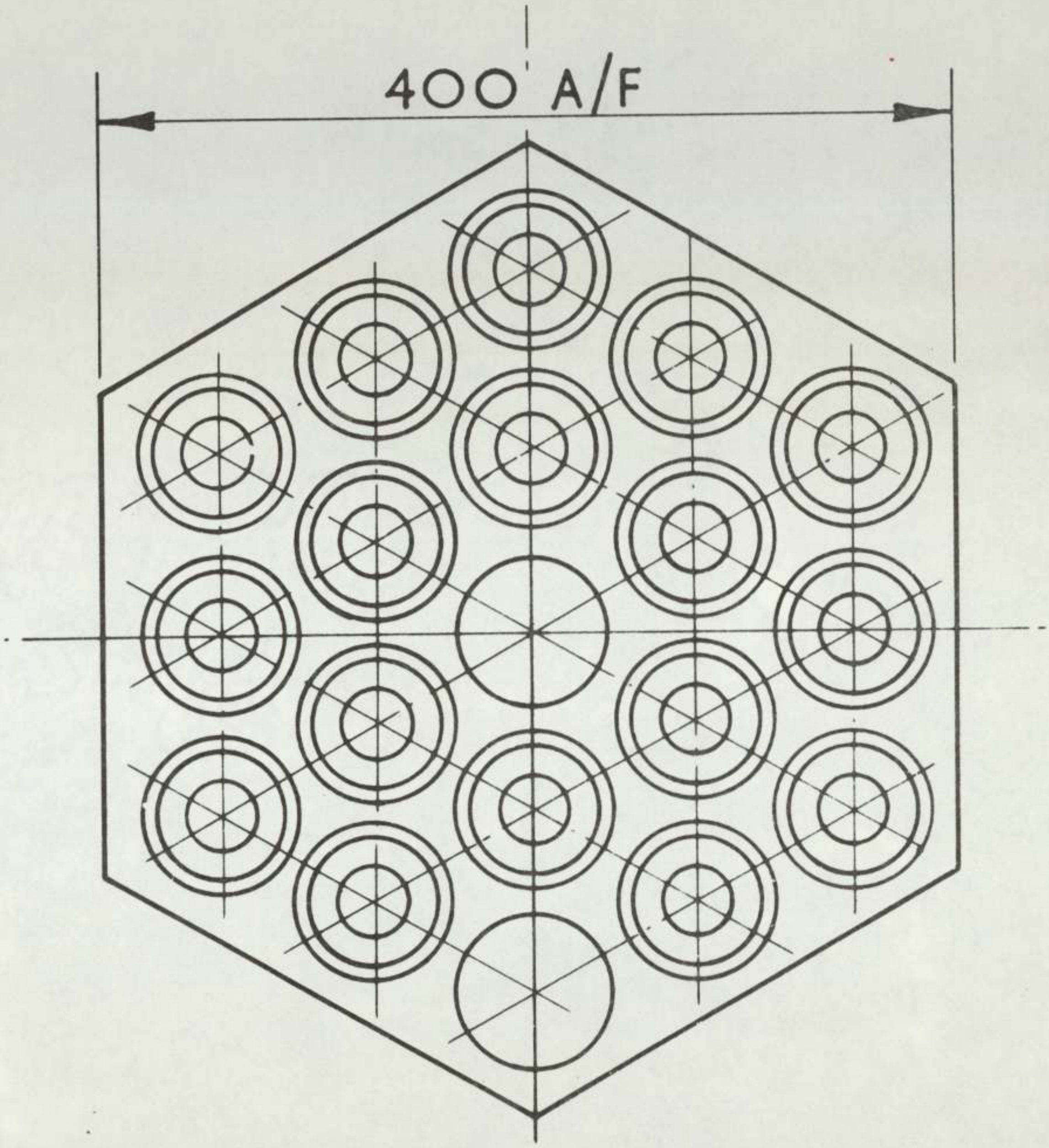

OLDBURY 'B' FUEL BRICK	FIG 2/4

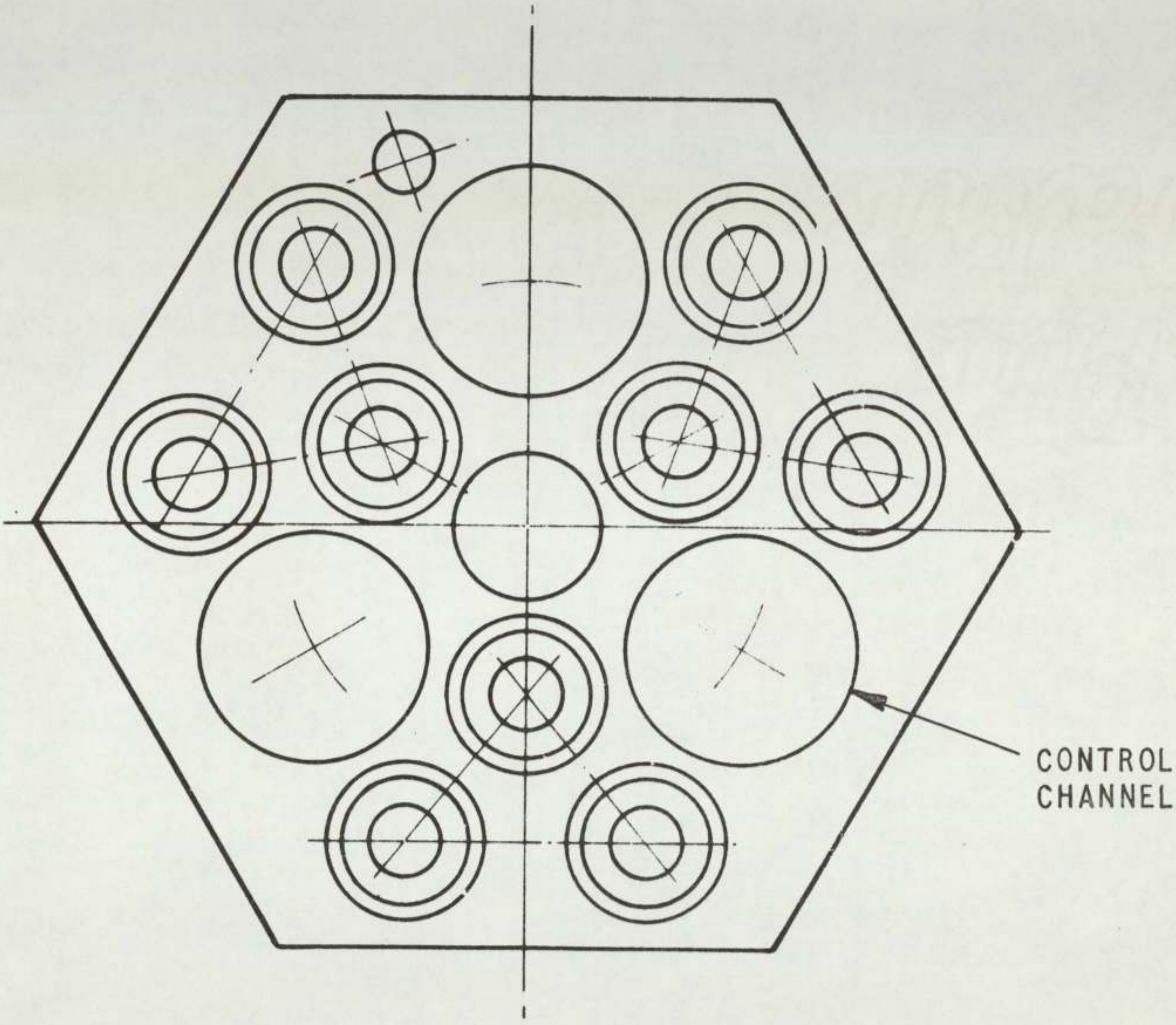

OLDBURY 'B' CONTROL BRICK	FIG 2/5

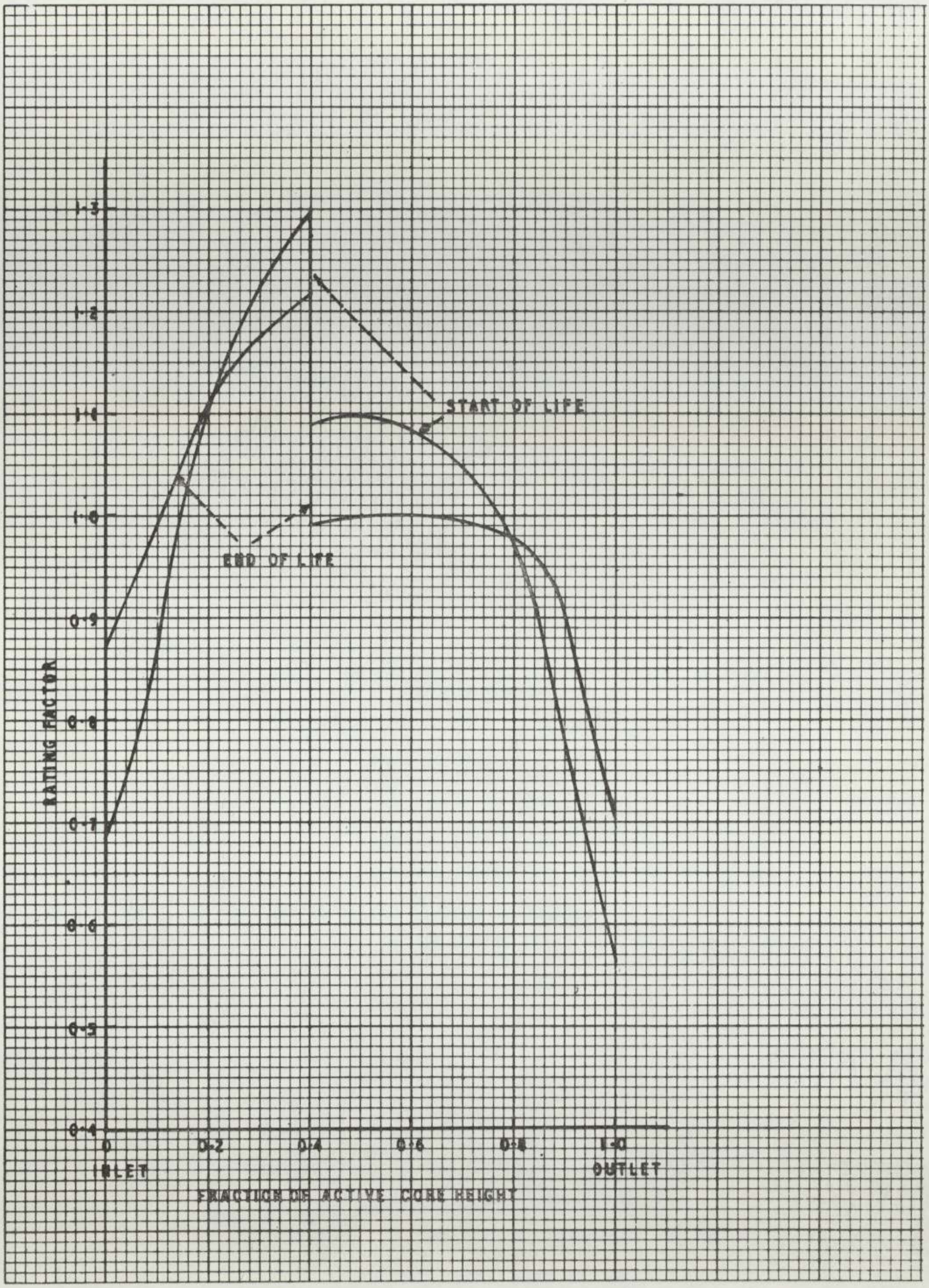

AXIAL RATING PROFILES AT THE START AND END OF LIFE OF A PEAK RATED CHANNEL	FIG 3/1

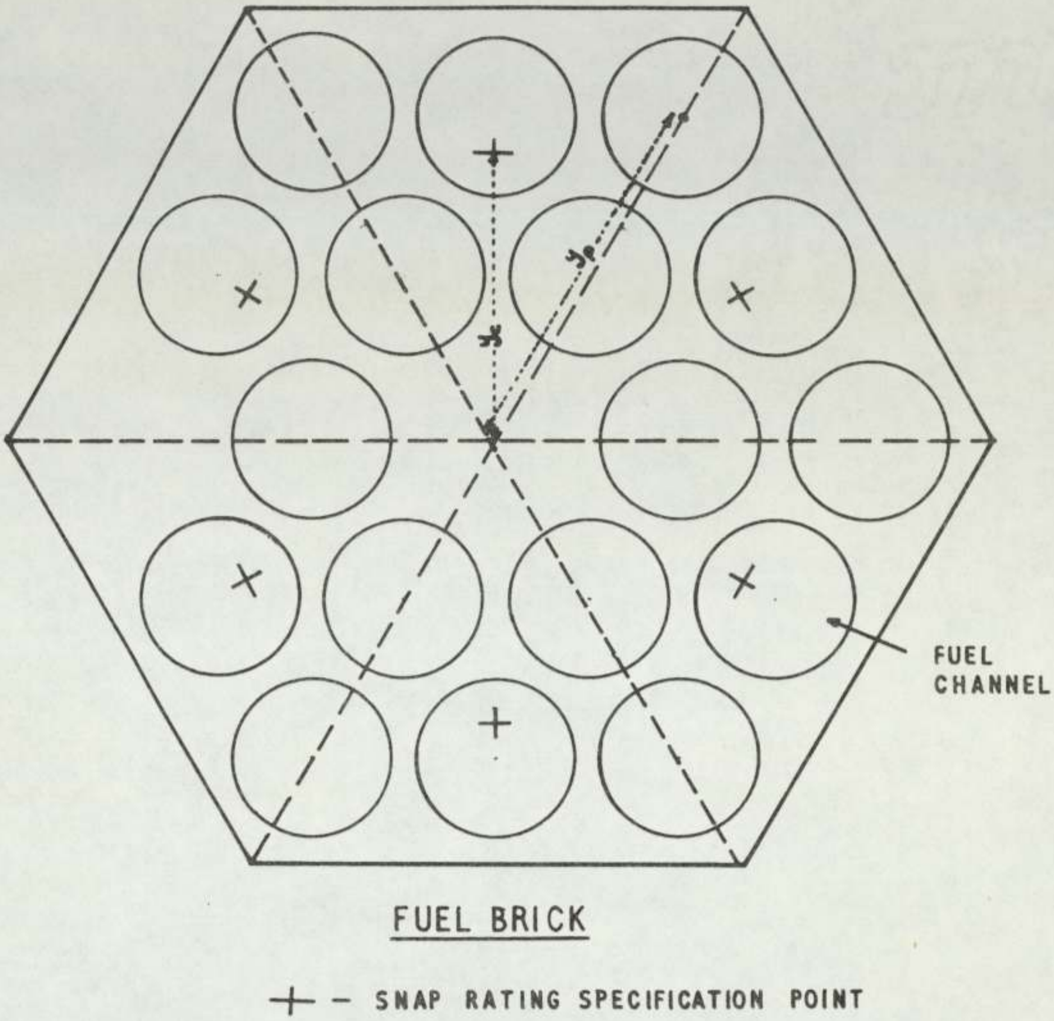

FUEL BRICK SHOWING RATING VALUES AS PRESENTED BY SNAP	FIG 3/2

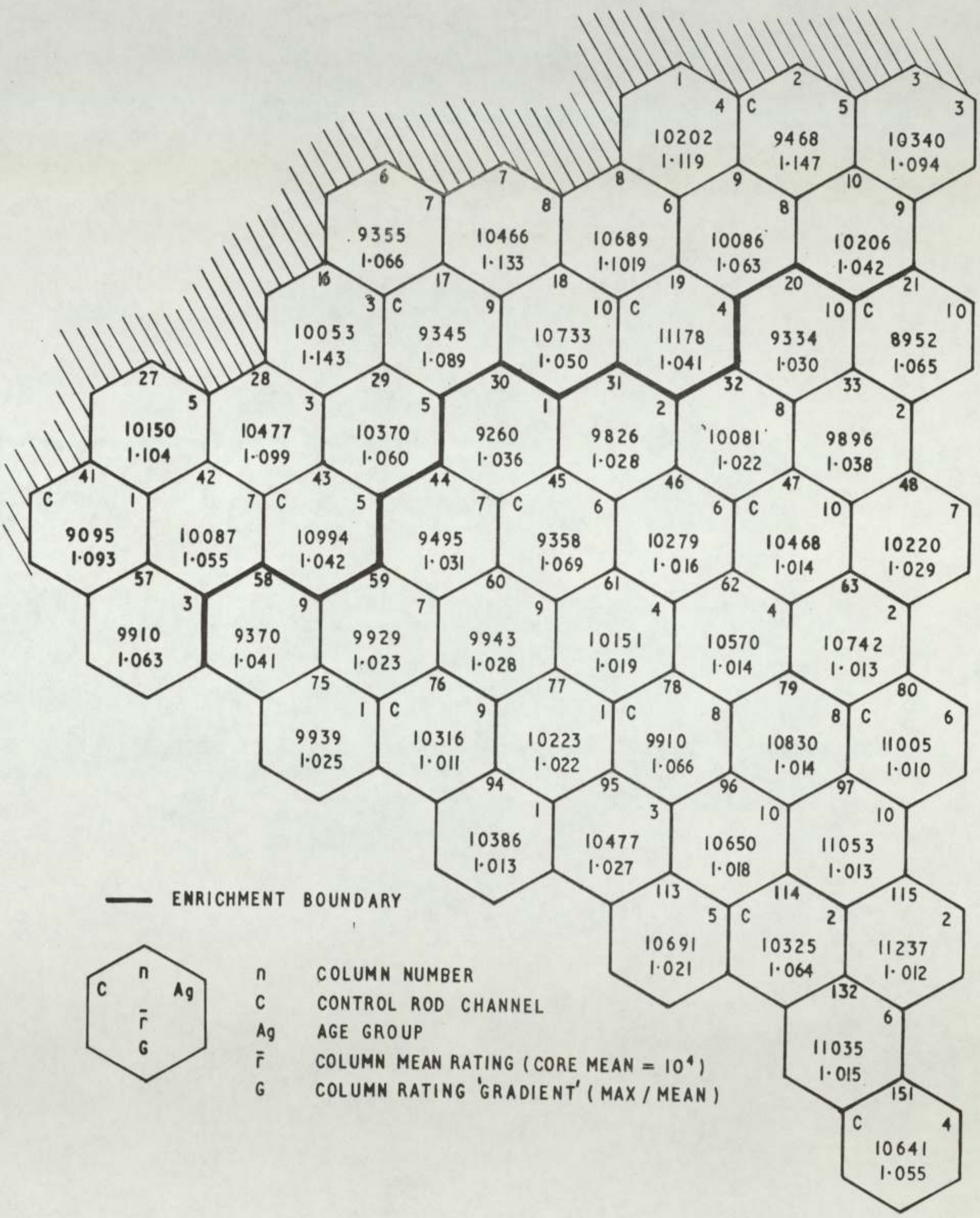

SEXTANT OF CORE SHOWING COLUMN RATINGS, GRADIENTS AND AGES	FIG 3/3

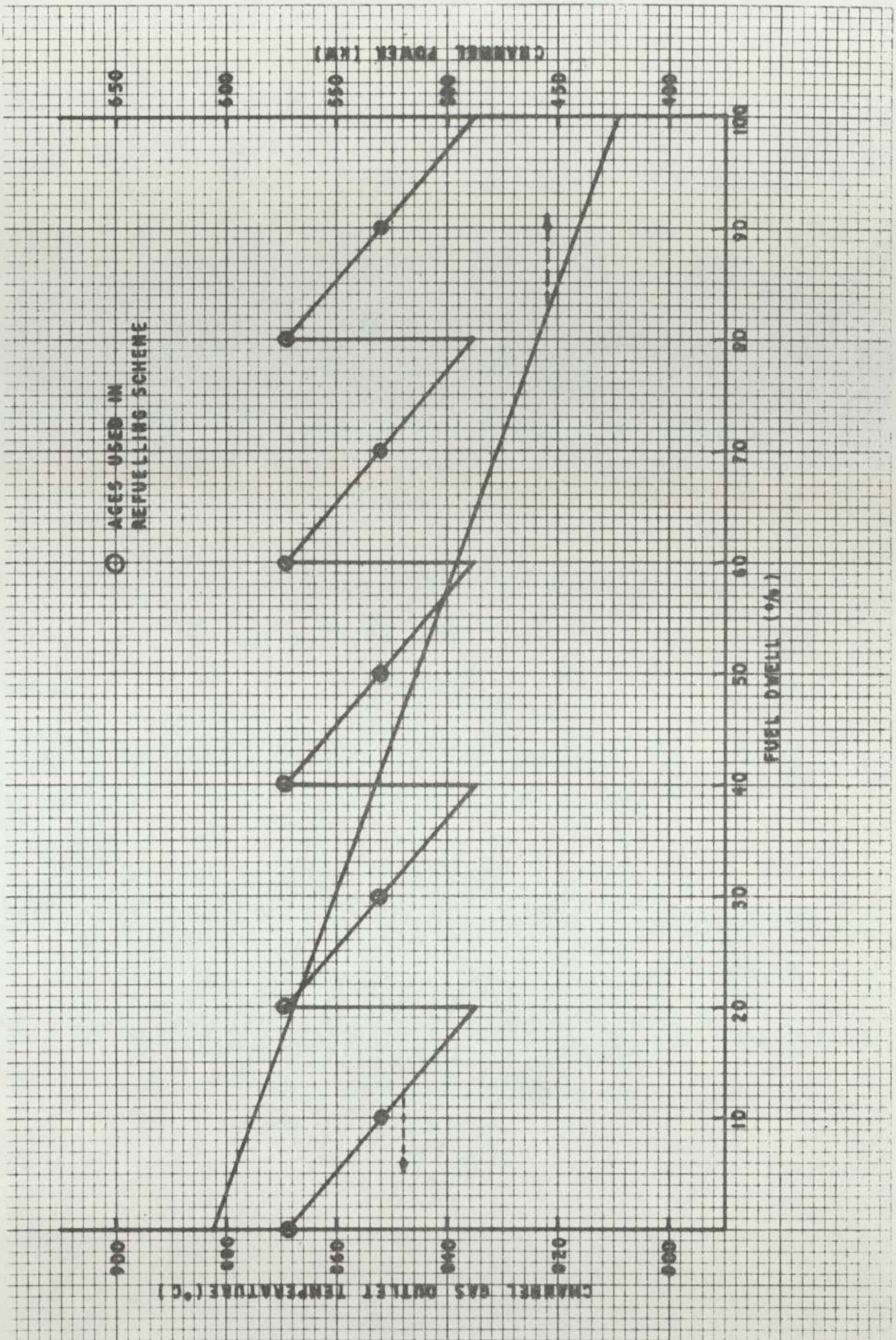

CHANNEL POWER AND GAS OUTLET TEMPERATURE TIME EVOLUTIONS FOR THE PEAK RATED CHANNEL	FIG 3/4

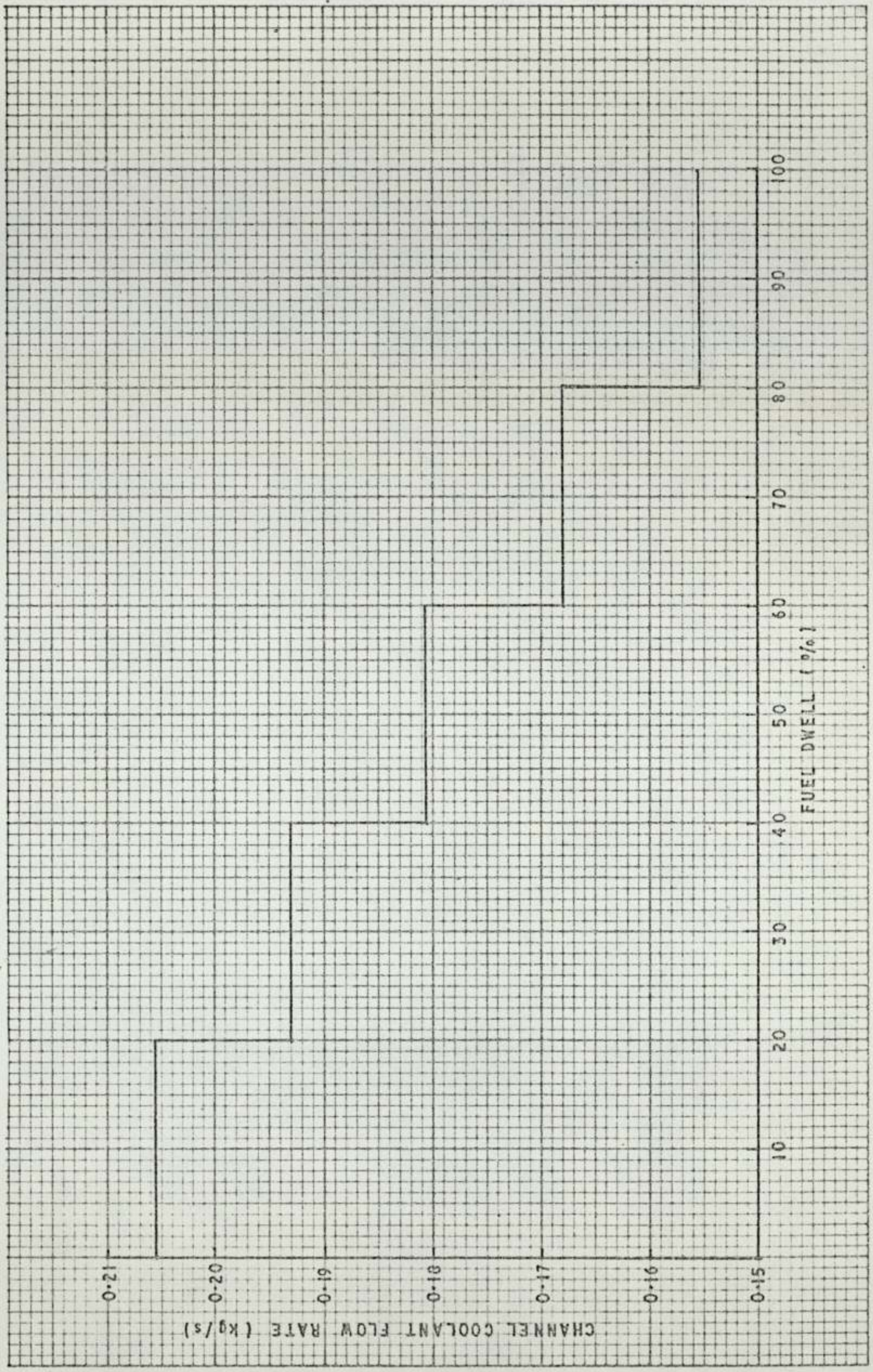

TIME EVOLUTION OF COOLANT FLOW RATE IN THE PEAK RATED CHANNEL	FIG 3/5

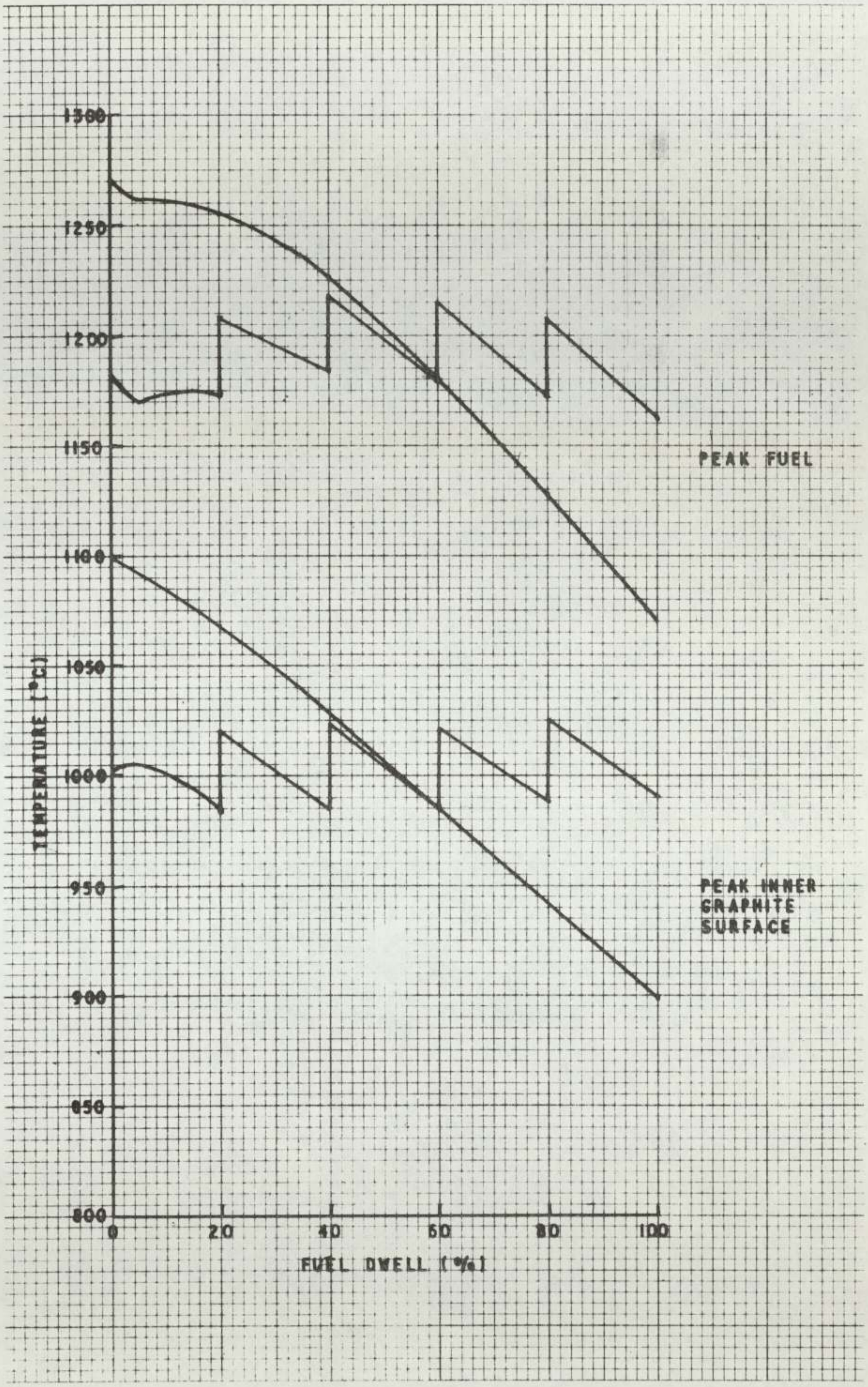

TIME EVOLUTIONS OF PEAK FUEL AND GRAPHITE TEMPERATURE FOR A FOUR AND NO-GAG CHANGE SCHEME	FIG 3/6

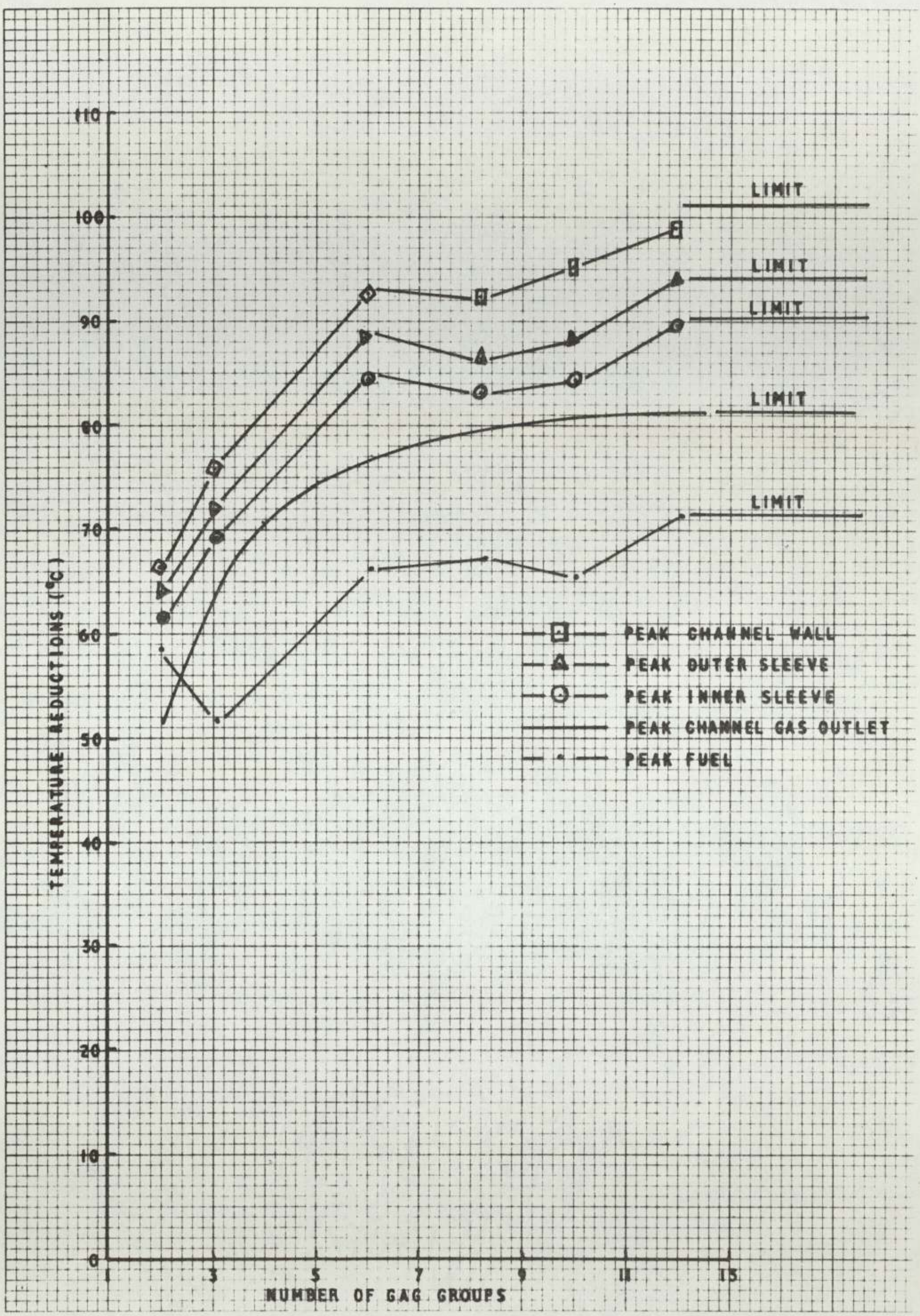

TEMPERATURE REDUCTIONS VERSUS NUMBER OF SPATIAL GAG GROUPS	FIG 3/7

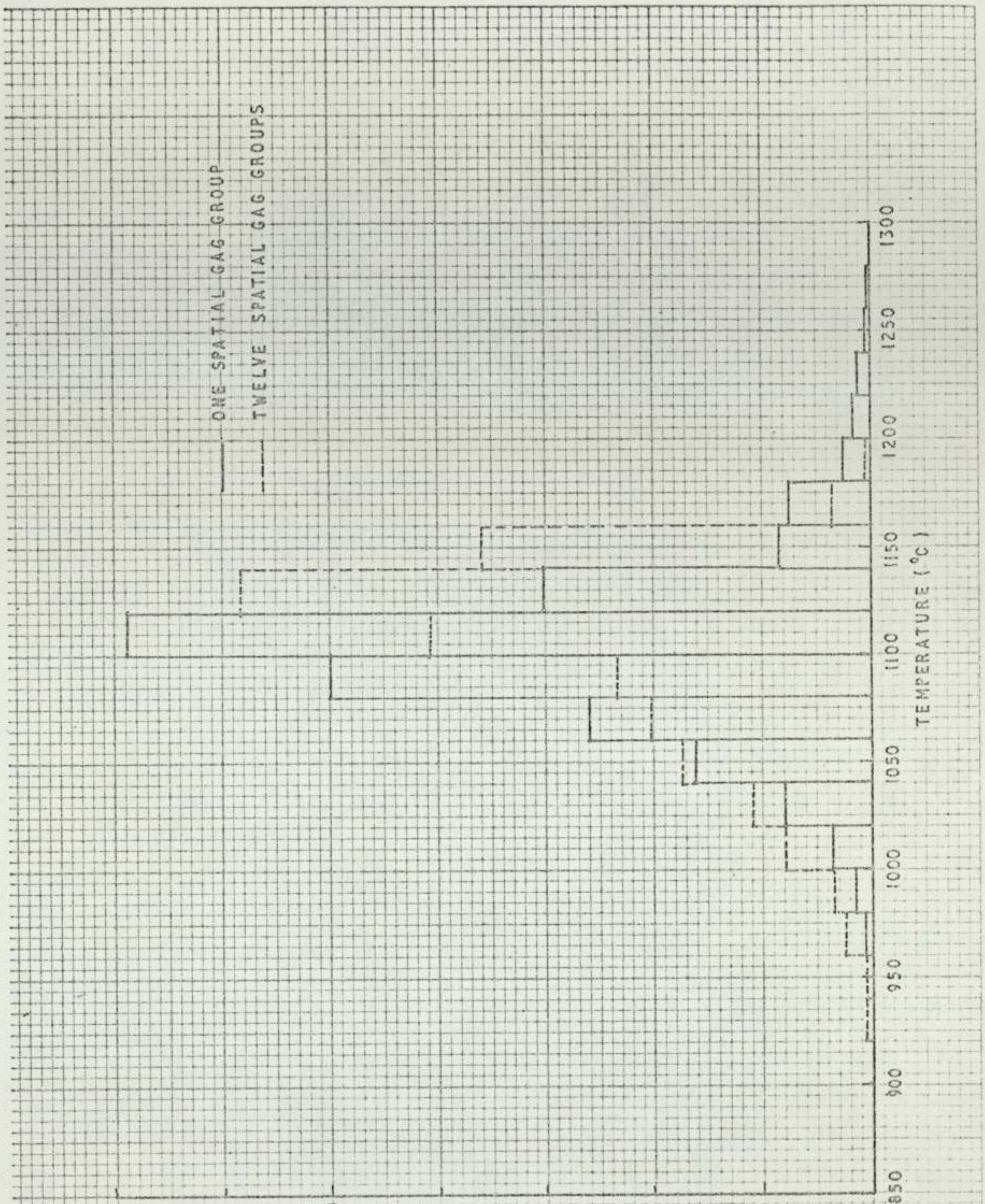

HISTOGRAM OF PEAK FUEL TEMPERATURE FOR ONE AND TWELVE GROUP SCHEMES	FIG 3/8

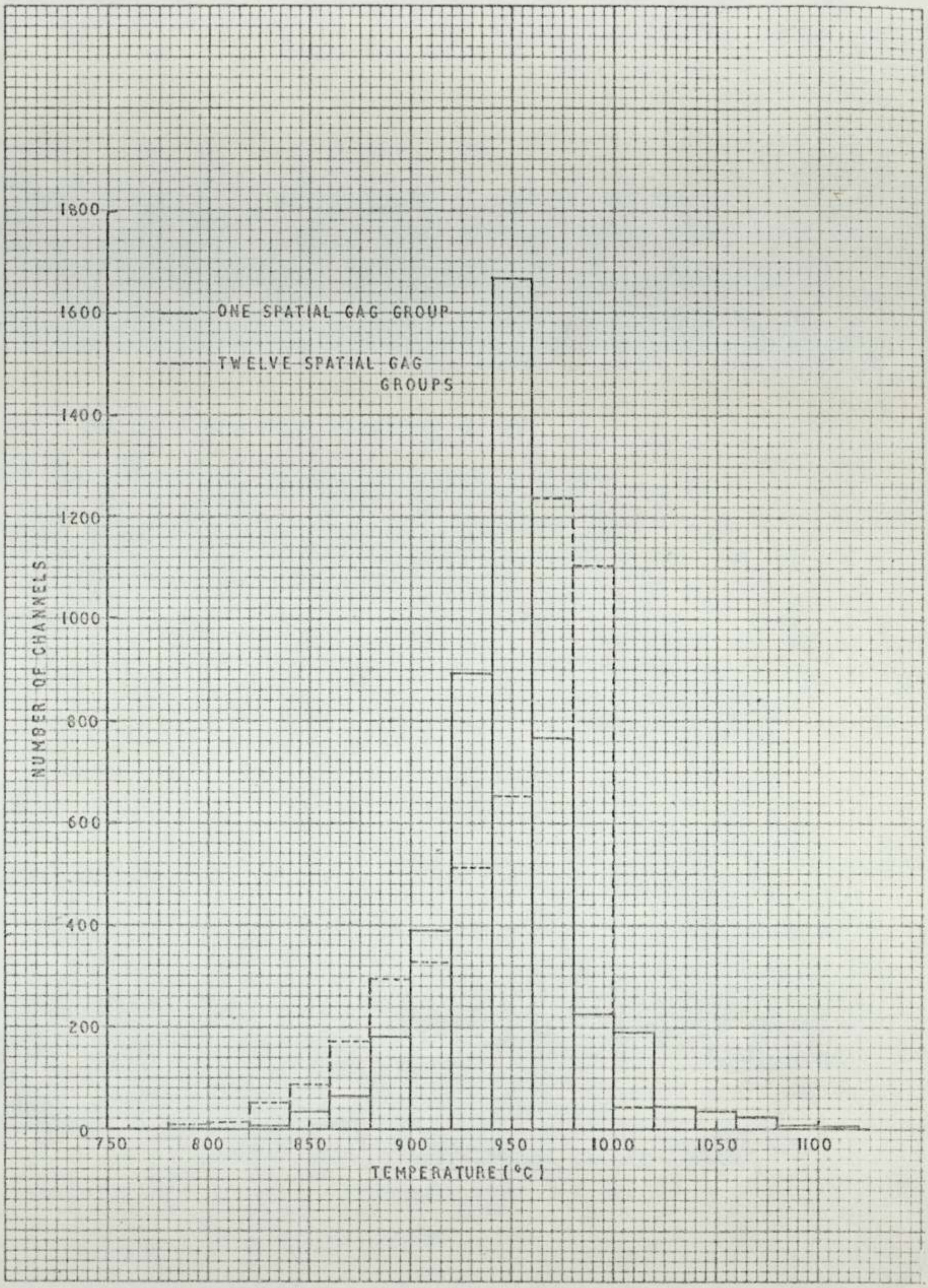

HISTOGRAM OF PEAK INNER SLEEVE TEMPERATURE FOR ONE AND TWELVE GROUP SCHEMES	FIG 3/9

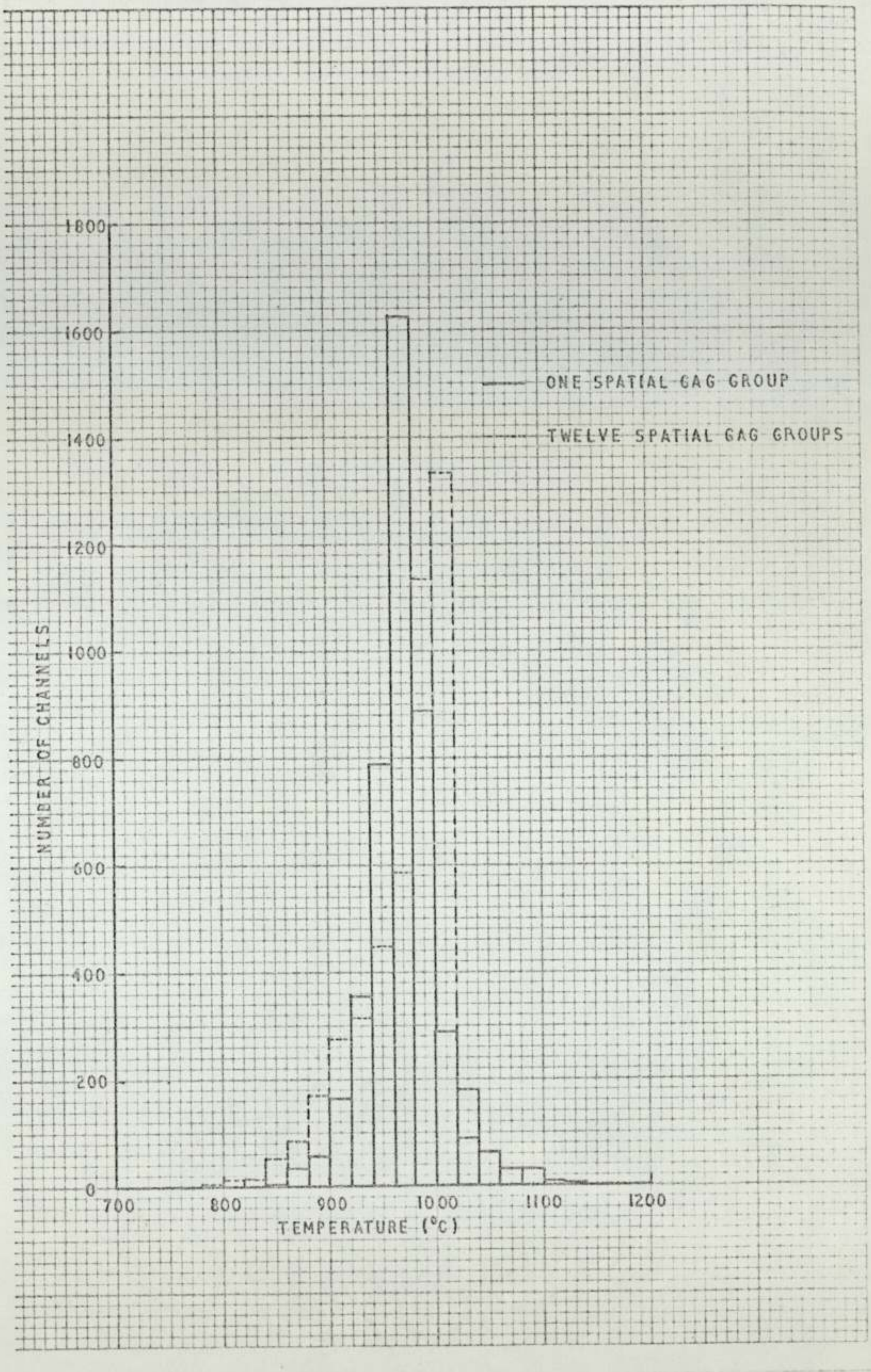

HISTOGRAM OF PEAK OUTER SLEEVE TEMPERATURE FOR ONE AND TWELVE GROUP SCHEMES	FIG 3/10

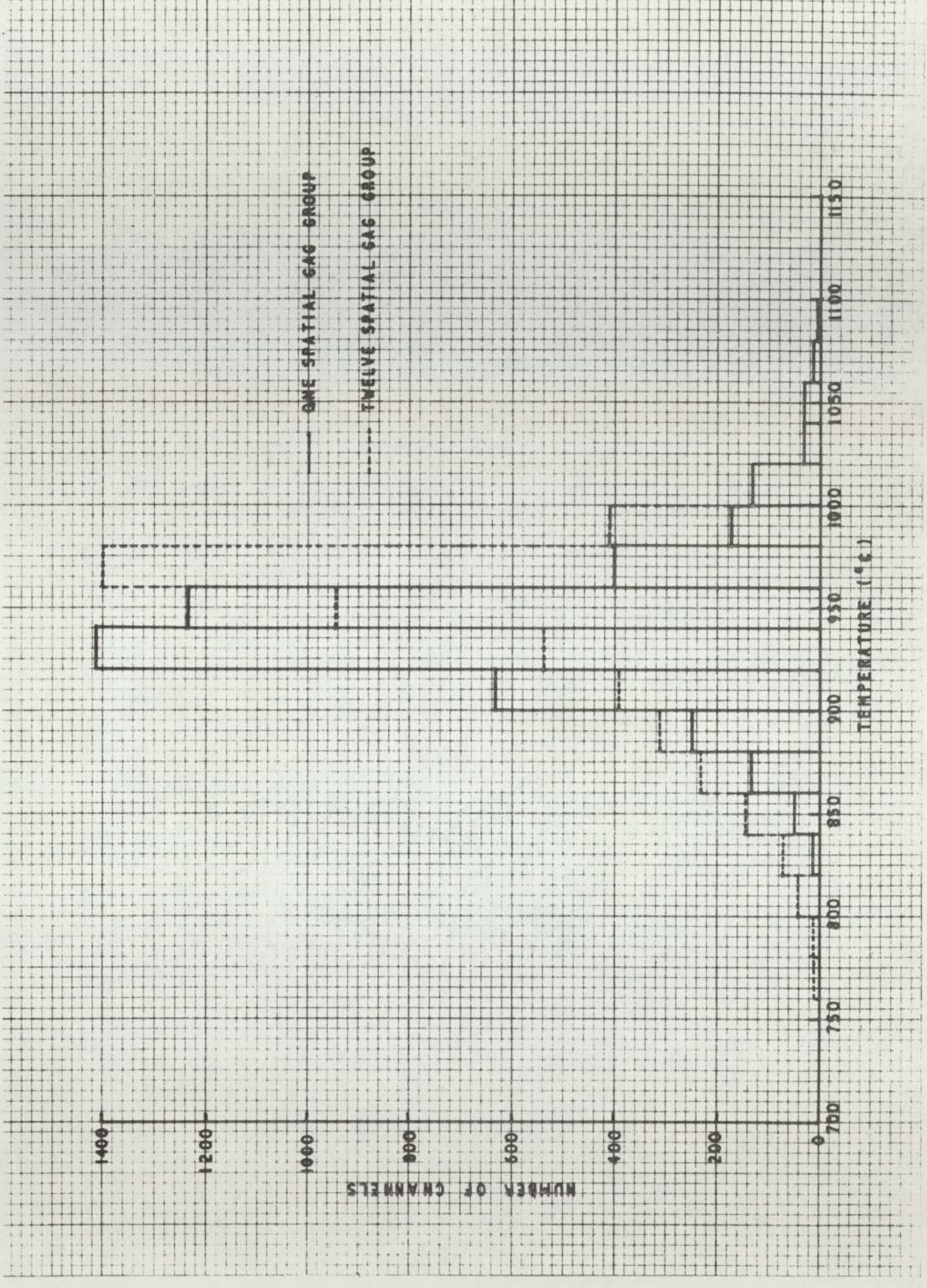

HISTOGRAM OF PEAK CHANNEL WALL TEMPERATURE FOR ONE AND TWELVE GROUP SCHEMES	FIG 3/11

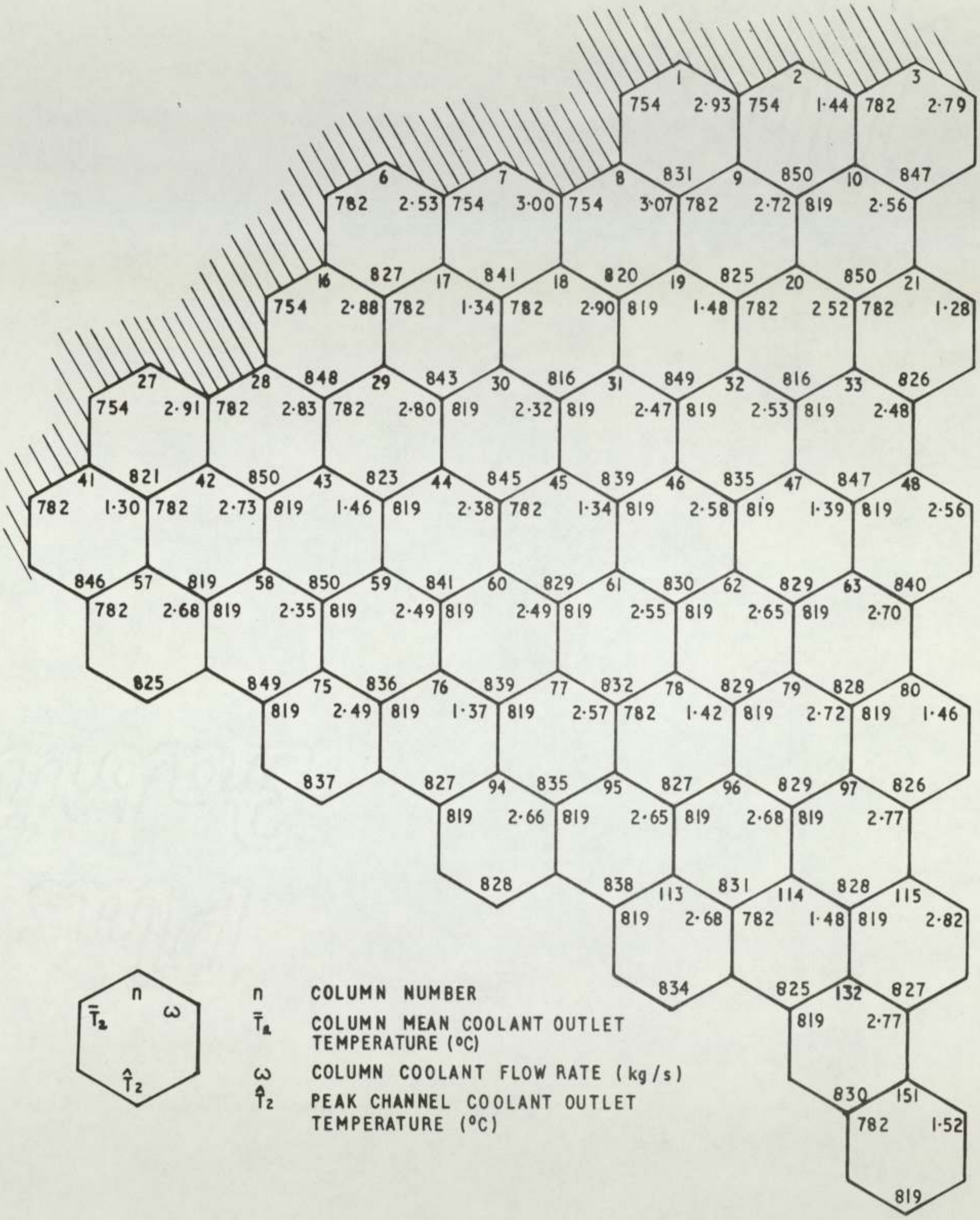

n COLUMN NUMBER

$\bar{T}_2$ COLUMN MEAN COOLANT OUTLET TEMPERATURE (°C)

ω COLUMN COOLANT FLOW RATE (kg/s)

$\hat{T}_2$ PEAK CHANNEL COOLANT OUTLET TEMPERATURE (°C)

SEXTANT OF CORE SHOWING COLUMN FLOWS, MEAN AND PEAK CHANNEL GAS OUTLET TEMPERATURES	FIG 3/12

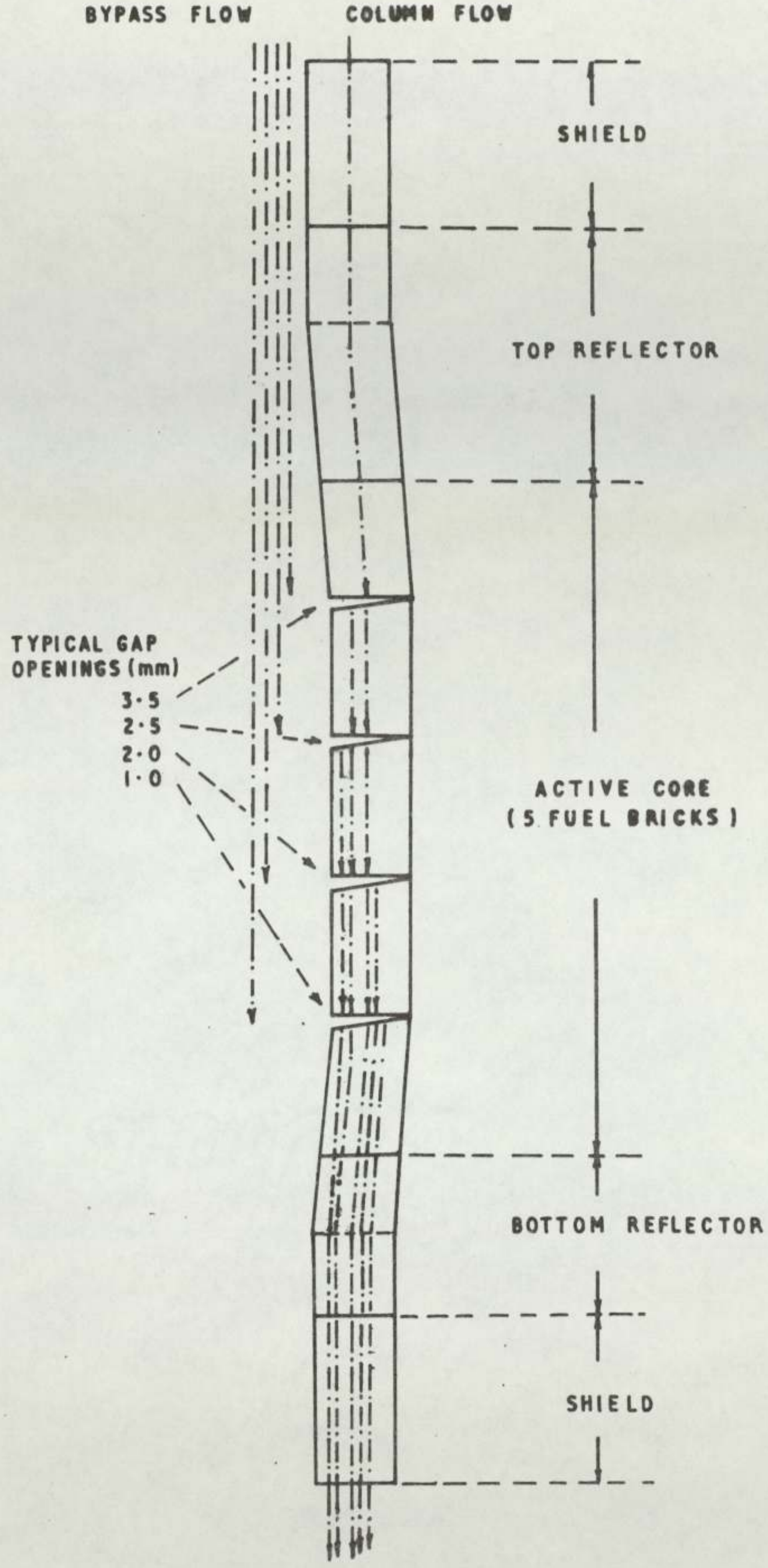

DIAGRAMMATIC SKETCH OF AN IRRADIATED COLUMN SHOWING TYPICAL GAP OPENINGS AND THEIR EFFECT ON FLOW DISTRIBUTION	FIG 3/13

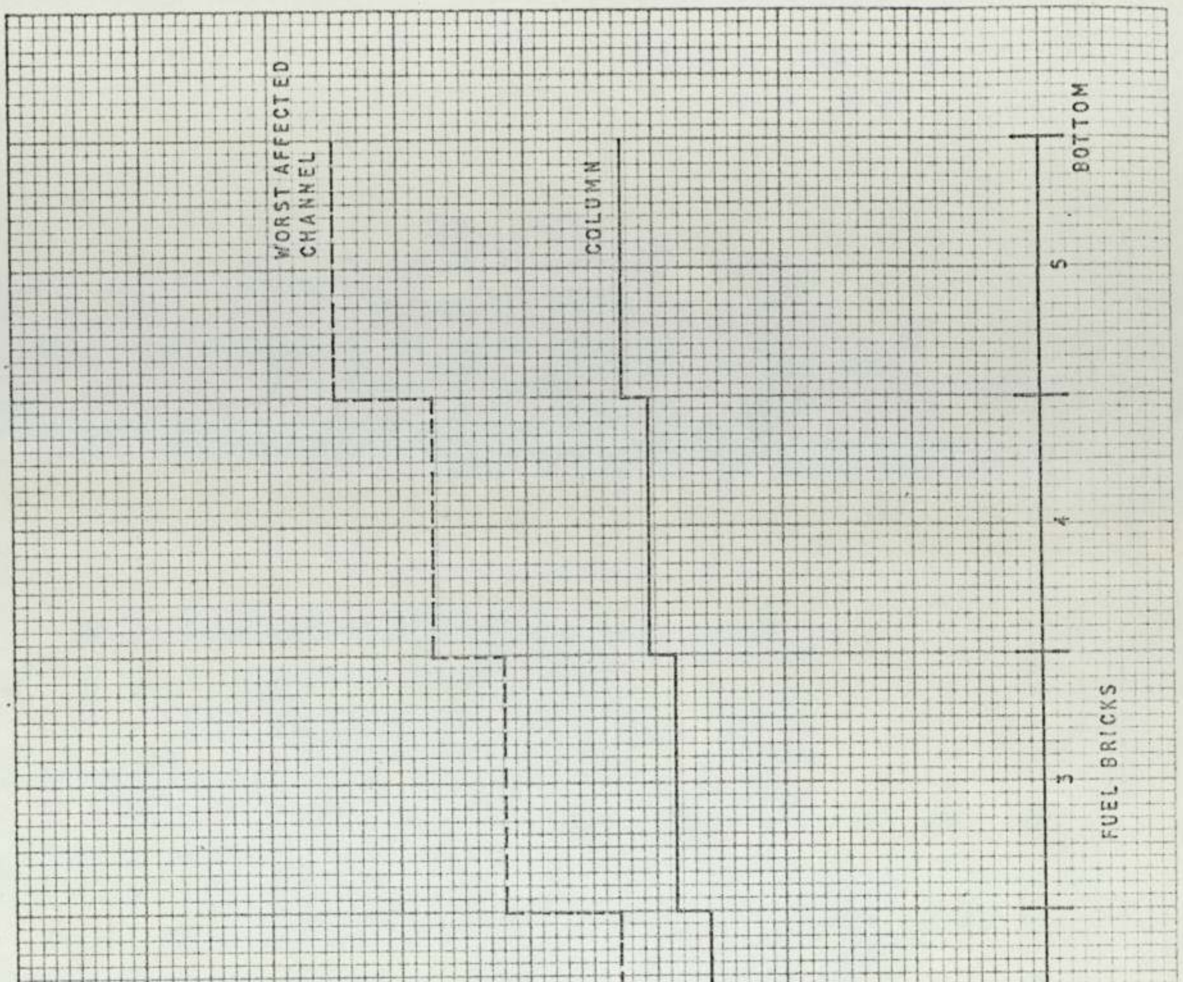

TYPICAL AXIAL VARIATION OF FLOW IN A LEAKING COLUMN	FIG 3/14

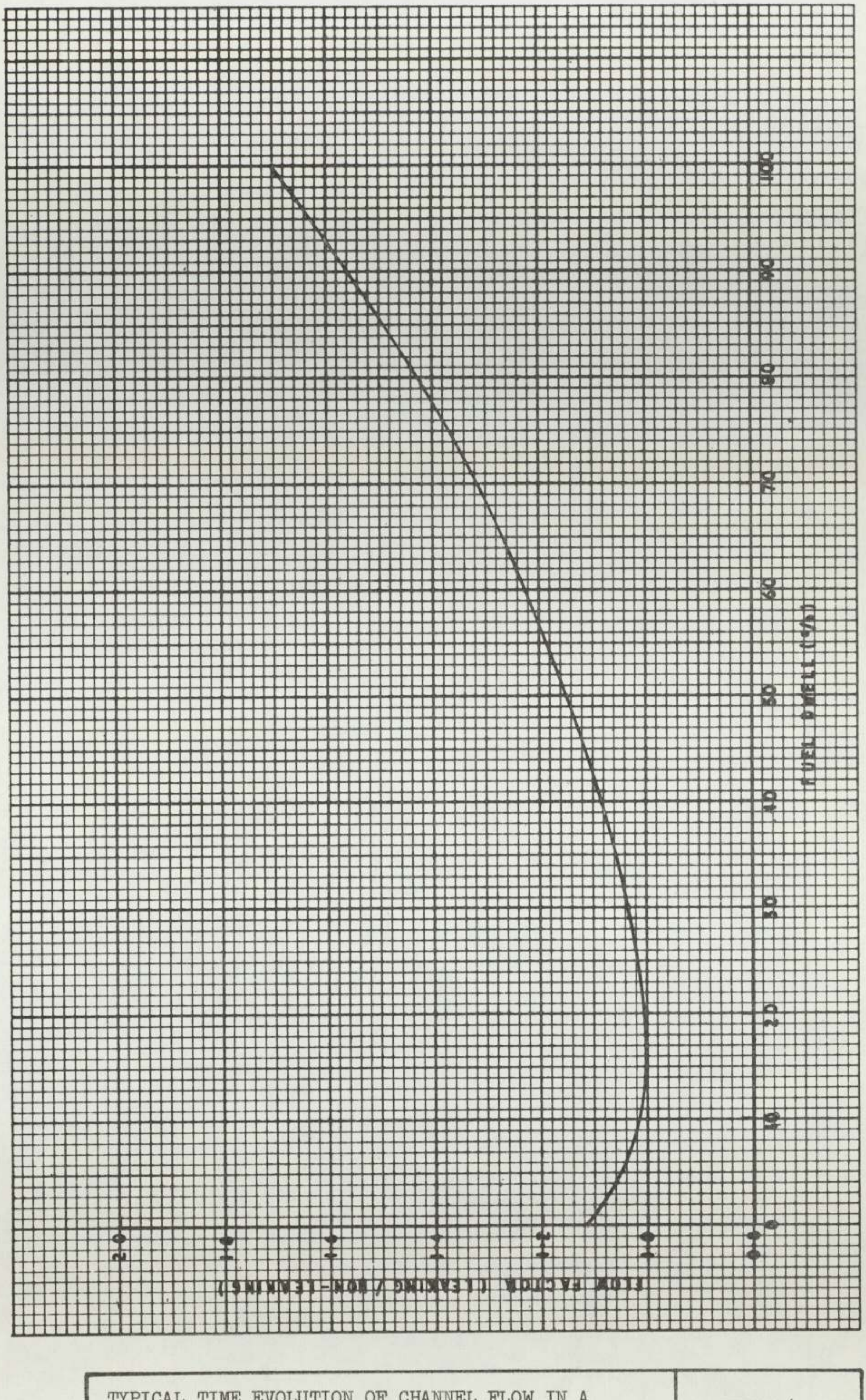

TYPICAL TIME EVOLUTION OF CHANNEL FLOW IN A LEAKING COLUMN	FIG 3/15

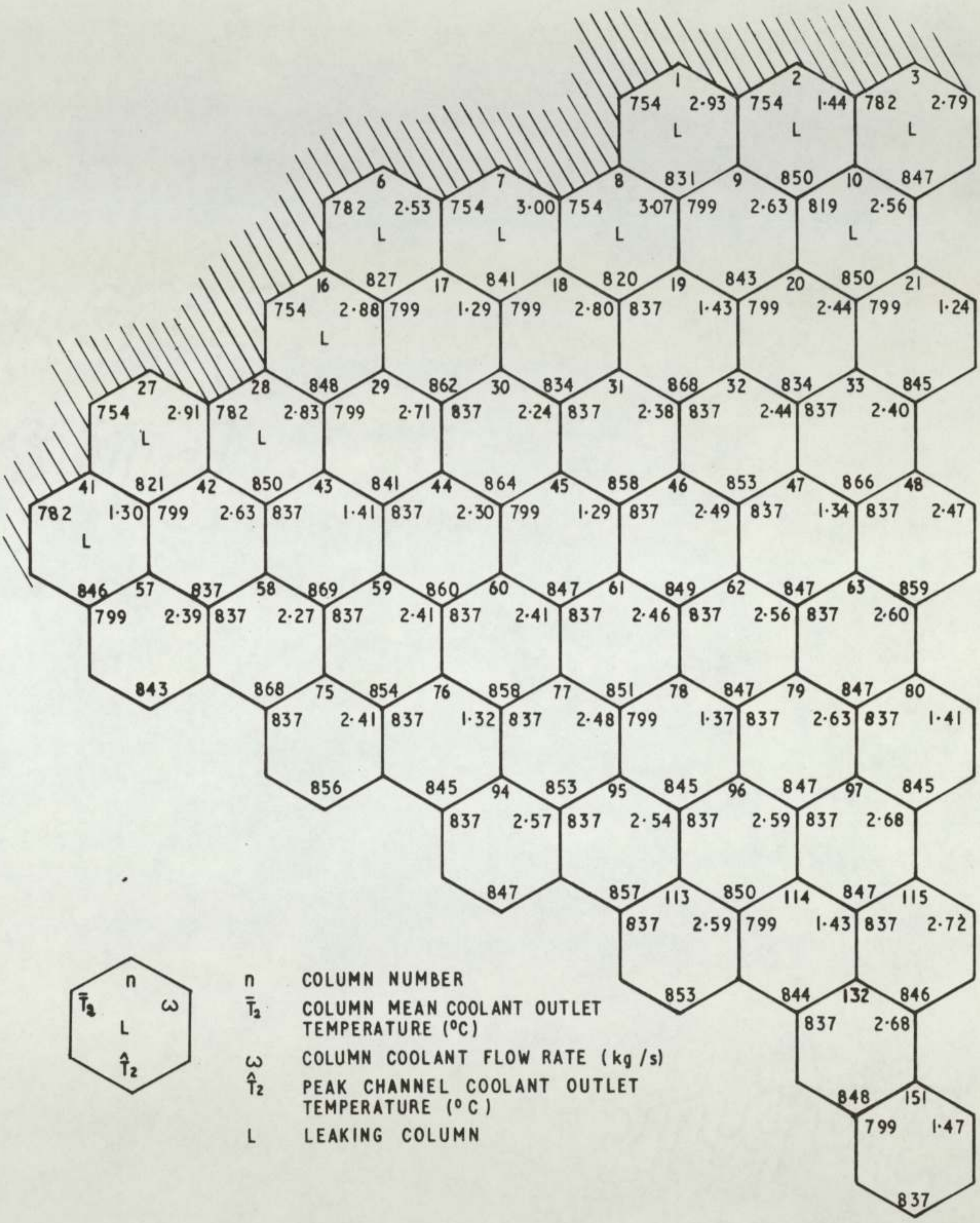

SPATIAL FLOW AND GAS OUTLET TEMPERATURE DISTRIBUTIONS IN A LEAKING CORE	FIG 3/16

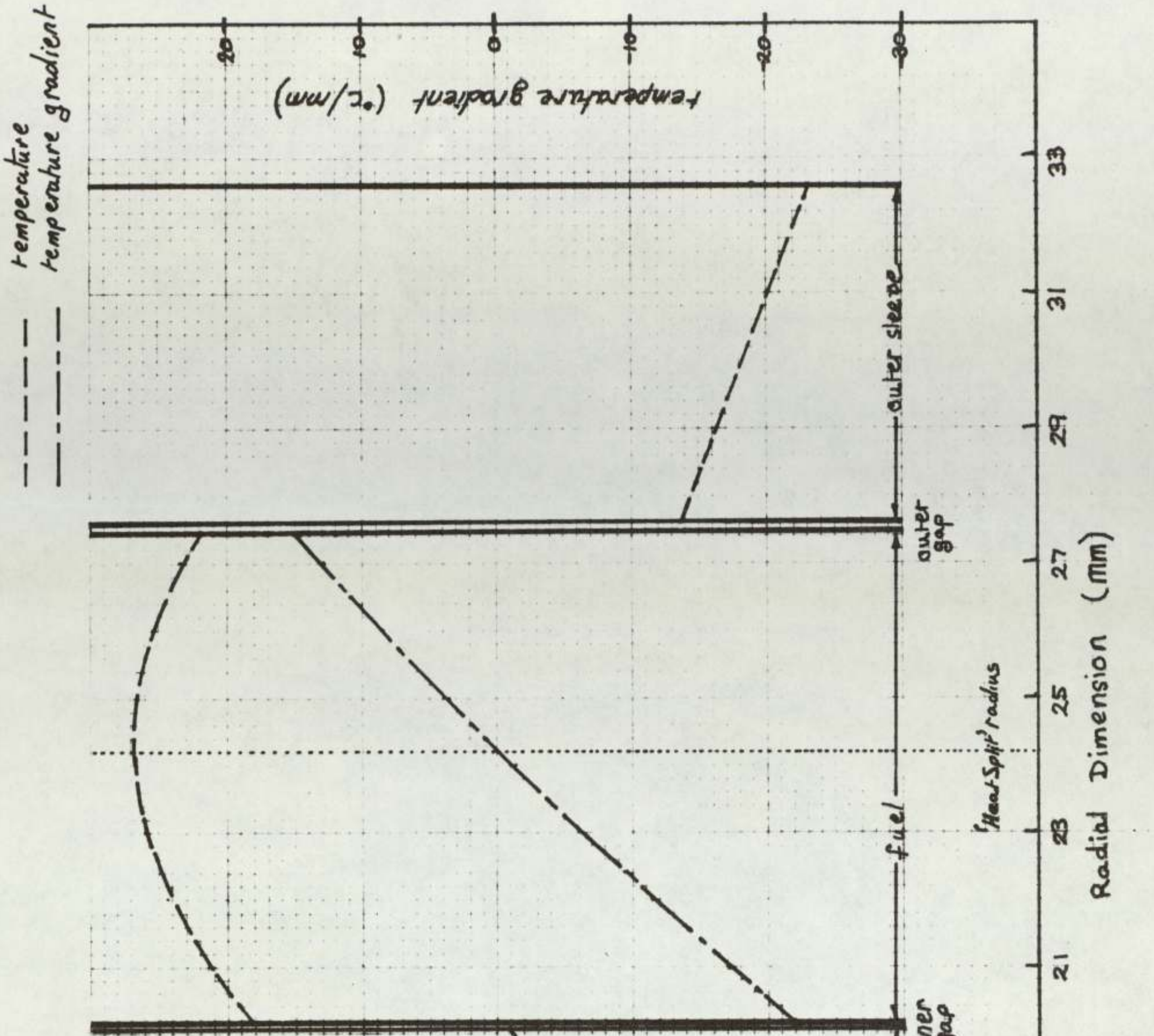

TYPICAL RADIAL TEMPERATURE DISTRIBUTION THROUGH A TUBULAR FUEL ELEMENT	FIG 4/1

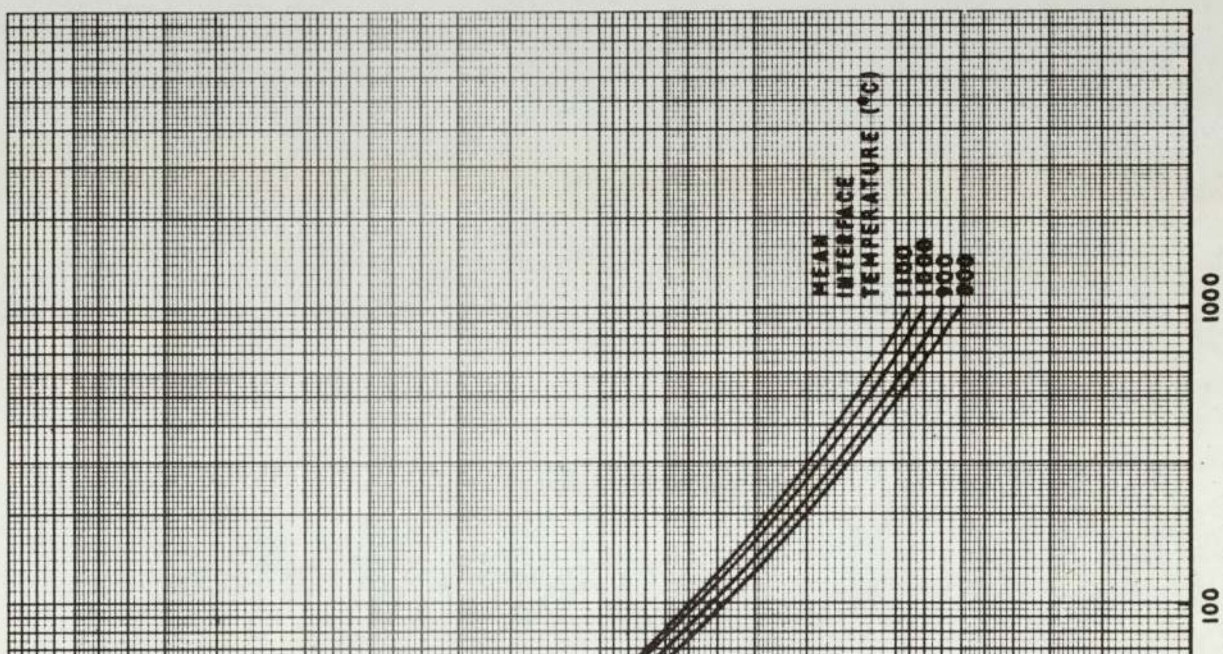

INTERFACE GAP CONDUCTANCE VERSUS RADIAL GAP WIDTH	FIG 4/2

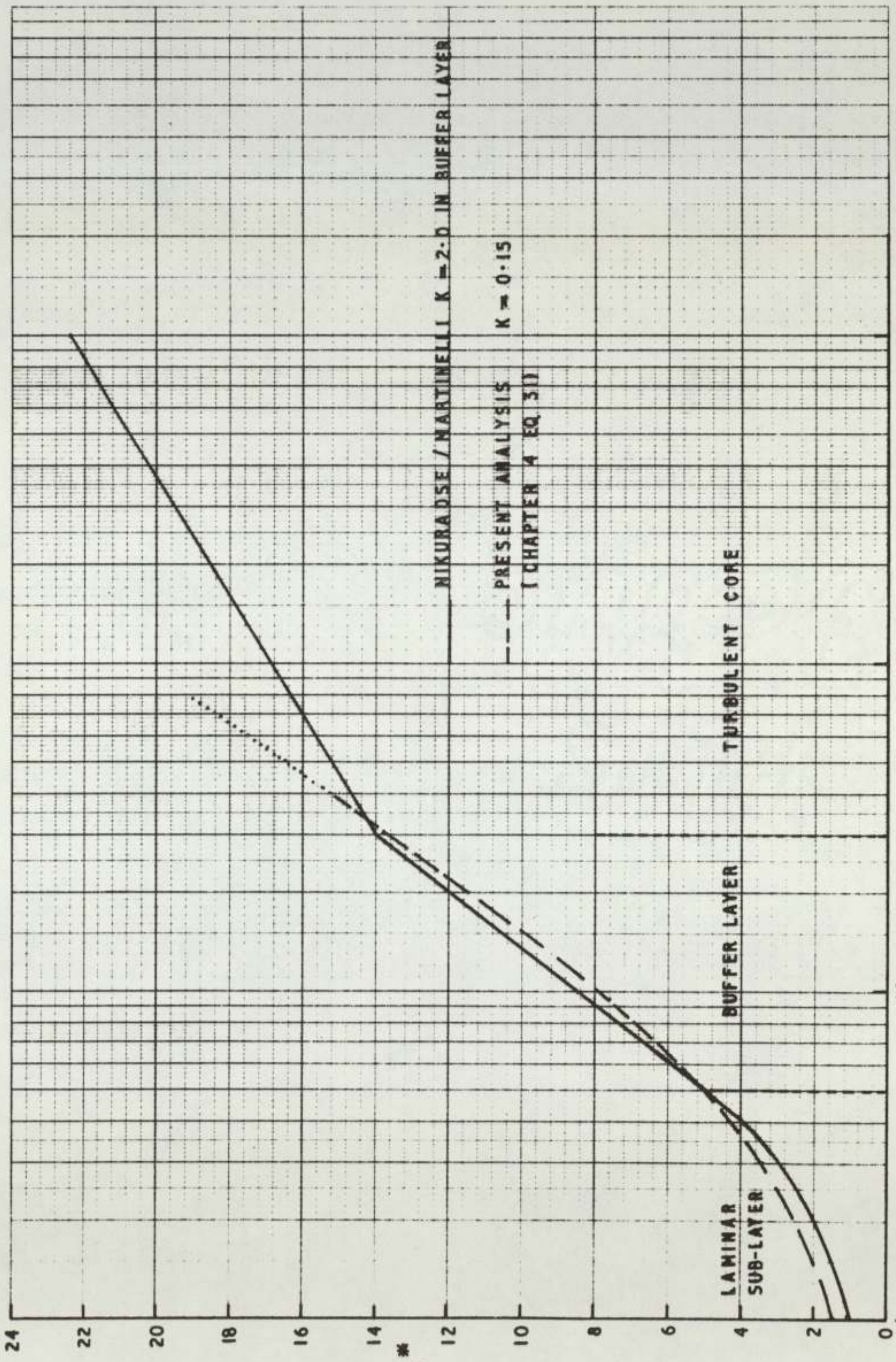

VELOCITY DISTRIBUTION CLOSE TO A WALL FOR A TURBULENT BOUNDARY LAYER	FIG 4/3

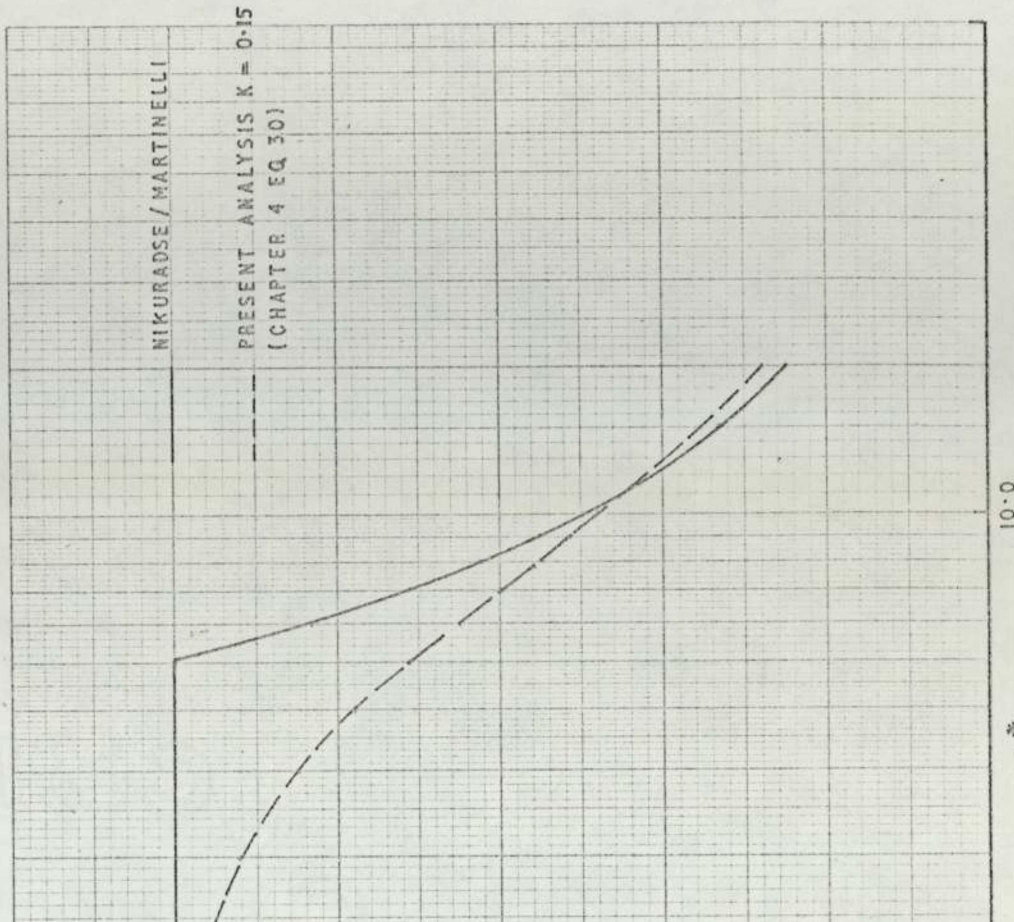

VELOCITY GRADIENT DISTRIBUTION CLOSE TO A WALL FOR A TURBULENT BOUNDARY LAYER	FIG 4/4

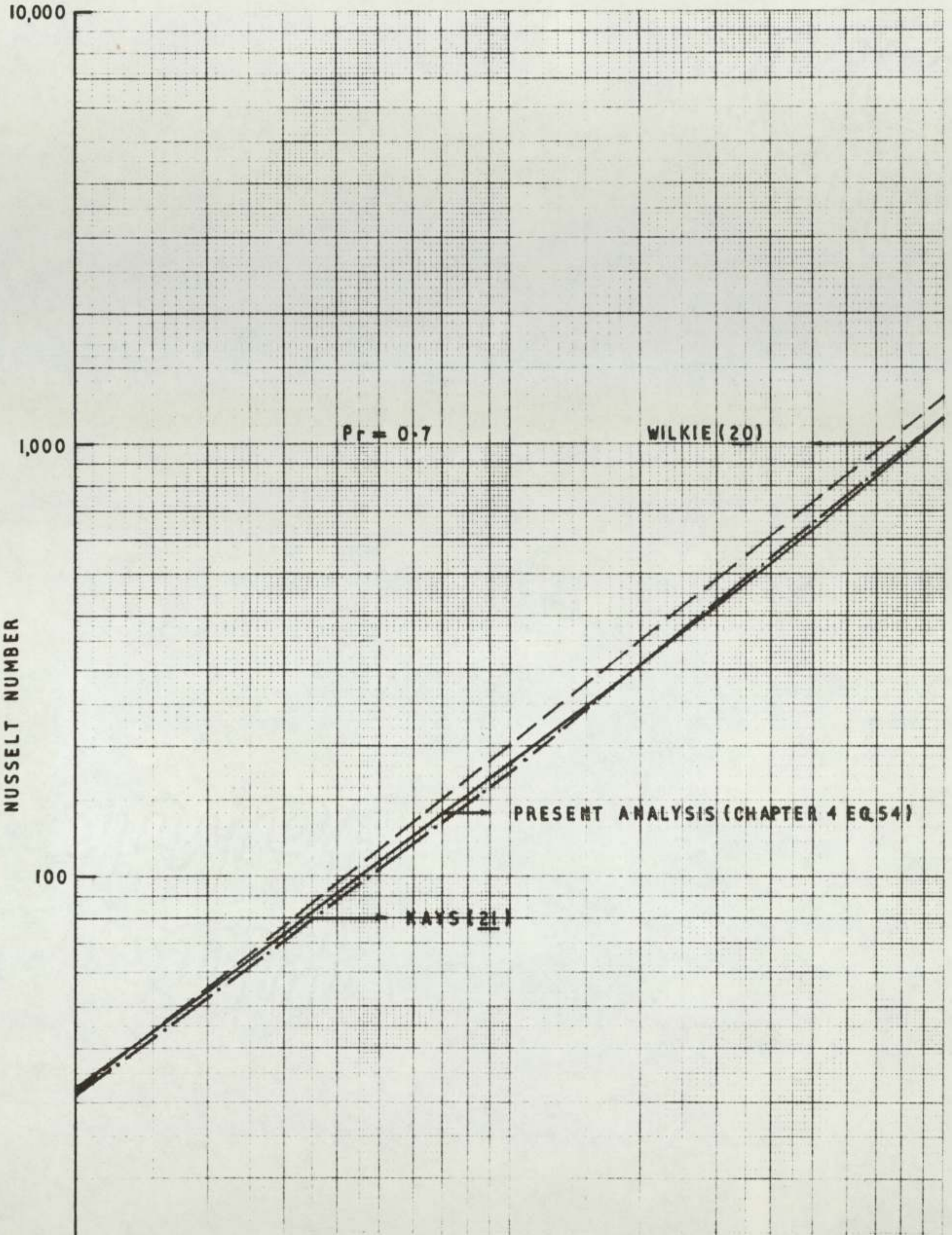

DEVELOPED NUSSELT NUMBERS IN SMOOTH TUBES - REYNOLDS NUMBER DEPENDENCE	FIG 4/5

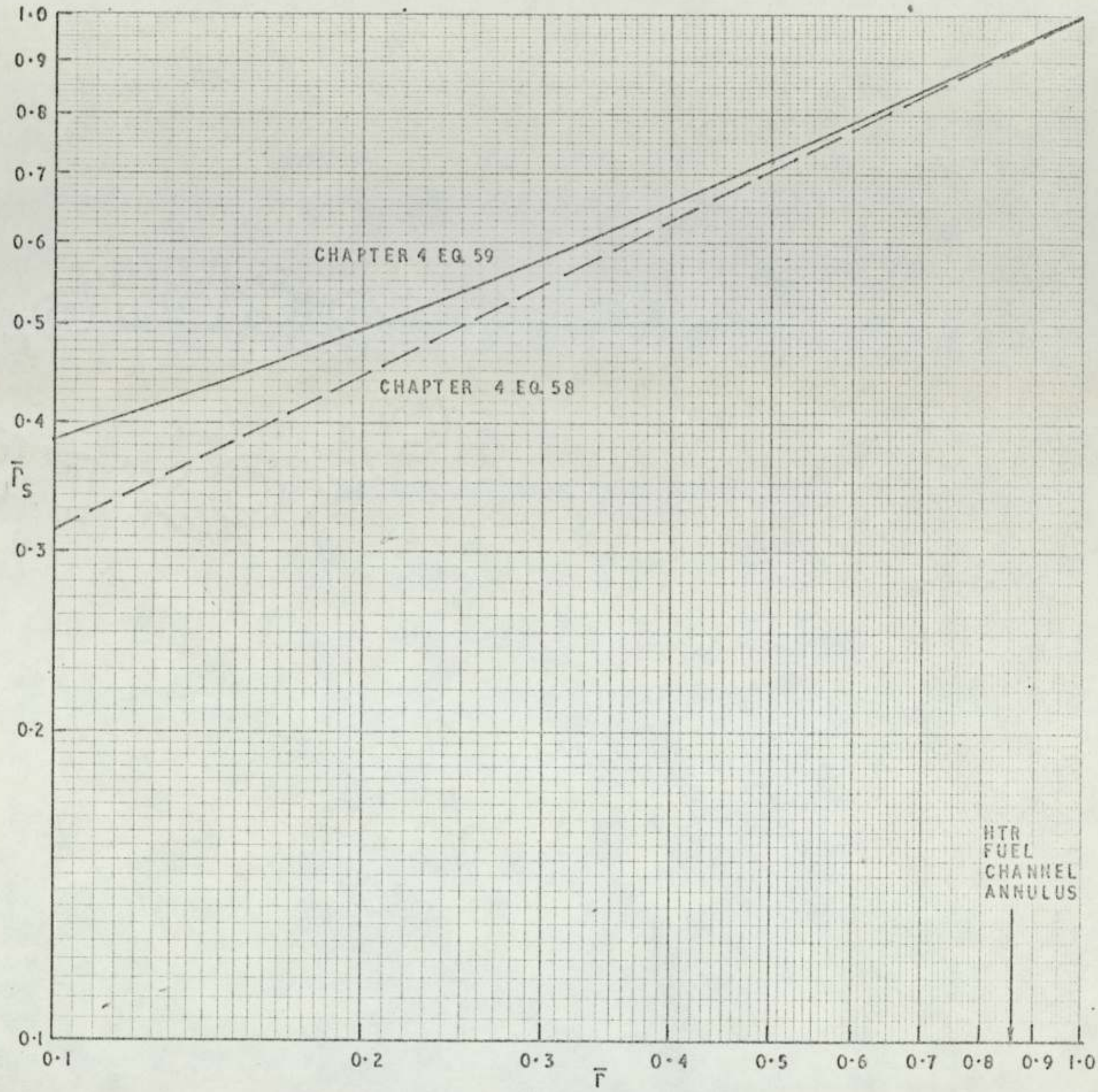

THE DEPENDENCE OF DIMENSIONLESS RADIUS OF NO SHEAR ($\bar{r}_s$) ON RADIUS RATIO ($\bar{r}$)	FIG 4/6

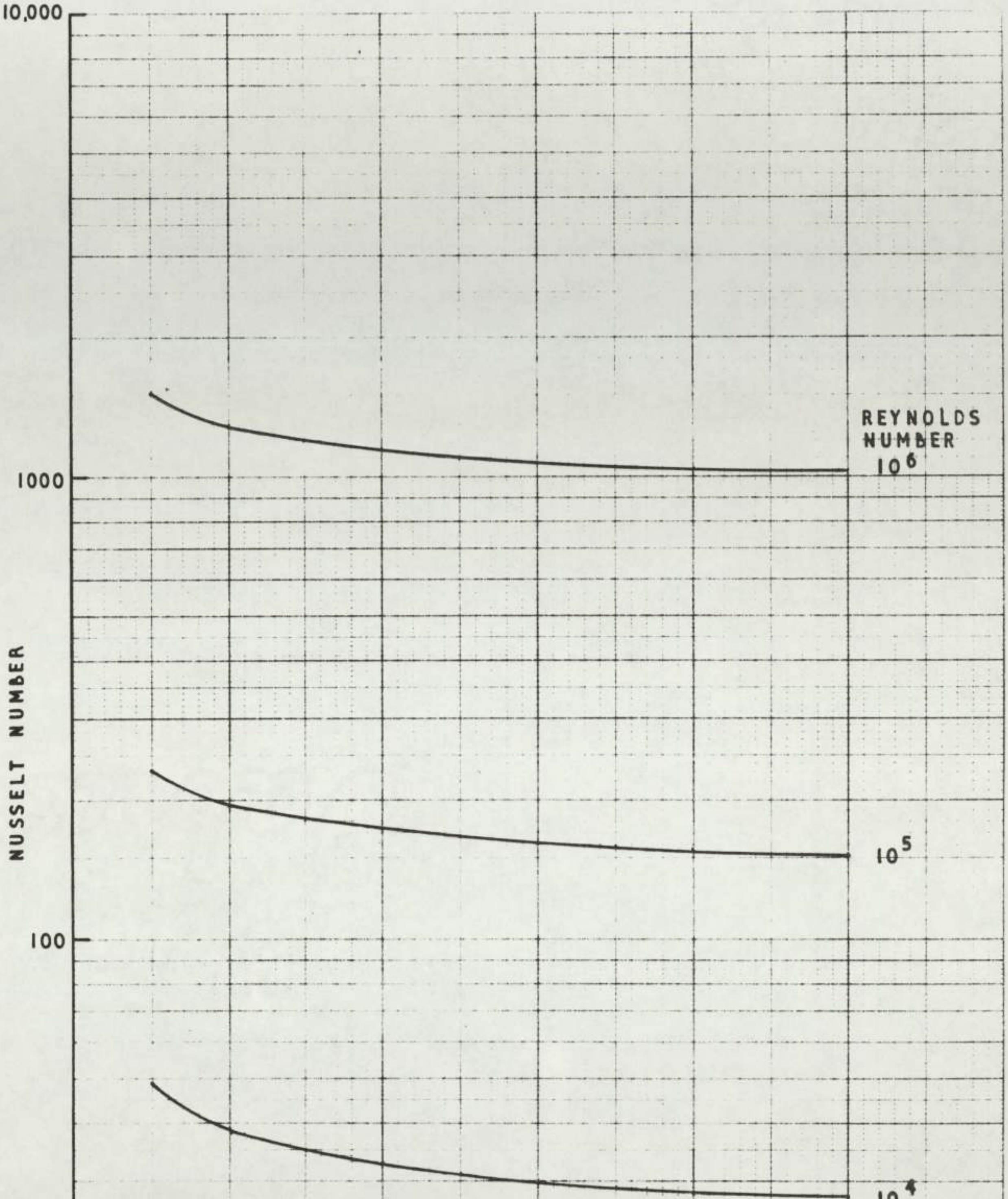

DEVELOPED NUSSELT NUMBERS IN SMOOTH CONCENTRIC ANNULI - RADIUS RATIO DEPENDENCE	FIG 4/7

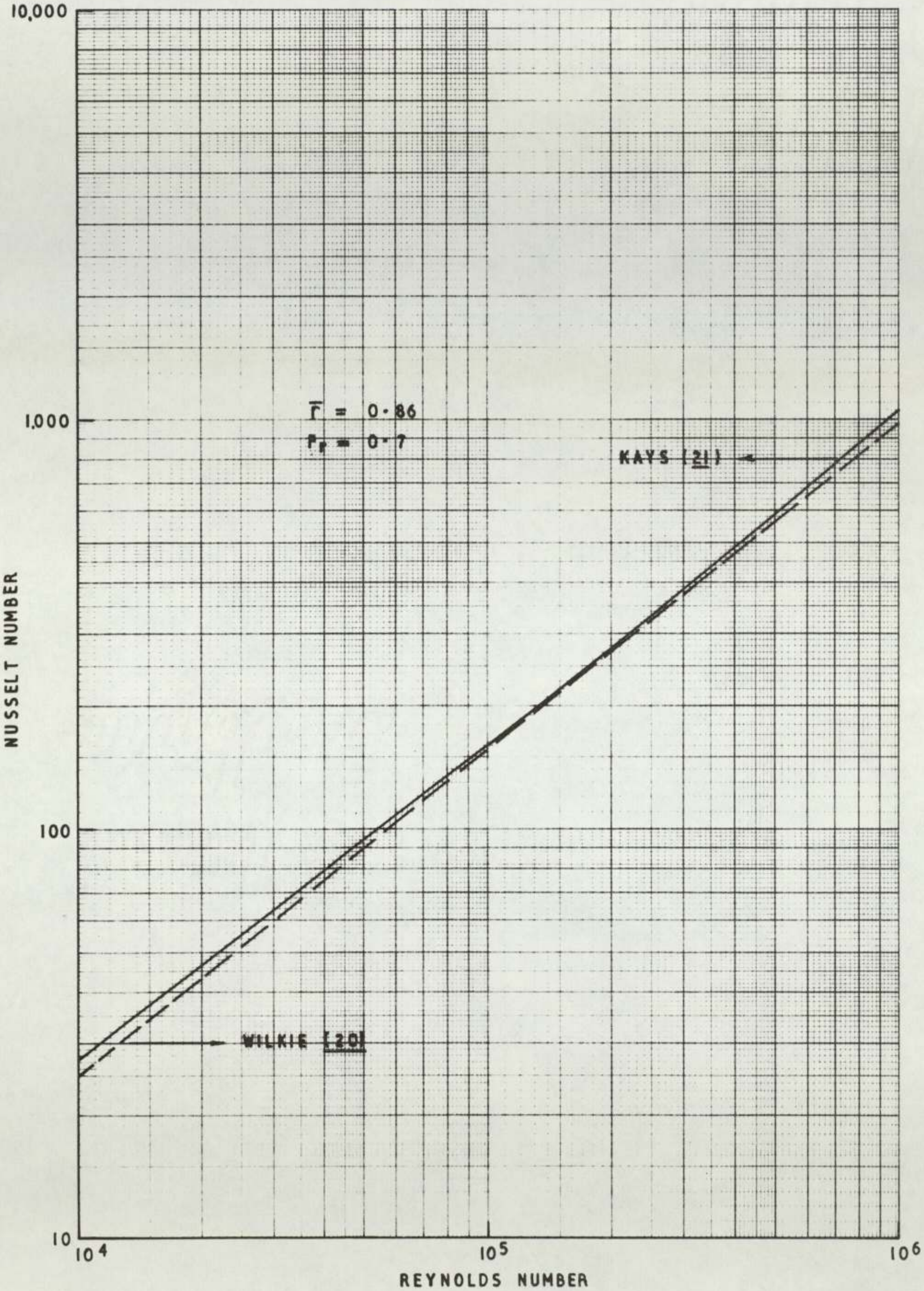

DEVELOPED NUSSELT NUMBERS IN SMOOTH CONCENTRIC ANNULI - REYNOLDS NUMBER DEPENDENCE ($\bar{r}$ = 0.86)	FIG 4/8

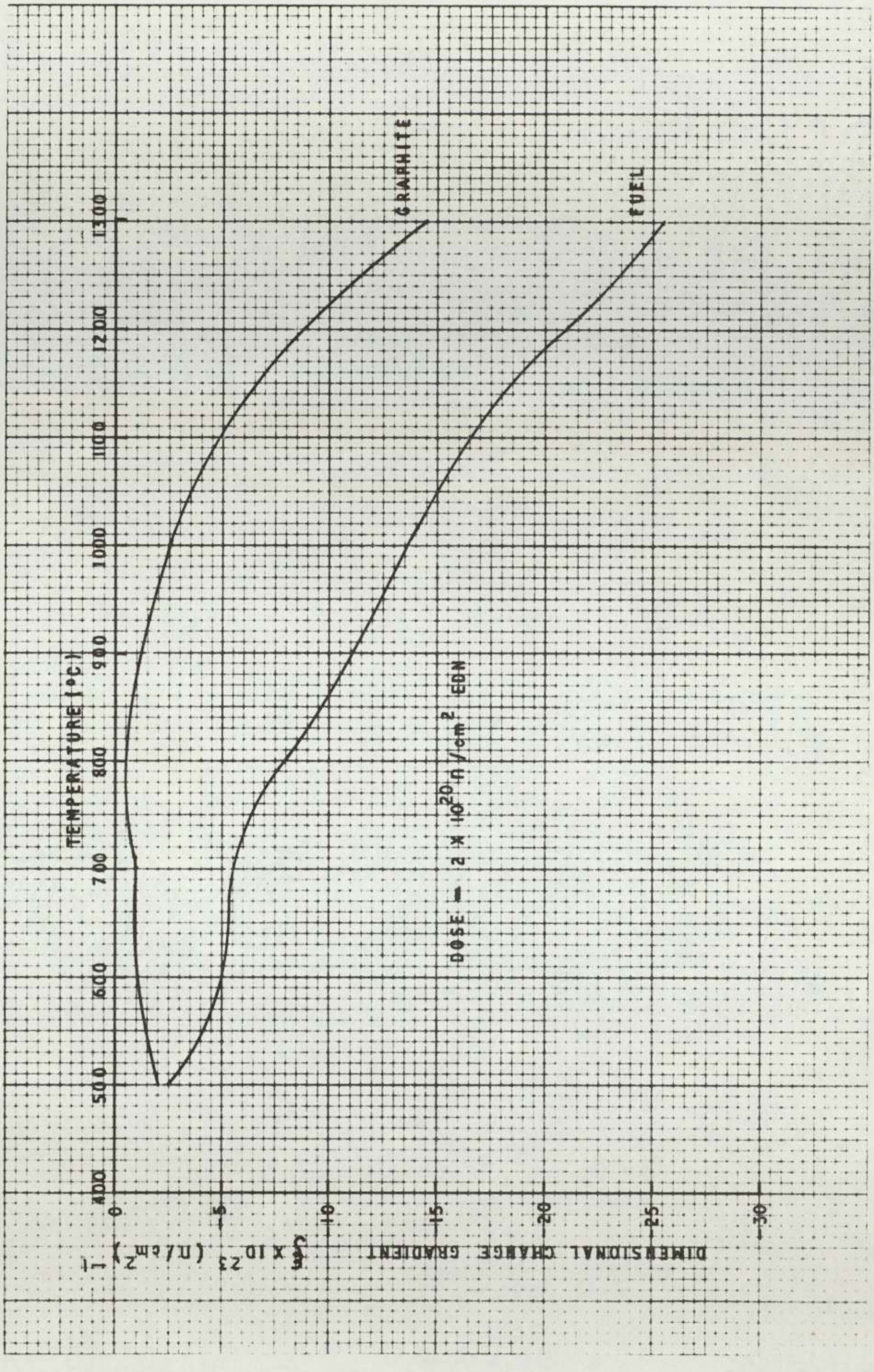

DEPENDENCE OF SHRINKAGE GRADIENT (ξ) ON TEMPERATURE	FIG 4/9

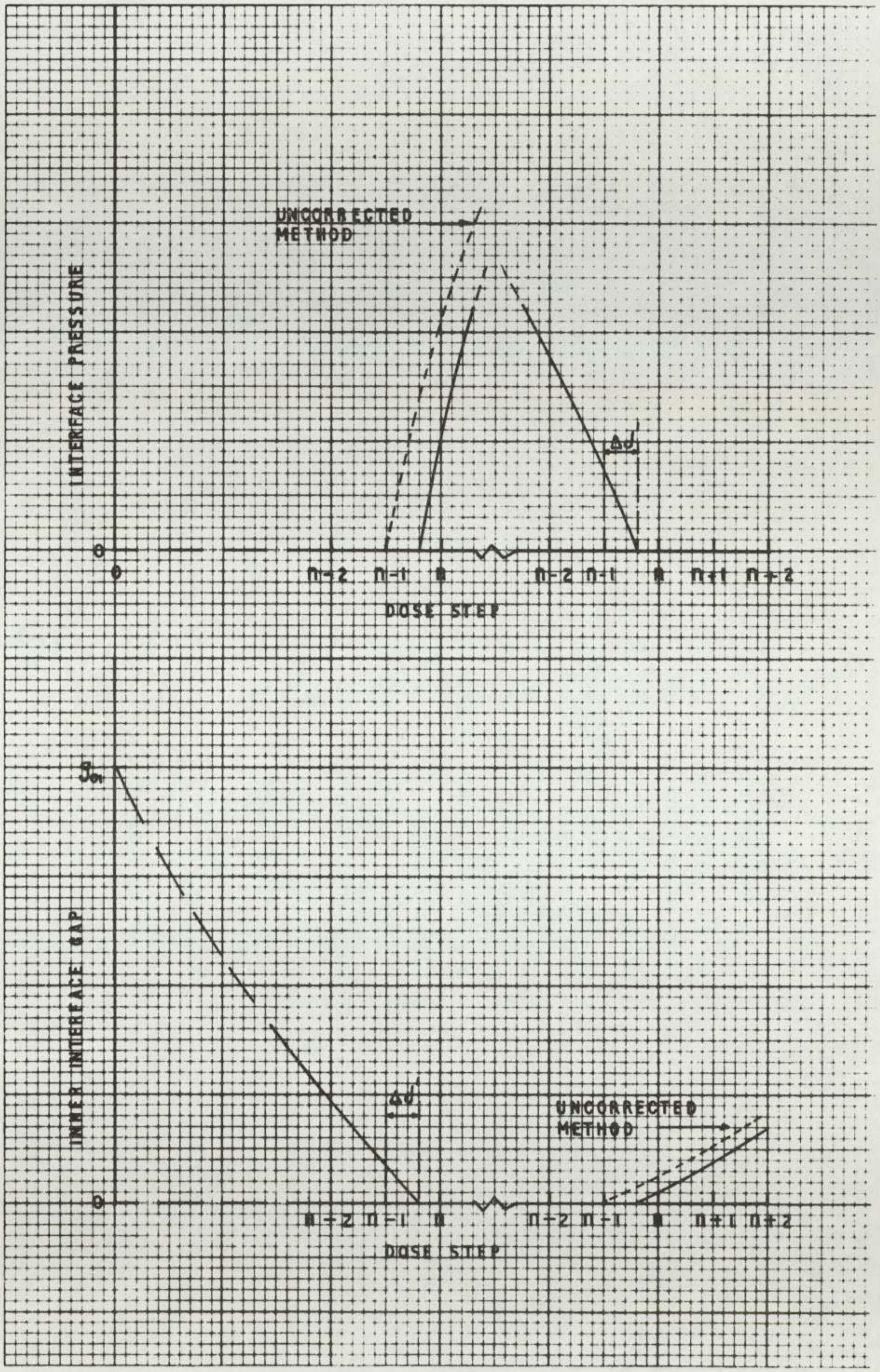

CORRECTION TO AZIMUSTAP 5 METHOD TO ALLOW FOR THE EFFECT OF FINITE DOSE INCREMENTS (.d)	FIG 4/10

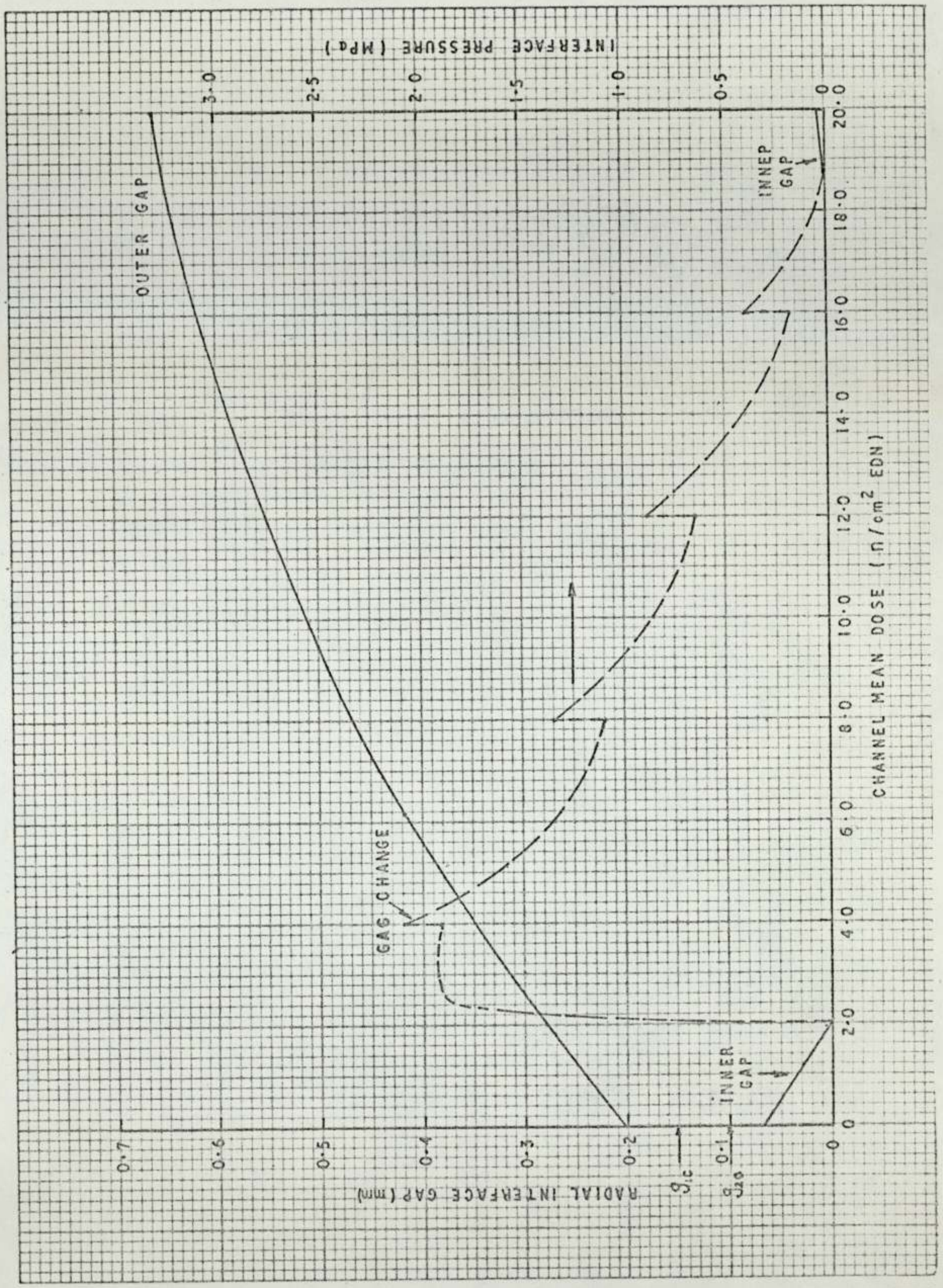

TIME EVOLUTION OF INTERFACE GAPS AND PRESSURES AT THE PEAK RATED AXIAL POSITION (2m FROM INLET)	FIG 4/11

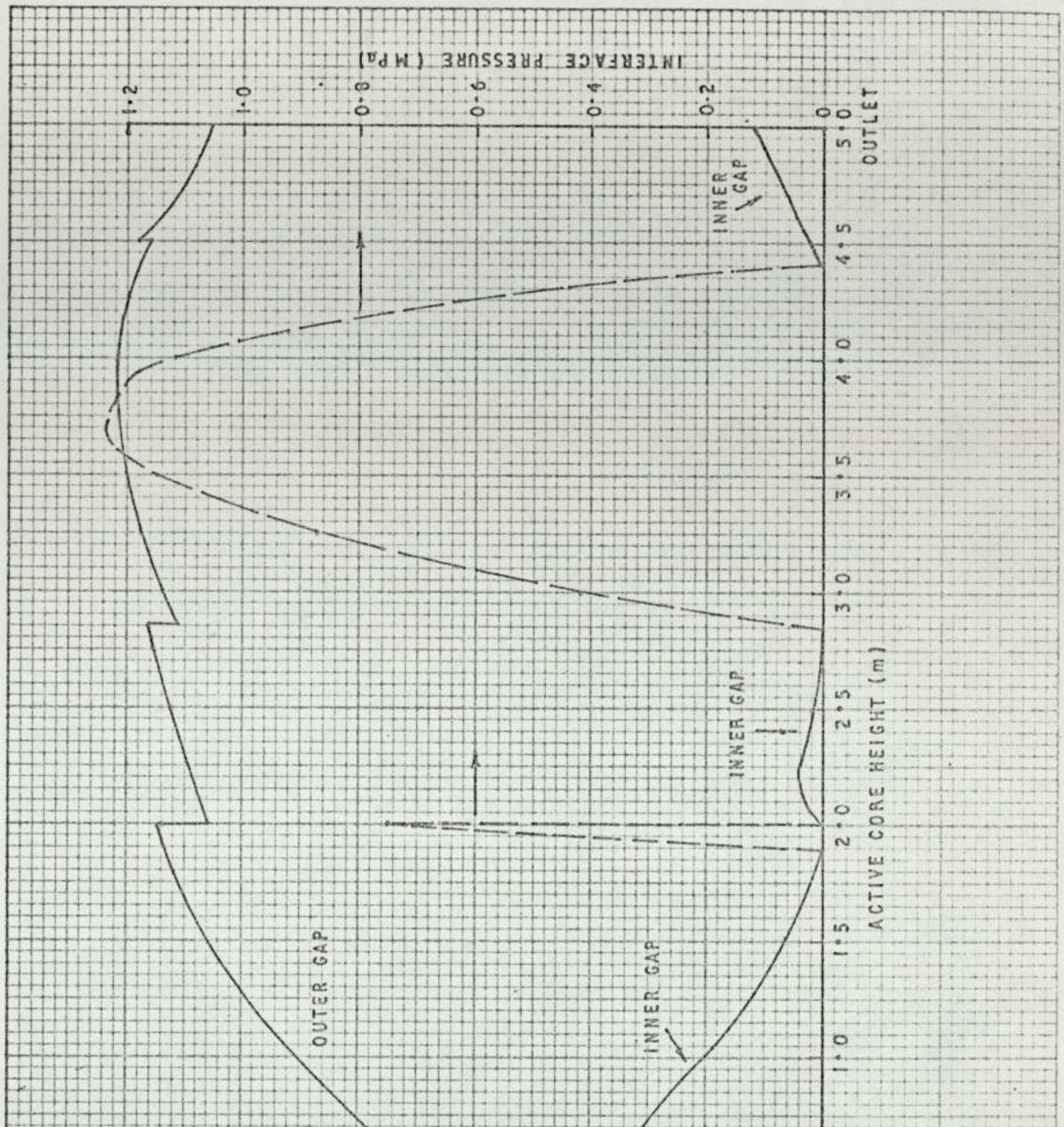

AXIAL DISTRIBUTION OF INTERFACE GAPS AND PRESSURES AT 2.0 x 10^{20} n/cm^2 EDN CHANNEL MEAN DOSE	FIG 4/12

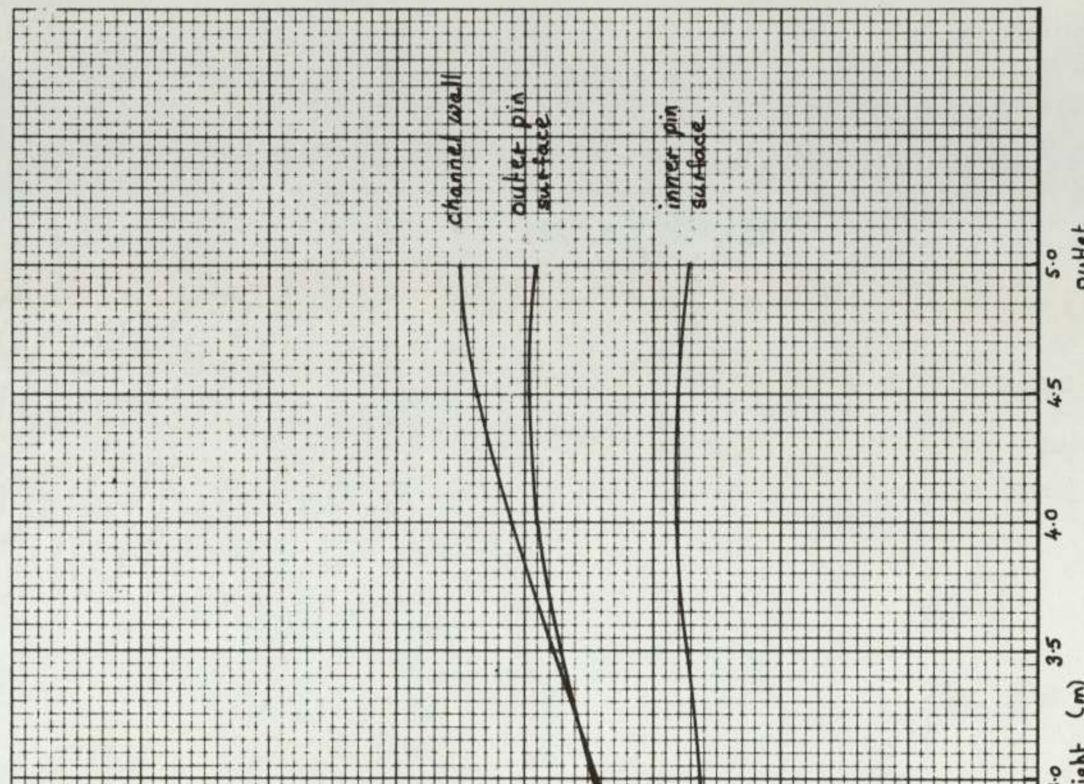

AXIAL DISTRIBUTION OF THERMAL EXPANSION INCREMENTS ON GRAPHITE SURFACE DIMENSIONS	FIG 4/13

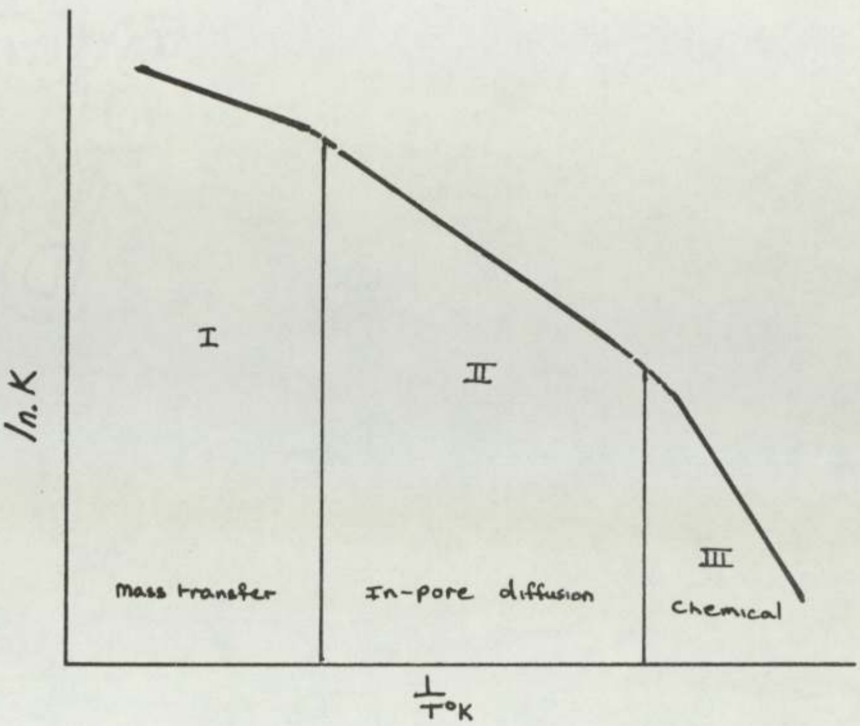

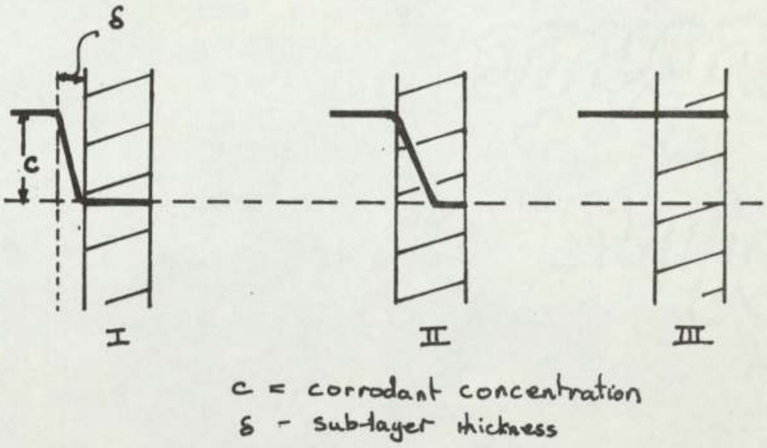

GRAPHITE CORROSION MECHANISMS	FIG 4/14

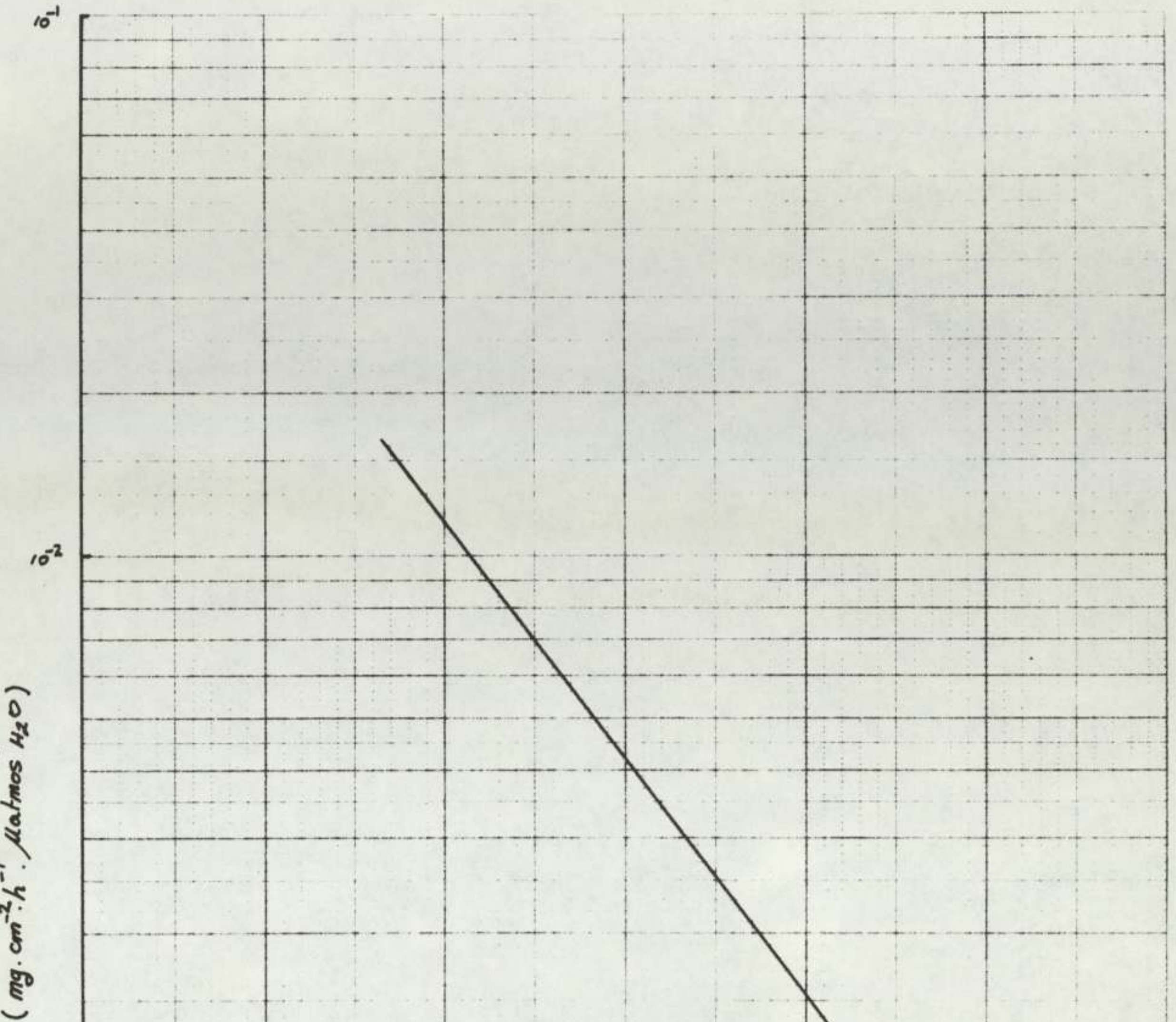

BURN-OFF RATE (k_{eff}) VERSUS GRAPHITE TEMPERATURE	FIG 4/15

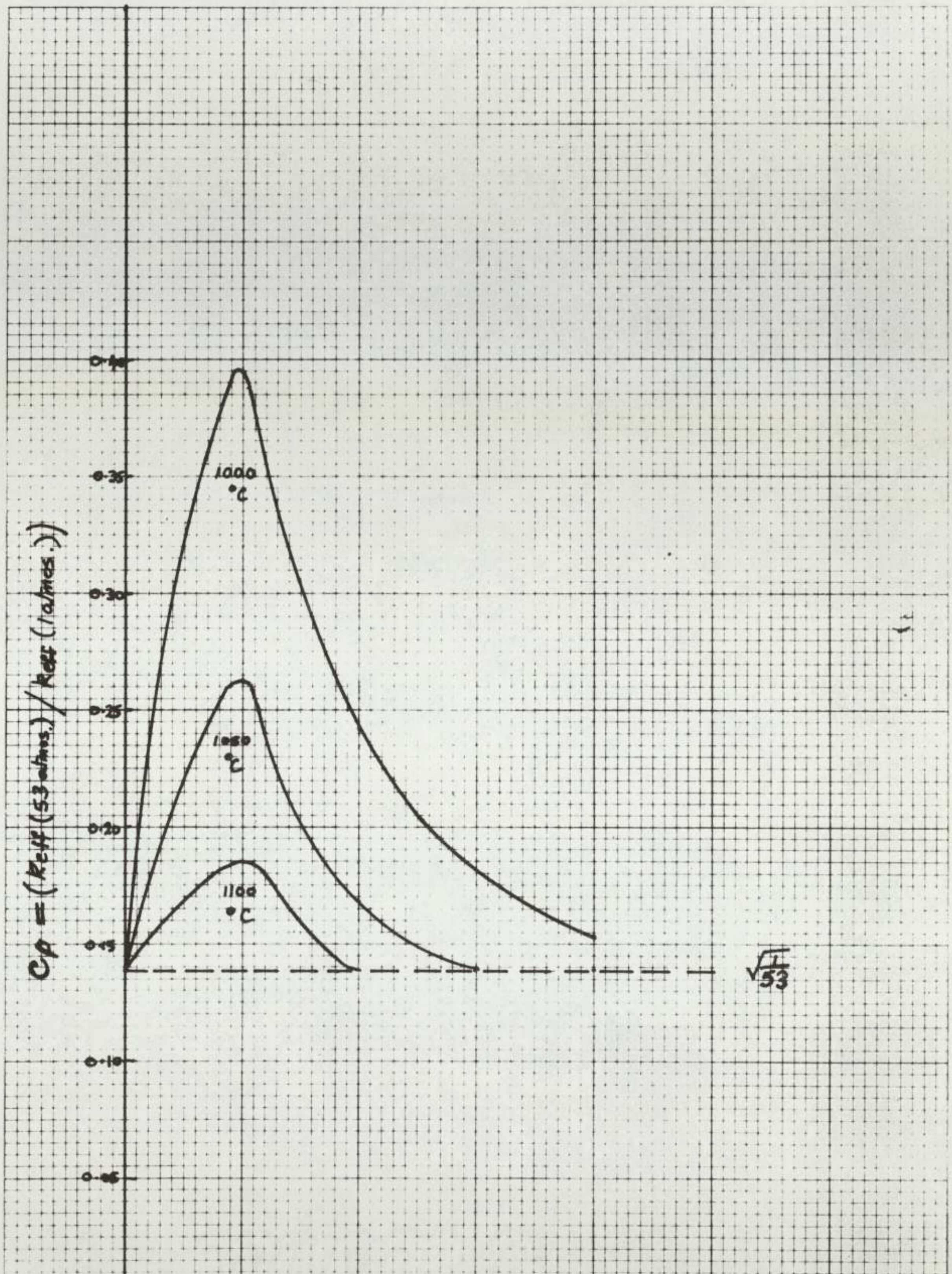

BURN-OFF RATE PRESSURE CONVERSION FACTOR VERSUS BURN-UP FOR VARIOUS GRAPHITE TEMPERATURES	FIG 4/16

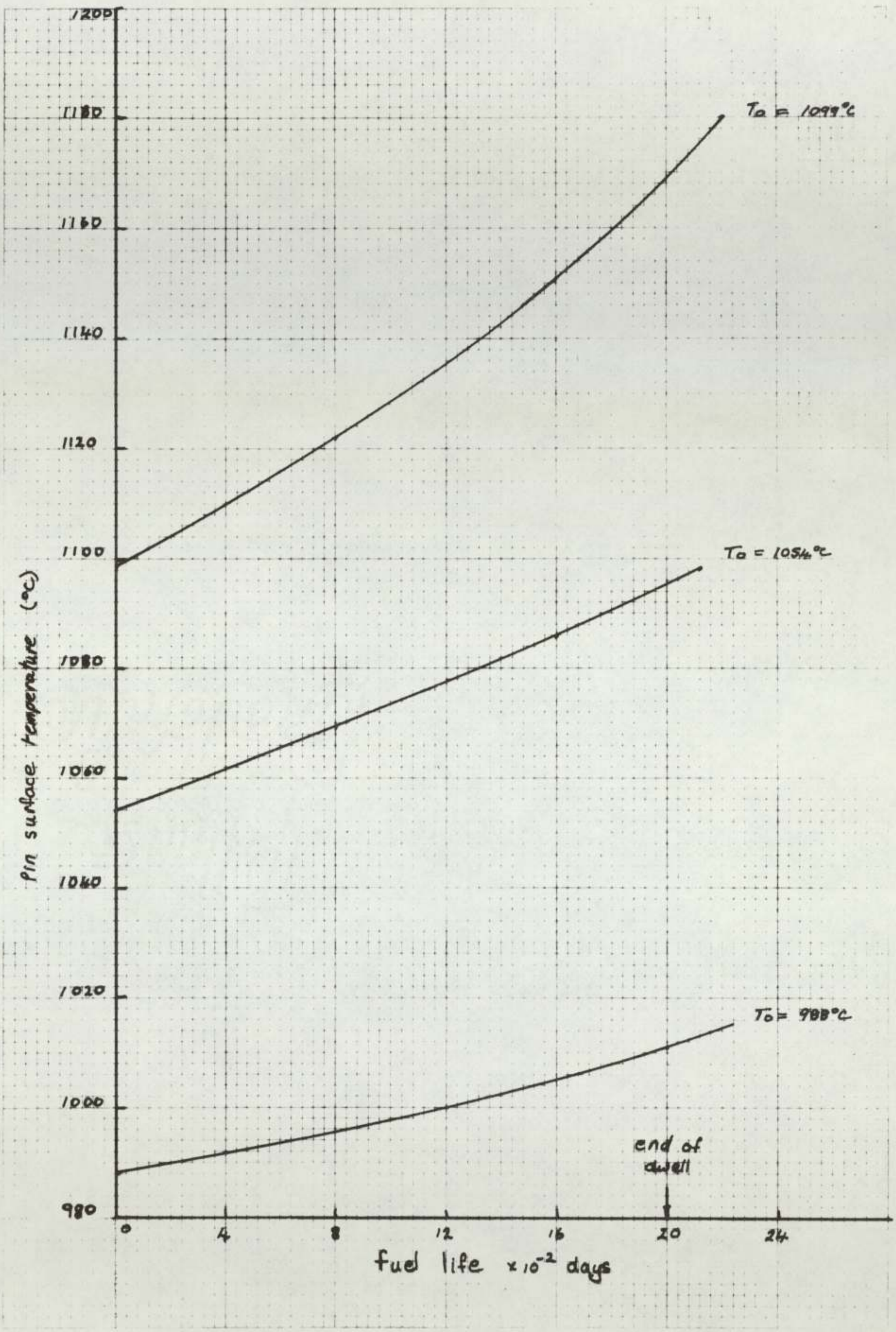

HOLLOW ROD SURFACE TEMPERATURE VERSUS FUEL DWELL FOR VARIOUS START-OF-LIFE VALUES (T_o)	FIG 4/17

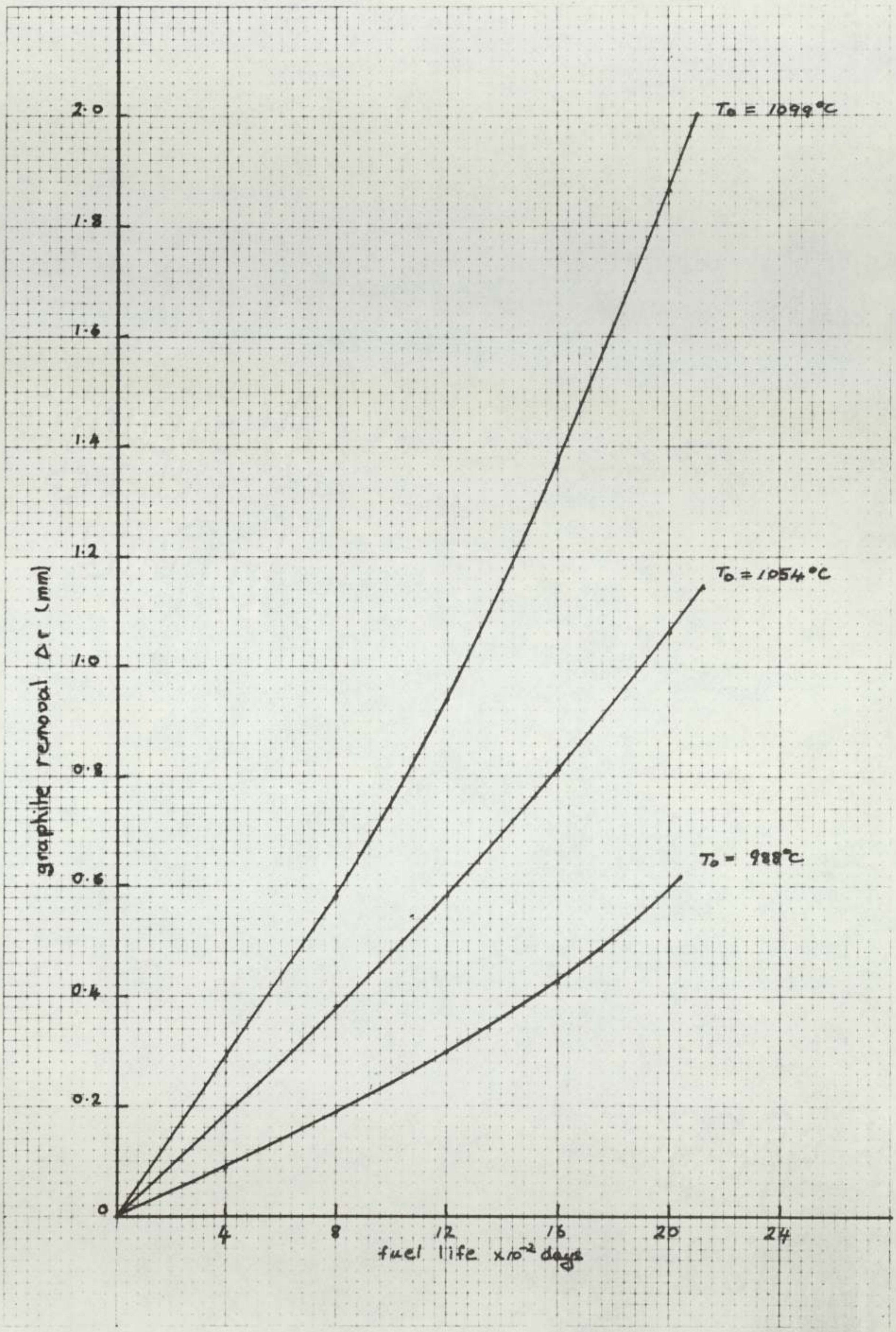

GRAPHITE REMOVAL VERSUS FUEL DWELL FOR VARIOUS START-OF-LIFE SURFACE TEMPERATURES	FIG 4/18

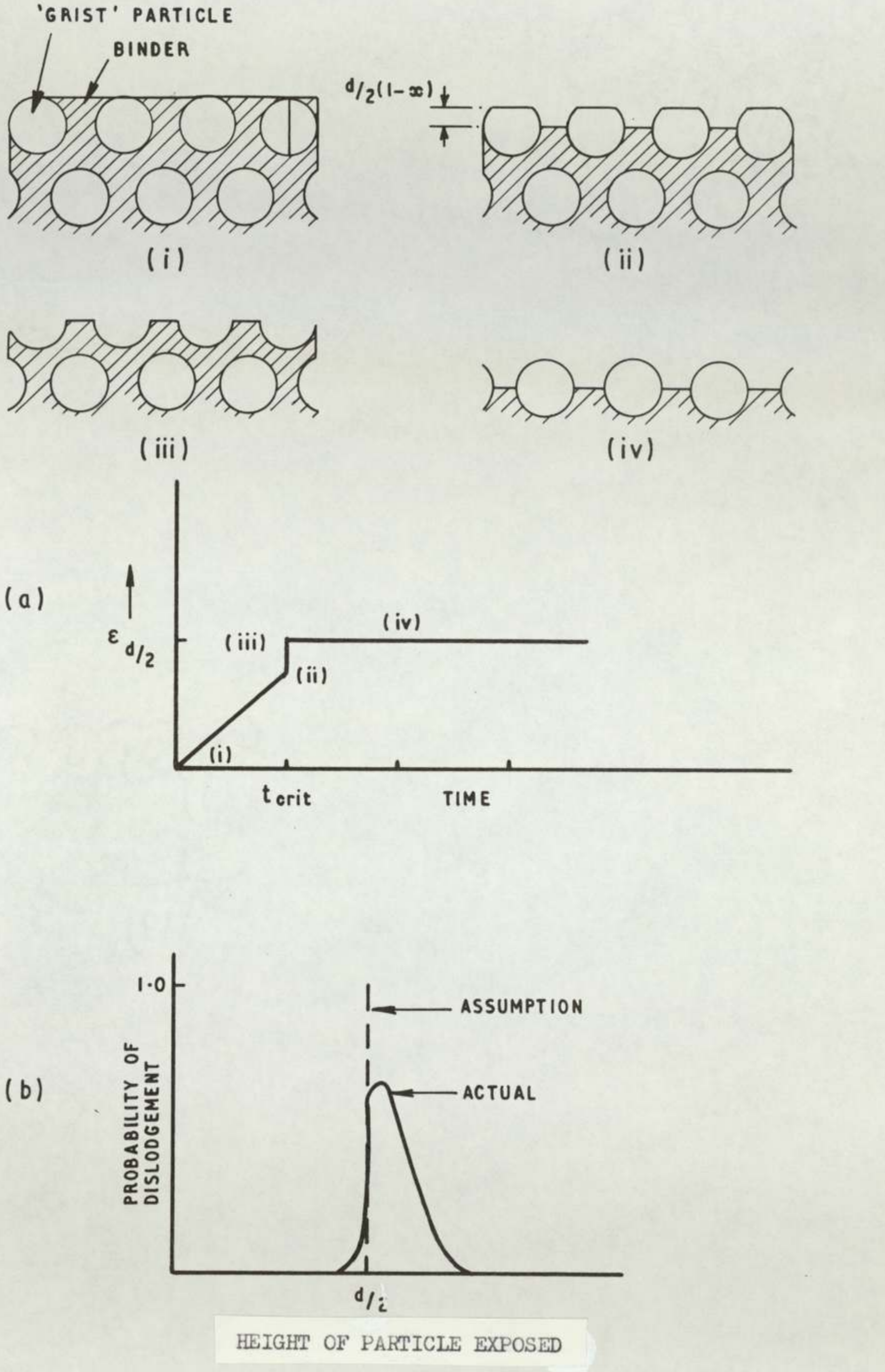

DEVELOPMENT OF SURFACE ROUGHNESS

FIG 4/19

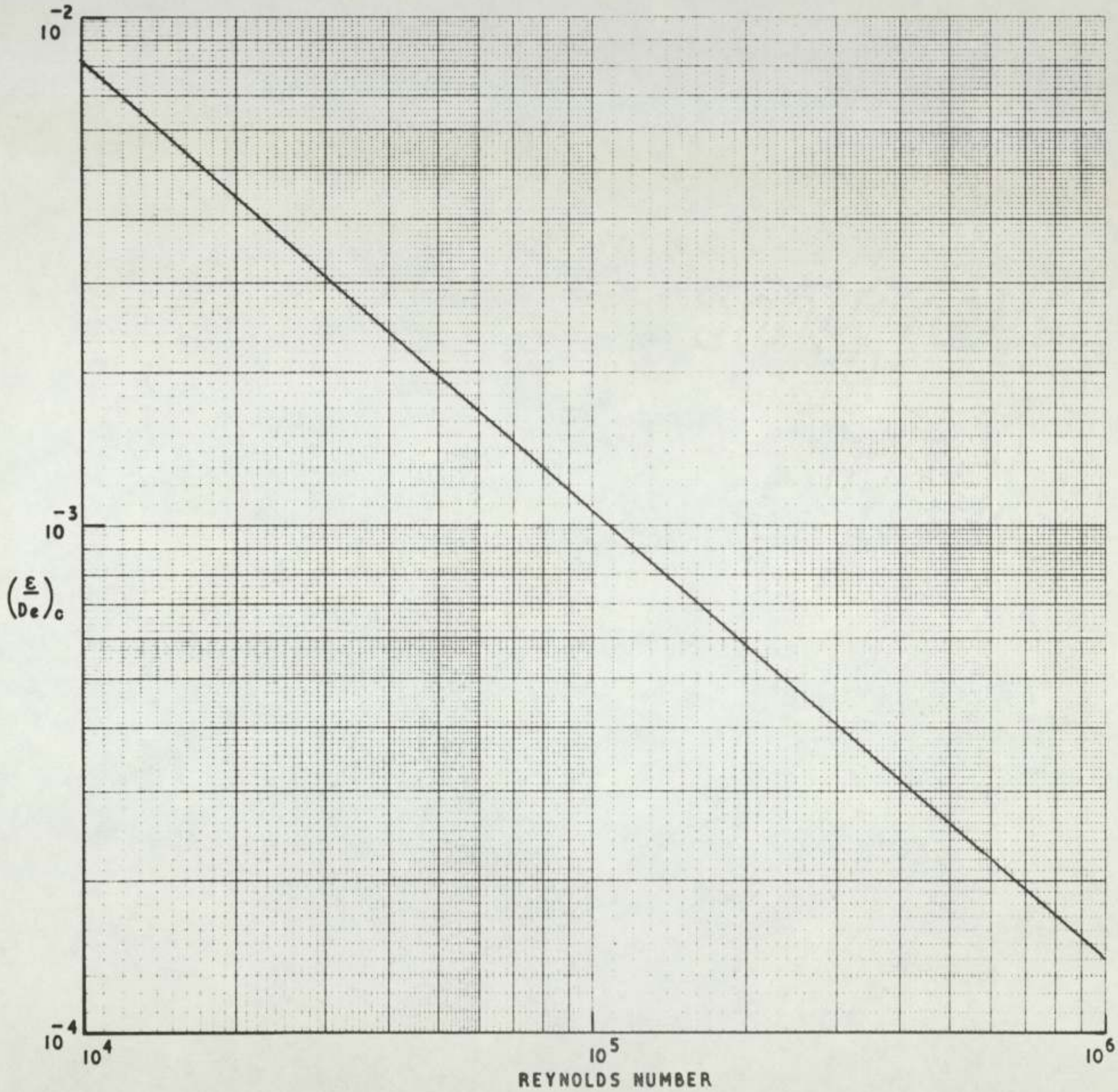

CRITICAL VALUES OF ROUGHNESS PARAMETER, $(\varepsilon/D_e)_c$: REYNOLDS NUMBER DEPENDENCE	FIG 4/20

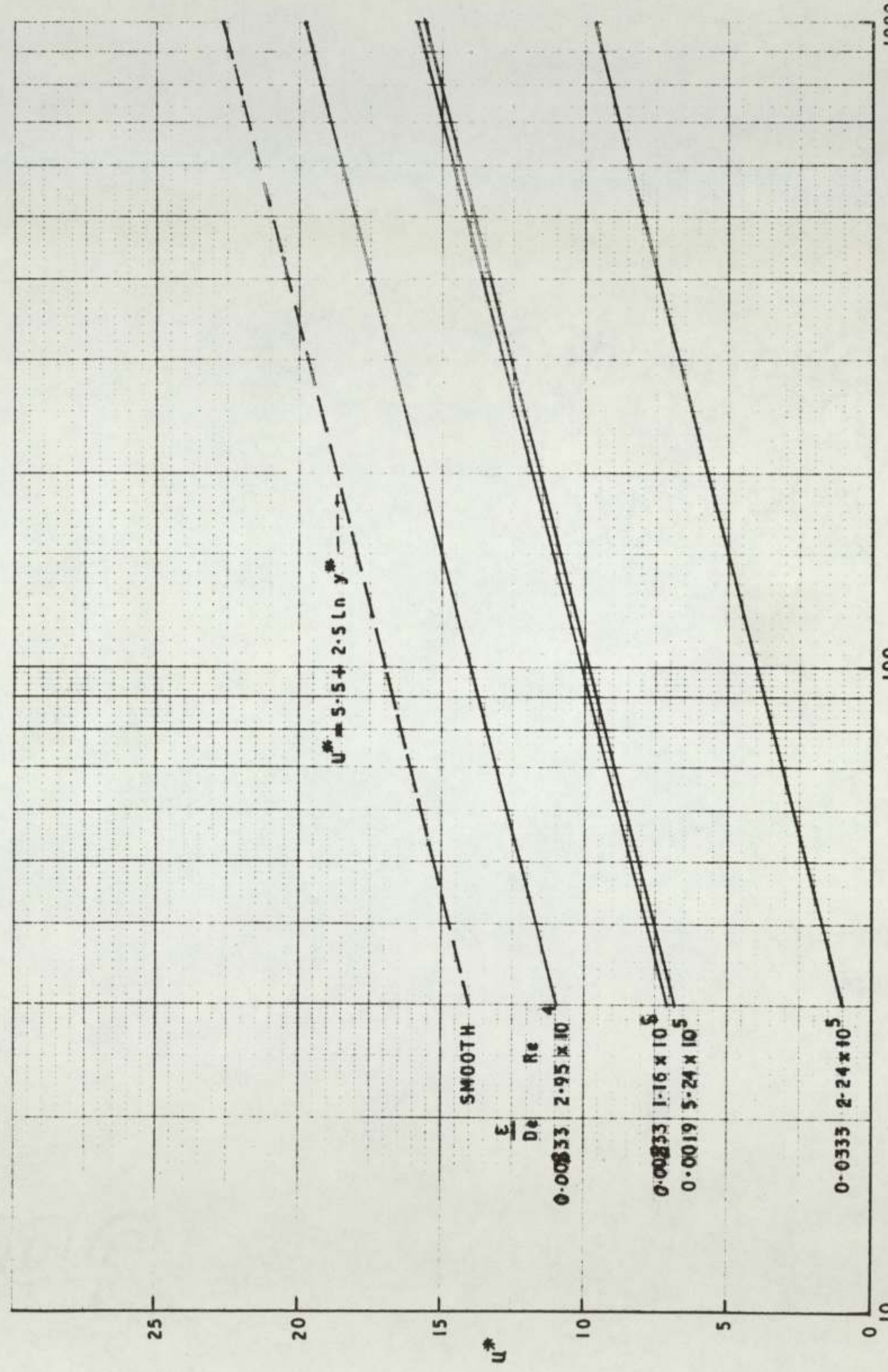

DIMENSIONLESS VELOCITY PROFILES FOR SMOOTH AND ROUGH TUBES	FIG 4/21

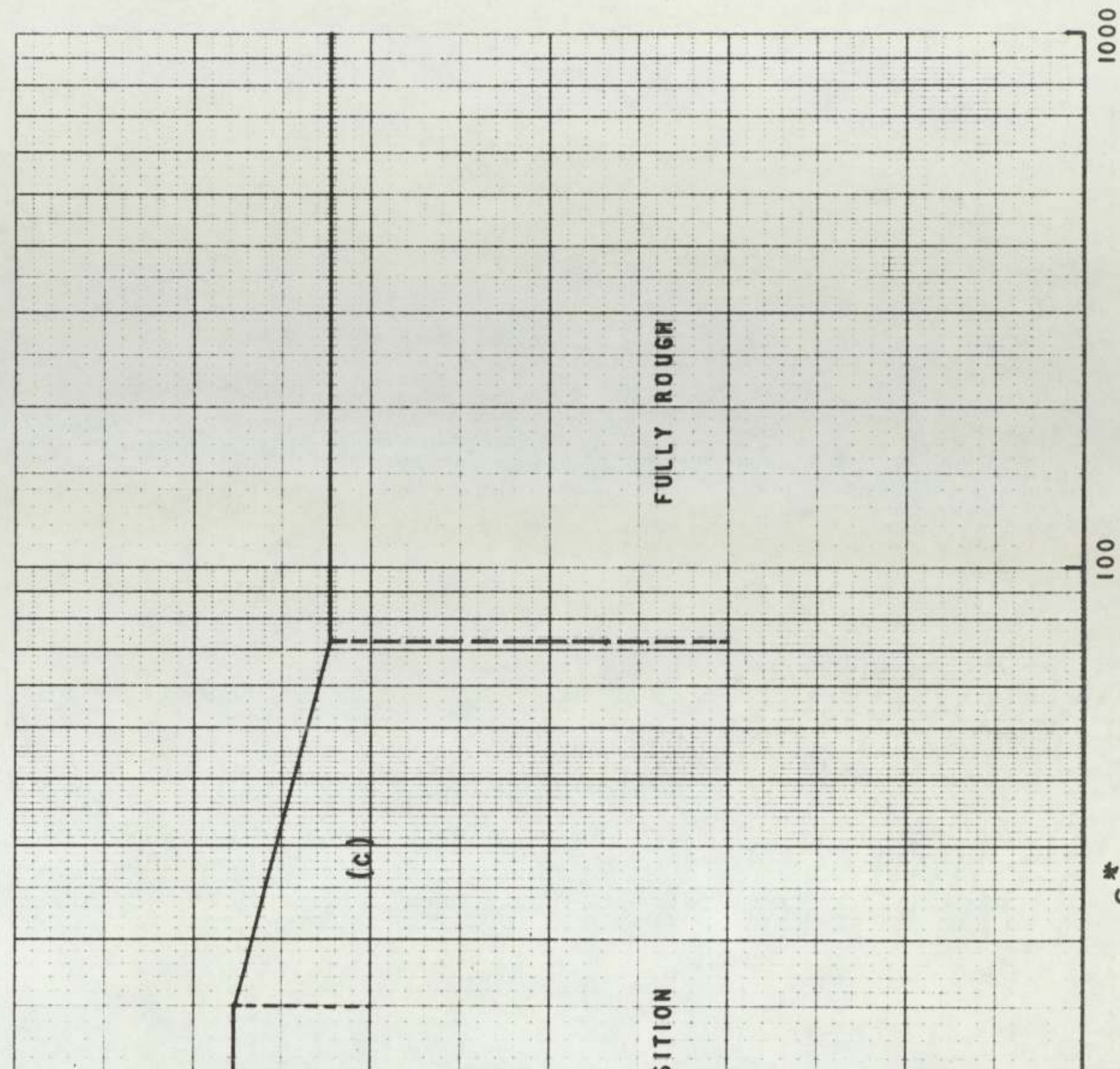

A* VERSUS ε* SHOWING ROUGHNESS REGIMES	FIG 4/22

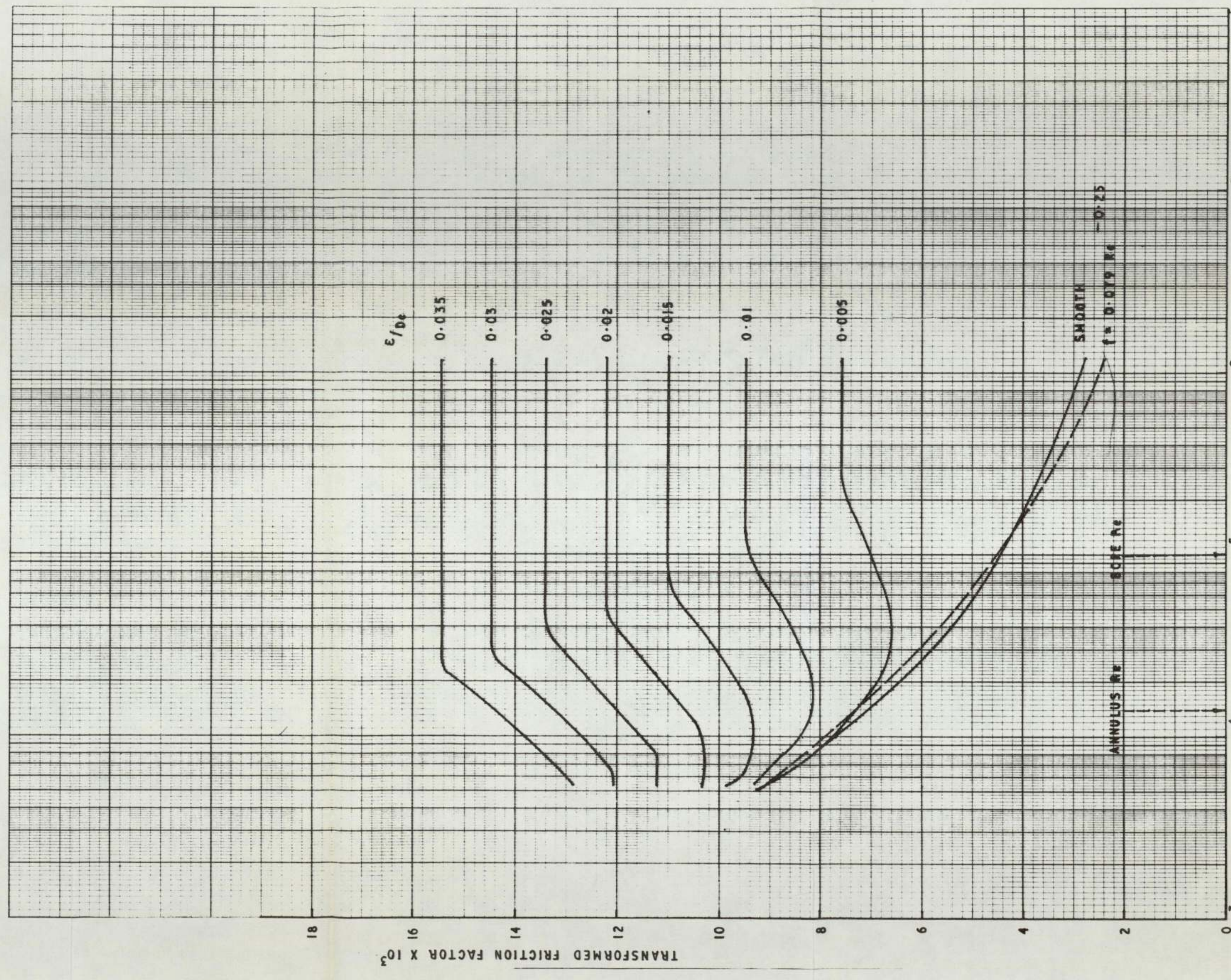

FRICTION FACTOR VERSUS REYNOLDS NUMBER FOR VARIOUS VALUES OF THE ROUGHNESS PARAMETER ε/D_e	FIG 4/23

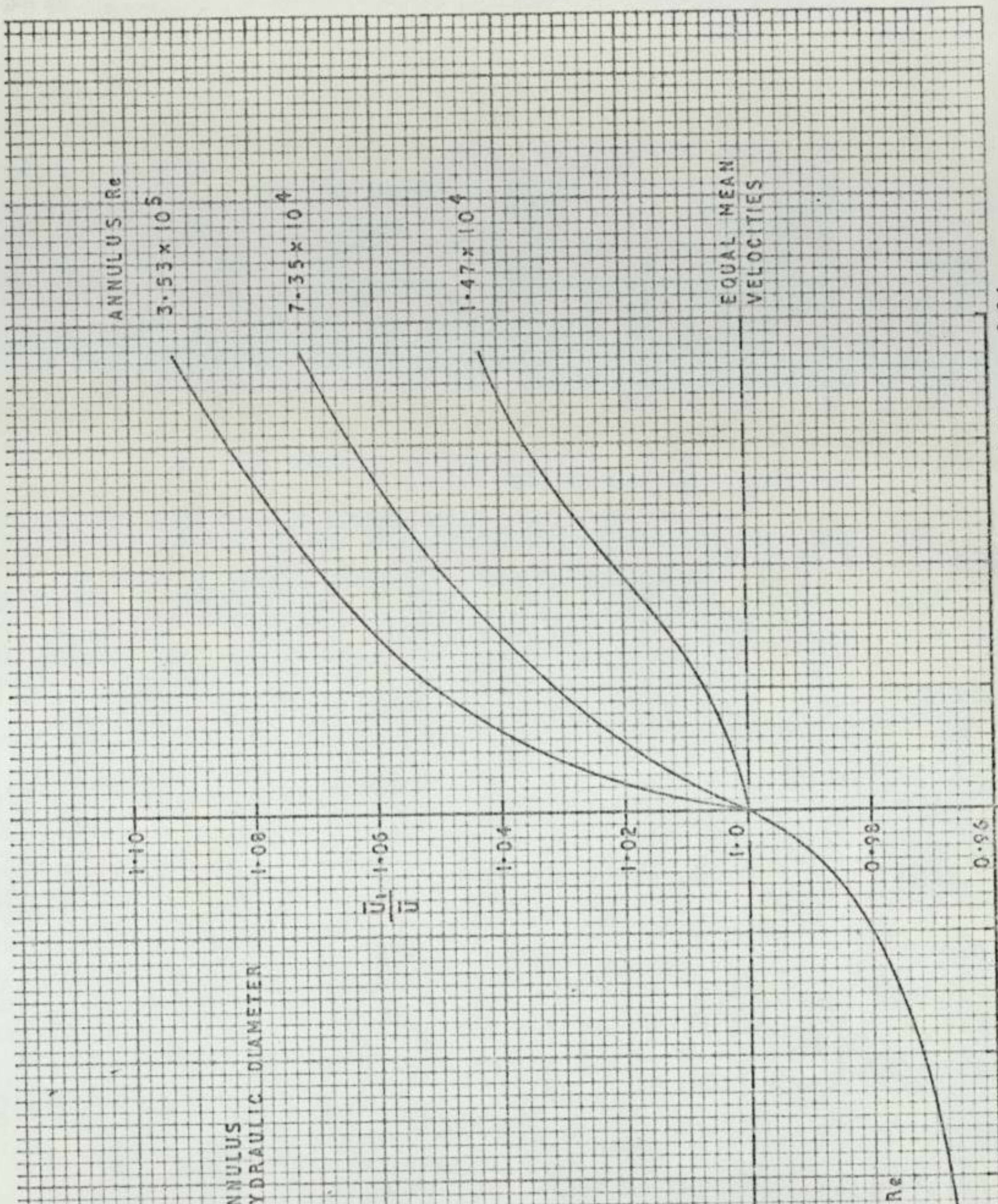

$\bar{u}_1/\bar{u}$ AGAINST ε/D_e AND REYNOLDS NUMBER IN AN ANNULUS	FIG 4/24

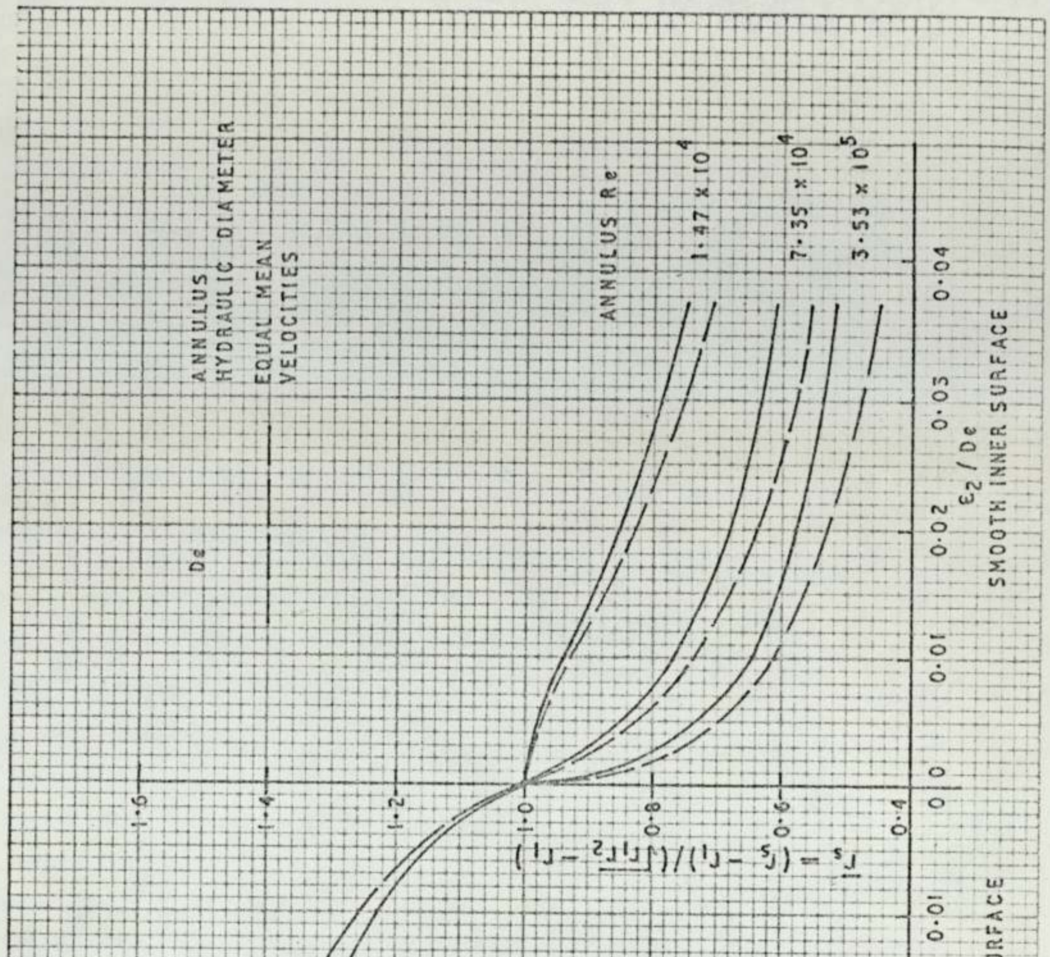

DIMENSIONLESS RADIUS OF NO-SHEAR ($\bar{r}_s$) AGAINST ε/D_e AND REYNOLDS NUMBER IN AN ANNULUS	FIG 4/25

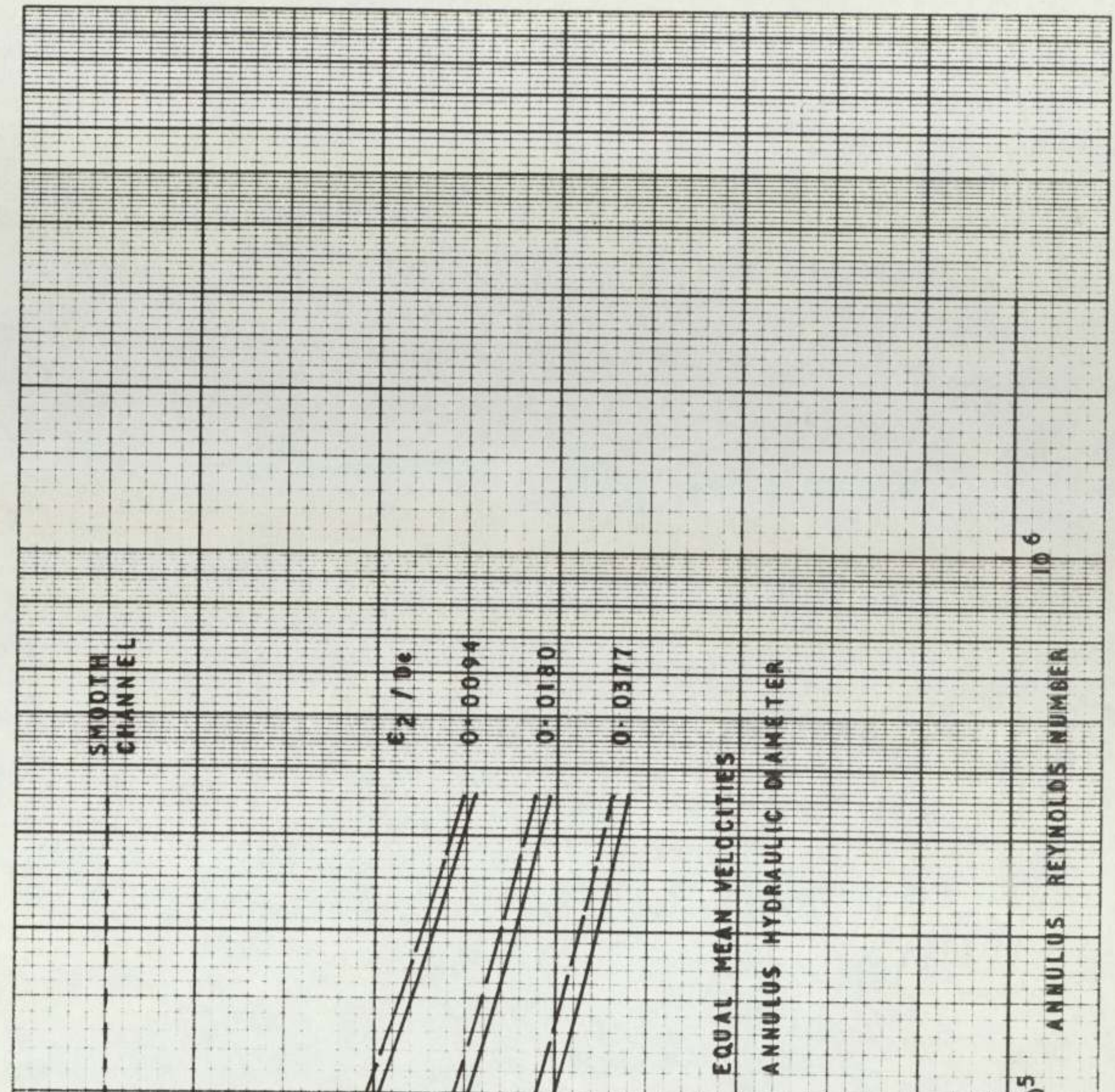

f_1/F VERSUS REYNOLDS NUMBER FOR VARIOUS VALUES OF ε_2/D_e	FIG 4/26

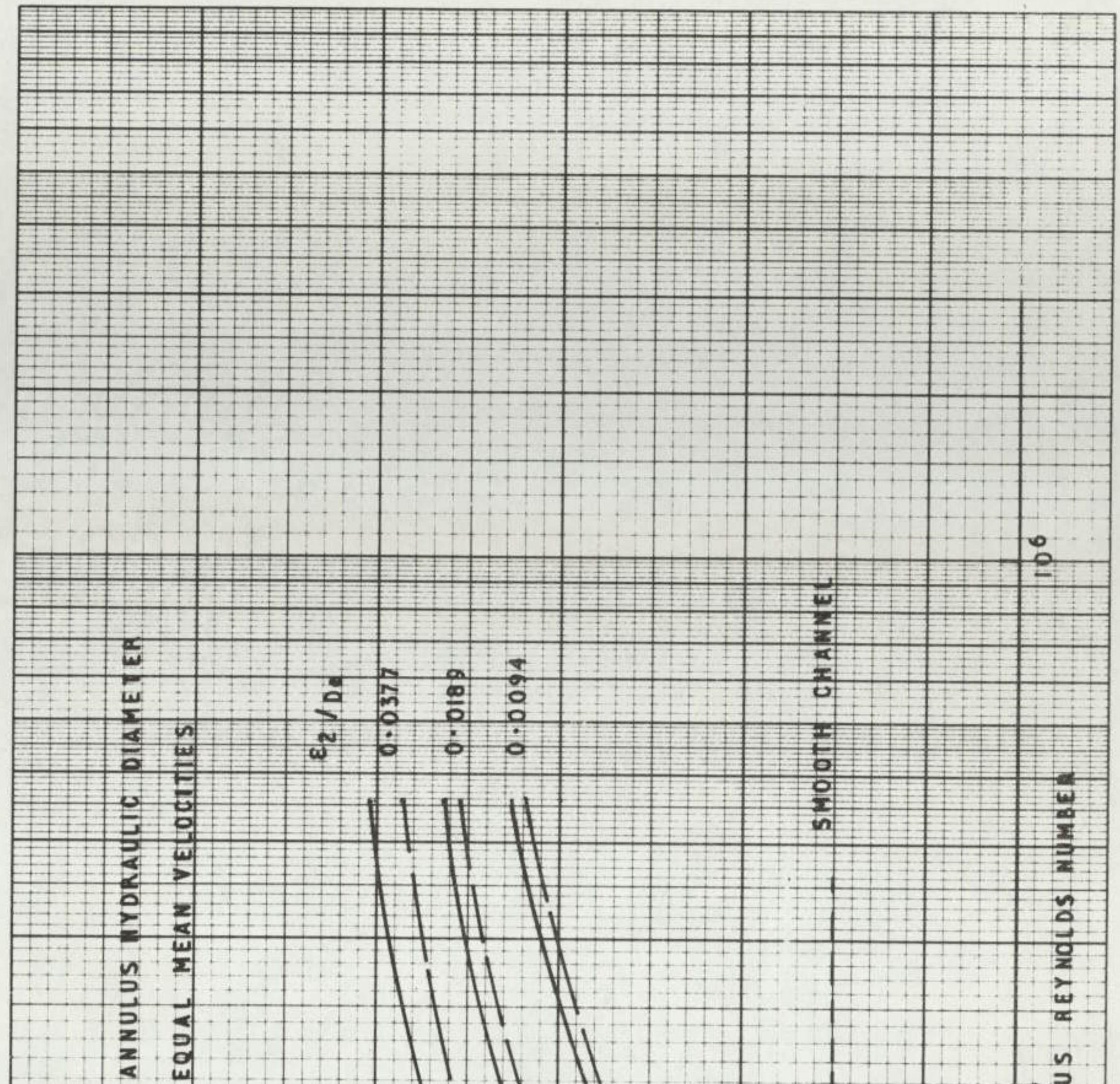

f_2/F VERSUS REYNOLDS NUMBER FOR VARIOUS VALUES OF ε_2/D_e	FIG 4/27

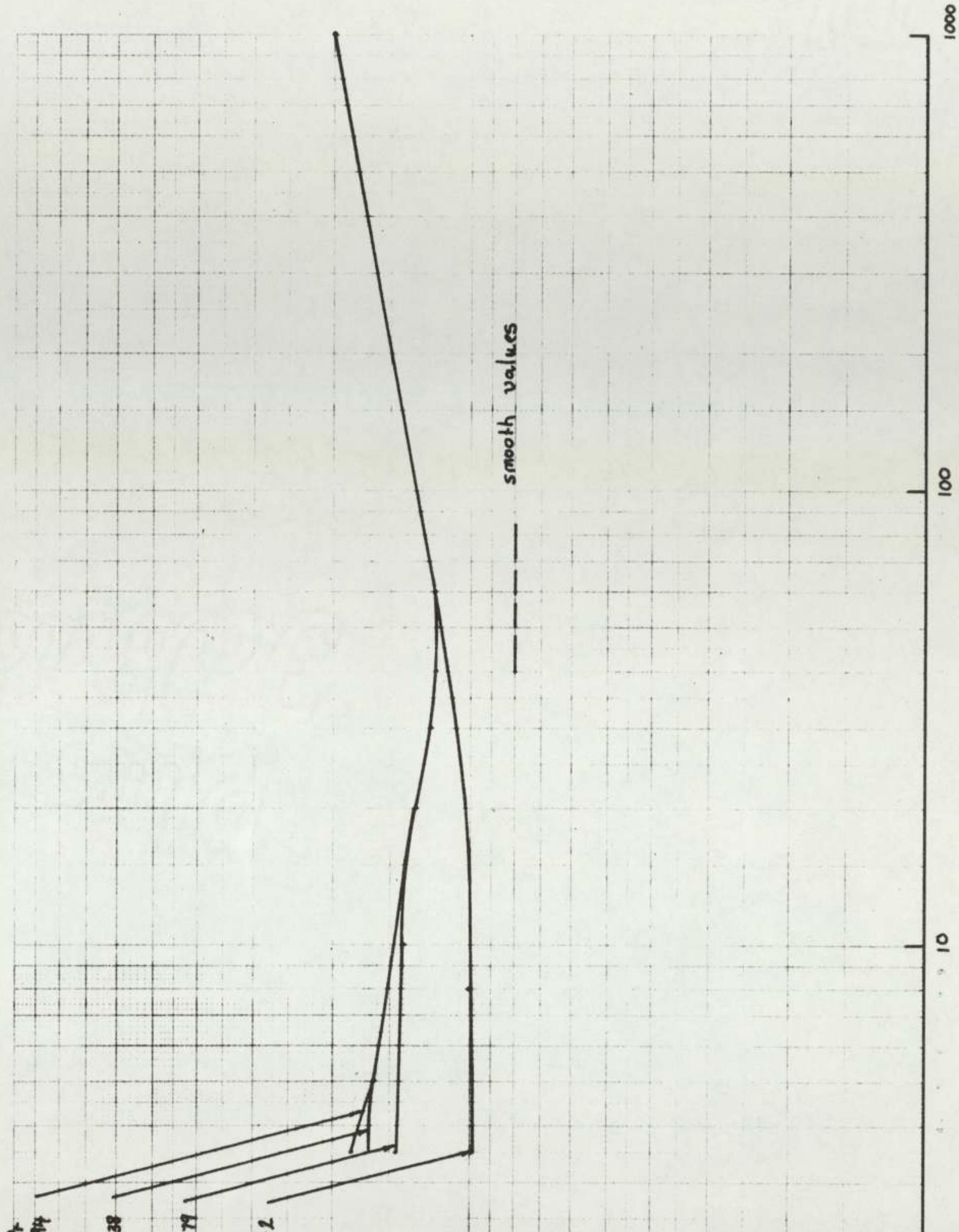

B* VERSUS ε* FOR PRANDTL NUMBERS: 5.94, 4.38, 2.79, 1.2

FIG 4/28

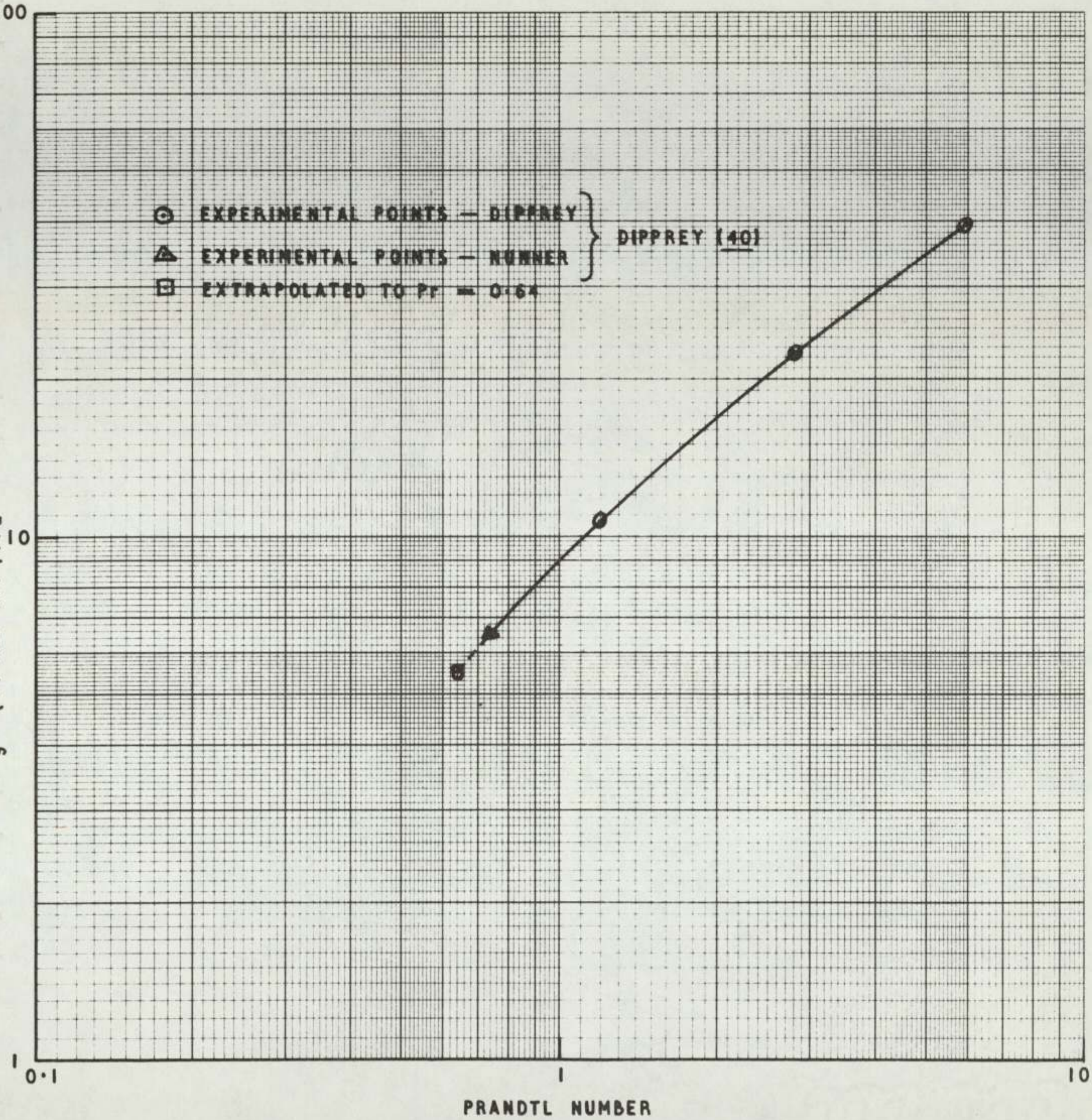

SMOOTH LIMITING VALUES OF g – PRANDTL NUMBER DEPENDENCE	FIG 4/29

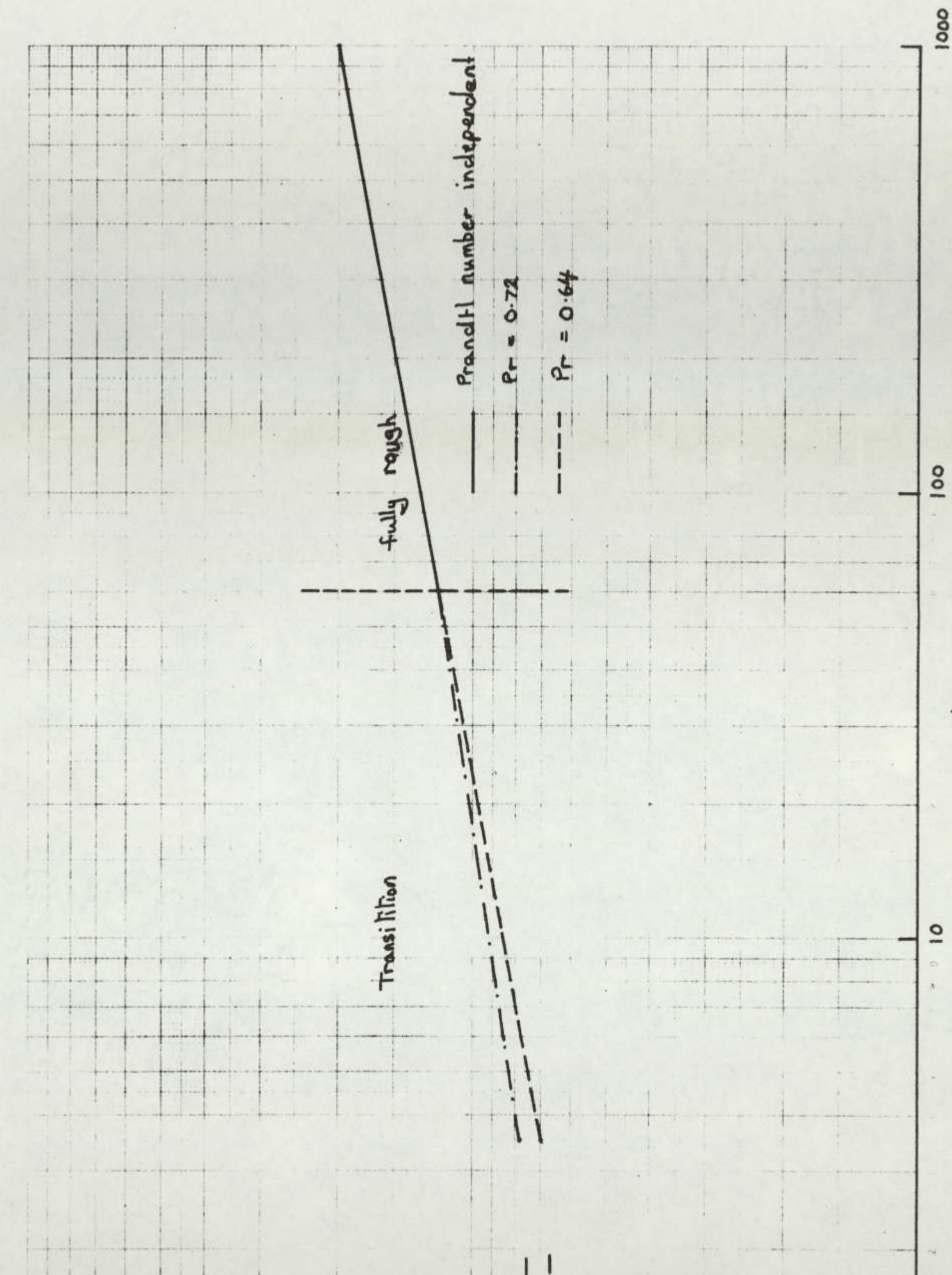

B* VERSUS ε* FOR PRANDTL NUMBERS: 0.72, 0.64	FIG 4/30

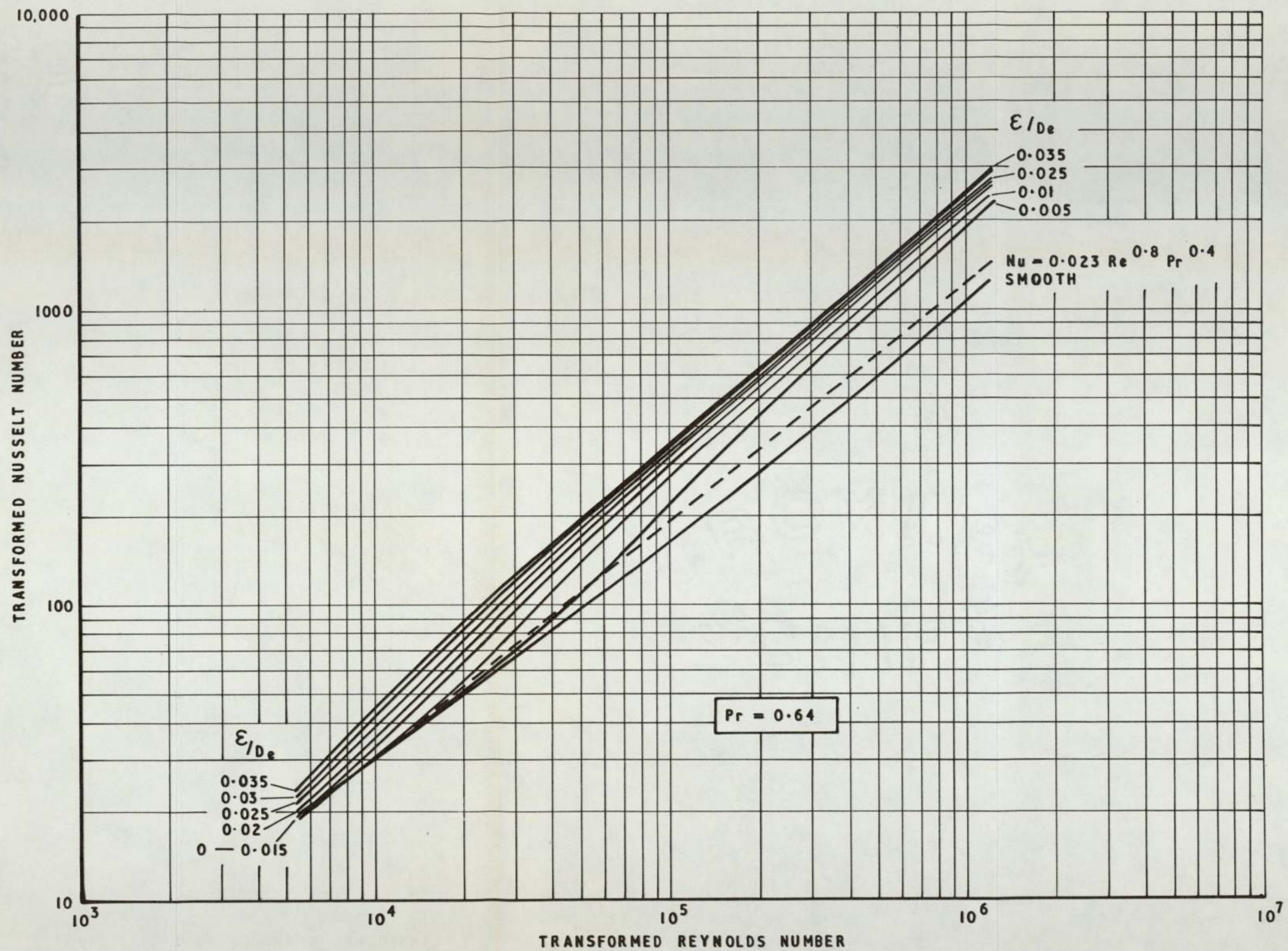

Nu VERSUS REYNOLDS NUMBER FOR VARIOUS VALUES OF /D_e	FIG 4/31

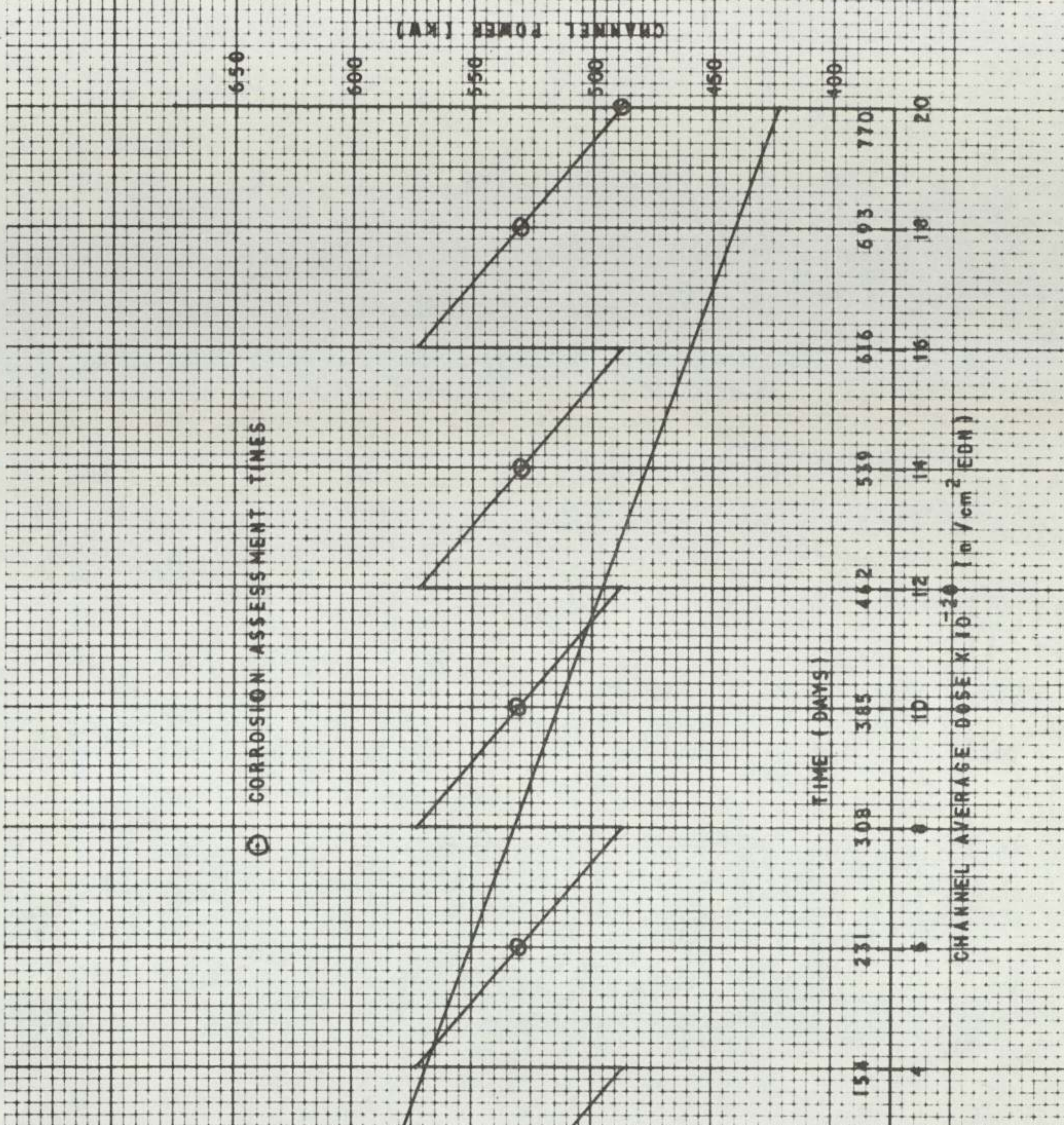

TIME EVOLUTION OF T_2 AND Q_{CH} SHOWING CORROSION ASSESSMENT CALCULATION POINTS

FIG 4/32

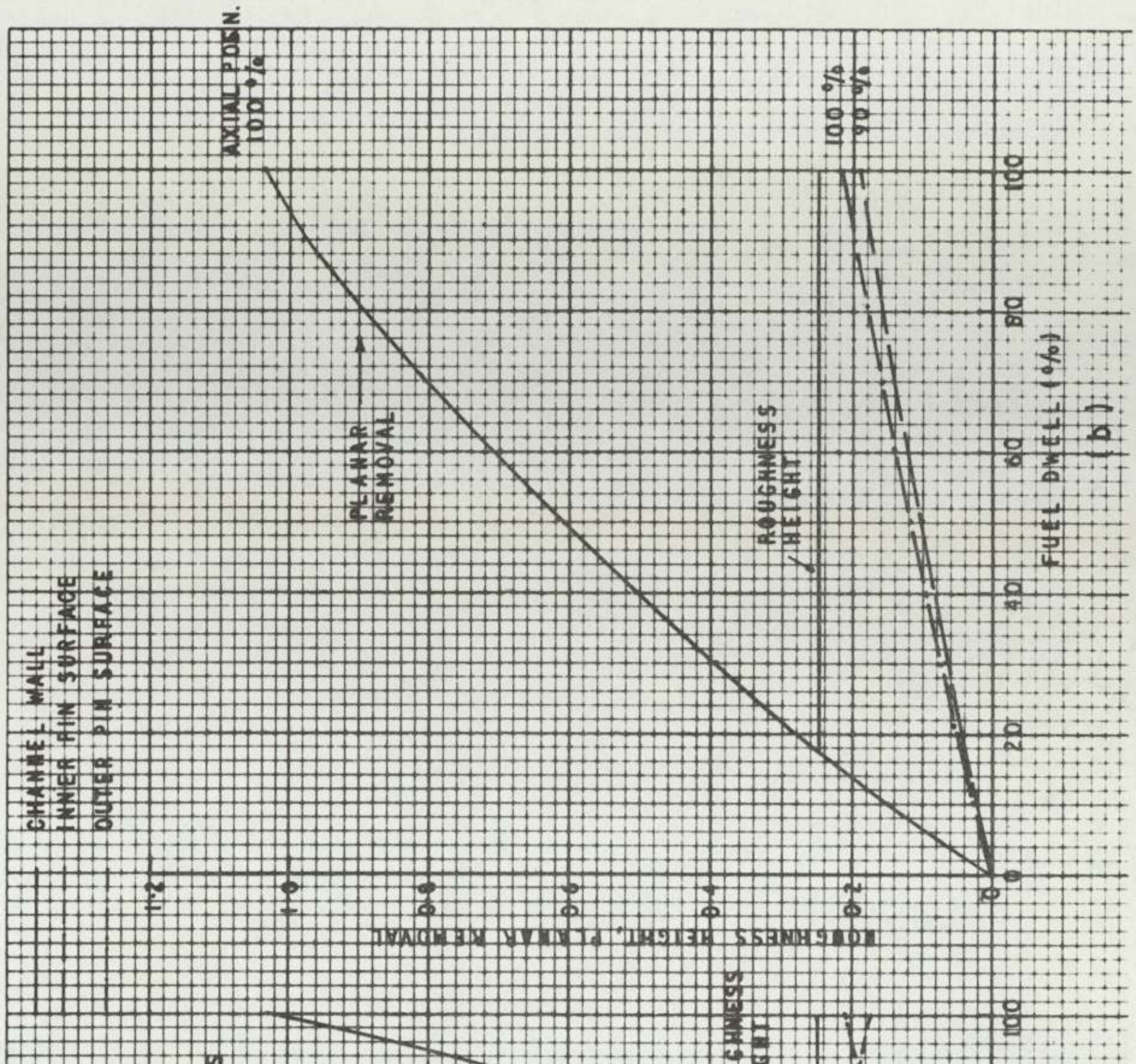

AXIAL (a) AND TIME (b) DISTRIBUTIONS OF ROUGHNESS HEIGHT AND PLANAR REMOVAL	FIG 4/33

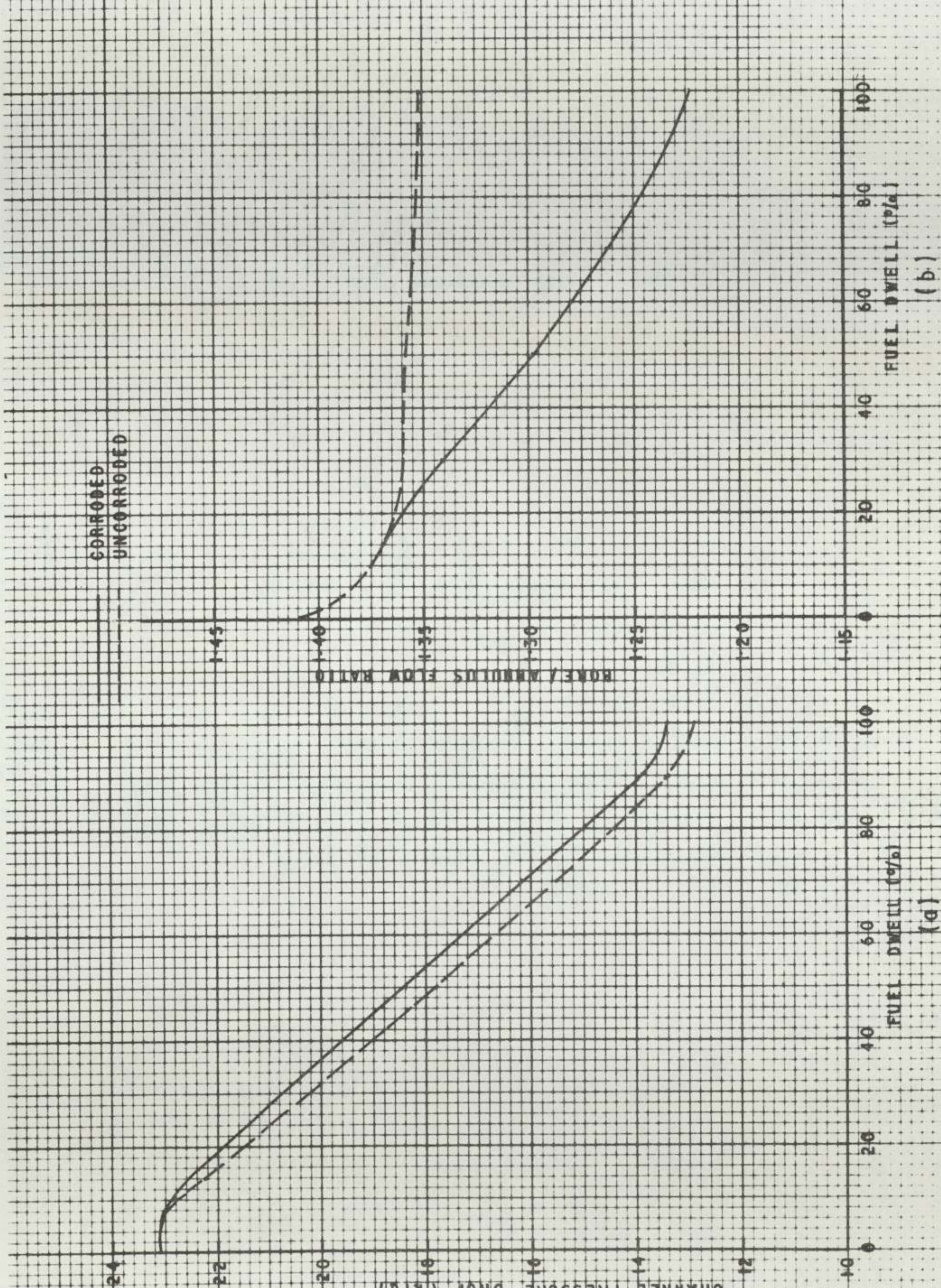

TIME EVOLUTIONS OF PRESSURE DROP (a) AND FLOW SPLIT (b)

FIG 4/34

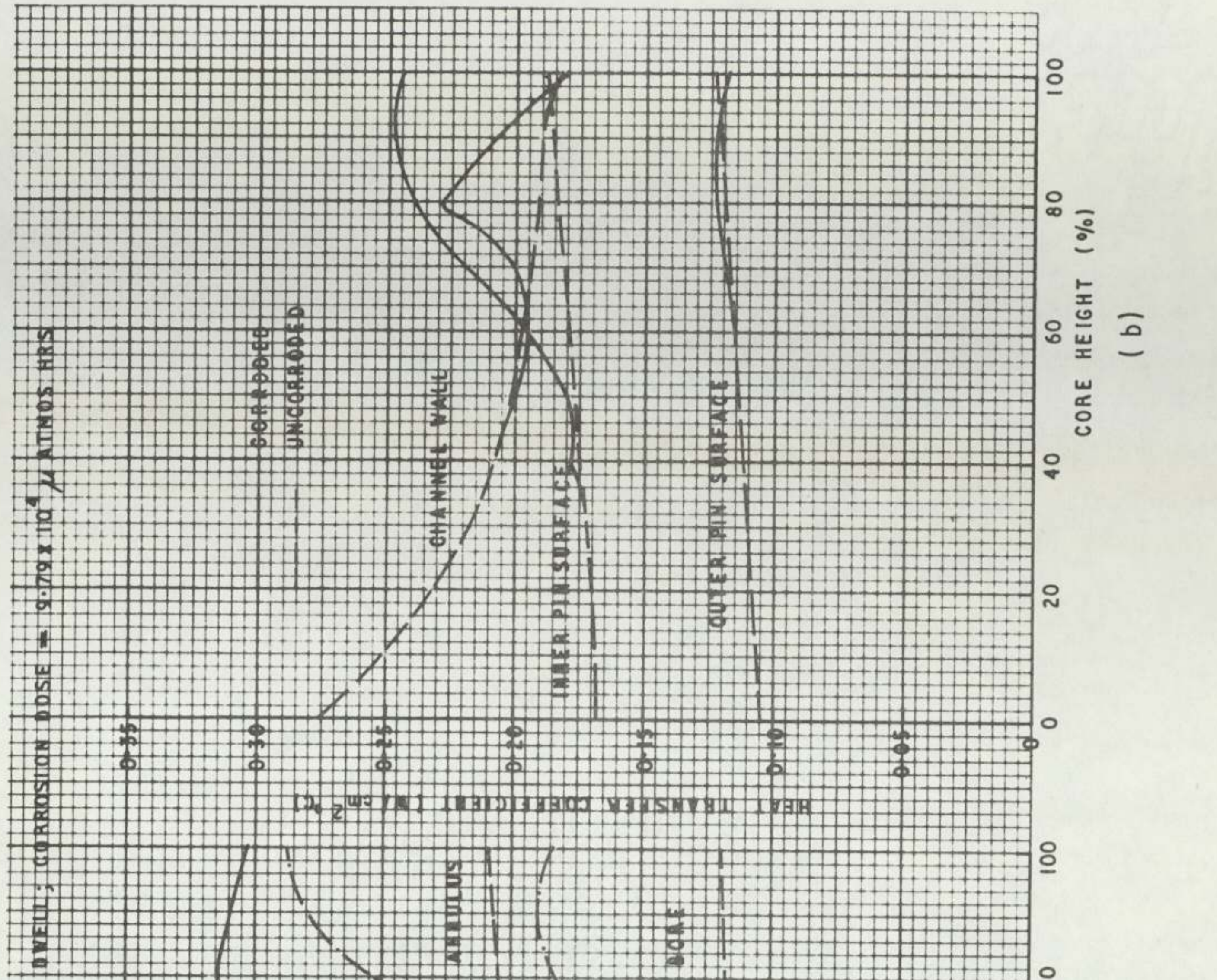

AXIAL DISTRIBUTION OF FRICTION FACTOR (a) AND HEAT TRANSFER COEFFICIENT (b)	FIG 4/35

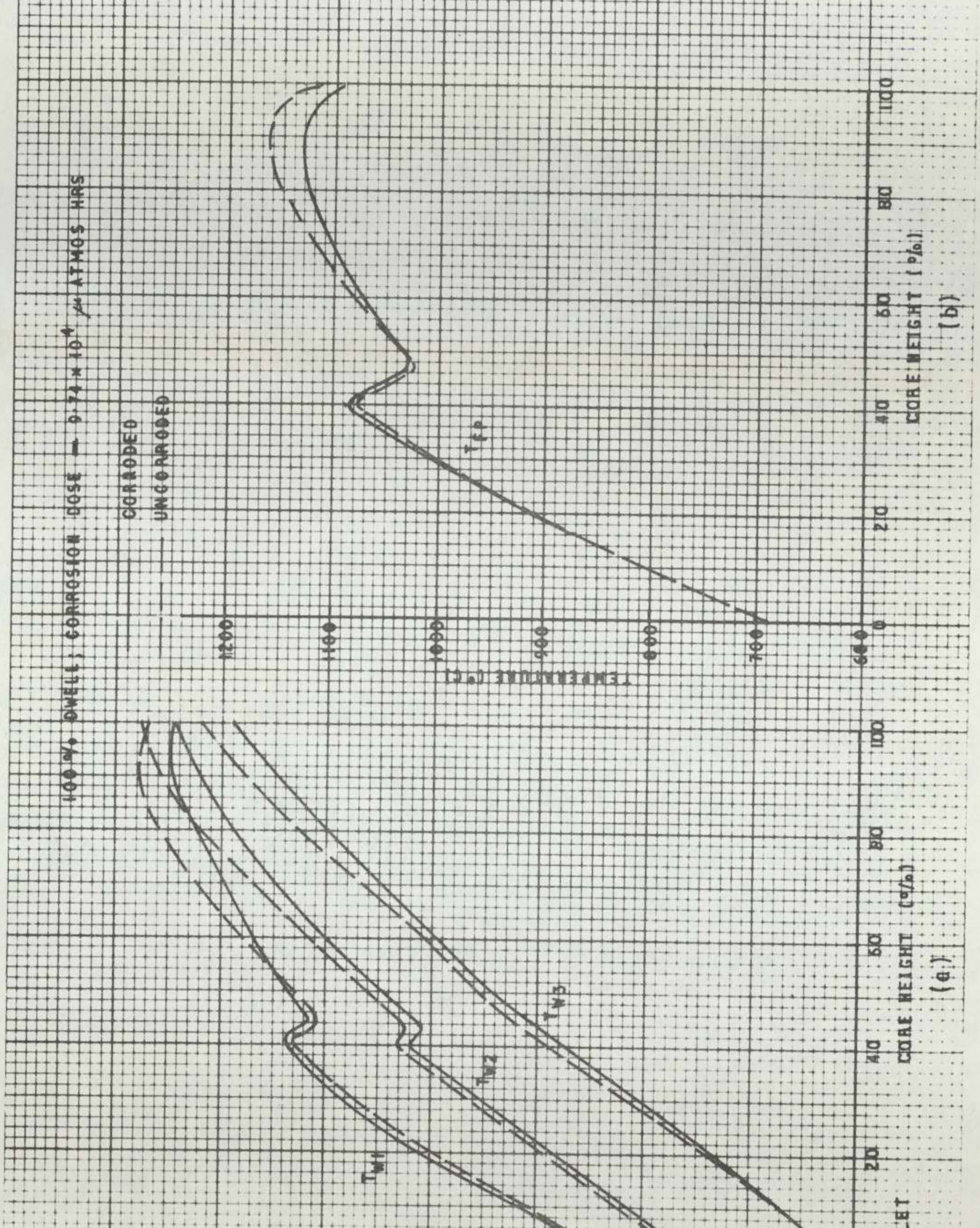

AXIAL DISTRIBUTIONS OF TEMPERATURE	FIG 4/36

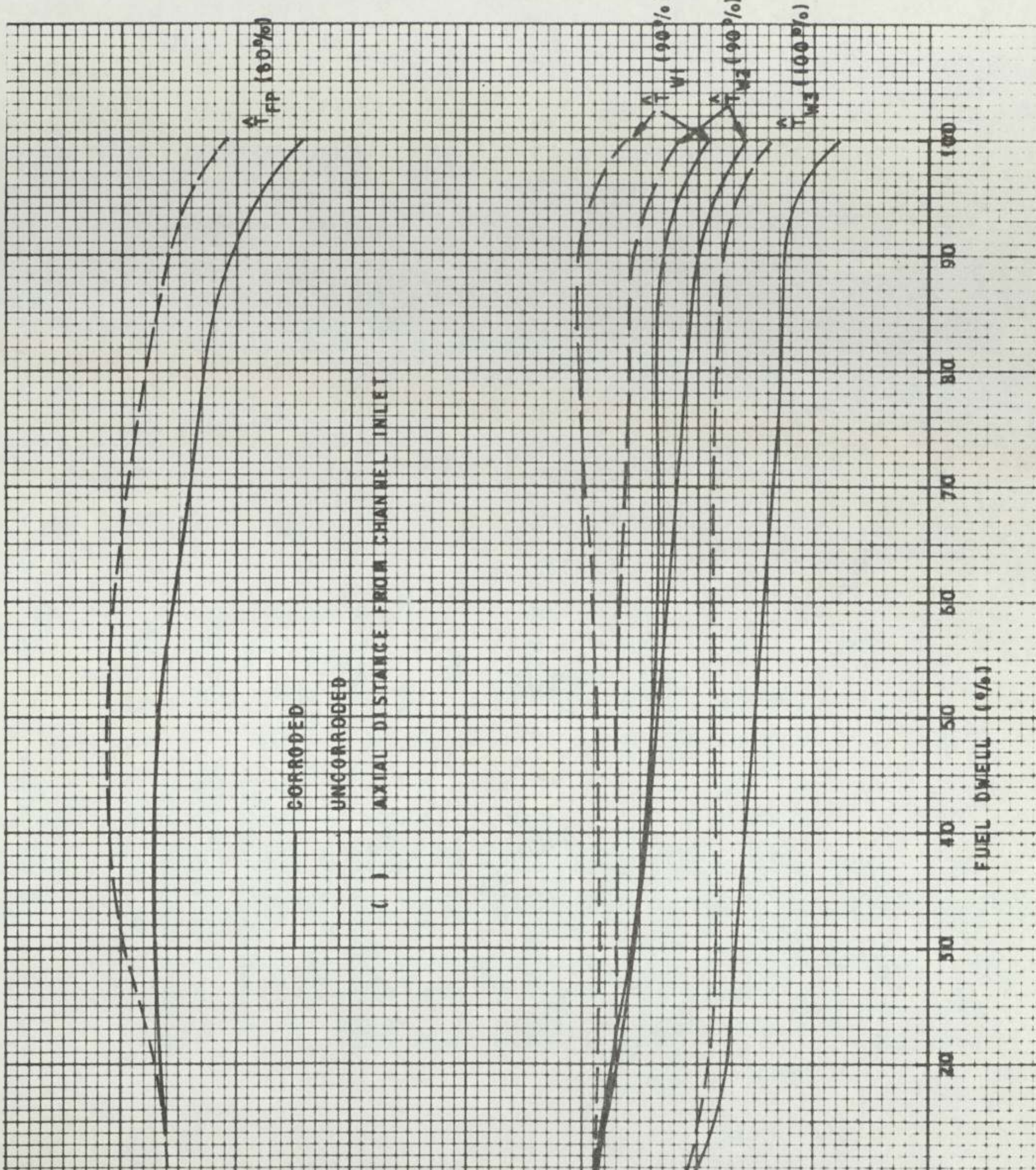

TIME EVOLUTIONS OF TEMPERATURE - HEATAX III

FIG 4/37

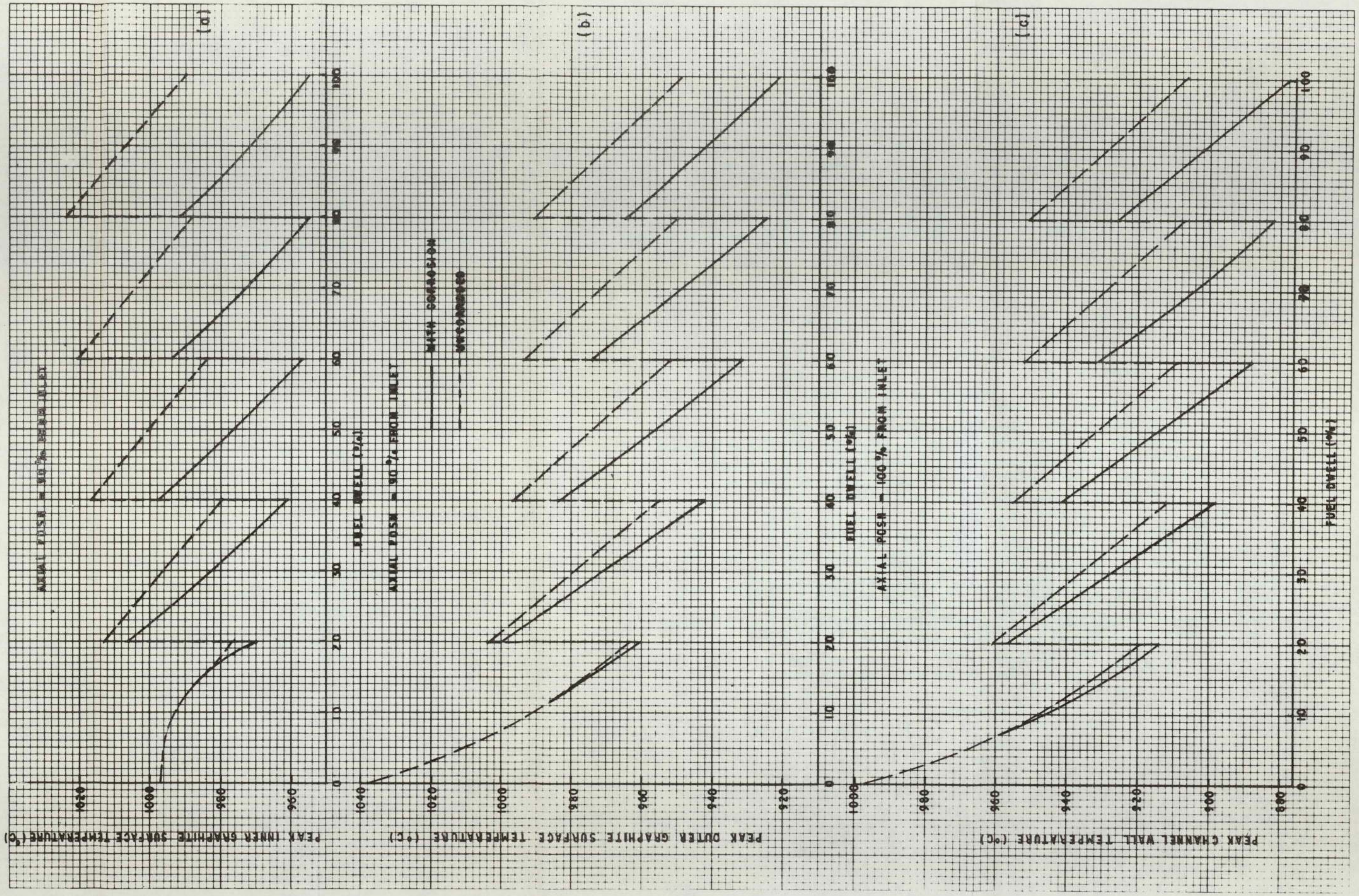

TIME EVOLUTIONS OF GRAPHITE SURFACE TEMPERATURE – HEATAX III/AZIMUSTAP 5	FIG 4/38

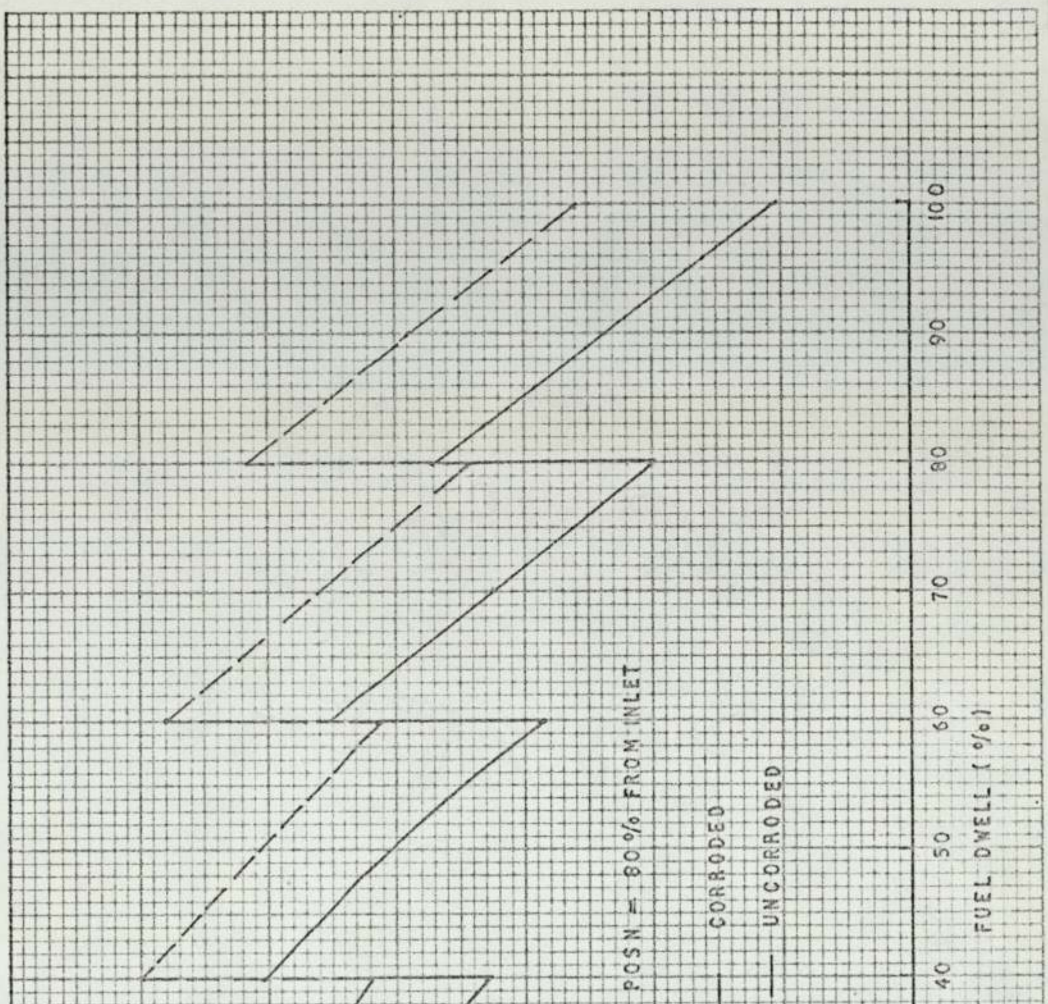

TIME EVOLUTION OF PEAK FUEL TEMPERATURE – HEATAX III/AZIMUSTAP 5	FIG 4/39

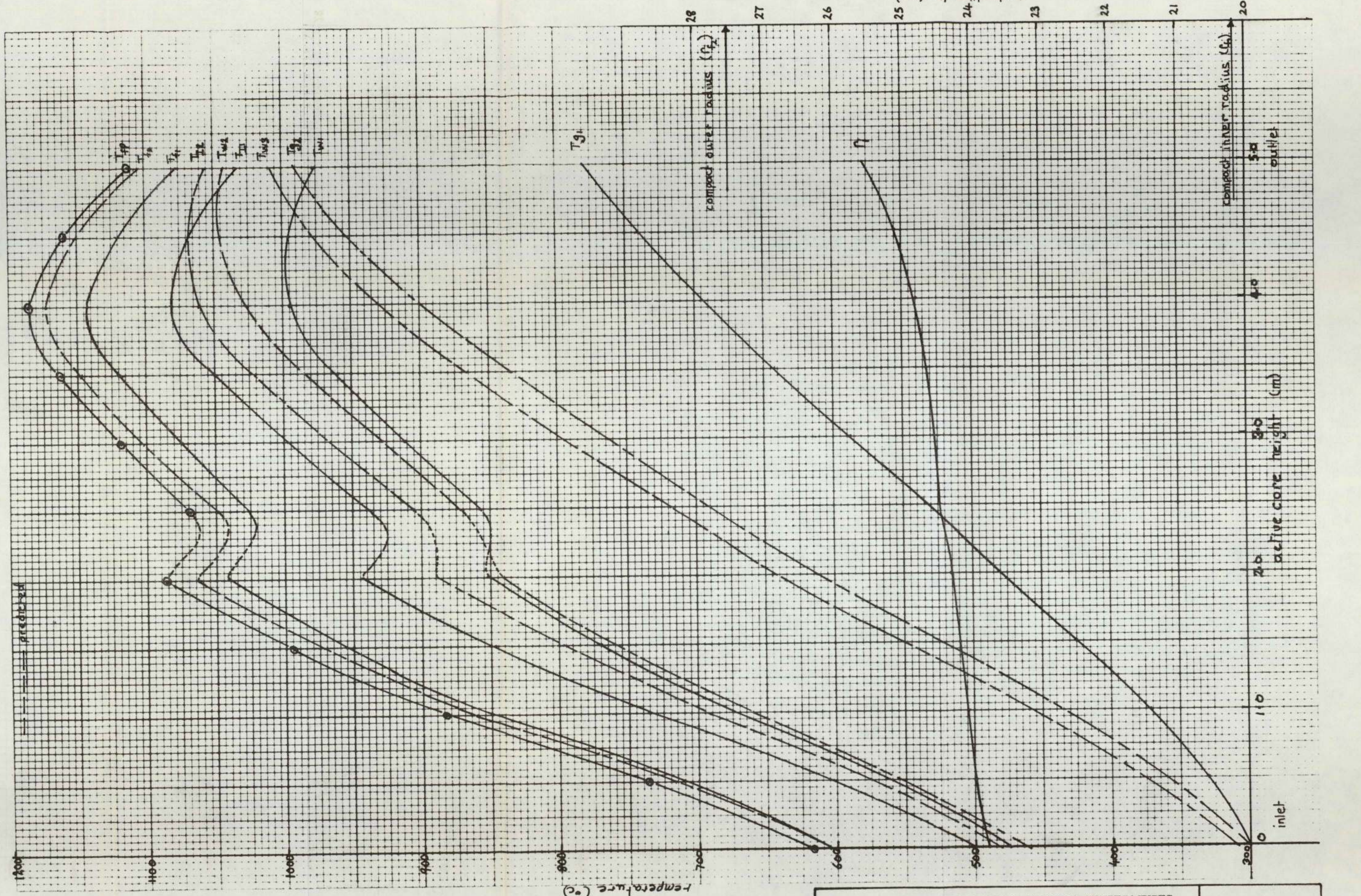

AXIAL DISTRIBUTIONS OF FUEL ELEMENT TEMPERATURES AND HEAT-SPLIT RADIUS	FIG 5/1

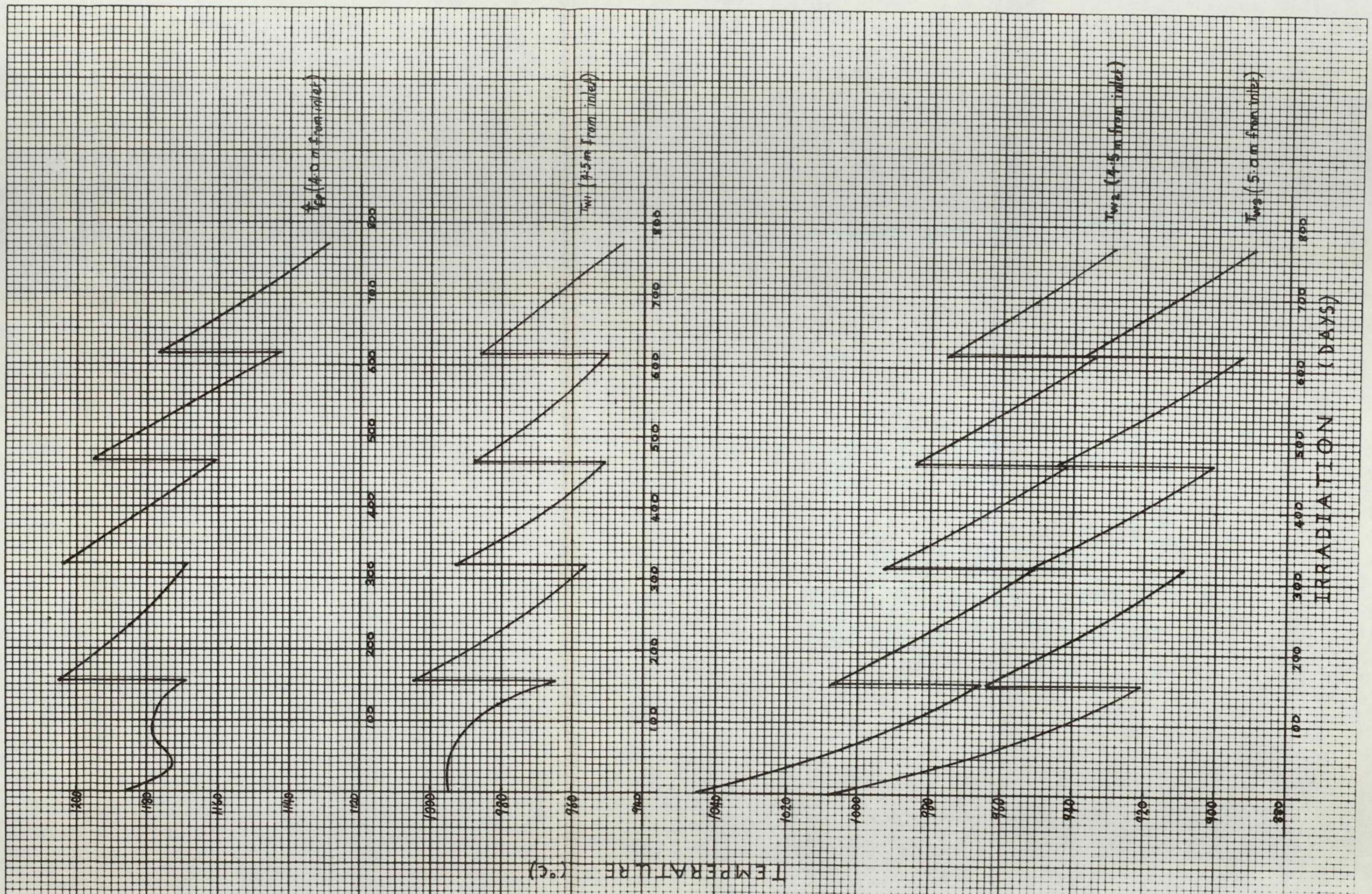

TIME EVOLUTIONS OF AXIAL PEAK FUEL AND GRAPHITE TEMPERATURES	FIG 5/2

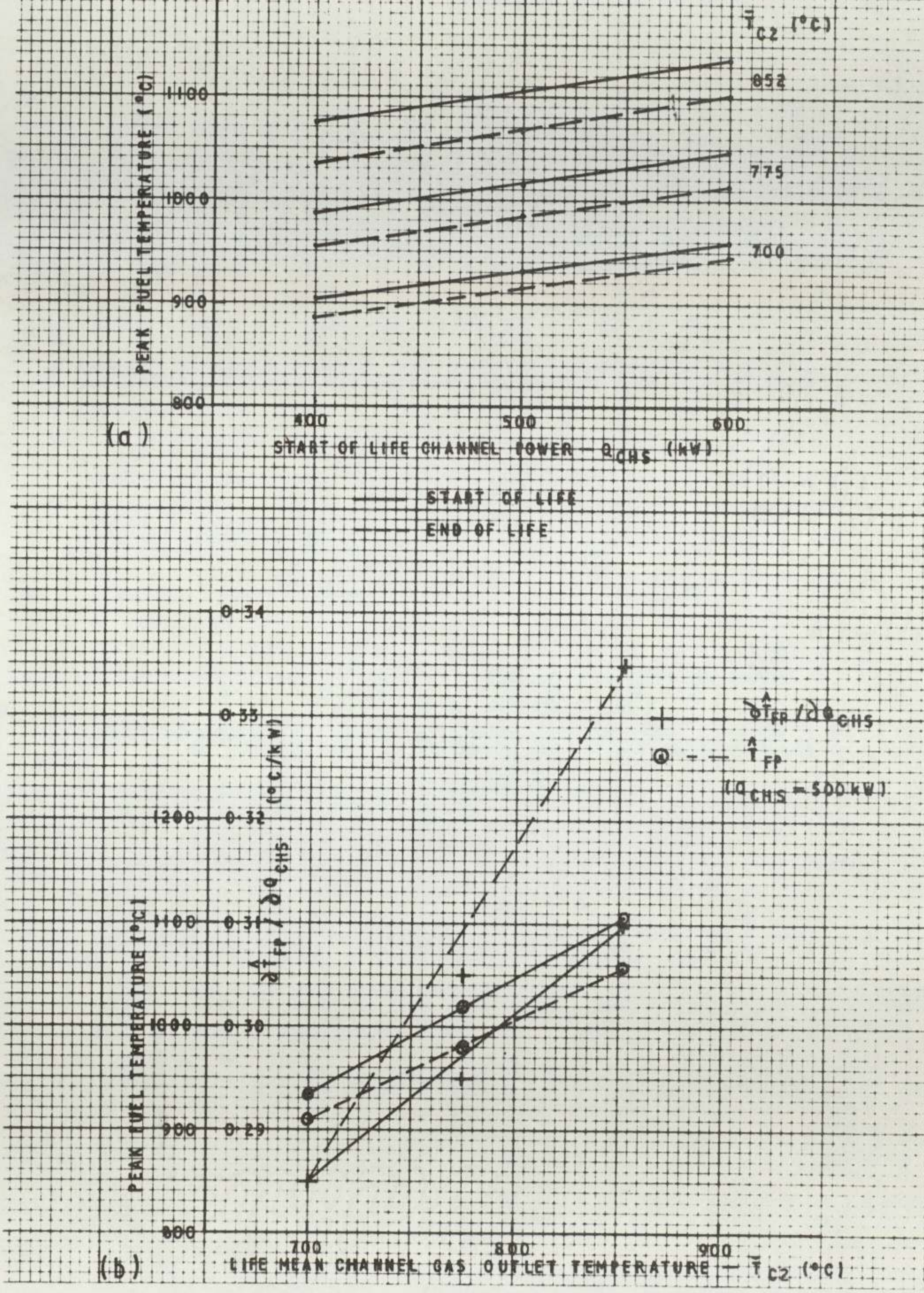

INTEGRAL DATA METHOD - PEAK FUEL TEMPERATURE	FIG 5/3

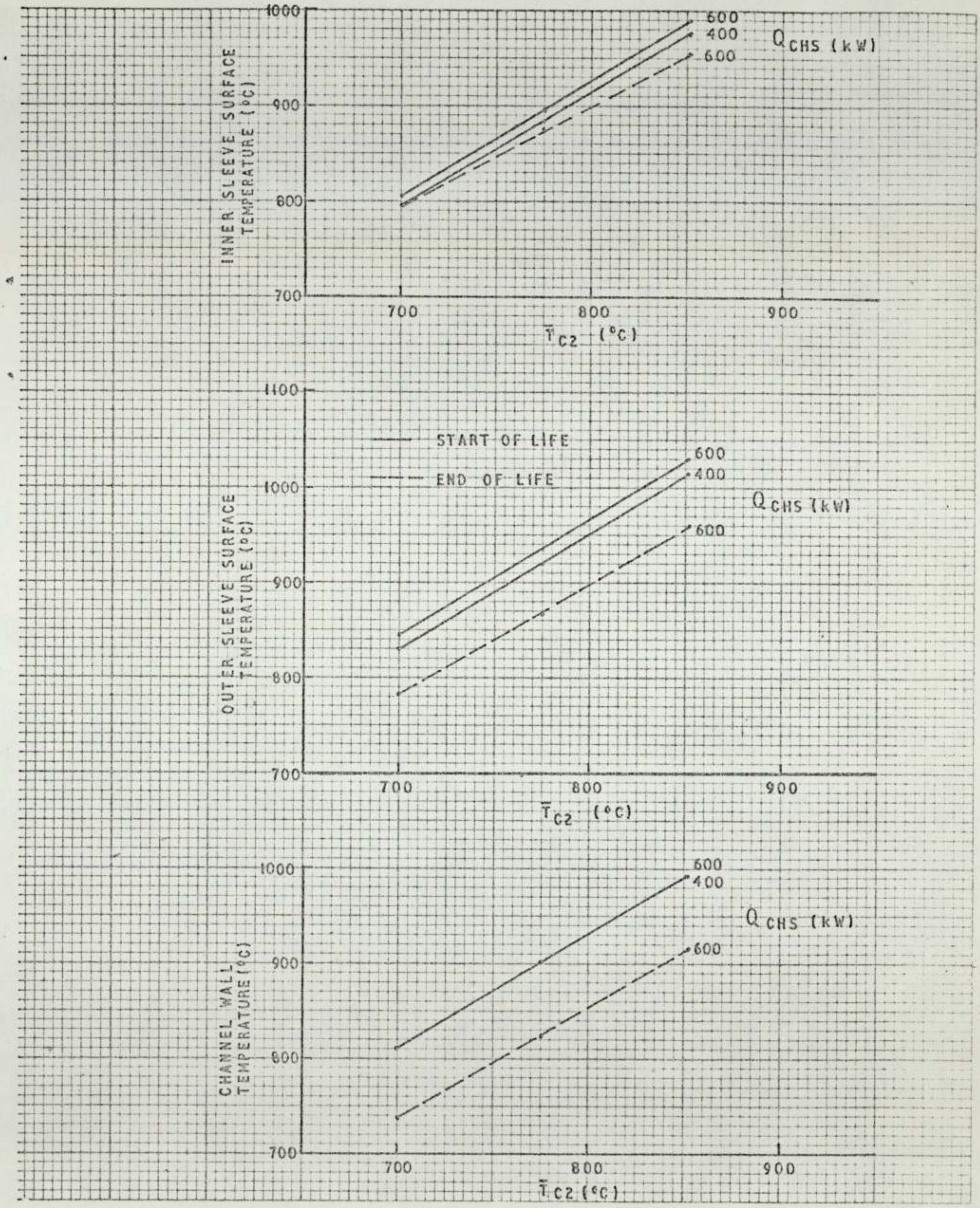

INTEGRAL DATA METHOD - PEAK GRAPHITE TEMPERATURES	FIG 5/4

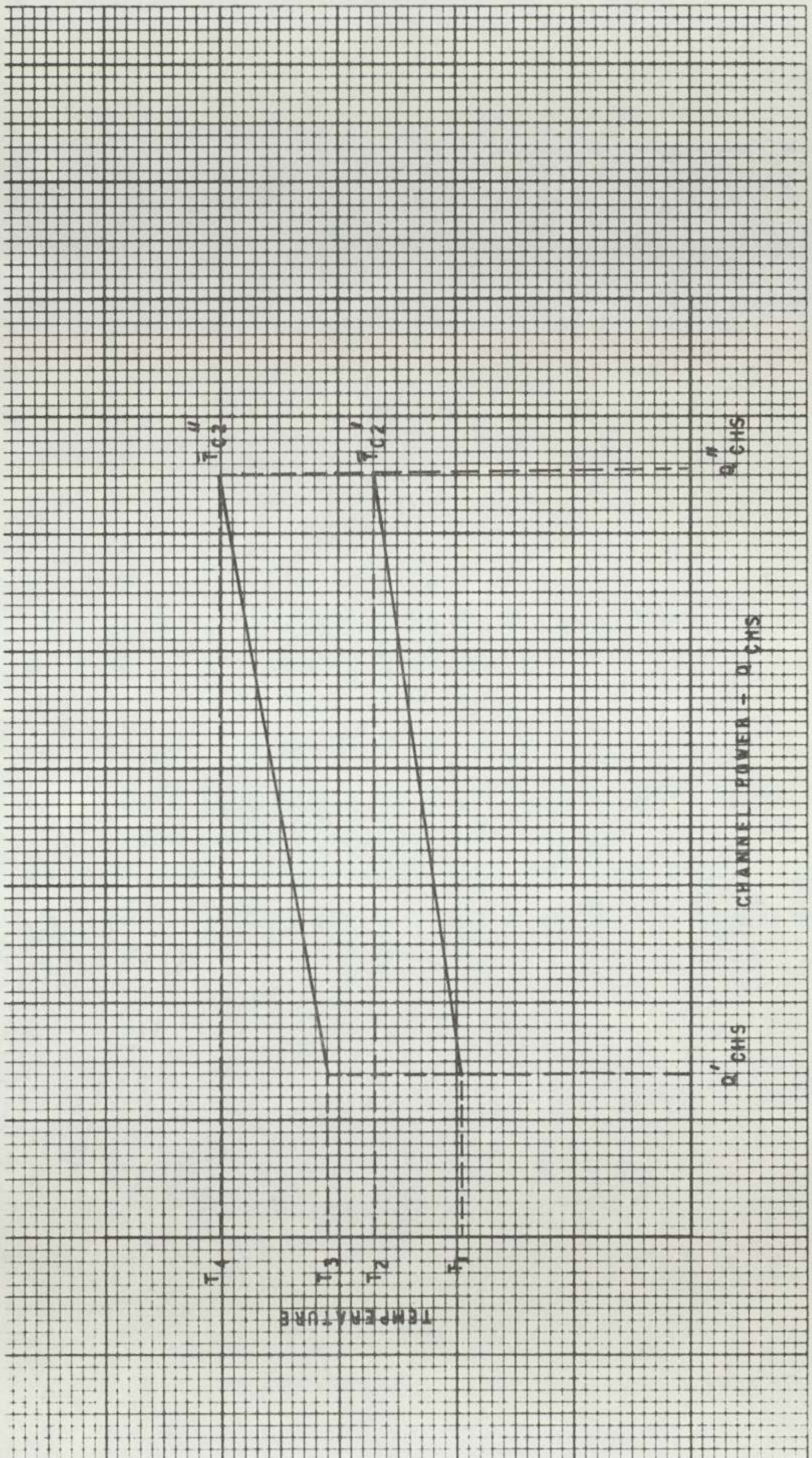

INTEGRAL DATA METHOD - DERIVATION OF CONSTANTS	FIG 5/5

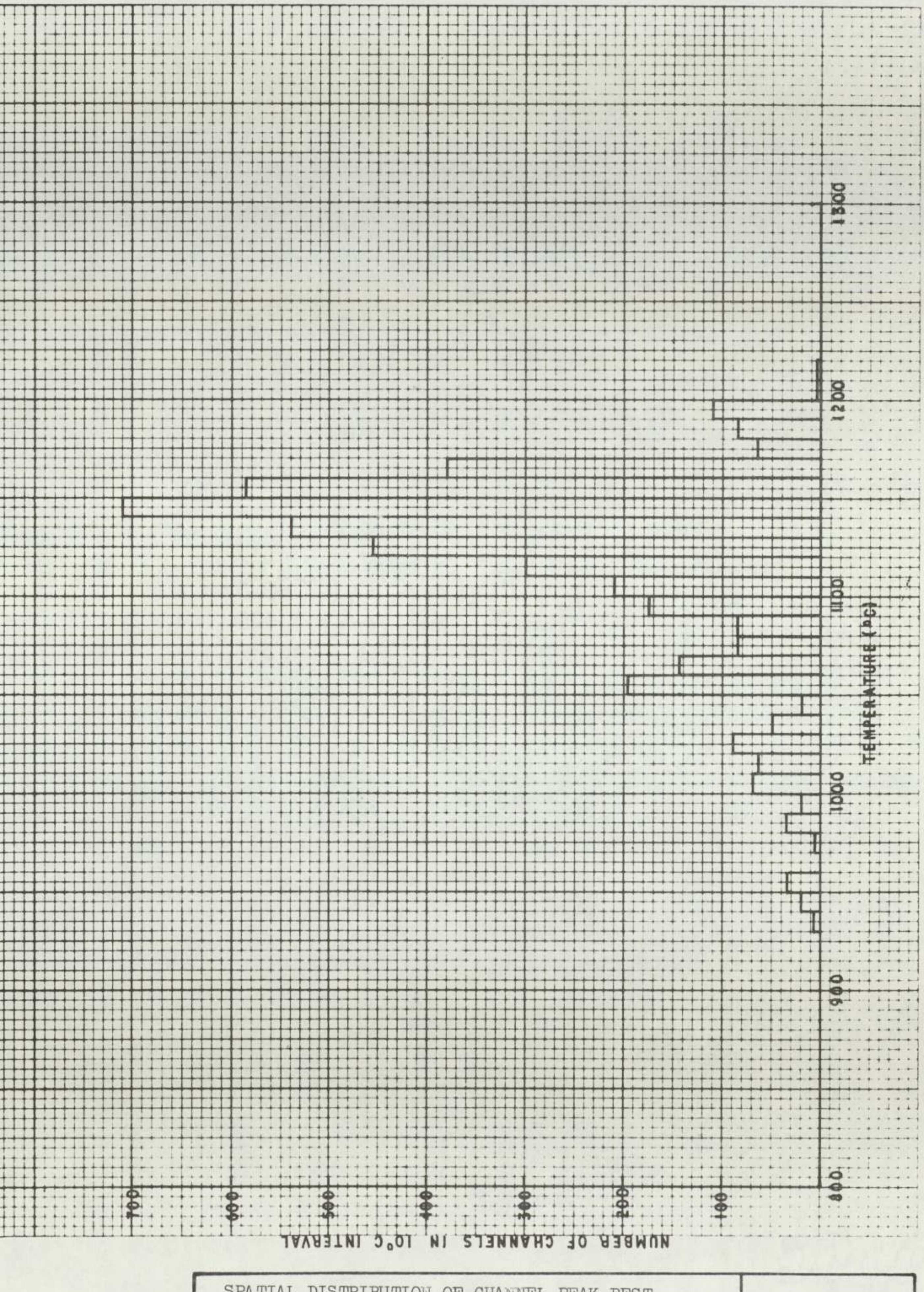

SPATIAL DISTRIBUTION OF CHANNEL PEAK BEST ESTIMATE FUEL TEMPERATURE	FIG 5/6

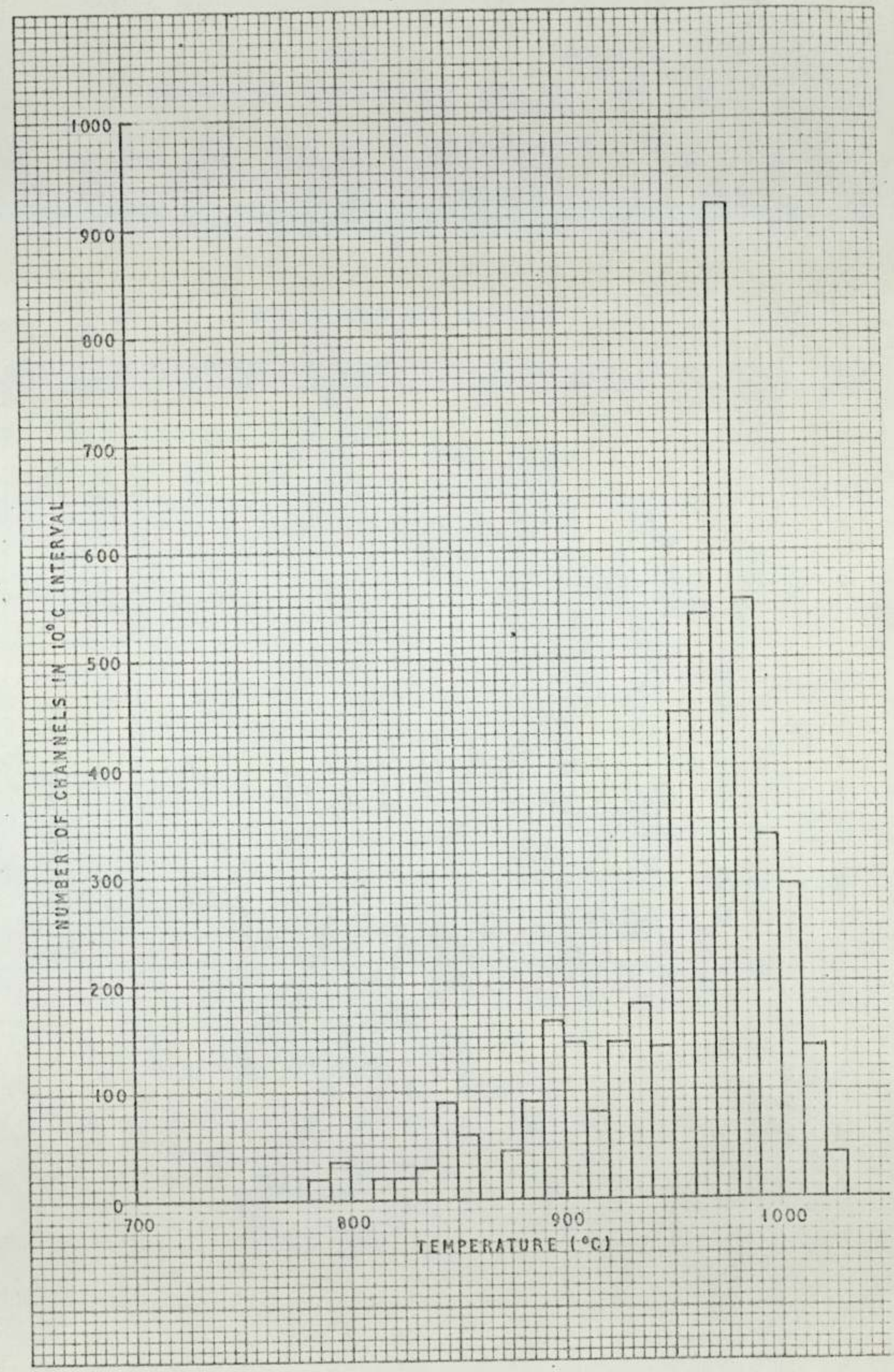

SPATIAL DISTRIBUTION OF CHANNEL PEAK BEST ESTIMATE INNER PIN SURFACE TEMPERATURE	FIG 5/7

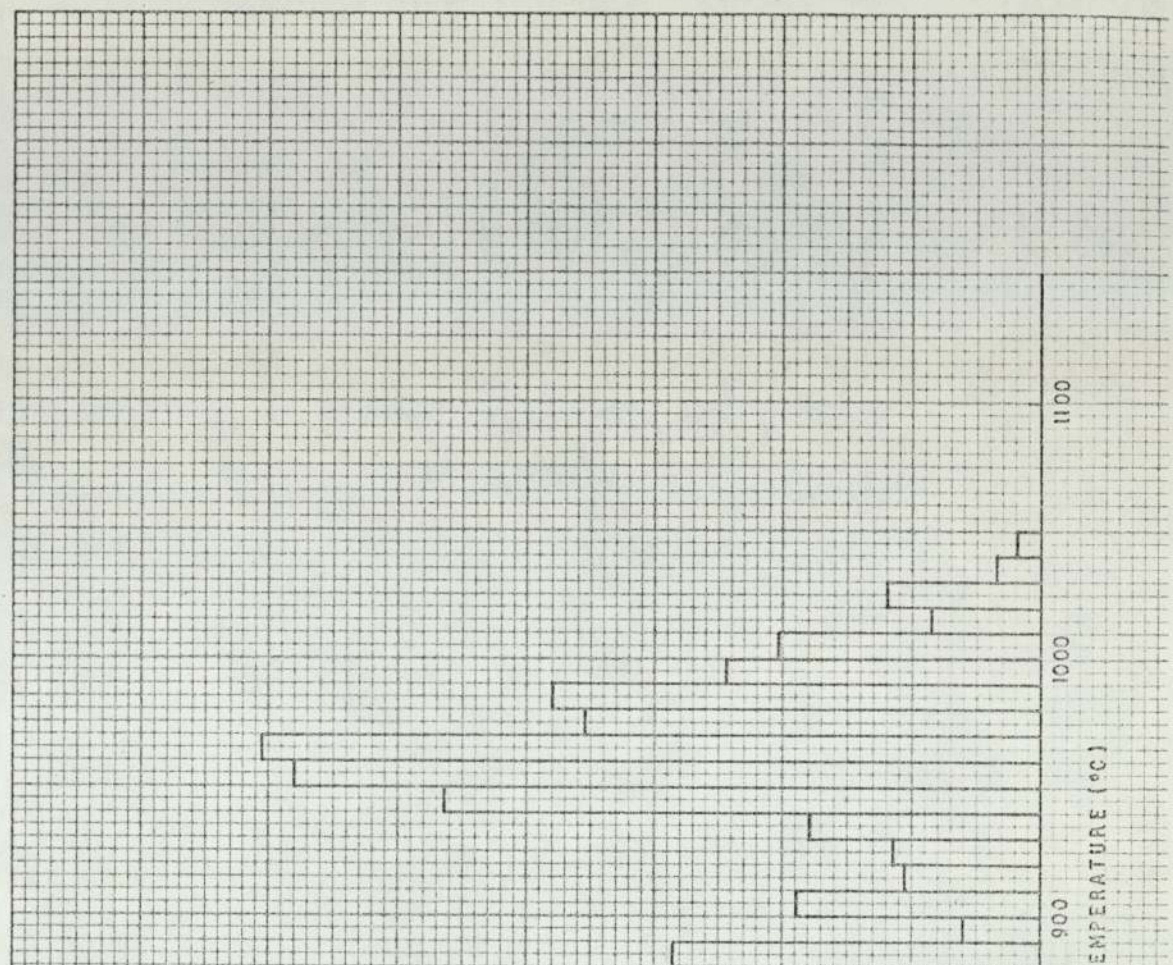

SPATIAL DISTRIBUTION OF CHANNEL PEAK BEST ESTIMATE OUTER PIN SURFACE TEMPERATURE	FIG 5/8

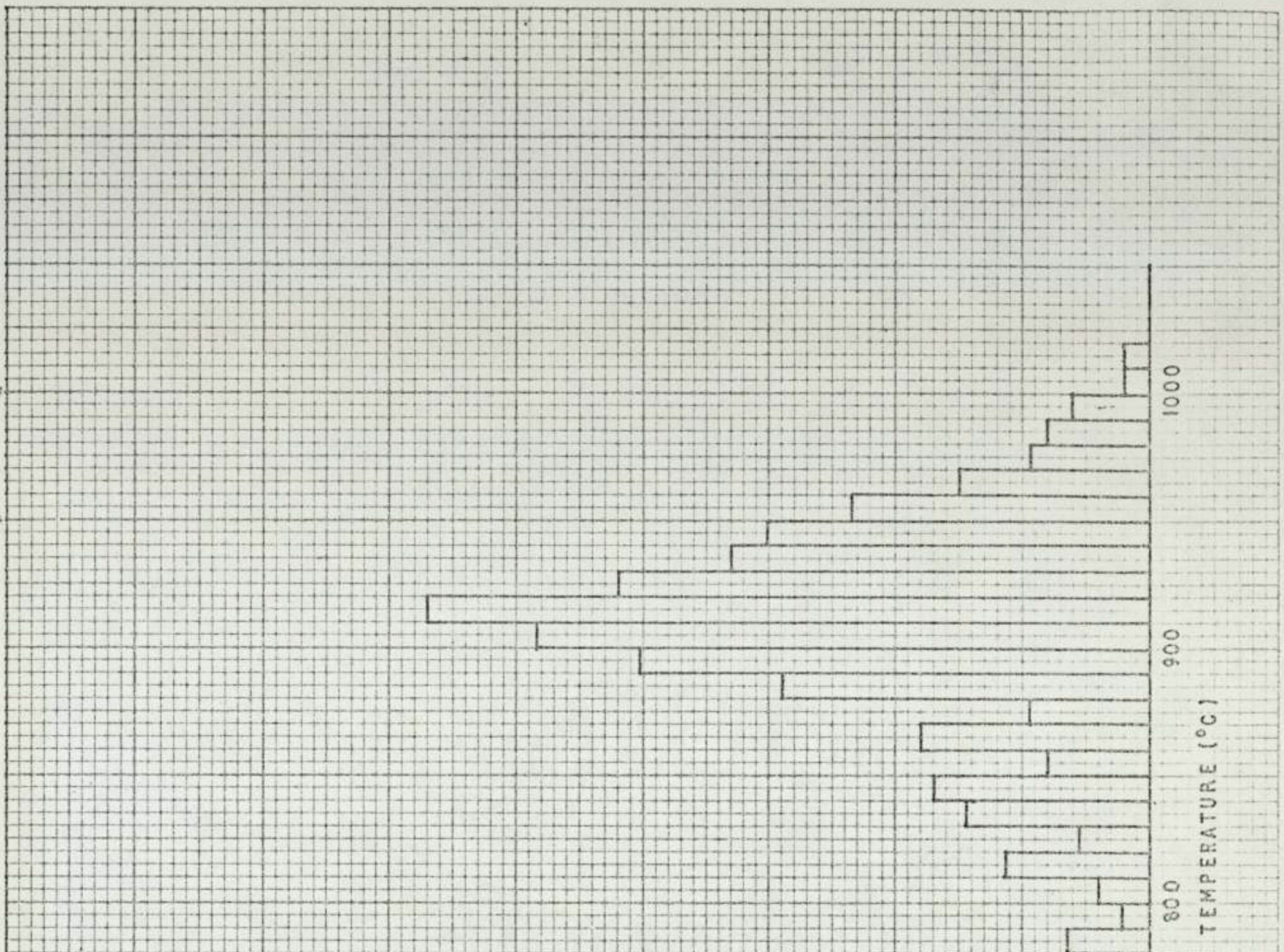

SPATIAL DISTRIBUTION OF CHANNEL PEAK BEST ESTIMATE CHANNEL WALL TEMPERATURE	FIG 5/9

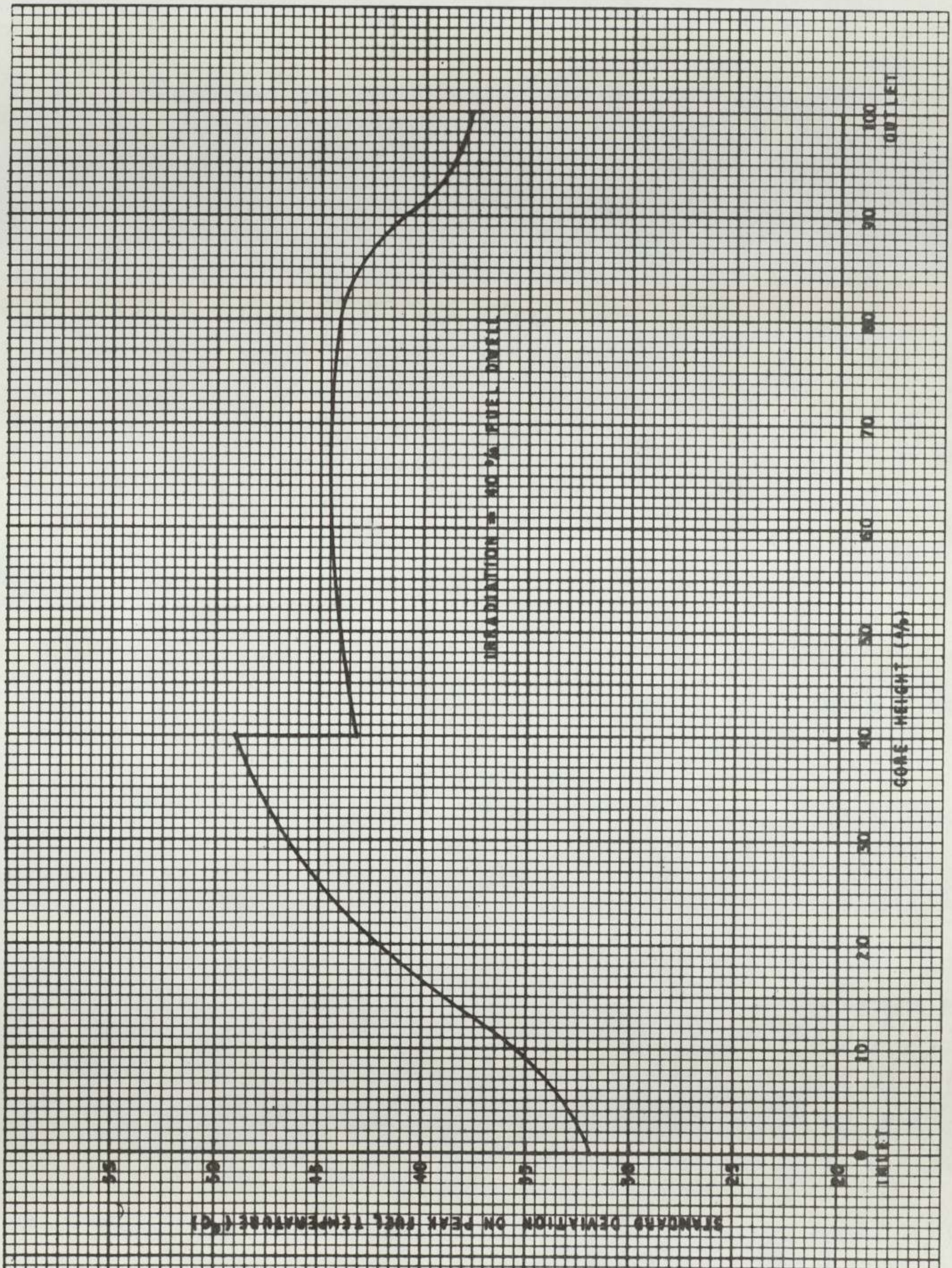

AXIAL DISTRIBUTION OF PEAK FUEL TEMPERATURE STANDARD DEVIATION	FIG 5/10

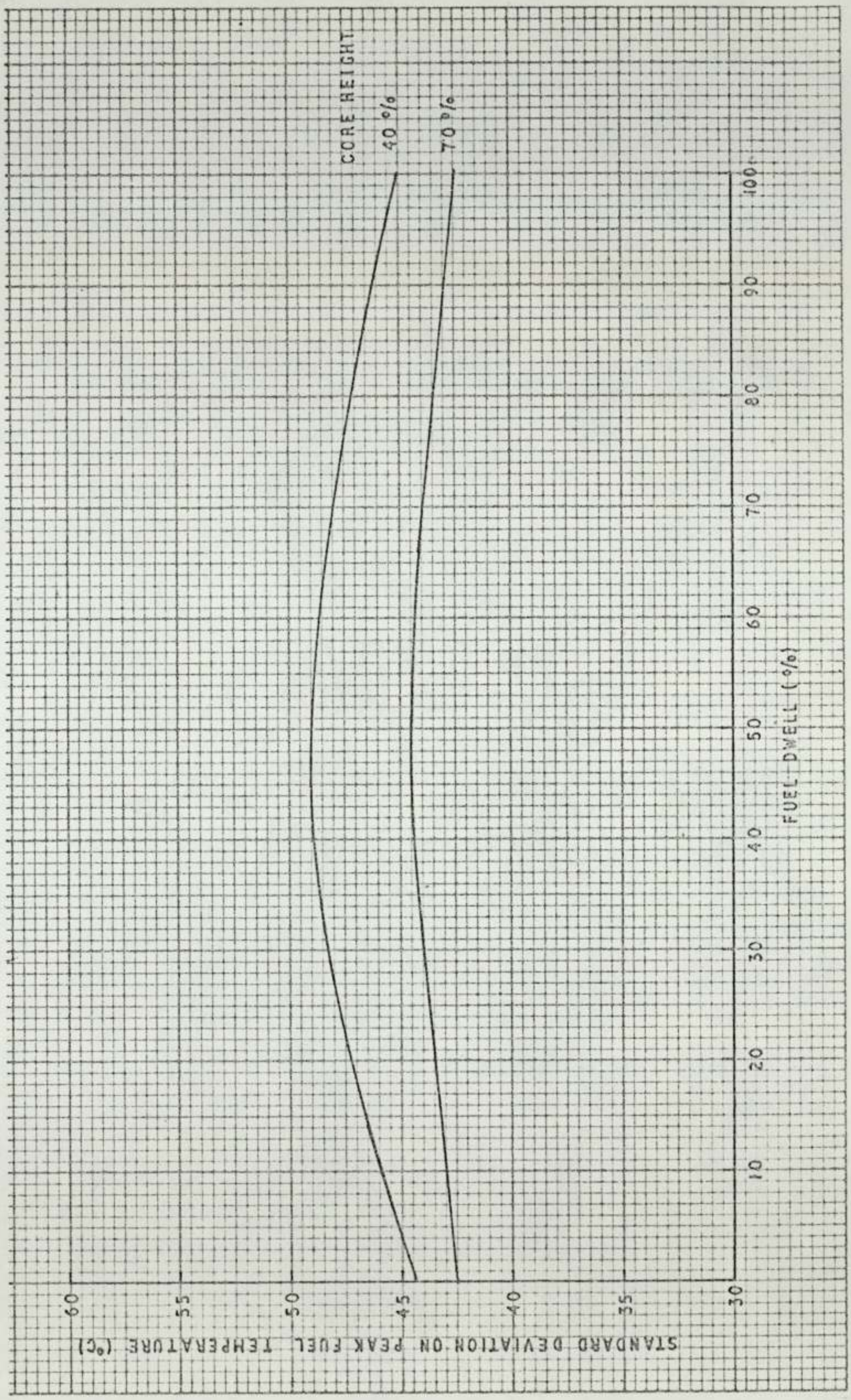

TIME EVOLUTION OF PEAK FUEL TEMPERATURE STANDARD DEVIATION	FIG 5/11

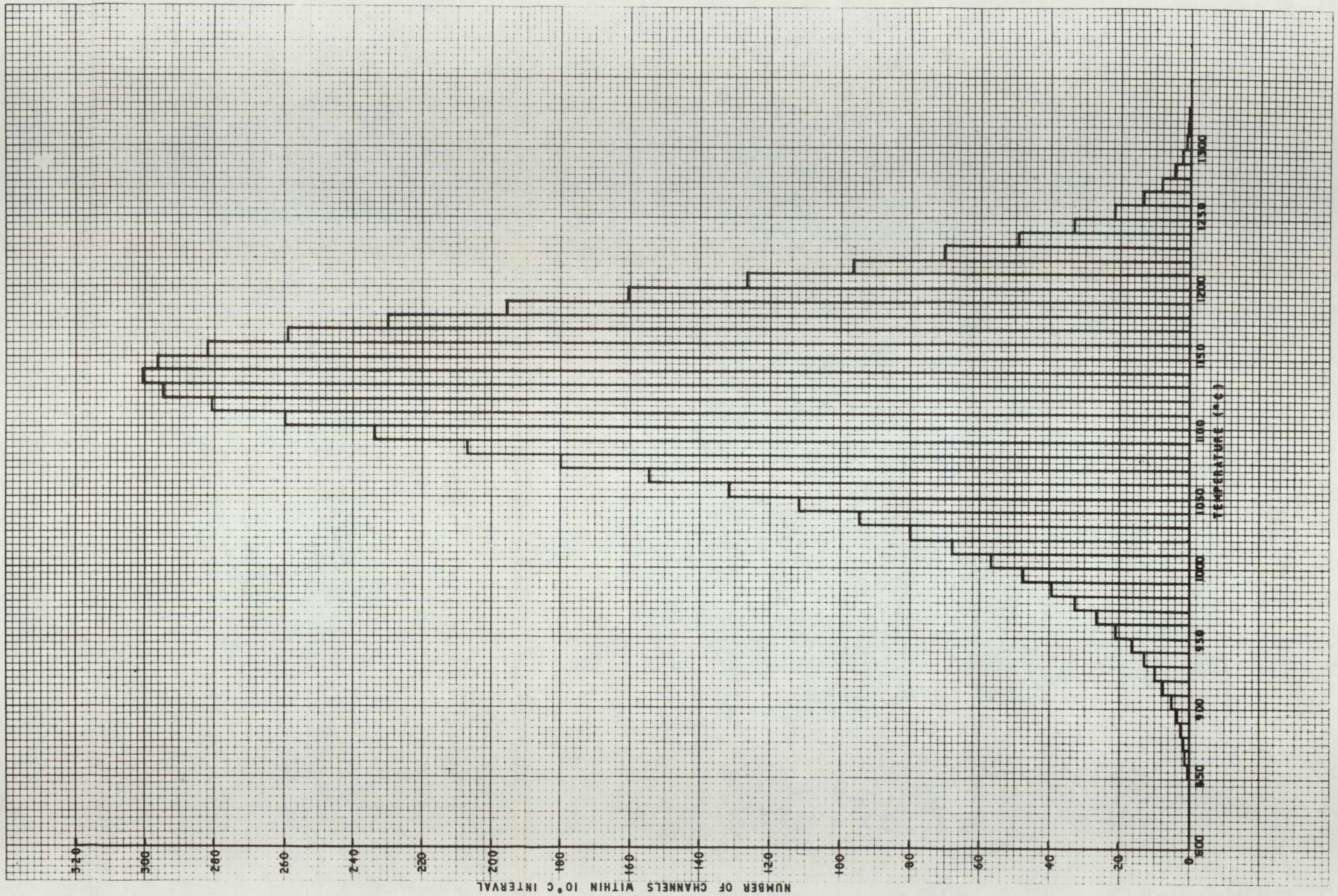

EXPECTED FREQUENCY DISTRIBUTION OF CHANNEL PEAK FUEL TEMPERATURE	FIG 5/12

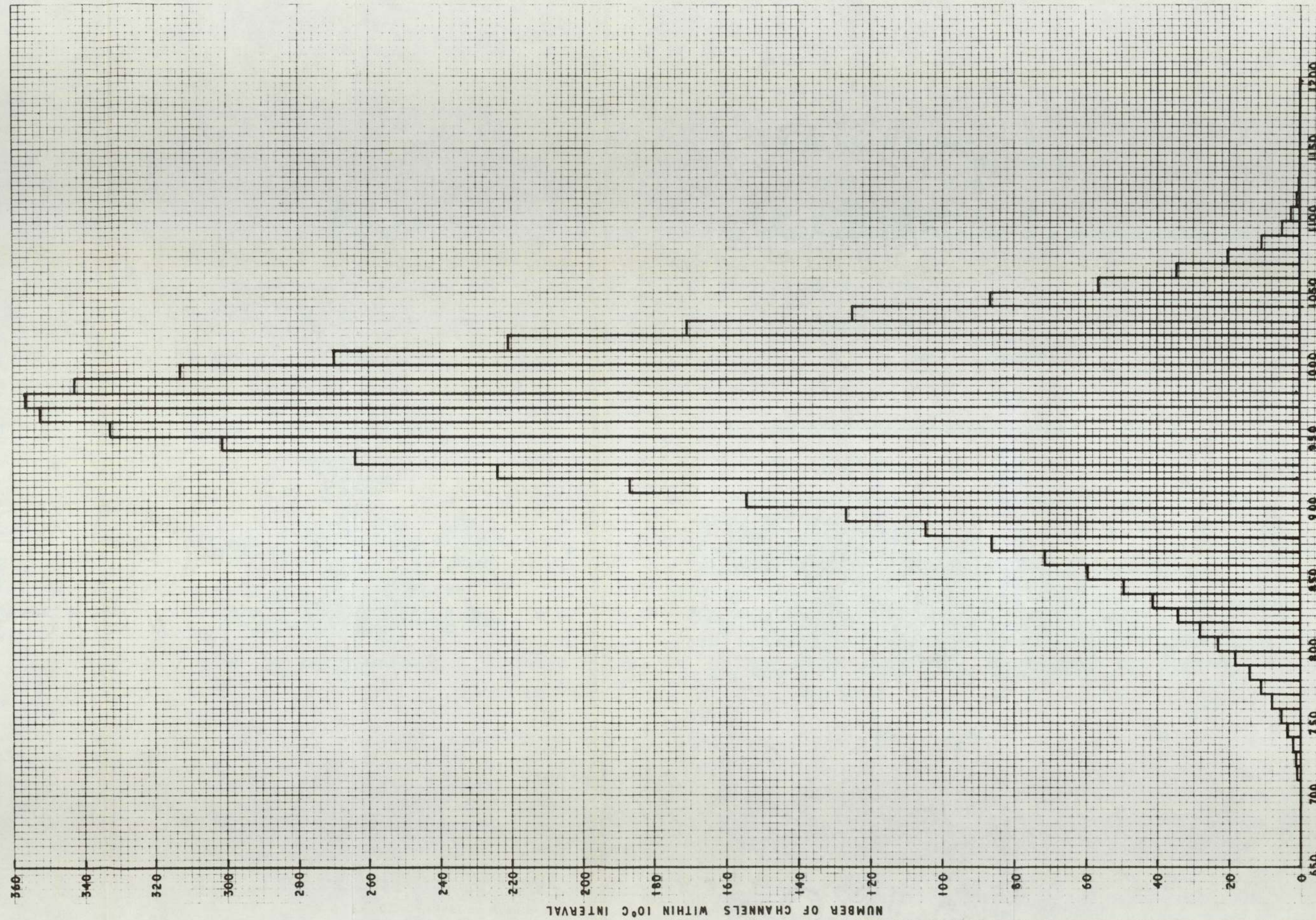

EXPECTED FREQUENCY DISTRIBUTION OF CHANNEL PEAK INNER PIN SURFACE TEMPERATURE	FIG 5/13

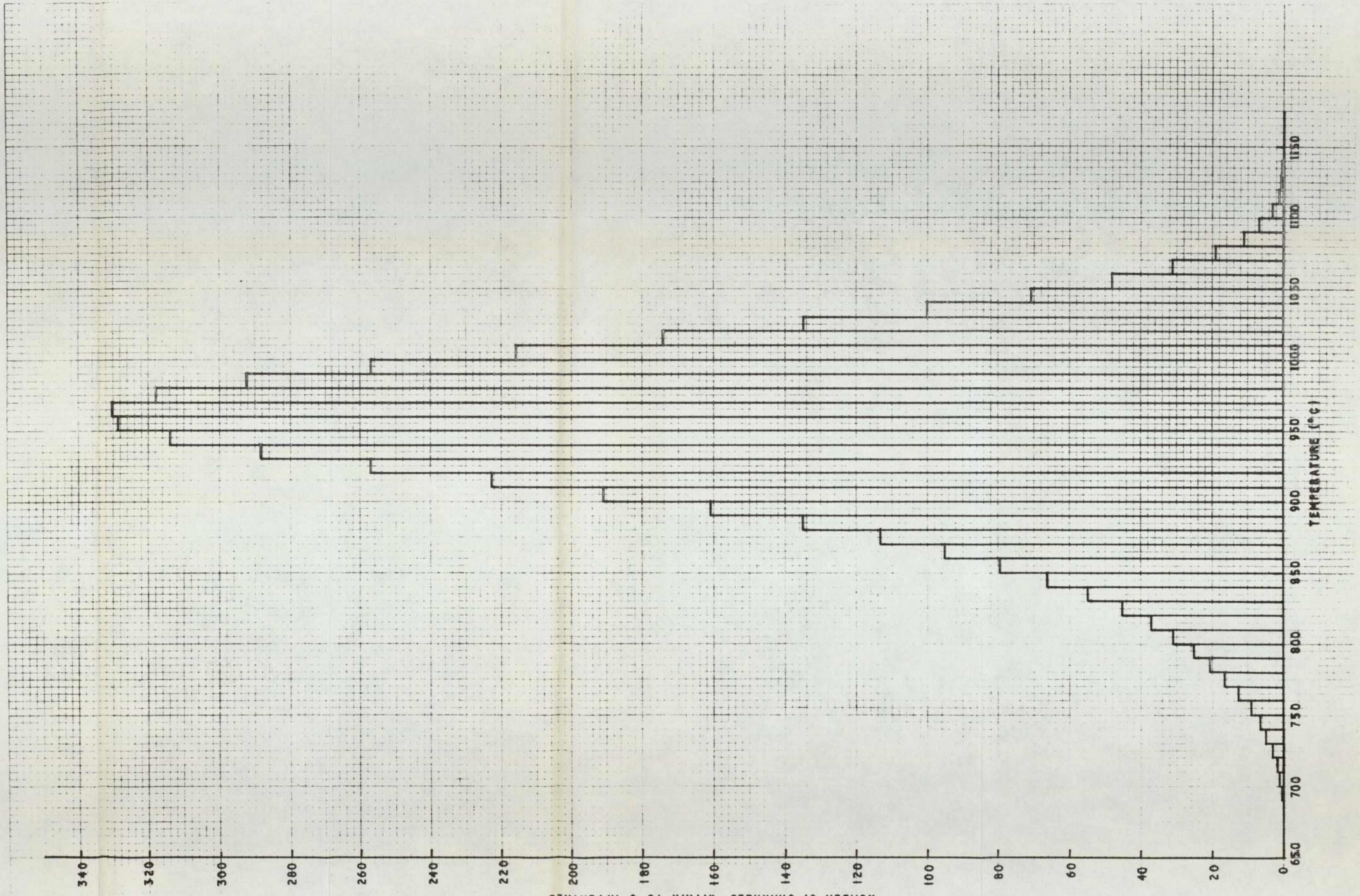

EXPECTED FREQUENCY DISTRIBUTION OF CHANNEL PEAK OUTER PIN SURFACE TEMPERATURE	FIG 5/14

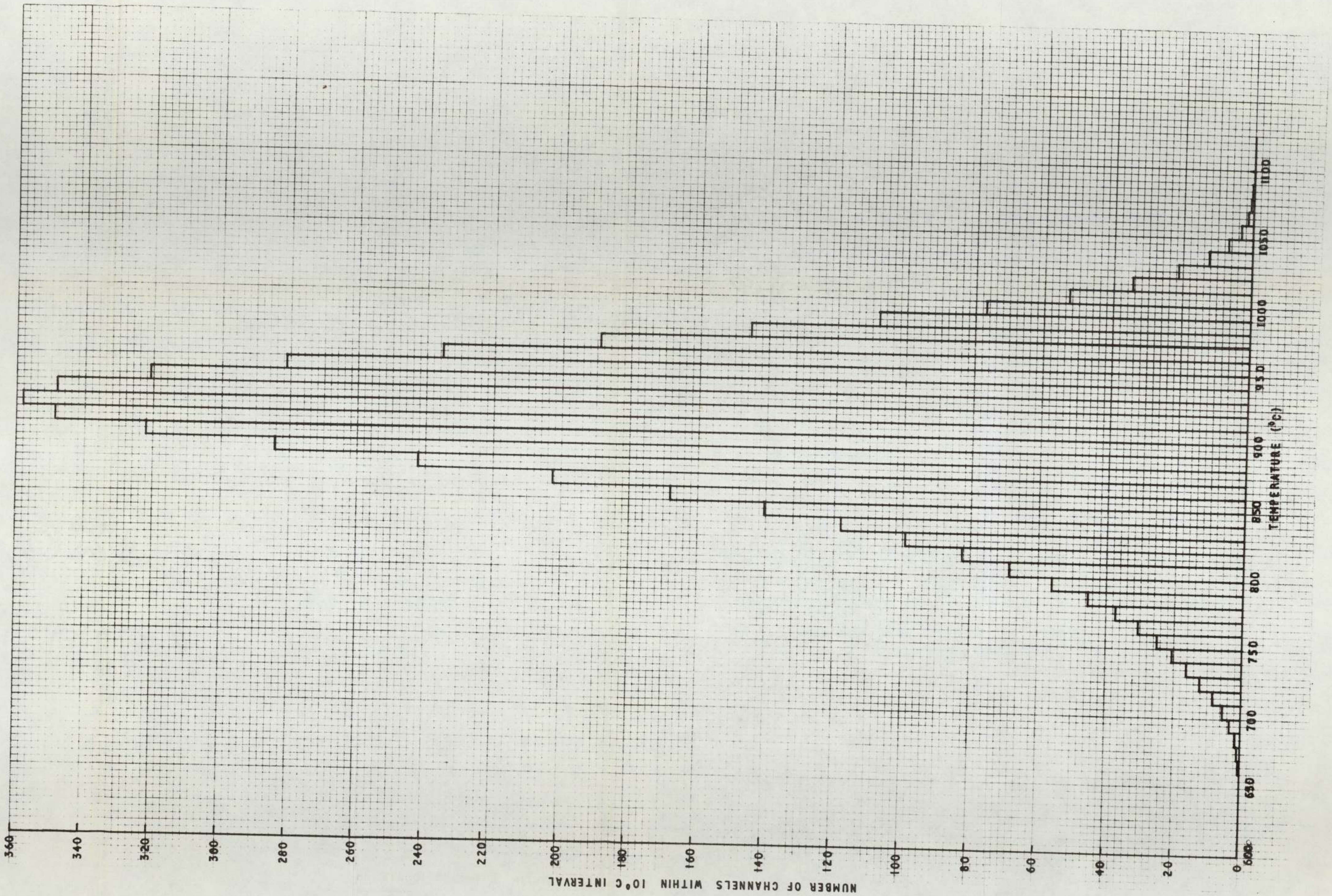

EXPECTED FREQUENCY DISTRIBUTION OF CHANNEL PEAK CHANNEL WALL TEMPERATURE	FIG 5/15

APPENDICES

APPENDIX I

THE GAGGING EFFECTS ON CHANNEL GAS OUTLET TEMPERATURE

It will be assumed that the channel power falls linearly with time (see Fig 3/4). The Age Factor, A, is then defined as the ratio of the start-of-life power to the half-life power.

Let there be n gag changes. At each gag change the flow is adjusted so as to obtain the same channel peak gas outlet temperature (Fig 3/4). This peak temperature is chosen so as to obtain the desired life mean channel gas outlet temperature ($\overline{T}_2$) as the mean for each gag interval.

If a full dwell = 1, the period of each gag interval is $1/(n+1)$ and as the temperature (T_2) falls linearly between gag changes it is desired that:

$$T_2(\tfrac{1}{2}(n+1)) = \overline{T}_2$$

If $\hat{T}_2$ is the gas outlet temperature at the start of the gag interval and T_1 is the channel inlet gas temperature:

$$\frac{\hat{T}_2 - T_1}{\overline{T}_2 - T_1} = \frac{Q_S}{Q_M}$$

where Q_S is the channel power at the start of the gag interval and Q_M is that at the mid-point. Q_M/Q_S is clearly given by:

$$\frac{Q_M}{Q_S} = 1 + \frac{1}{(n+1)} \left(\frac{1}{A} - 1\right)$$

Therefore:

$$\hat{T}_2 = T_1 + \frac{(\overline{T}_2 - T_1)}{\left(1 + \frac{1}{n+1}\left(\frac{1}{A} - 1\right)\right)}$$

In the case of a continuous gagging scheme:

$$n \rightarrow \infty \quad \text{and} \quad \hat{T}_2 \rightarrow \overline{T}_2$$

If there were no gag changes:

$$n = 0 \text{ and } \hat{T}_2 = T_1 + A(\overline{T}_2 - T_1)$$

APPENDIX II

CHANNEL FLOW VARIATIONS WITHIN A COLUMN

Given a uniform heat generation within a column the channel flow distribution would also be expected to be uniform. Rating tilts, however, cause density differences and, as the pressure drop across the column must be a constant for all channels, this leads to flow changes. Let us first ignore the density differences.

Let

$$G = r/\bar{r}$$

where r is the rating of a channel in a column of mean rating $\bar{r}$.

If $\bar{T}_2$ is the column mean gas outlet temperature and T_1 the column inlet temperature, the gas outlet temperature (T_2) of this particular channel is given by:

$$T_2 = T_1 + G(\bar{T}_2 - T_1) \qquad \text{.....AII/1}$$

This is assuming uniform flow.

Let us now consider flow variation effects.

If we define an equivalent flow area (Ae) and hydraulic diameter (D_e) for the channels then the pressure drop across a 'mean' channel in the column is given by the Guggenhiem equation (Chapter 4, Eq. 67):

$$\Delta P = \frac{1}{2\bar{\rho}} \left(\frac{\bar{W}}{Ae}\right)^2 \left[\frac{4fL}{D_e} + \frac{4(\bar{T}_2 - T_1)}{(\bar{T}_2 + T_1)} + K_L\right] \qquad \text{.....AII/2}$$

where:

- L = active core height
- $\bar{W}$ = column mean flow
- $\bar{\rho}$ = column mean density
- f = friction factor
- K_L = discontinuity losses

The equivalent for a single channel is:

$$\Delta P = \frac{1}{2\rho} \left(\frac{W}{A_e}\right)^2 \left[\frac{4fL}{D_e} + 4\frac{(T_2 - T_1)}{(T_2 + T_1)} + K_L\right] \qquad \text{.....AII/3}$$

$$W = G\overline{W}\frac{(\overline{T}_2 - T_1)}{(T_2 - T_1)}$$

The density ρ, for helium, is given by:

$$\rho = \frac{RP}{T}$$

It will be assumed that:

$$\overline{\rho} \propto \frac{1}{\overline{T}_2 + T_1}$$

and

$$\rho \propto \frac{1}{T_2 + T_1}$$

Substituting for W, ρ and $\overline{\rho}$ and setting

$$\frac{4fL}{D_e} + K_L = 4K \text{ ; assumed constant,}$$

we have:

$$\Delta P = C \left(\frac{\overline{W}}{Ae}\right)^2 \frac{4}{(\overline{T}_2 + T_1)} \left[K + \frac{(\overline{T}_2 - T_1)}{(\overline{T}_2 + T_1)}\right] \qquad \text{.....AII/4}$$

and

$$\Delta P = C\, G^2 \left(\frac{\overline{W}}{Ae}\right)^2 \left(\frac{\overline{T}_2 - T_1}{T_2 - T_1}\right)^2 \frac{4}{(T_2 + T_1)} \left[K + \frac{(T_2 - T_1)}{(T_2 + T_1)}\right] \qquad \text{.....AII/5}$$

C is a constant and since there must be a constant pressure across the column equations AII/4 and AII/5 can be equated, i.e.

$$G^2 \left(\frac{\overline{T}_2 - T_1}{T_2 - T_1}\right)^2 \left(\frac{\overline{T}_2 + T_1}{T_2 + T_1}\right) \left[K + \frac{(T_2 - T_1)}{(T_2 + T_1)}\right] = \left[K + \frac{(\overline{T}_2 - T_1)}{(\overline{T}_2 + T_1)}\right]$$

The following equation, quadratic in T_2, is obtained:

$$T_2^2 - T_2 \left[\frac{(K+1)(\overline{T}_2 - T_1)^2 G^2}{\overline{T}_2(K+1) + (K-1)\, T_1} + 2\, T_1\right] + \left[T_1^2 - \frac{(K+1)(\overline{T}_2 - T_1)^2 G^2 T_1}{\overline{T}_2(K+1) + T_1(K-1)}\right] = 0$$

.....AII/6

Using a value of $K = 2.7$ (mean channel) and assuming $\overline{T}_2 = 800^\circ C$ and $T_1 = 300^\circ C$, the dependence of channel T_2 on rating ratio G is determined.

Fig AII-1 shows $(T_2 - T_1)/(\bar{T}_2 - T_1)$ versus G. The equation to the curve is:

$$\frac{T_2 - T_1}{(\bar{T}_2 - T_1)} = G^{1.4} \qquad \text{.....AII/7}$$

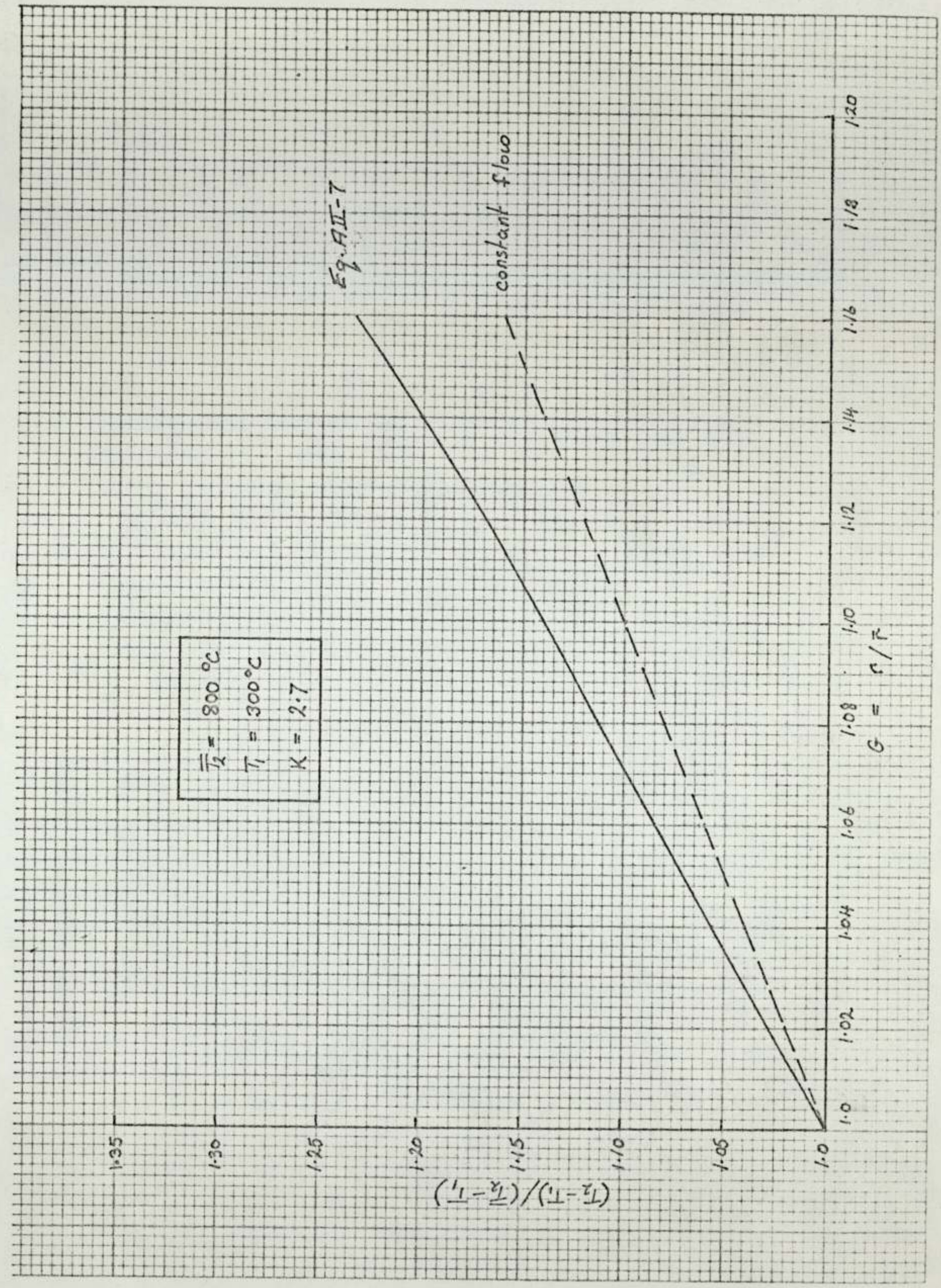

WITHIN COLUMN FLOW VARIATIONS - EFFECT ON ACROSS-COLUMN TEMPERATURE GRADIENTS	FIG AII-1

APPENDIX III

REFERENCE THREE GROUP GAGGING SCHEME

The object is to distribute the 301 columns between three groups and allocate respectively three column gas outlet temperatures such that there is a common peak channel gas outlet temperature between groups.

From the power map shown in Fig 3/3 the maximum rating 'gradient' is 1.147. The three groups are chosen, therefore, as:

0–1.05; 1.05–1.10; 1.10–1.147.

The following table gives the total heat generation (ΣR), in arbitary units, and maximum gradient ($\hat{G}$) of each group.

Group	ΣR	$\hat{G}$	F	T_2
1	467.9	1.042	1.059	819.2
2	207.1	1.099	1.141	782.1
3	96.17	1.147	1.210	754.4

F is the temperature tilt factor (Eq. AII/7).

From equations 5 and 6 (Chapter 3) the values of the group T_2 values can be found and are given in the table. The peak channel T_2 value that corresponds to this scheme is 850°C.

APPENDIX IV

THERMAL EXPANSION AS A FUNCTION OF TEMPERATURE

Consider Chapter 4, Eq. 75, expressed in a general form:

$$\frac{U_1}{r_1} = \frac{2r_1}{r_2^2 - r_1^2} \int_{r_1}^{r_2} r \alpha T \; dr$$

Let α = aT + B (a good approximation over a 100°C temperature range (TRG 1000(R) (43)).

$$\frac{U_1}{r_1} = \frac{2r_1}{r_2^2 - r_1^2} \int_{r_1}^{r_2} (r\, aT^2 + rbT)dr$$

to a good approximation for the graphite sleeve.

$$T = Ar + B$$

$$U_1 = \frac{2r_1}{r_2^2 - r_1^2} \int_{r_1}^{r_2} [\, ra(Ar + B)^2 + rb(Ar + B)\,] \; dr$$

$$\text{Strain } S = \frac{2}{r_2^2 - r_1^2} \left[\frac{aA^2}{4} (r_2^4 - r_1^4) + \frac{A(2aB+b)}{3}(r_2^3 - r_1^3) + \frac{B(aB+b)}{2}(r_2^2 - r_1^2)\right] \quad \text{....A1V/1}$$

Now let us assume α is constant but evaluated at $\overline{T}$

$$\overline{T} = \frac{2}{r_2^2 - r_1^2} \int_{r_1}^{r_2} r \; Tdr$$

Since T = Ar + B

$$\overline{T} = \frac{2A}{3} \frac{(r_2^3 - r_1^3)}{(r_2^2 - r_1^2)} + B \quad \text{.....AIV/2}$$

$$\text{and} \quad \alpha(\overline{T}) = \frac{2Aa}{3} \frac{(r_2^3 - r_1^3)}{(r_2^2 - r_1^2)} + aB + B$$

The corresponding strain $\overline{S} = (a\overline{T} + b)\overline{T}$

$$\overline{S} = a\left[\frac{2A}{3} \frac{(r_2^3 - r_1^3)}{(r_2^2 - r_1^2)} + B\right]^2 + \frac{2bA}{3} \frac{(r_2^3 - r_1^3)}{(r_2^2 - r_1^2)} + bB \quad \text{.....AIV/3}$$

The error between S and $\bar{S}$ is given by:

$$\varepsilon = \frac{\bar{S} - S}{\bar{S}}$$

$$\bar{S} - S = aA^2 \left[\frac{4}{9} \left(\frac{r_2^3 - r_1^3}{r_2^2 - r_1^2} \right)^2 - \frac{r_2^2 + r_1^2}{2} \right] \qquad \text{.....AIV/4}$$

Let us consider a graphite sleeve of radii 27.5/32.5 mm with surface temperatures of 1050/950°C respectively.

From TRG 1000(R) (43) $a = 1.214 \times 10^{-9}\ {}^{\circ}C^{-2}$

$b = 4.636 \times 10^{-6}\ {}^{\circ}C^{-1}$

Also $A = -20.0\ {}^{\circ}C\ mm^{-1}$

$B = 1600\ {}^{\circ}C$

and $\bar{T} = 1000^{\circ}C$

From Eq. AIV/3

$$\bar{S} = 5.85 \times 10^{-3}$$

From Eq. AIV/4

$$\bar{S} - S = 1.009 \times 10^{-6}$$

$$\therefore \quad \underline{\varepsilon = 1.7 \times 10^{-4}}$$

APPENDIX V

THE RUSTAN PROGRAM

The RUSTAN code was written in the FORTRAN IV language. It was designed to determine the friction factors in a rough annulus with arbitary specification of roughness height on the two walls and allowing for velocity profile effects.

Fig AV-1 is a flow diagram showing the main calculation steps. (See Chapter 4, section 4, for nomenclature and equations). At the end of this appendix the program listing is shown.

(a) Data input

r_1, r_2	channel inner, outer radii	
μ	coolant viscosity	
Nc	number of cases	
W	channel mass flow rate	) Nc values
ε_1, ε_2	inner, outer roughness height	)

(b) Initial guesses

The transformed friction factors f_1,f_2 are set equal to the smooth value, f_s, (Eq. 34) and preliminary values of Re, D_e, etc. determined by also assuming smooth walls.

(c) ε^*_1, ε^*_2

These are calculated using Eq. 146.

(d) A^*_1, A^*_2

Depending upon the values of ε^*_1 and ε^*_2 the relevant equation for the evaluation of A^*_1 and A^*_2 is used.

It will be noted from the listing that the limiting values of ε^* and the A^* equations are slightly different from those quoted in Chapter 4 equations 136. The values and equations in RUSTAN are taken from NIKURADSE (37) whereas those in the text apply to the HEATAX code. The reason for the discrepancy is given in Appendix VII.

(e) Friction factors

The revised values of transformed friction factor are calculated from Eq. 145.

(f) Parameters

Certain parameters are determined e.g. De_1 De_2, $\bar{u}_1/\bar{u}_2$, Re_1, Re_2 (See equations in Chapter 4, sub-section 4.4.2).

(g) Error

If present f_1, f_2, values differ by more than 0.1% from previous values and not more than 20 iterations have been carried out the calculation returns to (c) above. (Typical number of iterations is four).

(h) Print out

Table 4/4 is a typical RUSTAN output (Units are all S.I. e.g. kg, m, s.)

The parameters printed out are:

RC1, RC2	annulus inner, outer radii
FLOW	annulus mass flow rate
EH1, EH2	Inner, outer roughness height (mm)
RE1, RE2	Inner, outer transformed Reynolds number
RM	Radius of no shear
UR	Inner/outer mean velocity ratio
E*1, E*2	ε^*_1, ε^*_2
F1, F2	Inner, outer transformed friction factors

```
C*** R U S T A N ***
   20 FORMAT(I3)
   21 FORMAT(3F10.1)
      READ(5,21) RC1,RC2,VIS
      WRITE(6,40)
      WRITE(6,41)
      WRITE(6,42) RC1,RC2
      WRITE(6,43)
   22 FORMAT(4F10.1)
      READ(5,20) NC
      DO 30 N=1,NC
      READ(5,22) W,EH1,EH2
      I=0
      A=3.14159*(RC2*RC2-RC1*RC1)
      RE=2.0*W*(RC2-RC1)/(A*VIS)
      FS1=0.079/RE**0.25
      F1=FS1
      F2=FS1
      RE1=RE
      RE2=RE
      DE1=2.0*(RC2-RC1)
      DE2=DE1
    1 ESTAR1=RE1*SQRT(F1/2.0)*EH1/DE1
      ESTAR2=RE2*SQRT(F2/2.0)*EH2/DE2
      M=0
      ESTAR=ESTAR1
    9 IF(ESTAR.LT.3.5) GO TO 2
      IF(ESTAR.LT.7.0) GO TO 3
      IF(ESTAR.LT.14.0) GO TO 4
      IF(ESTAR.LT.68.0) GO TO 5
      ASTAR=8.48
      GO TO 6
    2 ASTAR=2.5*ALOG(ESTAR)+5.55
      GO TO 6
    3 ASTAR=1.52*ALOG(ESTAR)+6.59
      GO TO 6
    4 ASTAR=9.59
      GO TO 6
    5 ASTAR=11.5-0.705*ALOG(ESTAR)
    6 IF(M.EQ.0) GO TO 7
      ASTAR2=ASTAR
      GO TO 8
    7 ASTAR1=ASTAR
      M=1
      ESTAR=ESTAR2
      GO TO 9
    8 F1N=2.0/(ASTAR1-3.75-2.5*ALOG(2.0*EH1/DE1))**2.0
      F2N=2.0/(ASTAR2-3.75-2.5*ALOG(2.0*EH2/DE2))**2.0
      ERROR=F1N/F1-1.0
      IF(ABS(ERROR).LT.0.001) GO TO 10
      F1=F1N
      F2=F2N
      I=I+1
      IF(I.EQ.20) GO TO 25
      GO TO 11
   10 ERROR=F2N/F2-1.0
      IF(ABS(ERROR).LT.0.001) GO TO 12
      I=I+1
      F1=F1N
      F2=F2N
      IF(I.EQ.20) GO TO 25
   11 UR=(1.0+3.75*SQRT(F2/2.0))/(1.0+3.75*SQRT(F1/2.0))
      DR=F2/(UR*UR*F1)
      RM=SQRT((RC1*RC2+DR*RC1*RC1)/(DR+RC1/RC2))

      DE1=2.0*(RM*RM-RC1*RC1)/RC1
      DE2=2.0*(RC2*RC2-RM*RM)/RC2
      ROUM1=0.6366*W/(RC1*DE1+RC2*DE2/UR)
      ROUM2=ROUM1/UR
      RE1=ROUM1*DE1/VIS
      RE2=ROUM2*DE2/VIS
      GO TO 1
   12 EH1=1000.0*EH1
      EH2=1000.0*EH2
      DE1=1000.0*DE1
      DE2=1000.0*DE2
      RM=1000.0*RM
      WRITE(6,44) W,EH1,EH2,RE1,RE2,RE,DE1,DE2,RM,UR,ESTAR1,ESTAR2,F1,F2
     1,I
   30 CONTINUE
   40 FORMAT('1',20X,'R U S T A N    R E S U L T S')
   41 FORMAT(///,2X,'RC1',5X,'RC2',3X,'(M)')
   42 FORMAT(1X,2(F7.4))
   43 FORMAT(//,2X,'FLOW    EH1     EH2',6X,'RE1',6X,'RE2',5X,'RE',5X,'DE1
     1',5X,'DE2',3X,'RM     UR',6X,'E*1',5X,'E*2',3X,'F1',6X,'F2')
   44 FORMAT(/,1X,3(F7.4),3(F9.0),3(F6.2),F6.3,2(F8.2),2(F8.5),15X,I3)
   25 STOP
      END
```

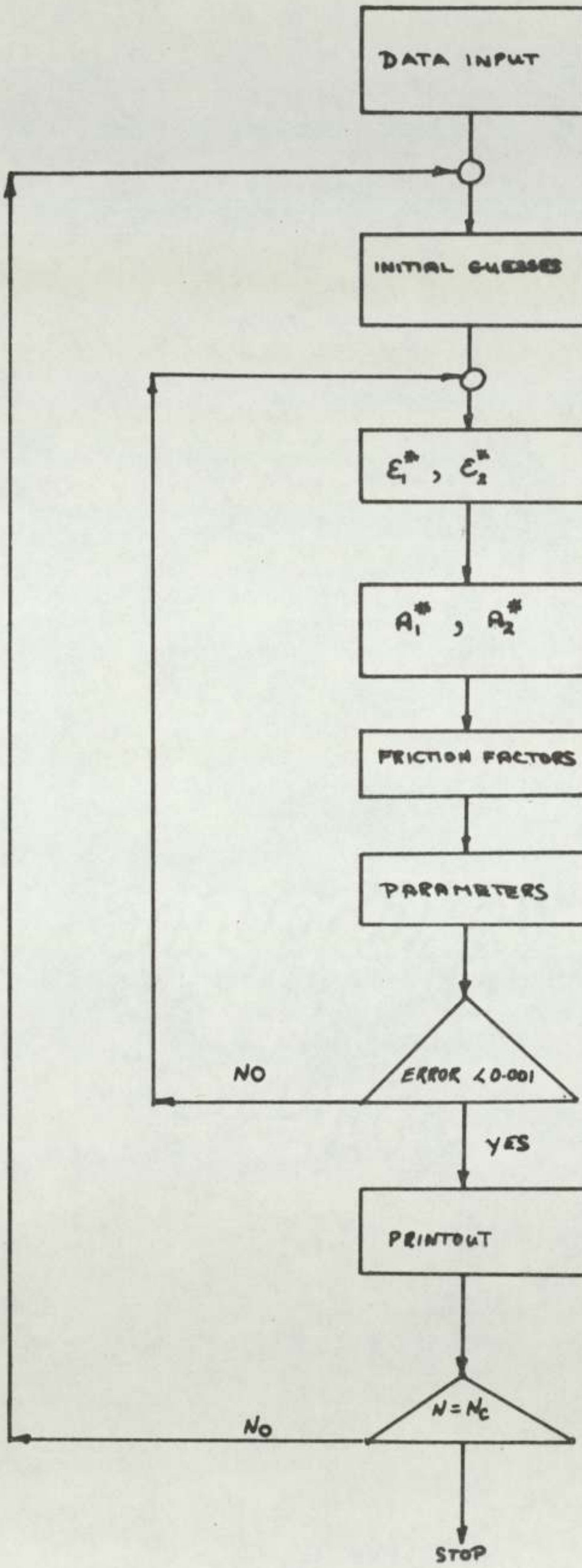

RUSTAN FLOWCHART	FIG AV-1

APPENDIX VI

THE AZIMUSTAP PROGRAM

There are two parts to the AXIMUSTAP 5 code:

(i) axial calculation

(ii) interface gap and time dependent calculation.

The specification for the latter was made by the Author and is described in Chapter 4, section 3. The axial calculation was not specified by the Author but will be described briefly to give useful background. The program was written by W.S. Sinclair and his report (SINCLAIR (51)) gives further details.

The fuel channel is divided into a number of axial slabs (N). The program performs N + 1 calculations starting at inlet to the fuel channel and finishing at outlet. The channel inlet and outlet gas temperatures are specified, together with the channel power, from which the channel mass flow rate can be determined.

$$W = Q_{CH}/C_P \; (T_2 - T_1)$$

In the case of a tubular element the first guess of the flow split is found from the application of a simplified Guggenheim equation.

Channel inlet gas temperature (T_1) provides the boundary conditions for the first axial calculation.

Fig AVI-1 shows a section through the fuel channel at axial position Z.

Thermal radiation across the annulus is at first neglected and the fuel element temperatures T_{FP}, T_{F1}, T_{W1} etc. found. The heat generation at the calculation point is determined by combining the axial rating shape and channel power. With values of T_{W2} and T_{W3} the thermal radiation component can be found and the temperatures recalculated. Within this iterative loop the temperature dependent material properties and interface gaps are continuously updated. On convergence, the heat transfer into the two passages can be found and the temperature rise within the step determined. The gas temperature boundary conditions are thus obtained for the next calculation step.

At each step the pressure rise within the step is determined for the two passages. When channel outlet is reached the two pressure drops are compared. If they differ by more than a certain percentage (usually 0.1%) the flow split is re-assessed and the axial calculation repeated. Generally, pressure convergence is achieved after two or three iterations.

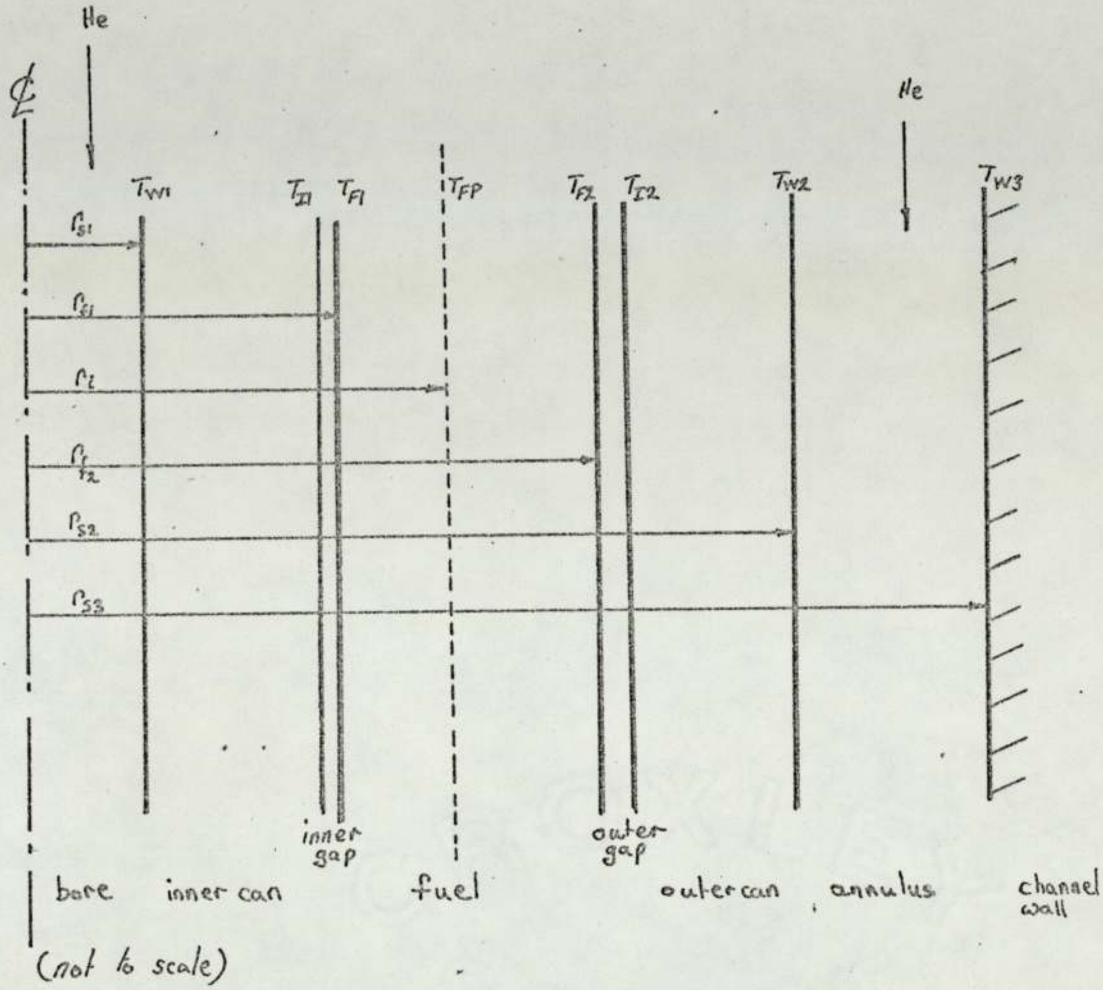

SECTION THROUGH TUBULAR FUEL ELEMENT	FIG AVI-1

APPENDIX VII

THE HEATAX PROGRAM

There were three stages of development of the FORTRAN IV code - HEATAX:

(i) HEATAX I

This program performed a single axial calculation (similar to the AZIMUSTAP program) given the flow split, channel power etc. Corrosion was neglected and the channel dimensions were independent of temperature. This program was intended as a fast running module to be built into a load following reactor physics code.

(ii) HEATAX II

This development included temperature dependent channel dimensions and the pressure drop calculation. Flow split and heat transfer effects of sleeve and channel thermal expansion could, therefore, be determined. (Chapter 4 sub-section 3.5).

(iii) HEATAX III

The final development of the program included the corrosion phenomenon where the flow split, pressure drop and heat transfer effects of temperature dependent planar removal and graphite roughness are determined. As corrosion is progressive the program was also developed to perform the axial calculation over a number of time steps.

This final version of the program will now be described in more detail.

1 Data input

NTIME - Number of time steps

NTIME sets of the following:

LTIME - time increment (days)

BKG	–	Graphite thermal conductivity – 19 values: 300°C to 1200°C in 50°C intervals (W/cm°C)
BKF	–	Fuel thermal conductivity – 25 values 300°C to 1500°C in 50°C intervals (w/cm°C)
QCH	–	Channel power (W)
NAX	–	Number of axial slabs
QZ	–	Axial rating value (NAX + 1 values)
ASLAB	–	Axial slab 'area' (NAX values) giving heat generation within slab.
HMAX	–	Conductance of nominally zero gap ($W/cm^{2\,o}C$)
RI	–	First guess of heat split radius (cm)
TG1	–	Bore inlet gas temperature (°C)
TG2	–	Annulus inlet gas temperature (°C)
E	–	Emmissivity (fuel and graphite)
RCOC	–	Cold bore radius (cm)
RC1C	–	Cold pin outer radius (cm)
RC2C	–	Cold channel wall radius (cm)
RF1	–	Fuel inner radius (cm)
RF2	–	Fuel outer radius (cm)
RHO	–	Fraction of channel heat generated in moderator
W1	–	Bore flow (g/s)
W2	–	Annulus flow (g/s)
RP	–	Rib height (cm)
RIBW	–	Rib width (cm)
AL	–	Active core height (cm)
FL	–	Fraction of core height containing fuel
PIN	–	Channel inlet pressure ($dynes/cm^2$)
NRIB	–	Number of ribs
GS1	–	Inner cold radial gap (cm) (NAX + 1 values)

GS2 - Outer cold radial gap (cm) (NAX + 1 values)

Appendix VIII is a typical data input for a seven time step, 10 axial step calculation.

2 The program

The program consists of three routines: MAIN, RUST and PRESS. A listing is shown at the end of this Appendix. The main steps in the calculation can be found by refering to the 'Comment' statements.

MAIN reads in the input data, performs the axial and time calculation and then prints out the results.

RUST performs the calculation of rough friction factors and heat transfer coefficients as according to Chapter 4 section 4.

PRESS calculates the pressure drop in the bore and annulus according to the Guggenheim equation and determines the flow split for the next iterative loop.

It should be pointed out that the $\varepsilon^* - A^*$ relations used in RUST and quoted in Chapter 4 section 4 are not those reported by NIKURADSE (37). By using the NIKURADSE equations it was found:

(i) If the smooth-rough transition was taken as $\varepsilon^* = 3.5$ (NIKURADSE) friction factors for ε^* values only a little above 3.5 were calculated as being less than the smooth values. This was overcome by reducing the critical ε^* to 3.05.

(ii) The NIKURADSE equations did not give the same values of A^* at the boundary values of ε^*. This was solved by changing slightly the boundary ε^* values.

3 Results output

RE At each axial calculation step three values of Reynolds number applying to the bore (1) and transformed annulus (2)

DE	Corresponding values of hydraulic diameter (cm)
RM	At each axial step - radius of no-shear (cm)
DWELL TIME	Cumulative dwell (days)
CHANNEL POWER	(W)
MIXED GAS OUTLET TEMPERATURE	(^{o}C)
INNER FLOW RATE	bore flow (g/s)
OUTER FLOW RATE	annulus flow (g/s)

For each calculation step:

Z	axial position (Z = 0 at inlet)	
TG1	T_{g1}	(^{o}C)
TW1	T_{W1}	(^{o}C)
TI1	T_{I1}	(^{o}C)
TF1	T_{F1}	(^{o}C)
TFM	T_{FP}	(^{o}C)
TF2	T_{F2}	(^{o}C)
TI2	T_{I2}	(^{o}C)
TW2	T_{W2}	(^{o}C)
TG2	T_{g2}	(^{o}C)
TW3	T_{W3}	(^{o}C)

INNER GAP	radial	(cm)
HEAT SPLIT RADIUS	(cm)	
OUTER GAP	radial	(cm)
RCO	r_{s1} (hot)	(cm)
RC1	r_{s2} (hot)	(cm)
RC2	r_{s3} (hot)	(cm)
PD (BORE)	bore pressure drop	(dynes/cm^2)
PD (ANNULUS)	annulus pressure drop	(dynes/cm^2)

PLANAR REMOVAL at r_{s1}, r_{s2}, r_{s3} (cm)

ROUGHNESS HEIGHT at r_{s1}, r_{s2}, r_{s3} (cm)

HEAT TRANSFER COEFFICIENT at r_{s1}, r_{s2}, r_{s3} $W/cm^{2o}C$

FRICTION FACTOR at r_{s1}, r_{s2}, r_{s3}

Appendix IX is a typical results output and shows the above values for the seven time steps.

```
      C      HEATAX
0001         DIMENSION  PI(50),TG1(50),TG2(50),TW1(50),TW2(50),TI1(50),
            1TI2(50),TF1(50),TF2(50),TFMAX(50),TWALL(50),QZ(50),ASLAB(50),
            2QSLAB(50),GOUT(50),BKG(30),BKF(30),TG(30),TF(30),
            3ITG1(50),ITG2(50),ITW1(50),ITW2(50),ITI1(50),ITI2(50),ITF1(50),
            4ITF2(50),ITFMAX(50),ITWALL(50),Z(50),IZ(50),GIN(50),GS1(50),GS2(50
            5),PCO(50),RC1(50),RC2(50),DPT1(50),DPT2(50),DRT1(20,20),DRT2(20,20
            6),DRT3(20,20),F1(20),F2(20),F3(20),HT1(20),HT2(20),HT3(20),LTIM(20
            7),FR1(20),FR2(20),FR3(20)
0002         COMMON W1,W2,AL,NAX,DE1,DE2,TG1,TG2,FLOA1,FLOA2,I,PIT1,DPT2,POUT,PO
            1IN,L,FF1,FF2
0003         DATA AX1,BX1,CX1,AX2,BX2,CX2/-4,083E-07,1.5724E-03,-0.2541,-6.38E-
            107,2.401E-03,4.087/
      C**STATEMENT FUNCTIONS**
0004         ALFAF(TF)=(AX1*TF*TF+BX1*TF+CX1)/1.0E+06
0005         ALFAG(TG)=(AX2*TG*TG+BX2*TG+CX2)/1.0E+06
0006         DELR1(T)=276.0/EXP(2.0174E+04/(T+273.0))
0007         DELR2(T)=2760.0/EXP(2.0174E+04/(T+273.0))
0008         LTIM(1)=0
0009         READ(5,100) NTIME
0010         NT=1
0011     400 NT=NT+1
0012         READ(5,99) LTIME
0013         MT=NT-1
0014      99 FORMAT(I5)
0015         LTIM(NT)=LTIM(MT)+LTIME
0016     100 FORMAT (I3)
0017     101 FORMAT (8F10.1)
      C      CONDUCTIVITY DATA
0018         READ(5,101)(BKG(N),N=1,19)
0019         READ(5,101)(BKF(N),N=1,25)
0020         TG(1)=573
0021         DO 50 N=2,19
0022         N1=N-1
0023         TG(N)=TG(N1)+50
0024      50 CONTINUE
0025         TF(1)=573
0026         DO 51 N=2,25
0027         N1=N-1
0028         TF(N)=TF(N1)+50
0029      51 CONTINUE
      C      RATING DATA
0030         READ(5,101) QCH
0031         READ(5,100) NAX
```



```
0032         N=NAX+1
0033         READ(5,101)(QZ(I1),I1=1,N)
0034         READ(5,101)(ASLAB(I1),I1=1,NAX)
      C      CHANNEL DATA
0035         READ(5,101) HMAX,PI(1),TG1(1),TG2(1),E,RCOC,RC1C,RC2C,RF1,RF2,RHO
            1,W1,W2,RP,RIBW,AL,FL,PIN
0036         READ(5,100) NRIB
0037         DO 55 I1=1,N
0038      55 READ(5,101) GS1(I1),GS2(I1)
      C*****---HEAT GENERATION---*****
0039         SUM=0
0040         DO 30 N=1,NAX
0041         SUM=SUM+ASLAB(N)
0042      30 CONTINUE
0043         CONST=QCH/SUM
0044         DO 31 N=1,NAX
0045         QSLAB(N)=CONST*ASLAB(N)
0046      31 CONTINUE
      C      FIRST GUESSES
0047         TG2(1)=TG2(1)+273
0048         TG1(1)=TG1(1)+273
0049         TF1(1)=TG1(1)+100
0050         TF2(1)=TG2(1)+100
0051         TFMAX(1)=TG2(1)+150
0052         TW1(1)=TG1(1)+50
0053         TI1(1)=TW1(1)+50
0054         TW2(1)=TG2(1)+50
0055         TWALL(1)=TG2(1)+50
0056         TI2(1)=TG2(1)+100
      C      CHANNEL CONSTANTS
0057         QL=QCH/AL
0058         R25=6.28318*RF2
0059         R26=6.28318*RF1
0060         R4=5.67*E/(2.0-E)
0061         NP=0
0062     500 I=0
      C      SLAB DATA
0063         WRITE(6,120)
0064       1 I=I+1
0065         Z(I)=AL*(I-1)/NAX
      C .    SLAB CONSTANTS
0066         AMU1=1.855E-04*(TG1(I)/273.16)**0.68
0067         AMU2=1.855E-04*(TG2(I)/273.16)**0.68
0068         AKH1=1.456E-03*(TG1(I)/273.16)**0.7
```

```
0069            AKH2=1,456E-03*(TG2(I)/273,16)**0,7                       00092000
0070            PR1=AMU1*5,19/AKH1                                         00093000
0071            PR2=AMU2*5,19/AKH2                                         00094000
0072             D3=1,0/(6,28318*HMAY*HF1)                                  00095000
0073             DELTAT=TG2(I)-TG1(I)                                       00096000
0074            QLF=QL*QZ(I)*(1,0-RHO)/FL                                  00097000
0075            QLM=QL*QZ(I)*RHO                                           00098000
0076            IZ=0                                                       00099000
0077         10 IF(IZ,GT,20) GO TO 8                                       00100000
0078            IZ=IZ+1                                                    00101000
          C      SLAB VARIABLES                                            00102000
0079             IF(I,EQ,1) GO TO 11                                       00103000
0080             IF(IZ,GT,1) GO TO 11                                      00104000
0081             N=I-1                                                     00105000
0082             GO TO 12                                                  00106000
0083         11  N=I                                                       00107000
          C      CALCULATION OF CONDUCTIVITY                               00108000
0084         12 TGM1=(TW1(N)+TI1(N))/2,0                                   00109000
0085            TGM2=(TW2(N)+TI2(N))/2,0                                   00110000
0086            TFM =(TF1(N)+TF2(N)+2,0*TFMAX(N))/4,0                      00111000
0087            IF(TGM1,LE,TG(1)) GO TO 52                                 00112000
0088            IF (TGM2,LE,TG(1)) GO TO 52                                00113000
0089            IF (TFM,LE,TF(1)) GO TO 52                                 00114000
0090            DO 20 N2=1,19                                              00115000
0091            IF(TGM1,LE,TG(N2)) GO TO 21                                00116000
0092         20 CONTINUE                                                   00117000
0093         21 N1=N2-1                                                    00118000
0094            AKG1=BKG(N1)+(TGM1-TG(N1))*(BKG(N2)-BKG(N1))/(TG(N2)-TG(N1))  00119000
0095            DO 22 N2=1,19                                              00120000
0096            IF(TGM2,LE,TG(N2)) GO TO 23                                00121000
0097         22 CONTINUE                                                   00122000
0098         23 N1=N2-1                                                    00123000
0099            AKG2=BKG(N1)+(TGM2-TG(N1))*(BKG(N2)-BKG(N1))/(TG(N2)-TG(N1))  00124000
0100            DO 24 N2=1,25                                              00125000
0101            IF(TFM,LE,TF(N2)) GO TO 25                                 00126000
0102         24 CONTINUE                                                   00127000
0103         25 N1=N2-1                                                    00128000
0104            AKF=BKF(N1)+(TFM-TF(N1))*(BKF(N2)-BKF(N1))/(TF(N2)-TF(N1))  00129000
          C      CALCULATION OF C,T,F,                                     00130000
0105            TFM=TFM-273                                                00131000
0106            TGM1=TGM1-273                                              00132000
0107            TGM2=TGM2-273                                              00133000
          C      CALCULATION OF GAPS                                       00134000
0108            GIN(I)=GS1(I)+RF1*(ALFAF(TFM)*(TFM-20,0)-ALFAG(TGM1)*(TGM1-20,0)) 00135000
```



```
0109            GOUT(I)=GS2(I)+RF2*(ALFAG(TGM2)*(TGM2-20,0)-ALFAF(TFM)*(TFM-20,0))00136000
          C**CALCULATION OF DIMENSIONS**                                   00137000
          C*THERMAL EXPANSION                                              00138000
0110            RC0(I)=RC0C*(ALFAG(TGM1)*(TGM1-20)+1)                      00139000
0111            RC1(I)=RC1C*(ALFAG(TGM2)*(TGM2-20)+1)                      00140000
0112            RC2(I)=RC2C*(ALFAG(TWALL(N))*(TWALL(N)-293)+1)             00141000
          C*****CORROSION CALCULATIONS                                     00142000
0113            TW1C=TW1(N)-273,0                                          00143000
0114            TW2C=TW2(N)-273,0                                          00144000
0115            TWALLC=TWALL(N)-273,0                                      00145000
0116            DR1=DELR1(TW1C)*LTIME                                      00146000
0117            DR2=DELR1(TW2C)*LTIME                                      00147000
0118            DR3=DELR2(TWALLC)*LTIME                                    00148000
0119            IF(DR1,LE,0,0) DR1=0,0                                     00149000
0120            IF(DR2,LE,0,0) DR2=0,0                                     00150000
0121            IF(DR3,LE,0,0) DR3=0,0                                     00151000
0122            DRT1(I,1)=0,0                                              00152000
0123            DRT2(I,1)=0,0                                              00153000
0124            DRT3(I,1)=0,0                                              00154000
0125            DRT1(I,NT)=DRT1(I,MT)+DR1                                  00155000
0126            DRT2(I,NT)=DRT2(I,MT)+DR2                                  00156000
0127            DRT3(I,NT)=DRT3(I,MT)+DR3                                  00157000
0128            RC0(I)=RC0(I)+DRT1(I,NT)                                   00158000
0129            RC1(I)=RC1(I)-DRT2(I,NT)                                   00159000
0130            RC2(I)=RC2(I)+DRT3(I,NT)                                   00160000
0131            IF(DRT1(I,NT),GE,RP) GO TO 401                             00161000
0132            E1=DRT1(I,NT)                                              00162000
0133            GO TO 402                                                  00163000
0134        401 E1=RP                                                      00164000
0135        402 IF(DRT2(I,NT),GE,RP) GO TO 403                             00165000
0136            E2=DRT2(I,NT)                                              00166000
0137            GO TO 404                                                  00167000
0138        403 E2=RP                                                      00168000
0139        404 IF(DRT3(I,NT),GE,RP) GO TO 405                             00169000
0140            E3=DRT3(I,NT)                                              00170000
0141            GO TO 406                                                  00171000
0142        405 E3=RP                                                      00172000
          C*****FRICTION FACTOR *****                                      00173000
          C**   INNER CHANNEL                                              00174000
0143        406 FLOA1=3,14159*RC0(I)*RC0(I)                                00175000
0144            DE1=2,0*RC0(I)                                             00176000
0145            RE1=W1*DE1/(FLOA1*AMU1)                                    00177000
0146            HN1=0,023*RE1**0,8*PR1**0,4                                00178000
0147            FF1=0,079/RE1**0,25                                        00179000
```

```
0148          IF(E1.LE.0.00001) GO TO 470                                     00180000
0149          CALL RUST(RE1,DE1,E1,PR1,FF1,HN1)                               00181000
        C**   OUTER CHANNEL                                                   00182000
0150      470 K2=0                                                            00183000
0151          RM1=SQRT(RC1(I)*RC2(I))                                         00184000
0152          A1=6.28318*RC1(I)-NRIB*RIBW*(RM1-RC1(I))*NRIB*2.0               00185000
0153          A2=6.28318*RC2(I)-NRIB*RIBW*(RC2(I)-RM1)*NRIB*2.0               00186000
0154          FLOA2=3.14159*(RC2(I)*RC2(I)-RC1(I)*RC1(I))-NRIB*RIBW*(RC2(I)-RC1(00187000
             1I))                                                             00188000
0155          DE2=4.0*FLOA2/(A1+A2)                                           00189000
0156          DE3=DE2                                                         00190000
0157          RE2=W2*DE2/(FLOA2*AMU2)                                         00191000
0158          RE3=RE2                                                         00191500
0159          HN2=0.023*RE2**0.8*PR2**0.4                                     00192000
0160          HN3=HN2                                                         00193000
0161          FF2=0.0877/RE2**0.25                                            00194000
0162          FF3=FF2                                                         00195000
0163          IF(E2.LE.0.00001) GO TO 471                                     00196000
0164          GO TO 420                                                       00197000
0165      471 IF(E3.LE.0.00001) GO TO 490                                     00198000
0166          GO TO 420                                                       00199000
0167      421 K2=K2+1                                                         00200000
0168          IF(K2.GT.20) GO TO 300                                          00201000
0169          A3=FF2*A1/(FF3*A2)                                              00202000
0170          A=3.14159*(1.0+A3)                                              00203000
0171          B=-NRIB*RIBW*(1.0+A3)                                           00204000
0172          C=NRIB*RIBW*(RC1(I)+A3*RC2(I))-3.14159*(A3*RC2(I)*RC2(I)+RC1(I)*RC00205000
             11(I))                                                           00206000
0173          RM=(-B+SQRT(B*B-4.0*A*C))/(2.0*A)                               00207000
0174          DE2=4.0*(3.14159*(RM*RM-RC1(I)*RC1(I))-NRIB*RIBW*(RM-RC1(I)))/A1  00208000
0175          DE3=4.0*(3.14159*(RC2(I)*RC2(I)-RM*RM)-NRIB*RIBW*(RC2(I)-RM))/A2  00209000
0176      420 RE2=W2*DE2/(FLOA2*AMU2)                                         00210000
0177          RE3=W2*DE3/(FLOA2*AMU2)                                         00211000
0178          CALL RUST(RE2,DE2,E2,PR2,FF2A,HN2)                              00212000
0179          CALL RUST(RE3,DE3,E3,PR2,FF3A,HN3)                              00213000
0180          ERROR=(FF2A*1.101-FF2)/FF2                                      00214000
0181          IF(ABS(ERROR).GT.0.01) GO TO 422                                00215000
0182          ERROR=(FF3A*1.101-FF3)/FF3                                      00216000
0183          IF(ABS(ERROR).LE.0.01) GO TO 423                                00217000
0184      422 FF2=FF2A*1.101                                                  00218000
0185          FF3=FF3A*1.101                                                  00219000
0186          GO TO 421                                                       00220000
0187      423 FF2=FF2A*1.101                                                  00221000
0188          FF3=FF3A*1.101                                                  00222000
```



```
0189          GO TO 472                                                       00223000
0190      490 RM=RM1                                                          00224000
0191      472 B20=6.28318*RC1(I)                                              00225000
0192          B5=1.0/E+(RC1(I)/RC2(I))*(1.0/E-1)                              00226000
0193          B6=5.67/B5                                                      00227000
        C     CALCULATION OF CONDUCTANCES                                     00228000
0194          B1=ALOG(RF1/RC0C)/(6.28318*AKG1)                                00229000
0195          B2=ALOG(RC1C/RF2)/(6.28318*AKG2)                                00230000
0196          B16=12.5663*AKF                                                 00231000
0197           B12=2*RI(N)*RI(N)/(RI(N)*RI(N)-RF1*RF1)                        00232000
0198           B7=(B12*ALOG(RI(N)/RF1)-1)/B16                                 00233000
0199           B17=2.0*RI(N)*RI(N)/(RF2*RF2-RI(N)*RI(N))                      00234000
0200           B8=(1.0-B17*ALOG(RF2/RI(N)))/B16                               00235000
0201           H1=HN1*(TG1(I)/TW1(N))**0.15*AKH1/DE1                          00236000
0202           H2=HN2*(TG2(I)/TW2(N))**0.15*AKH2/DE2                          00237000
0203           H3=HN3*(TG2(I)/TWALL(N))**0.15*AKH2/DE3                        00238000
0204           B9=1.0/(6.28318*RC0(I)*H1)                                     00239000
        C     CALCULATION OF GAP CONDUCTANCES                                 00240000
0205           TIMEN1=(TI1(N)+TF1(N))/2.0                                     00241000
0206           TIMEN2=(TI2(N)+TF2(N))/2.0                                     00242000
0207           HKG1=1.456E-3*(TIMEN1/273.16)**0.7                             00243000
0208           HKG2=1.456E-3*(TIMEN2/273.16)**0.7                             00244000
0209           IF (GIN(I).LE.0.0) GO TO 200                                   00245000
0210          RADG1=(TF1(N)+TI1(N))*(TF1(N)*TF1(N)+TI1(N)*TI1(N))/1.0E12      00246000
0211          B30=1/(((B4*RADG1)+(HKG1/GIN(I)))*B26)                          00247000
0212      200 RADG2=(TF2(N)+TI2(N))*(TF2(N)*TF2(N)+TI2(N)*TI2(N))/1.0E12      00248000
0213          IF (B30.LT.B3) B30=B3                                           00249000
0214           B11=1/(((B4*RADG2)+(HKG2/GOUT(I)))*B25)                        00250000
0215           B18=(TW2(N)*TW2(N)-TWALL(N)*TWALL(N))*(TW2(N)*TW2(N)+TWALL(N)  00251000
             1 *TWALL(N))/1.0E12                                              00252000
0216          IF(I2.EQ.1) GO TO 201                                           00253000
0217          QA=HEATLO/B20-B6*B18                                            00254000
0218          QB=(QLM+B6*B18*B20)/(6.28318*RC2(I))                            00255000
0219          FAC1=1.0+0.25*(1.0-QB/QA)                                       00256000
0220          FAC2=1.0+0.125*(1.0-QA/QB)                                      00257000
0221          H2=H2/FAC1                                                      00258000
0222          H3=H3/FAC2                                                      00259000
0223      201  B19=(B18*B6*B20+QLM)/(6.28318*RC2(I)*H3)                       00260000
0224           B10=1/((B6*B18/(TW2(N)-TG2(I))+H2)*B20)                        00261000
        C      CALCULATION OF THE HEAT SPLIT RADIUS                           00262000
0225           B13=B7+B30+B1+B9                                               00263000
0226           B14=B8+B11+B2+B10                                              00264000
0227           B15=RF2*RF2-RF1*RF1                                            00265000
0228           B21=(DELTAT/QLF)+B14                                           00266000
```

```
      B22=B15*B21/(B13+B14)+RF1*RF1
      RID=SQRT(B22)
C     CALCULATION OF HEAT FLUXES AND TEMPERATURES
      HEATLO=QLF*(RF2**2.0-B22)/B15
      TW2(I)=TG2(I)+HEATLO*B10
      TI2(I)=TW2(I)+HEATLO*B2
      TF2D=TI2(I)+HEATLO*B11
      TWALL(I)=TF2(I)+B19
      HEATLI=QLF*(RID*RID-RF1*RF1)/B15
      TW1(I)=TG1(I)+HEATLI*B9
      TI1(I)=TW1(I)+HEATLI*B1
      TF1(I)=TI1(I)+HEATLI*B30
      TFMAX(I)=TF2D+HEATLO*B8
      B23=ABS((RID-RI(N))/RI(N))
      IF(B23.GT.0.001) GO TO 4
      GO TO 5
    4 RI(I)=RID
      TF2(I)=TF2D
      GO TO 10
    5 RI(I)=RID
      B24=ABS(TF2D-TF2(I))
      IF (B24.GT.1.0) GO TO 6
      GO TO 7
    6 TF2(I)=TF2D
      GO TO 10
    7 TF2(I)=TF2D
      FF1=FF1*(TW1(I)/TG1(I))**0.05
      FF2=FF2*(TW2(I)/TG2(I))**0.05
      FF3=FF3*(TWALL(I)/TG2(I))**0.05
      F1(I)=FF1
      F2(I)=FF2
      F3(I)=FF3
      HT1(I)=H1
      HT2(I)=H2
      HT3(I)=H3
      ER1(I)=E1
      ER2(I)=E2
      ER3(I)=E3
  194 FORMAT(//,1X,'*RE*',3(2X,E12.5),2X,'*DE*',3(2X,E12.5),2X,'*RM*',2X
     1,E12.5)
      WRITE(6,194) RE1,RE2,RE3,DE1,DE2,DE3,RM
      IF(I.EQ.1) GO TO 210
C********--PRESSURE  PRESSURE  PRESSURE-----****
      CALL PRESS
```



```
    9 IF(I.EQ.NAX+1) GO TO 8
  210 HETIN=QSLAB(I)*(1-RHO)*(RI(I)*RI(I)-RF1*RF1)/B15
      HETOUT=QSLAB(I)*(1-RHO)*(RF2*RF2-RI(I)*RI(I))/B15+QSLAB(I)*RHO
      N=I+1
      TG1(N) =TG1(I)+HETIN/(W1*5.19)
      TG2(N) =TG2(I)+HETOUT/(W2*5.19)
      GO TO 1
C     PRINTOUT SEGMENT
    8 N1=NAX+1
      DO 40 N=1,N1
      IZ(N)=IFIX(Z(N))
      ITG1(N)=IFIX(TG1(N))-273
      ITG2(N)=IFIX(TG2(N))-273
      ITW1(N)=IFIX(TW1(N))-273
      ITW2(N)=IFIX(TW2(N))-273
      ITI1(N)=IFIX(TI1(N))-273
      ITI2(N)=IFIX(TI2(N))-273
      ITF1(N)=IFIX(TF1(N))-273
      ITF2(N)=IFIX(TF2(N))-273
      ITFMAX(N)=IFIX(TFMAX(N))-273
      ITWALL(N)=IFIX(TWALL(N))-273
   40 CONTINUE
  119 FORMAT(//,'   Z       INNER GAP         HEAT SPLIT RADIUS        OUTER G
     1AP')
  142 FORMAT(1X,I3,4X,E12.5,2(8X,E12.5))
  140 FORMAT('1','        GRAPHITE  SURFACE  DIMENSIONS',///,'    Z
     1RC0              RC1                RC2')
  143 FORMAT(1X,I3,3(4X,E12.5))
  144 FORMAT(1X,I3,2(4X,E12.5))
  141 FORMAT(//,'          PRESSURE  DROPS',/,'   Z        PD(BORE)          PD(
     1ANNULUS)')
  120 FORMAT ('1',25X,'H E A T A N D   R E S U L T S')
  121 FORMAT('0',23H              CHANNEL POWER)
  122 FORMAT(11X,E12.5)
  123 FORMAT('0',44H              INNER FLOW RATE     OUTER FLOW RATE)
  124 FORMAT(5X,2(6X,E12.5))
  125 FORMAT('0',28H                   TEMPERATURES)
  126 FORMAT(1X,I3,10(5X,I5))
  127 FORMAT(1X,103H  Z          TG1         TW1          TI1           TF1          TF
     1M        TF2        TI2         TW2         TG2          TW3)
  128 FORMAT(1X,26HCONDUCTIVITY OUTSIDE RANGE)
      GO TO 53
   52 WRITE(6,128)
   53 TGO=(W1*TG1(N1)+W2*TG2(N1))/(W1+W2)-273.0
```

```
      175 FORMAT(//,11X,'FIXED GAS OUTLET TEMPERATURE',5X,F5.1)
          WRITE(6,189) LTIM(NT)
          WRITE(6,121)
          WRITE(6,122) OCH
          WRITE(6,175) TGB
          WRITE(6,123)
          WRITE(6,124) W1,W2
          WRITE(6,125)
          WRITE(6,127)
          DO 41 N=1,N1
       41 WRITE(6,126)IZ(N),ITG1(N),ITM1(N),ITI1(N),ITF1(N),ITFMAX(N),
         2ITF2(N),ITI2(N),ITW2(N),ITG2(N),ITWALL(N)
          WRITE(6,119)
          DO 42 N=1,N1
       42 WRITE(6,142) IZ(N), GIN(N),FI(N),GOUT(N)
          WRITE(6,140)
          DO 43 N=1,N1
       43 WRITE(6,143) IZ(N),RCO(N),RC1(N),RC2(N)
          WRITE(6,141)
          DO 44 N=1,N1
       44 WRITE(6,144) IZ(N), DPT1(N),DPT2(N)
C***      CORROSION ADDITIONAL PRINTOUT
      189 FORMAT('1',11X,'DWELL TIME  =  ',I5,' DAYS')
      190 FORMAT('1',6X,'CORROSION  DATA',///,17X,'PLANAR  REMOVAL',32X,'ROU
         1GHNESS  HEIGHTS')
      191 FORMAT(/////,25X,'HEAT TRANSFER COEFF.',7X,'AND',7X,'FRICTION  FAC
         1TOR  (TRANSFORMED)')
      192 FORMAT(/,3X,'Z',5X,'RCO',13X,'RC1',13X,'RC2',13X,'RCO',13X,'RC1',1
         13X,'RC2')
      193 FORMAT(1X,I3,6(4X,E12.5))
          WRITE(6,190)
          WRITE(6,192)
          DO 45 N=1,N1
       45 WRITE(6,193) IZ(N),DPT1(N,NT),DPT2(N,NT),DRT3(N,NT),ER1(N),ER2(N),
         1ER3(N)
          WRITE(6,191)
          WRITE(6,192)
          DO 46 N=1,N1
       46 WRITE(6,193) IZ(N),HT1(N),HT2(N),HT3(N),F1(N),F2(N),F3(N)
          NP=NP+1
          IF(NP.EQ.6) GO TO 300
          IF(L.EQ.1)  GO TO 301
          WTOT=W1+W2
          DPC=(DPT1(I)+DPT2(I))/2.0
```



```
          W1=W1*(DPC/DPT1(I))**0.5714
          W2=W2*(DPC/DPT2(I))**0.5714
          W1=W1*WTOT/(W1+W2)
          W2=W2*WTOT/(W1+W2)
          GO TO 500
      301 IF(NT.LE.NTIME) GO TO 400
      300 STOP
          END
```

```
      SUBROUTINE  RUST(RE,DE,E,PR,FF,HN)
      K1=0
      HN=0,023*RE**0,8*PR**0,4
      HNS=HN
      FF=0,079/RE**0,25
      FFS=FF
  407 K1=K1+1
      IF(K1,GT,20) GO TO 450
      ESTAR=RE*(FF/2,0)**0,5*E/DE
      IF(ESTAR,LT,3,64) GO TO 470
C*** FRICTION FACTOR
      IF(ESTAR,LT,7,2) GO TO 409
      IF(ESTAR,LT,15,0) GO TO 410
      IF(ESTAR,LT,73,0) GO TO 411
      ASTAR=8,48
      GO TO 412
  411 ASTAR=11,5-0,705*ALOG(ESTAR)
      GO TO 412
  410 ASTAR=9,59
      GO TO 412
  409 ASTAR=1,52*ALOG(ESTAR)+6,59
      GO TO 412
  470 ASTAR=2,5*ALOG(ESTAR)+5,5
  412 FFA=2,0/(ASTAR-3,75-2,5*ALOG(2,0*E/DE))**2,0
      ERROR=(FFA-FF)/FF
      IF(ABS(ERROR),LT,0,005) GO TO 413
      FF=FFA
      GO TO 407
C*** HEAT TRANSFER COEFF,
  413 FF=FFA
      IF(ESTAR,LE,3,5) GO TO 451
      BSTAR=5,58*ESTAR**0,1805
      GR=BSTAR*PR**0,44
      HNR=0,5*RE*PR*FF/(1,0-(8,48-GR)*SQRT(FF/2,0))
C*** NORMALISATION
  451 K3=0
      FFS2=FFS
  414 IF(K3,GT,20) GO TO 450
      K3=K3+1
      FFS1=1,0/(1,7684*ALOG(RE*SQRT(FFS2))-0,566)**2,0
      ERROR=(FFS1-FFS2)/FFS2
      IF(ABS(ERROR),LE,0,001) GO TO 415
      FFS2=FFS1
      GO TO 414
```



```
  415 FFA=FFA*FFS/FFS1
      FF=FFA
      IF(ESTAR,LE,3,5) GO TO 408
      HNS1=0,5*RE*PR*FFS1/(1,0-3,01*SQRT(FFS1/2,0))
      IF(HNR,LT,HNS1) HNR=HNS1
      HN=HNR*HNS/HNS1
      GO TO 408
  450 WRITE(6,460)
  460 FORMAT('1',/// ,'ITERATION NUMBER EXCEEDED IN RUST')
  408 RETURN
      END
```

```
0001          SUBROUTINE  PRESS
        C****--PRESSURE DROP CALCULATION--***
0002          DIMENSION TG1(50),TG2(50),P1(50),P2(50),DPT1(50),DPT2(50)
0003          COMMON W1,W2,AL,NAX,DE1,DE2,TG1,TG2,FLOA1,FLOA2,I,DPT1,DPT2,POUT,P
             1IN,L,FF1,FF2
        C ***--STATEMENT FUNCTION--***
0004          DEN(TGAS,P)=48,139E-09*P/TGAS
0005          N=I-1
0006          P1(1)=PIN
0007          P2(1)=PIN
0008          DPT1(1)=0,0
0009          DPT2(1)=0,0
0010          L=0
0011          TBAR1=(TG1(N)+TG1(I))/2,0
0012          TBAR2=(TG2(N)+TG2(I))/2,0
0013          DP1=W1*W1*(4,0*FF1*AL/(NAX*DE1)+2,0*(TG1(I)-TG1(N))/TBAR1+1,4/NAX)
             1/(FLOA1*FLOA1*DEN(TBAR1,P1(I))*2,0)
0014          DP2=W2*W2*(4,0*FF2*AL/(NAX*DE2)+2,0*(TG2(I)-TG2(N))/TBAR2+4,5/NAX)
             1/(FLOA2*FLOA2*DEN(TBAR2,P2(I))*2,0)
0015          P1(I)=P1(N)+DP1
0016          P2(I)=P2(N)+DP2
0017          DPT1(I)=DPT1(N)+DP1
0018          DPT2(I)=DPT2(N)+DP2
0019          IF(I,NE,NAX+1) GO TO 600
0020          ERRORP=2,0*(DPT1(I)-DPT2(I))/(DPT1(I)+DPT2(I))
0021          IF (ABS(ERRORP),LE,0,005) L=1
0022          IF (L,EQ,1) GO TO 550
0023          GO TO 600
0024      550 POUT=(P1(I)+P2(I))/2,0
0025      600 RETURN
0026          END
```

APPENDIX VIII

HEATAX III INPUT DATA

Input data for a seven time, ten axial step calculation for the peak rated channel (Tables 4/1, 5/1)

7							
0							
0,807	0,759	0,711	0,667	0,626	0,591	0,560	0,527
0,498	0,473	0,450	0,431	0,410	0,398	0,380	0,367
0,353	0,345	0,336					
0,288	0,288	0,288	0,288	0,288	0,285	0,285	0,285
0,285	0,285	0,285	0,285	0,285	0,285	0,285	0,285
0,285	0,285	0,285	0,285	0,285	0,285	0,285	0,285
0,285							
6,07E+05							
10							
0,684	0,869	1,098	1,223	1,293	1,198	1,083	1,153
0,974	0,779	0,554					
0,743	0,991	1,176	1,258	1,096	1,092	1,074	1,024
0,889	0,658						
2,00	2,6	300,0	300,0	0,87	1,515	3,26	3,79
2,015	2,75	0,08	117,0	88,58	0,025	0,5	500,0
0,94	5,5E+07						
3							
0,015	0,01						
0,015	0,01						
0,015	0,01						
0,015	0,01						
0,015	0,01						
0,015	0,01						
0,015	0,01						
0,015	0,01						
0,015	0,01						
0,015	0,01						
0,015	0,01						
77							
0,284	0,320	0,363	0,391	0,395	0,400	0,390	0,384
0,370	0,369	0,358	0,350	0,348	0,337	0,335	0,323
0,320	0,315	0,307					
0,215	0,215	0,215	0,215	0,205	0,205	0,200	0,2
0,2	0,2	0,2	0,2	0,2	0,2	0,2	0,2
0,2	0,2	0,2	0,2	0,2	0,2	0,2	0,2
0,2							
5,89E+05							
10							
0,695	0,879	1,101	1,222	1,269	1,194	1,082	1,153
0,976	0,783	0,562					
0,752	0,999	1,173	1,255	1,091	1,088	1,072	1,022
0,891	0,661						
2,00	2,6	300,0	300,0	0,87	1,515	3,26	3,79
2,015	2,75	0,08	115,7	89,66	0,025	0,5	500,0
0,94	5,5E+07						
3							
0,0187	0,0099						
0,0131	0,0124						
0,0101	0,0166						
0,0083	0,0195						
0,0073	0,021						
0,008	0,0201						
0,0079	0,0195						
0,0083	0,0204						
0,00815	0,0204						
0,0087	0,0189						
0,011	0,0155						

154							
0,135	0,180	0,220	0,250	0,272	0,280	0,281	0,281
0,282	0,282	0,282	0,283	0,283	0,283	0,284	0,284
0,284	0,284	0,284					
0,155	0,155	0,155	0,155	0,1475	0,1475	0,1425	0,1425
0,1425	0,1425	0,1425	0,1425	0,1425	0,1425	0,1425	0,1425
0,1425	0,1425	0,1425	0,1425	0,1425	0,1425	0,1425	0,1425
0,1425							
5,51E+05							
10							
0,716	0,897	1,104	1,216	1,277	1,082	1,076	1,051
0,979	0,789	0,577					
0,771	1,016	1,167	1,249	1,082	1,08	1,067	1,019
0,894	0,668						
2,00	2,6	300,0	300,0	0,87	1,505	3,26	3,79
2,015	2,75	0,08	107,9	84,62	0,025	0,5	500,0
0,94	5,5E+07						
3							
0,0117	0,0134						
0,0088	0,0177						
0,0064	0,0241						
0,0073	0,0292						
0,0081	0,0335						
0,0081	0,0303						
0,0085	0,0303						
0,0089	0,0313						
0,0093	0,0303						
0,0091	0,0273						
0,0085	0,0223						
154							
0,08	0,135	0,177	0,209	0,229	0,241	0,246	0,246
0,246	0,246	0,249	0,257	0,257	0,257	0,257	0,257
0,257	0,257	0,257					
0,12	0,12	0,12	0,12	0,1175	0,1175	0,11	0,11
0,11	0,11	0,11	0,11	0,11	0,11	0,11	0,11
0,11	0,11	0,11	0,11	0,11	0,11	0,11	0,11
0.11							
5,14E+05							
10							
0,757	0,921	1,107	1,205	1,261	1,06	1,058	1,036
0,978	0,817	0,609					
0,807	1,029	1,162	1,234	1,059	1,06	1,05	1,016
0,907	0,699						
2,00	2,6	300,0	300,0	0,87	1,505	3,26	3,79
2,015	2,75	0,08	100,4	79,15	0,025	0,5	500,0
0,94	5,5E+07						
3							
0,0101	0,0168						
0,0056	0,0223						
0,0069	0,0298						
0,0079	0,0362						
0,0085	0,0418						
0,0085	0,0377						
0,0087	0,0376						
0,0095	0,0380						
0,0099	0,0363						
0,0095	0,0328						
0,0091	0.0267						

```
  154
0,065     0,120     0,162     0,195     0,215     0,235     0,240     0,242
0,245     0,245     0,245     0,245     0,245     0,245     0,245     0,245
0,245     0,245     0,245
0,1075    0,1075    0,1075    0,1075    0,1025    0,1025    0,0975    0,0975
0,0975    0,0975    0,0975    0,0975    0,0975    0,0975    0,0975    0,0975
0,0975    0,0975    0,0975    0,0975    0,0975    0,0975    0,0975    0,0975
0,0975
  4,77E+05
  10
0,802     0,947     1,110     1,193     1,245     1,036     1,037     1,020
0,975     0,850     0,643
0,847     1,042     1,157     1,218     1,053     1,038     1,03      1,001
0,922     0,736
2,00      2,6       300,0     300,0     0,87      1,505     3,26      3,79
2.015     2,75      0,08      93,03     73,59     0,025     0,5       500,0
       0,94   5,5E+07
  3
0,0073    0,0209
0,0060    0,0256
0,0075    0,0547
0,0077    0,0425
0,0079    0,0495
0,0083    0,0441

0,0087    0,0430
0,0093    0,0433
0,0095    0,0413
0,0099    0,0367
0,0097    0,0302
  154
0,058     0,115     0,155     0,180     0,210     0,215     0,220     0,231
0,238     0,238     0,238     0,238     0,238     0,238     0,238     0,238
0,238     0,238     0,238
0,1       0,1       0,1       0,1       0,095     0,095     0,0925    0,0925
0,0925    0,0925    0,0925    0,0925    0,0925    0,0925    0,0925    0,0925
0,0925    0,0925    0,0925    0,0925    0,0925    0,0925    0,0925    0,0925
0,0925
  4,40E+05
  10
0,847     0,972     1,113     1,181     1,228     1,012     1,016     1,003
0,971     0,883     0,678
0,886     1,055     1,152     1,201     1,007     1,115     1,011     0,992
0,937     0,773
2,00      2,6       300,0     300,0     0,87      1,505     3,26      3,79
2.015     2,75      0,08      85,79     67,91     0,025     0,5       500,0
       0,94   5,5E+07
  3
0,0054    0,0247
0,0064    0,0292
0,0075    0,0386
0,0073    0,0482
0,0066    0,0552
0,0073    0,0499
0,0077    0,0481
0,0083    0,0472
0,0089    0,0450
0,0097    0,0404
0,0099    0,0336
  77
0,058     0,115     0,155     0,180     0,210     0,215     0,220     0,231
0,238     0,238     0,238     0,238     0,238     0,238     0,238     0,238
0,238     0,238     0,238
0,1       0,1       0.1       0,1       0,095     0,095     0.0925    0,0925
0,0925    0,0925    0,0925    0,0925    0,0925    0,0925    0,0925    0,0925
0,0925    0,0925    0,0925    0,0925    0,0925    0,0925    0,0925    0,0925
0,0925
  4.218E+05
  10
0,847     0,972     1.113     1,181     1,228     1,012     1,016     1,003
0,971     0,883     0,678
0,886     1,055     1,152     1,201     1,007     1,015     1,011     0,992

0,937     0,773
2,00      2,6       300,0     300,0     0,87      1,515     3,26      3,79
2.015     2,75      0,08      84,73     67,18     0,025     0,5       500,0
       0,94   5,5E+07
  3
0.0054    0.0247
[illegible]    0.0292
0.0075    0.0386
0.0073    0.0482
0.0056    0.0552
0.0073    0.0499
0.0077    0.0481
0.0083    0.0472
0.0089    0.045.
0.0097    [illegible]
0.0099    0.0336
```

APPENDIX IX

HEATAX III RESULTS

Results output for a seven time, ten axial step calculation for the peak rated channel (Appendix VIII)

(a) UNCORRODED CASE

HEATAX RESULTS

RE	0.16563E 06	0.24979E 05	0.24979E 05	*DE*	0.30172E 01	0.98130E 00	0.98130E 00	*RM*	0.35217E 01
RE	0.15981E 06	0.23364E 05	0.23364E 05	*DE*	0.30189E 01	0.98057E 00	0.98057E 00	*RM*	0.35233E 01
RE	0.15247E 06	0.21621E 05	0.21621E 05	*DE*	0.30212E 01	0.97975E 00	0.97975E 00	*RM*	0.35255E 01
RE	0.14453E 06	0.19960E 05	0.19960E 05	*DE*	0.30233E 01	0.98033E 00	0.98033E 00	*RM*	0.35277E 01
RE	0.13687E 06	0.18529E 05	0.18529E 05	*DE*	0.30251E 01	0.98113E 00	0.98113E 00	*RM*	0.35298E 01
RE	0.13086E 06	0.17495E 05	0.17495E 05	*DE*	0.30251E 01	0.98349E 00	0.98349E 00	*RM*	0.35309E 01
RE	0.12519E 06	0.16632E 05	0.16632E 05	*DE*	0.30263E 01	0.98455E 00	0.98455E 00	*RM*	0.35325E 01
RE	0.12005E 06	0.15898E 05	0.15898E 05	*DE*	0.30274E 01	0.98540E 00	0.98540E 00	*RM*	0.35340E 01
RE	0.11551E 06	0.15282E 05	0.15282E 05	*DE*	0.30281E 01	0.98659E 00	0.98659E 00	*RM*	0.35353E 01
RE	0.11181E 06	0.14811E 05	0.14811E 05	*DE*	0.30279E 01	0.98827E 00	0.98827E 00	*RM*	0.35361E 01
RE	0.10911E 06	0.14510E 05	0.14510E 05	*DE*	0.30274E 01	0.98988E 00	0.98988E 00	*RM*	0.35363E 01

DWELL TIME = 0 DAYS

CHANNEL POWER
0.60700E 06

MIXED GAS OUTLET TEMPFRATURE 868.

INNER FLOW RATE 0.12049E 03 OUTER FLOW RATE 0.85402E 02

TEMPERATURES

Z	TG1	TW1	TI1	TF1	TFM	TF2	TI2	TW2	TG2	TW3
0	300	474	501	599	617	600	480	462	300	308
50	330	562	602	711	737	717	576	551	358	372
100	372	675	736	850	884	861	695	660	434	455
150	425	770	847	955	995	971	797	755	522	548
200	482	853	944	1042	1087	1063	888	841	613	645
250	534	857	939	1026	1068	1049	906	868	690	719
300	587	911	997	1075	1118	1101	966	928	764	794
350	642	960	1049	1118	1152	1147	1021	983	834	866
400	695	995	1082	1143	1186	1173	1062	1027	899	930
450	742	995	1069	1121	1159	1151	1069	1045	954	979
500	780	976	1033	1076	1110	1106	1057	1043	991	1008

Z	INNER GAP	HEAT SPLIT RADIUS	OUTER GAP
0	0.10847E-01	0.23805E 01	0.15418E-01
50	0.10012E-01	0.23961E 01	0.16541E-01
100	0.86519E-02	0.24082E 01	0.17956E-01
150	0.78136E-02	0.24196E 01	0.19210E-01
200	0.68306E-02	0.24299E 01	0.20427E-01
250	0.68357E-02	0.24483E 01	0.20922E-01
300	0.62373E-02	0.24586E 01	0.21309E-01
350	0.56722E-02	0.24681E 01	0.22660E-01
400	0.52805E-02	0.24813E 01	0.23385E-01
450	0.52962E-02	0.25089E 01	0.23741E-01
500	0.55176E-02	0.25557E 01	0.23831E-01

GRAPHITE SURFACE DIMENSIONS

Z	RC0	RC1	RC2
0	0.15086E 01	0.32675E 01	0.37957E 01
50	0.15096E 01	0.32693E 01	0.37971E 01
100	0.15106E 01	0.32717E 01	0.37990E 01
150	0.15117E 01	0.32737E 01	0.38013E 01
200	0.15126E 01	0.32756E 01	0.38037E 01
250	0.15126E 01	0.32761E 01	0.38055E 01
300	0.15131E 01	0.32775E 01	0.38074E 01
350	0.15137E 01	0.32788E 01	0.38092E 01
400	0.15140E 01	0.32797E 01	0.38109E 01
450	0.15140E 01	0.32800E 01	0.38121E 01
500	0.15137E 01	0.32799E 01	0.38129E 01

PRESSURE DROPS

Z	PD(BOFE)	PD(ANNULUS)
0	0.0	0.0
50	0.16139E 05	0.14596E 05
100	0.34221E 05	0.31305E 05
150	0.54538E 05	0.50292E 05
200	0.76711E 05	0.71550E 05
250	0.99536E 05	0.94419E 05
300	0.12385E 06	0.11902E 06
350	0.14950E 06	0.14530E 06
400	0.17629E 06	0.17307E 06
450	0.20370E 06	0.20195E 06
500	0.23109E 06	0.23142E 06

CORROSION DATA

	PLANAR REMOVAL			ROUGHNESS HEIGHTS		
Z	RC0	RC1	RC2	RC0	RC1	RC2
0	0.0	0.0	0.0	0.0	0.0	0.0
50	0.0	0.0	0.0	0.0	0.0	0.0
100	0.0	0.0	0.0	0.0	0.0	0.0
150	0.0	0.0	0.0	0.0	0.0	0.0
200	0.0	0.0	0.0	0.0	0.0	0.0
250	0.0	0.0	0.0	0.0	0.0	0.0
300	0.0	0.0	0.0	0.0	0.0	0.0
350	0.0	0.0	0.0	0.0	0.0	0.0
400	0.0	0.0	0.0	0.0	0.0	0.0
450	0.0	0.0	0.0	0.0	0.0	0.0
500	0.0	0.0	0.0	0.0	0.0	0.0

HEAT TRANSFER COEFF. AND FRICTION FACTOR (TRANSFORMED)

Z	RC0	RC1	RC2	RC0	RC1	RC2
0	0.22600E 00	0.12694E 00	0.41327E 00	0.39683E-02	0.70073E-02	0.69254E-02
50	0.22549E 00	0.12903E 00	0.35019E 00	0.40159E-02	0.71311E-02	0.70443E-02
100	0.22544E 00	0.13173E 00	0.30309E 00	0.40755E-02	0.72748E-02	0.71851E-02
150	0.22716E 00	0.13499E 00	0.27789E 00	0.41339E-02	0.74143E-02	0.73316E-02
200	0.22968E 00	0.13837E 00	0.25829E 00	0.41901E-02	0.75430E-02	0.74703E-02
250	0.23411E 00	0.14156E 00	0.24857E 00	0.42242E-02	0.76291E-02	0.75759E-02
300	0.23683E 00	0.14409E 00	0.23938E 00	0.42674E-02	0.77175E-02	0.76721E-02
350	0.23950E 00	0.14670E 00	0.22958E 00	0.43080E-02	0.77971E-02	0.77591E-02
400	0.24248E 00	0.14904E 00	0.22355E 00	0.43435E-02	0.78655E-02	0.78352E-02
450	0.24600E 00	0.15145E 00	0.21767E 00	0.43684E-02	0.79144E-02	0.78942E-02
500	0.24932E 00	0.15411E 00	0.20974E 00	0.43839E-02	0.79428E-02	0.79321E-02

H E A T A X   R E S U L T S

0.16364E 06	0.25328E 05	0.25328E 05	*DE*	0.30171E 01	0.98090E 00	0.98090E 00	*RM*	0.35218E 01
0.15823E 06	0.23675E 05	0.23675E 05	*DE*	0.30192E 01	0.98081E 00	0.98081E 00	*RM*	0.35233E 01
0.15076E 06	0.22008E 05	0.22008E 05	*DE*	0.30220E 01	0.98085E 00	0.98085E 00	*RM*	0.35251E 01
0.14238E 06	0.20497E 05	0.20497E 05	*DE*	0.30241E 01	0.98116E 00	0.98116E 00	*RM*	0.35270E 01
0.13438E 06	0.19174E 05	0.19174E 05	*DE*	0.30259E 01	0.98165E 00	0.98165E 00	*RM*	0.35289E 01
0.12830E 06	0.18186E 05	0.18186E 05	*DE*	0.30256E 01	0.98364E 00	0.98364E 00	*RM*	0.35299E 01
0.12268E 06	0.17340E 05	0.17340E 05	*DE*	0.30266E 01	0.98439E 00	0.98439E 00	*RM*	0.35314E 01
0.11768E 06	0.16597E 05	0.16597E 05	*DE*	0.30276E 01	0.98527E 00	0.98527E 00	*RM*	0.35329E 01
0.11332E 06	0.15965E 05	0.15965E 05	*DE*	0.30282E 01	0.98634E 00	0.98634E 00	*RM*	0.35341E 01
0.10981E 06	0.15470E 05	0.15470E 05	*DE*	0.30279E 01	0.98790E 00	0.98790E 00	*RM*	0.35349E 01
0.10728E 06	0.15143E 05	0.15143E 05	*DE*	0.30273E 01	0.98935E 00	0.98935E 00	*RM*	0.35352E 01

DWELL TIME = 0 DAYS

CHANNEL POWER
0.58900E 06

MIXED GAS OUTLET TEMPERATURE 852.

INNER FLOW RATE OUTER FLOW RATE
0.11904E 03 0.86597E 02

TEMPERATURES

TG1	TW1	TI1	TF1	TFM	TF2	TI2	TW2	TG2	TW3
300	462	503	623	646	619	497	466	300	307
325	556	626	714	751	726	575	540	359	372
371	698	784	833	889	862	669	628	430	450
427	797	902	933	999	971	757	711	507	532
485	876	990	1023	1093	1065	842	792	587	616
543	873	972	1001	1063	1041	860	819	656	682
598	921	1021	1050	1112	1090	919	878	722	750
652	967	1067	1095	1157	1136	973	933	788	816
705	997	1093	1120	1179	1161	1014	978	850	877
751	993	1072	1094	1145	1133	1025	997	902	924
787	970	1030	1047	1089	1081	1017	999	939	955

INNER GAP	HEAT SPLIT RADIUS	OUTER GAP
0.14662E-01	0.23604E 01	0.15409E-01
0.79463E-02	0.24079E 01	0.18799E-01
0.34546E-02	0.24414E 01	0.24029E-01
0.56507E-03	0.24534E 01	0.27969E-01
-0.12868E-02	0.24557E 01	0.30556E-01
-0.33417E-03	0.24668E 01	0.30192E-01
-0.11437E-02	0.24680E 01	0.30468E-01
-0.12250E-02	0.24729E 01	0.32175E-01
-0.16967E-02	0.24792E 01	0.32879E-01
-0.10634E-02	0.24972E 01	0.31303E-01
0.15048E-02	0.25276E 01	0.28598E-01

GRAPHITE SURFACE DIMENSIONS

Z	RC0	RC1	RC2
0	0.15086E 01	0.32677E 01	0.37957E 01
50	0.15096E 01	0.32692E 01	0.37971E 01
100	0.15110E 01	0.32710E 01	0.37990E 01
150	0.15121E 01	0.32726E 01	0.38009E 01
200	0.15129E 01	0.32746E 01	0.38029E 01
250	0.15128E 01	0.32751E 01	0.38046E 01
300	0.15133E 01	0.32764E 01	0.38063E 01
350	0.15138E 01	0.32776E 01	0.38080E 01
400	0.15141E 01	0.32786E 01	0.38096E 01
450	0.15140E 01	0.32789E 01	0.38108E 01
500	0.15136E 01	0.32788E 01	0.38116E 01

PRESSURE DROPS

Z	PD(BORE)	PD(ANNULUS)
0	0.0	0.0
50	0.15443E 05	0.14977E 05
100	0.23276E 05	0.31687E 05
150	0.53526E 05	0.50802E 05
200	0.75713E 05	0.71761E 05
250	0.98438E 05	0.94212E 05
300	0.12256E 06	0.11830E 06
350	0.14789E 06	0.14400E 06
400	0.17427E 06	0.17116E 06
450	0.20120E 06	0.19943E 06
500	0.22803E 06	0.22834E 06

CORROSION DATA

	PLANAR REMOVAL			ROUGHNESS HEIGHTS		
Z	RC0	RC1	RC2	RC0	RC1	RC2
0	0.0	0.0	0.0	0.0	0.0	0.0
50	0.0	0.0	0.0	0.0	0.0	0.0
100	0.0	0.0	0.0	0.0	0.0	0.0
150	0.0	0.0	0.0	0.0	0.0	0.0
200	0.0	0.0	0.0	0.0	0.0	0.0
250	0.0	0.0	0.0	0.0	0.0	0.0
300	0.0	0.0	0.0	0.0	0.0	0.0
350	0.0	0.0	0.0	0.0	0.0	0.0
400	0.0	0.0	0.0	0.0	0.0	0.0
450	0.0	0.0	0.0	0.0	0.0	0.0
500	0.0	0.0	0.0	0.0	0.0	0.0

HEAT TRANSFER COEFF. AND FRICTION FACTOR (TRANSFORMED)

Z	RC0	RC1	RC2	RC0	RC1	RC2
0	0.22434E 00	0.12814E 00	0.45162E 00	0.39772E-02	0.69849E-02	0.69009E-02
50	0.22288E 00	0.13082E 00	0.34711E 00	0.40276E-02	0.71025E-02	0.70208E-02
100	0.22226E 00	0.13373E 00	0.29747E 00	0.40921E-02	0.72321E-02	0.71527E-02
150	0.22426E 00	0.13671E 00	0.27616E 00	0.41540E-02	0.73559E-02	0.72824E-02
200	0.22728E 00	0.13957E 00	0.26022E 00	0.42117E-02	0.74730E-02	0.74057E-02
250	0.23205E 00	0.14243E 00	0.25229E 00	0.42458E-02	0.75526E-02	0.75021E-02
300	0.23502E 00	0.14462E 00	0.24517E 00	0.42884E-02	0.76368E-02	0.75918E-02
350	0.23784E 00	0.14677E 00	0.23888E 00	0.43282E-02	0.77142E-02	0.76751E-02
400	0.24083E 00	0.14878E 00	0.23421E 00	0.43624E-02	0.77816E-02	0.77490E-02
450	0.24436E 00	0.15075E 00	0.22998E 00	0.43859E-02	0.78312E-02	0.78082E-02
500	0.24765E 00	0.15260E 00	0.22459E 00	0.43999E-02	0.78615E-02	0.78476E-02

HEATAX RESULTS

0.15266E 06	0.23895E 05	0.23895E 05	*DE*	0.30177E 01	0.98126E 00	0.98126E 00	*RM*	0.35217E 01
0.14691E 06	0.22427E 05	0.22427E 05	*DE*	0.30198E 01	0.98108E 00	0.98108E 00	*RM*	0.35231E 01
0.13949E 06	0.20909E 05	0.20909E 05	*DE*	0.30224E 01	0.98089E 00	0.98089E 00	*RM*	0.35249E 01
0.13174E 06	0.19503E 05	0.19503E 05	*DE*	0.30244E 01	0.98112E 00	0.98112E 00	*RM*	0.35268E 01
0.12442E 06	0.18249E 05	0.18249E 05	*DE*	0.30260E 01	0.98170E 00	0.98170E 00	*RM*	0.35286E 01
0.11885E 06	0.17320E 05	0.17320E 05	*DE*	0.30257E 01	0.98355E 00	0.98355E 00	*RM*	0.35296E 01
0.11375E 06	0.16513E 05	0.16513E 05	*DE*	0.30268E 01	0.98427E 00	0.98427E 00	*RM*	0.35311E 01
0.10919E 06	0.15802E 05	0.15802E 05	*DE*	0.30277E 01	0.98512E 00	0.98512E 00	*RM*	0.35325E 01
0.10522E 06	0.15194E 05	0.15194E 05	*DE*	0.30282E 01	0.98614E 00	0.98614E 00	*RM*	0.35338E 01
0.10200E 06	0.14711E 05	0.14711E 05	*DE*	0.30280E 01	0.98765E 00	0.98765E 00	*RM*	0.35346E 01
0.99702E 05	0.14387E 05	0.14387E 05	*DE*	0.30273E 01	0.98904E 00	0.98904E 00	*RM*	0.35350E 01

DWELL TIME = 0 DAYS

CHANNEL POWER
0.55100E 06

MIXED GAS OUTLET TEMPERATURE 851.

INNER FLOW RATE	OUTER FLOW RATE
0.11108E 03	0.81697E 02

TEMPERATURES

TG1	TW1	TI1	TF1	TFM	TF2	TI2	TW2	TG2	TW3
300	486	549	613	651	622	493	452	300	308
332	588	673	709	766	736	568	524	355	369
379	708	817	843	919	886	665	614	423	442
436	[illegible]	921	950	1035	1001	751	696	497	522
497	878	1006	1037	1130	1093	831	774	576	604
551	872	982	1009	1089	1060	850	803	643	668
606	922	1031	1058	1139	1109	919	862	709	736
[illegible]	967	1075	1101	1181	1153	963	918	774	802
712	997	1099	1123	1199	1174	1006	964	835	863
758	992	1077	1097	1151	1143	1018	986	889	911
794	971	1036	1052	1104	1092	1013	992	927	943

INNER GAP	HEAT SPLIT RADIUS	OUTER GAP
0.72358E-02	0.23980E 01	0.18754E-01
0.32230E-02	0.24311E 01	0.23879E-01
-0.65433E-03	0.24486E 01	0.31263E-01
-0.50[illegible]86E-03	0.24546E 01	0.37347E-01
-0.51687E-03	0.24587E 01	0.42651E-01
-0.42812E-03	0.24648E 01	0.4[illegible]059E-01
-0.54604E-03	0.24659E 01	0.40931E-01
-0.61876E-03	0.24692E 01	0.42752E-01
-0.52897E-03	0.24733E 01	0.42496E-01
-0.64962E-03	0.24866E 01	0.39977E-01
-0.10056E-02	0.25084E 01	0.35244E-01

GRAPHITE SURFACE DIMENSIONS

Z	RCO	RC1	RC2
0	0.15089E 01	0.32675E 01	0.37957E 01
50	0.15099E 01	0.32690E 01	0.37970E 01
100	0.15112E 01	0.32708E 01	0.37989E 01
150	0.15122E 01	0.32726E 01	0.38007E 01
200	0.15132E 01	0.32743E 01	0.38027E 01
250	0.15129E 01	0.32748E 01	0.38042E 01
300	0.15134E 01	0.32761E 01	0.38060E 01
350	0.15138E 01	0.32773E 01	0.38076E 01
400	0.15141E 01	0.32783E 01	0.38092E 01
450	0.15140E 01	0.32787E 01	0.38105E 01
500	0.15137E 01	0.32787E 01	0.38113E 01

PRESSURE DROPS

Z	PD(BORE)	PD(ANNULUS)
0	0.0	0.0
50	0.13996E 05	0.13322E 05
100	0.3[illegible]111E 05	0.26321E 05
150	0.48128E 05	0.45080E 05
200	0.67783E 05	0.63652E 05
250	0.87927E 05	0.83537E 05
300	0.10924E 06	0.10489E 06
350	0.13163E 06	0.12769E 06
400	0.15492E 06	0.15181E 06
450	0.17872E 06	0.17697E 06
500	0.20241E 06	0.20274E 06

CORROSION DATA

	PLANAR REMOVAL			ROUGHNESS HEIGHTS		
Z	RCO	RC1	RC2	RCO	RC1	RC2
0	0.0	0.0	0.0	0.0	0.0	0.0
50	0.0	0.0	0.0	0.0	0.0	0.0
100	0.0	0.0	0.0	0.0	0.0	0.0
150	0.0	0.0	0.0	0.0	0.0	0.0
200	0.0	0.0	0.0	0.0	0.0	0.0
250	0.0	0.0	0.0	0.0	0.0	0.0
300	0.0	0.0	0.0	0.0	0.0	0.0
350	0.0	0.0	0.0	0.0	0.0	0.0
400	0.0	0.0	0.0	0.0	0.0	0.0
450	0.0	0.0	0.0	0.0	0.0	0.0
500	0.0	0.0	0.0	0.0	0.0	0.0

	HEAT TRANSFER COEFF.		AND	FRICTION FACTOR (TRANSFORMED)		
Z	RCO	RC1	RC2	RCO	RC1	RC2
0	0.21114E 00	0.12297E 00	0.37090E 00	0.40532E-02	0.70805E-02	0.70028E-02
50	0.21[illegible]38E 00	0.12524E 00	0.30975E 00	0.41[illegible]E-02	0.71944E-02	0.71169E-02
100	0.21[illegible]66E 00	0.12767E 00	0.27883E 00	0.41720E-02	0.73231E-02	0.72450E-02
150	0.21283E 00	0.13035E 00	0.26040E 00	0.42334E-02	0.74468E-02	0.73734E-02
200	0.21567E 00	0.13310E 00	0.24695E 00	0.42916E-02	0.75640E-02	0.74976E-02
250	0.22027E 00	0.13569E 00	0.24077E 00	0.43252E-02	0.76448E-02	0.75940E-02
300	0.22296E 00	0.13779E 00	0.23381E 00	0.43682E-02	0.77305E-02	0.76851E-02
350	0.22557E 00	0.13981E 00	0.22798E 00	0.44082E-02	0.78097E-02	0.77699E-02
400	0.22834E 00	0.14169E 00	0.22373E 00	0.44425E-02	0.78792E-02	0.78457E-02
450	0.23166E 00	0.14350E 00	0.22046E 00	0.44659E-02	0.79314E-02	0.79071E-02
500	0.23468E 00	0.14565E 00	0.21689E 00	0.44802E-02	0.79647E-02	0.79490E-02

H E A T A X   R E S U L T S

0.14228E 06	0.22305E 05	0.22305E 05	*DE*	0.30181E 01	0.98128E 00	0.98128E 00	*RM*	0.35218E 01
0.13651E 06	0.20916E 05	0.20916E 05	*DE*	0.30201E 01	0.98126E 00	0.98126E 00	*RM*	0.35232E 01
0.12943E 06	0.19514E 05	0.19514E 05	*DE*	0.30225E 01	0.98096E 00	0.98096E 00	*RM*	0.35249E 01
0.12231E 06	0.18210E 05	0.18210E 05	*DE*	0.30243E 01	0.98130E 00	0.98130E 00	*RM*	0.35267E 01
0.11561E 06	0.17058E 05	0.17058E 05	*DE*	0.30259E 01	0.98188E 00	0.98188E 00	*RM*	0.35285E 01
0.11056E 06	0.16209E 05	0.16209E 05	*DE*	0.30256E 01	0.98372E 00	0.98372E 00	*RM*	0.35295E 01
0.10590E 06	0.15466E 05	0.15466E 05	*DE*	0.30266E 01	0.98440E 00	0.98440E 00	*RM*	0.35309E 01
0.10174E 06	0.14807E 05	0.14807E 05	*DE*	0.30275E 01	0.98520E 00	0.98520E 00	*RM*	0.35324E 01
0.98069E 05	0.14233E 05	0.14233E 05	*DE*	0.30281E 01	0.98613E 00	0.98613E 00	*RM*	0.35337E 01
0.95056E 05	0.13768E 05	0.13768E 05	*DE*	0.30280E 01	0.98749E 00	0.98749E 00	*RM*	0.35346E 01
0.92848E 05	0.13444E 05	0.13444E 05	*DE*	0.30275E 01	0.98868E 00	0.98868E 00	*RM*	0.35350E 01

DWELL TIME = 0 DAYS

CHANNEL POWER
0.51400E 06

MIXED GAS OUTLET TEMPERATURE 851.

INNER FLOW RATE	OUTER FLOW RATE
0.10354E 03	0.76264E 02

TEMPERATURES

TG1	TW1	TI1	TF1	TFM	TF2	TI2	TW2	TG2	TW3
300	501	575	624	676	642	500	453	300	309
335	600	695	714	788	752	570	522	356	370
364	709	824	849	941	901	666	611	423	443
446	796	920	947	1051	1009	747	699	497	521
501	872	1002	1031	1142	1099	825	765	574	602
554	863	974	999	1094	1059	842	793	640	664
607	913	1023	1048	1143	1108	900	853	704	731
661	957	1066	1090	1184	1150	955	908	768	796
712	991	1094	1117	1206	1175	1001	958	830	857
758	994	1082	1101	1180	1155	1021	986	884	908
795	975	1044	1059	1122	1107	1019	994	925	944

INNER GAP	HEAT SPLIT RADIUS	OUTER GAP
0.54402E-02	0.24103E 01	0.22140E-01
-0.14267E-03	0.24394E 01	0.28609E-01
0.44215E-06	0.24486E 01	0.35374E-01
0.15819E-03	0.24561E 01	0.44216E-01
-0.25599E-04	0.24597E 01	0.50793E-01
0.85659E-04	0.24651E 01	0.47295E-01
-0.22860E-03	0.24650E 01	0.48060E-01
0.10760E-03	0.24668E 01	0.49294E-01
0.16319E-03	0.24694E 01	0.48378E-01
-0.25608E-03	0.24793E 01	0.45434E-01
-0.45265E-03	0.24967E 01	0.39583E-01

GRAPHITE SURFACE DIMENSIONS

Z	RC0	RC1	RC2
0	0.15091E 01	0.32676E 01	0.37958E 01
50	0.15101E 01	0.32689E 01	0.37971E 01
100	0.15112E 01	0.32708E 01	0.37989E 01
150	0.15122E 01	0.32725E 01	0.38007E 01
200	0.15132E 01	0.32741E 01	0.38026E 01
250	0.15128E 01	0.32746E 01	0.38041E 01
300	0.15133E 01	0.32759E 01	0.38058E 01
350	0.15137E 01	0.32771E 01	0.38075E 01
400	0.15141E 01	0.32782E 01	0.38091E 01
450	0.15140E 01	0.32787E 01	0.38104E 01
500	0.15137E 01	0.32789E 01	0.38112E 01

PRESSURE DROPS

Z	PD(BORE)	PD(ANNULUS)
0	0.0	0.0
50	0.12512E 05	0.11768E 05
100	0.26825E 05	0.24990E 05
150	0.42670E 05	0.39752E 05
200	0.59921E 05	0.56078E 05
250	0.77560E 05	0.73529E 05
300	0.96216E 05	0.92257E 05
350	0.11579E 06	0.11225E 06
400	0.13621E 06	0.13342E 06
450	0.15711E 06	0.15557E 06
500	0.17801E 06	0.17835E 06

CORROSION DATA

	PLANAR REMOVAL			ROUGHNESS HEIGHTS		
Z	RC0	RC1	RC2	RC0	RC1	RC2
0	0.0	0.0	0.0	0.0	0.0	0.0
50	0.0	0.0	0.0	0.0	0.0	0.0
100	0.0	0.0	0.0	0.0	0.0	0.0
150	0.0	0.0	0.0	0.0	0.0	0.0
200	0.0	0.0	0.0	0.0	0.0	0.0
250	0.0	0.0	0.0	0.0	0.0	0.0
300	0.0	0.0	0.0	0.0	0.0	0.0
350	0.0	0.0	0.0	0.0	0.0	0.0
400	0.0	0.0	0.0	0.0	0.0	0.0
450	0.0	0.0	0.0	0.0	0.0	0.0
500	0.0	0.0	0.0	0.0	0.0	0.0

HEAT TRANSFER COEFF. AND FRICTION FACTOR (TRANSFORMED)

Z	RC0	RC1	RC2	RC0	RC1	RC2
0	0.19898E 00	0.11649E 00	0.33404E 00	0.41294E-02	0.72038E-02	0.71249E-02
50	0.19871E 00	0.11672E 00	0.28535E 00	0.41850E-02	0.73197E-02	0.72424E-02
100	0.19951E 00	0.12097E 00	0.26034E 00	0.42495E-02	0.74492E-02	0.73712E-02
150	0.20164E 00	0.12356E 00	0.24324E 00	0.43108E-02	0.75731E-02	0.75009E-02
200	0.20433E 00	0.12612E 00	0.23125E 00	0.43689E-02	0.76904E-02	0.76251E-02
250	0.20868E 00	0.12853E 00	0.22594E 00	0.44018E-02	0.77705E-02	0.77208E-02
300	0.21114E 00	0.13045E 00	0.21977E 00	0.44649E-02	0.78567E-02	0.78119E-02
350	0.21356E 00	0.13233E 00	0.21461E 00	0.44848E-02	0.79368E-02	0.78972E-02
400	0.21606E 00	0.13408E 00	0.21078E 00	0.45201E-02	0.80089E-02	0.79750E-02
450	0.21897E 00	0.13575E 00	0.20803E 00	0.45456E-02	0.80653E-02	0.80396E-02
500	0.22177E 00	0.13786E 00	0.20017E 00	0.45611E-02	0.81022E-02	0.80857E-02

HEATAX RESULTS

0.13188E 06	0.20728E 05	0.20728E 05	*DE*	0.30185E 01	0.98140E 00	0.98140E 00	*RM*	0.35218E 01
0.12602E 06	0.19435E 05	0.19435E 05	*DE*	0.30203E 01	0.98128E 00	0.98128E 00	*RM*	0.35232E 01
0.11943E 06	0.18123E 05	0.18123E 05	*DE*	0.30225E 01	0.98120E 00	0.98120E 00	*RM*	0.35249E 01
0.11289E 06	0.16926E 05	0.16926E 05	*DE*	0.30242E 01	0.98162E 00	0.98162E 00	*RM*	0.35266E 01
0.10680E 06	0.15873E 05	0.15873E 05	*DE*	0.30258E 01	0.98221E 00	0.98221E 00	*RM*	0.35283E 01
0.10224E 06	0.15104E 05	0.15104E 05	*DE*	0.30253E 01	0.98400E 00	0.98400E 00	*RM*	0.35293E 01
0.98019E 05	0.14425E 05	0.14425E 05	*DE*	0.30263E 01	0.98461E 00	0.98461E 00	*RM*	0.35307E 01
0.94264E 05	0.13819E 05	0.13819E 05	*DE*	0.30273E 01	0.98536E 00	0.98536E 00	*RM*	0.35321E 01
0.9083[illegible]E 05	0.13287E 05	0.13287E 05	*DE*	0.30280E 01	0.98620E 00	0.98620E 00	*RM*	0.35335E 01
0.88062E 05	0.12842E 05	0.12842E 05	*DE*	0.30281E 01	0.98712E 00	0.98712E 00	*RM*	0.35345E 01
0.85944E 05	0.12516E 05	0.12516E 05	*DE*	0.30276E 01	0.98852E 00	0.98852E 00	*RM*	0.35350E 01

DWELL TIME = 0 DAYS

CHANNEL POWER
0.47700E 06

MIXED GAS OUTLET TEMPERATURE 851.

INNER FLOW RATE 0.95984E 02
OUTER FLOW RATE 0.70871E 02

TEMPERATURES

TG1	TW1	TI1	TF1	TFM	TF2	TI2	TW2	TG2	TW3
300	522	600	622	685	651	497	450	300	310
339	608	700	719	798	760	570	523	356	371
388	711	820	843	941	899	658	607	424	444
445	793	912	937	1046	1003	736	682	497	521
505	867	993	1019	1134	1090	812	756	573	601
557	855	961	983	1081	1046	828	782	636	660
610	904	1010	1032	1129	1094	887	842	699	725
662	949	1053	1075	1171	1136	942	897	762	789
713	985	1085	1106	1198	1165	990	948	822	850
759	997	1085	1103	1187	1159	1019	982	878	904
797	982	1051	1065	1133	1115	1021	995	922	942

INNER GAP	HEAT SPLIT RADIUS	OUTER GAP
0.23784E-02	0.24293E 01	0.26178E-01
0.19718E-03	0.24404E 01	0.31685E-01
0.65162E-03	0.24511E 01	0.41583E-01
0.12666E-04	0.24574E 01	0.50382E-01
-0.55262E-03	0.24612E 01	0.58334E-01
-0.13627E-04	0.24661E 01	0.53531E-01
-0.12076E-03	0.24649E 01	0.53303E-01
0.12282E-04	0.24661E 01	0.54433E-01
-0.16104E-03	0.24675E 01	0.53231E-01
0.10136E-03	0.24725E 01	0.49301E-01
0.82301E-04	0.24888E 01	0.43172E-01

GRAPHITE SURFACE DIMENSIONS

GRAPHITE SURFACE DIMENSIONS

Z	RC0	RC1	RC2
0	0.15093E 01	0.32675E 01	0.37958E 01
50	0.15101E 01	0.32690E 01	0.37972E 01
100	0.15112E 01	0.32707E 01	0.37988E 01
150	0.15121E 01	0.32723E 01	0.38006E 01
200	0.15129E 01	0.32739E 01	0.38026E 01
250	0.15127E 01	0.32743E 01	0.38040E 01
300	0.15132E 01	0.32756E 01	0.38057E 01
350	0.15136E 01	0.32769E 01	0.38073E 01
400	0.15140E 01	0.32780E 01	0.38089E 01
450	0.15141E 01	0.32787E 01	0.38102E 01
500	0.15138E 01	0.32789E 01	0.38112E 01

PRESSURE DROPS

Z	PD(BORE)	PD(ANNULUS)
0	0.0	0.0
50	0.11145E 05	0.10295E 05
100	0.23680E 05	0.21868E 05
150	0.37508E 05	0.34756E 05
200	0.52519E 05	0.48985E 05
250	0.67808E 05	0.64164E 05
300	0.83986E 05	0.80439E 05
350	0.10095E 06	0.97602E 05
400	0.11864E 06	0.11620E 06
450	0.13686E 06	0.13551E 06
500	0.15515E 06	0.15544E 06

CORROSION DATA

	PLANAR REMOVAL			ROUGHNESS HEIGHTS		
Z	RC0	RC1	RC2	RC0	RC1	RC2
0	0.0	0.0	0.0	0.0	0.0	0.0
50	0.0	0.0	0.0	0.0	0.0	0.0
100	0.0	0.0	0.0	0.0	0.0	0.0
150	0.0	0.0	0.0	0.0	0.0	0.0
200	0.0	0.0	0.0	0.0	0.0	0.0
250	0.0	0.0	0.0	0.0	0.0	0.0
300	0.0	0.0	0.0	0.0	0.0	0.0
350	0.0	0.0	0.0	0.0	0.0	0.0
400	0.0	0.0	0.0	0.0	0.0	0.0
450	0.0	0.0	0.0	0.0	0.0	0.0
500	0.0	0.0	0.0	0.0	0.0	0.0

HEAT TRANSFER COEFF. AND FRICTION FACTOR (TRANSFORMED)

Z	RC0	RC1	RC2	RC0	RC1	RC2
0	0.18649E 00	0.11011E 00	0.29105E 00	0.42141E-02	0.73359E-02	0.72575E-02
50	0.18710E 00	0.11201E 00	0.26378E 00	0.42702E-02	0.74557E-02	0.73770E-02
100	0.18811E 00	0.11426E 00	0.24098E 00	0.43348E-02	0.75862E-02	0.75093E-02
150	0.19027E 00	0.11669E 00	0.22628E 00	0.43959E-02	0.77102E-02	0.76393E-02
200	0.19278E 00	0.11909E 00	0.21548E 00	0.44542E-02	0.78276E-02	0.77636E-02
250	0.19686E 00	0.12132E 00	0.21098E 00	0.44863E-02	0.79065E-02	0.78581E-02
300	0.19912E 00	0.12308E 00	0.20560E 00	0.45294E-02	0.79930E-02	0.79490E-02
350	0.20131E 00	0.12481E 00	0.20100E 00	0.45696E-02	0.80738E-02	0.80347E-02
400	0.20354E 00	0.12643E 00	0.19758E 00	0.46056E-02	0.81473E-02	0.81133E-02
450	0.20602E 00	0.12848E 00	0.19078E 00	0.46336E-02	0.82081E-02	0.81817E-02
500	0.20869E 00	0.13006E 00	0.18764E 00	0.46507E-02	0.82497E-02	0.82319E-02

H E A T A X   R E S U L T S

0.12159E 06	0.19132E 05	0.19132E 05	*DE*	0.30188E 01	0.98134E 00	0.98134E 00	*RM*	0.35218E 01
0.11586E 06	0.17904E 05	0.17904E 05	*DE*	0.30204E 01	0.98119E 00	0.98119E 00	*RM*	0.35232E 01
0.10975E 06	0.16692E 05	0.16692E 05	*DE*	0.30224E 01	0.98142E 00	0.98142E 00	*RM*	0.35249E 01
0.10377E 06	0.15604E 05	0.15604E 05	*DE*	0.30241E 01	0.98197E 00	0.98197E 00	*RM*	0.35265E 01
0.98226E 05	0.14655E 05	0.14655E 05	*DE*	0.30256E 01	0.98257E 00	0.98257E 00	*RM*	0.35282E 01
0.94131E 05	0.13966E 05	0.13966E 05	*DE*	0.30251E 01	0.98433E 00	0.98433E 00	*RM*	0.35291E 01
0.90314E 05	0.13355E 05	0.13355E 05	*DE*	0.30261E 01	0.98489E 00	0.98489E 00	*RM*	0.35305E 01
0.86388E 05	0.12804E 05	0.12804E 05	*DE*	0.30270E 01	0.98557E 00	0.98557E 00	*RM*	0.35319E 01
0.83826E 05	0.12314E 05	0.12314E 05	*DE*	0.30278E 01	0.98633E 00	0.98633E 00	*RM*	0.35333E 01
0.81167E 05	0.11892E 05	0.11892E 05	*DE*	0.30282E 01	0.98704E 00	0.98704E 00	*RM*	0.35344E 01
0.79135E 05	0.11572E 05	0.11572E 05	*DE*	0.30278E 01	0.98841E 00	0.98841E 00	*RM*	0.35350E 01

DWELL TIME = 0 DAYS

CHANNEL POWER
0.44000E 06

MIXED GAS OUTLET TEMPERATURE 851.

INNER FLOW RATE	OUTER FLOW RATE
0.68501E 02	0.65414E 02

TEMPERATURES

TG1	TW1	TI1	TF1	TFM	TF2	TI2	TW2	TG2	TW3
300	535	618	633	700	666	500	453	300	311
341	615	706	724	805	767	572	524	358	374
391	711	816	837	934	894	654	604	426	446
448	789	902	925	1031	990	726	676	498	522
508	860	979	1003	1114	1073	800	748	572	600
559	847	946	966	1050	1027	814	772	634	657
611	895	994	1014	1107	1074	873	831	695	720
662	940	1037	1057	1149	1116	928	886	756	783
712	979	1073	1092	1181	1149	979	939	816	843
760	1001	1087	1104	1187	1159	1016	979	873	900
799	989	1057	1071	1139	1119	1022	996	919	940

INNER GAP	HEAT SPLIT RADIUS	OUTER GAP
0.32756E-03	0.24344E 01	0.29980E-01
0.51400E-03	0.24427E 01	0.35294E-01
0.65866E-03	0.24534E 01	0.45556E-01
-0.33675E-03	0.24603E 01	0.55998E-01
-0.17726E-02	0.24631E 01	0.63937E-01
-0.91712E-03	0.24688E 01	0.59201E-01
-0.10156E-02	0.24665E 01	0.58262E-01
-0.98333E-03	0.24663E 01	0.58194E-01
-0.68680E-03	0.24668E 01	0.56804E-01
-0.13947E-03	0.24690E 01	0.52945E-01
0.20901E-03	0.24838E 01	0.46561E-01

GRAPHITE SURFACE DIMENSIONS

Z	RC0	RC1	RC2
0	0.15094E 01	0.32676E 01	0.37958E 01
50	0.151[illegible]2[illegible]E 01	0.32690E 01	0.37971E 01
100	0.15112[illegible]E 01	0.327[illegible]6E 01	0.37989E 01
150	0.15122[illegible]E 01	0.32721E 01	0.38[illegible]7E 01
200	0.15128[illegible]E 01	0.32737E 01	0.38026E 01
250	0.15125E 01	0.32741E 01	0.38040E 01
300	0.1513[illegible]E 01	0.32754E 01	0.38056E 01
350	0.15135E 01	0.32766E 01	0.38072E 01
400	0.15139E 01	0.32777E 01	0.38087E 01
450	0.15141E 01	0.32787E 01	0.38101E 01
500	0.15139E 01	0.32789E 01	0.38111E 01

PRESSURE DROPS

Z	PD(BORE)	PD(ANNULUS)
0	0.0	0.0
50	0.97255E 04	0.89370E 04
100	0.2[illegible]582[illegible]E 05	0.16963E 05
150	0.325[illegible]7[illegible]E 05	0.30102E 05
200	0.45410E 05	0.42368E 05
250	0.58531E 05	0.55427E 05
300	0.72412E 05	0.694[illegible]8E 05
350	0.8[illegible]966E 05	0.84313E 05
400	0.10216E 06	0.10012E 06
450	0.11787E 06	0.11675E 06
500	0.13372E 06	0.13397E 06

CORROSION DATA

	PLANAR REMOVAL			ROUGHNESS HEIGHTS		
Z	RC0	RC1	RC2	RC0	RC1	RC2
0	0.0	0.0	0.0	0.0	0.0	0.0
50	0.0	0.0	0.0	0.0	0.0	0.0
100	0.0	0.0	0.0	0.0	0.0	0.0
150	0.0	0.0	0.0	0.0	0.0	0.0
200	0.0	0.0	0.0	0.0	0.0	0.0
250	0.0	0.0	0.0	0.0	0.0	0.0
300	0.0	0.0	0.0	0.0	0.0	0.0
350	0.0	0.0	0.0	0.0	0.0	0.0
400	0.0	0.0	0.0	0.0	0.0	0.0
450	0.0	0.0	0.0	0.0	0.0	0.0
500	0.0	0.0	0.0	0.0	0.0	0.0

HEAT TRANSFER COEFF. AND FRICTION FACTOR (TRANSFORMED)

Z	RC0	RC1	RC2	RC0	RC1	RC2
0	0.17434E 00	0.10333E 00	0.26323E 00	0.43040E-02	0.74658E-02	0.74050E-02
50	0.17528E 00	0.10529E 00	0.23810E 00	0.43614E-02	0.76097E-02	0.75304E-02
100	0.17654E 00	0.10741E 00	0.22156E 00	0.44264E-02	0.77414E-02	0.76651E-02
150	0.17666E 00	0.10971E 00	0.20855E 00	0.44876E-02	0.78652E-02	0.77961E-02
200	0.18104E 00	0.11191E 00	0.19930E 00	0.45462E-02	0.79823E-02	0.79200E-02
250	0.18[illegible]8[illegible]E 00	0.11396E 00	0.19535E 00	0.45777E-02	0.80600E-02	0.80133E-02
300	0.18690E 00	0.11556E 00	0.19079E 00	0.46211E-02	0.81463E-02	0.81035E-02
350	0.18891E 00	0.11713E 00	0.18690E 00	0.46616E-02	0.82276E-02	0.81892E-02
400	0.19090E 00	0.11862E 00	0.18389E 00	0.46987E-02	0.83030E-02	0.82690E-02
450	0.19300E 00	0.12059E 00	0.17720E 00	0.47297E-02	0.83683E-02	0.83409E-02
500	0.19550E 00	0.12214E 00	0.17432E 00	0.47485E-02	0.84142E-02	0.83955E-02

HEATAX RESULTS

0.12015E 06	0.18916E 05	0.18916E 05	*DE*	0.30186E 01	0.98152E 00	0.98152E 00	*RM*	0.35218E 01
0.11467E 06	0.17737E 05	0.17737E 05	*DE*	0.30202E 01	0.98138E 00	0.98138E 00	*RM*	0.35231E 01
0.10876E 06	0.16568E 05	0.16568E 05	*DE*	0.30221E 01	0.98160E 00	0.98160E 00	*RM*	0.35247E 01
0.10295E 06	0.15516E 05	0.15516E 05	*DE*	0.30237E 01	0.98214E 00	0.98214E 00	*RM*	0.35263E 01
0.97566E 05	0.14595E 05	0.14595E 05	*DE*	0.30252E 01	0.98271E 00	0.98271E 00	*RM*	0.35279E 01
0.93574E 05	0.13924E 05	0.13924E 05	*DE*	0.30247E 01	0.98441E 00	0.98441E 00	*RM*	0.35288E 01
0.89849E 05	0.13327E 05	0.13327E 05	*DE*	0.30257E 01	0.98493E 00	0.98493E 00	*RM*	0.35301E 01
0.86500E 05	0.12788E 05	0.12788E 05	*DE*	0.30266E 01	0.98559E 00	0.98559E 00	*RM*	0.35315E 01
0.83500E 05	0.12307E 05	0.12307E 05	*DE*	0.30273E 01	0.98632E 00	0.98632E 00	*RM*	0.35328E 01
0.80896E 05	0.11893E 05	0.11893E 05	*DE*	0.30277E 01	0.98702E 00	0.98702E 00	*RM*	0.35339E 01
0.78913E 05	0.11577E 05	0.11577E 05	*DE*	0.30273E 01	0.98834E 00	0.98834E 00	*RM*	0.35345E 01

DWELL TIME = 0 DAYS

CHANNEL POWER
0.42180E 06

MIXED GAS OUTLET TEMPERATURE 834.

INNER FLOW RATE OUTER FLOW RATE
0.87450E 02 0.64675E 02

TEMPERATURES

TG1	TW1	TI1	TF1	TFM	TF2	TI2	TW2	TG2	TW3
300	527	607	622	686	653	494	448	300	311
340	605	693	710	788	752	563	517	356	371
389	699	799	820	913	875	643	594	422	442
444	775	883	905	1007	969	712	664	492	515
502	844	958	981	1083	1049	783	734	563	590
552	831	926	946	1036	1005	797	757	623	645
602	878	973	992	1082	1050	854	814	682	706
652	922	1015	1034	1123	1091	907	868	741	767
701	959	1050	1068	1154	1124	957	918	799	825
747	981	1064	1080	1160	1133	993	958	854	880
786	969	1035	1048	1113	1094	999	974	899	919

INNER GAP	HEAT SPLIT RADIUS	OUTER GAP
0.40722E-03	0.24350E 01	0.29928E-01
0.61848E-03	0.24431E 01	0.35216E-01
0.78861E-03	0.24544E 01	0.45449E-01
-0.18562E-03	0.24615E 01	0.55860E-01
-0.16022E-02	0.24644E 01	0.53762E-01
-0.75149E-03	0.24698E 01	0.59010E-01
-0.83970E-03	0.24674E 01	0.58041E-01
-0.69025E-03	0.24672E 01	0.57945E-01
-0.48388E-03	0.24675E 01	0.55528E-01
0.74860E-04	0.24696E 01	0.52643E-01
0.42035E-03	0.24838E 01	0.46246E-01

GRAPHITE SURFACE DIMENSIONS

Z	RCC	RC1	RC2
1	0.15093E 01	0.32675E 01	0.37958E 01
50	0.15101E 01	0.32688E 01	0.37971E 01
100	0.15111E 01	0.32704E 01	0.37988E 01
150	0.15119E 01	0.32718E 01	0.38005E 01
200	0.15126E 01	0.32733E 01	0.38023E 01
250	0.15126E 01	0.32737E 01	0.38037E 01
300	0.15128E 01	0.32750E 01	0.38052E 01
350	0.15133E 01	0.32761E 01	0.38067E 01
400	0.15137E 01	0.32773E 01	0.38083E 01
450	0.15139E 01	0.32782E 01	0.38096E 01
500	0.15137E 01	0.32784E 01	0.38106E 01

PRESSURE DROPS

Z	PD(BORE)	PD(ANNULUS)
0	0.0	0.0
50	0.94359E 04	0.87078E 04
100	0.19945E 05	0.18448E 05
150	0.31475E 05	0.29241E 05
200	0.43938E 05	0.41099E 05
250	0.56618E 05	0.53708E 05
300	0.69999E 05	0.67190E 05
350	0.84032E 05	0.81548E 05
400	0.98671E 05	0.96755E 05
450	0.11380E 06	0.11275E 06
500	0.12906E 06	0.12930E 06

CORROSION DATA

	PLANAR REMOVAL			ROUGHNESS HEIGHTS		
Z	RC0	RC1	RC2	RC0	RC1	RC2
0	0.0	0.0	0.0	0.0	0.0	0.0
50	0.0	0.0	0.0	0.0	0.0	0.0
100	0.0	0.0	0.0	0.0	0.0	0.0
150	0.0	0.0	0.0	0.0	0.0	0.0
200	0.0	0.0	0.0	0.0	0.0	0.0
250	0.0	0.0	0.0	0.0	0.0	0.0
300	0.0	0.0	0.0	0.0	0.0	0.0
350	0.0	0.0	0.0	0.0	0.0	0.0
400	0.0	0.0	0.0	0.0	0.0	0.0
450	0.0	0.0	0.0	0.0	0.0	0.0
500	0.0	0.0	0.0	0.0	0.0	0.0

HEAT TRANSFER COEFF. AND FRICTION FACTOR (TRANSFORMED)

Z	RC0	RC1	RC2	RC0	RC1	RC2
0	0.17294E 00	0.10249E 00	0.26086E 00	0.43147E-02	0.75043E-02	0.74258E-02
50	0.17384E 00	0.10436E 00	0.23651E 00	0.43709E-02	0.76259E-02	0.75677E-02
100	0.17501E 00	0.10640E 00	0.22004E 00	0.44346E-02	0.77535E-02	0.76793E-02
150	0.17705E 00	0.10861E 00	0.20728E 00	0.44947E-02	0.78745E-02	0.78068E-02
200	0.17934E 00	0.11073E 00	0.19821E 00	0.45523E-02	0.79891E-02	0.79277E-02
250	0.18303E 00	0.11271E 00	0.19433E 00	0.45833E-02	0.81651E-02	0.80195E-02
300	0.18504E 00	0.11424E 00	0.18986E 00	0.46260E-02	0.81498E-02	0.81074E-02
350	0.18699E 00	0.11576E 00	0.18597E 00	0.46658E-02	0.82296E-02	0.81915E-02
400	0.18891E 00	0.11720E 00	0.18292E 00	0.47123E-02	0.83036E-02	0.82699E-02
450	0.19096E 00	0.11906E 00	0.17558E 00	0.47328E-02	0.83679E-02	0.83405E-02
500	0.19340E 00	0.12055E 00	0.17374E 00	0.47516E-02	0.84132E-02	0.83944E-02

(b) CORRODED CASE

HEATAX RESULTS

RE	0,16563E 06	0,24979E 05	0,24979E 05	*DE*	0,30172E 01	0,98130E 00	0,98130E 00	*RM*	0,35217E 01
RE	0,15981E 06	0,23364E 05	0,23364E 05	*DE*	0,30189E 01	0,98057E 00	0,98057E 00	*RM*	0,35233E 01
RE	0,15247E 06	0,21621E 05	0,21621E 05	*DE*	0,30212E 01	0,97975E 00	0,97975E 00	*RM*	0,35255E 01
RE	0,14453E 06	0,19960E 05	0,19960E 05	*DE*	0,30233E 01	0,98033E 00	0,98033E 00	*RM*	0,35277E 01
RE	0,13687E 06	0,18529E 05	0,18529E 05	*DE*	0,30251E 01	0,98113E 00	0,98113E 00	*RM*	0,35298E 01
RE	0,13086E 06	0,17495E 05	0,17495E 05	*DE*	0,30251E 01	0,98349E 00	0,98349E 00	*RM*	0,35309E 01
RE	0,12519E 06	0,16632E 05	0,16632E 05	*DE*	0,30263E 01	0,98455E 00	0,98455E 00	*RM*	0,35325E 01
RE	0,12005E 06	0,15898E 05	0,15898E 05	*DE*	0,30274E 01	0,98540E 00	0,98540E 00	*RM*	0,35340E 01
RE	0,11551E 06	0,15282E 05	0,15282E 05	*DE*	0,30281E 01	0,98659E 00	0,98659E 00	*RM*	0,35353E 01
RE	0,11181E 06	0,14811E 05	0,14811E 05	*DE*	0,30279E 01	0,98827E 00	0,98827E 00	*RM*	0,35361E 01
RE	0,10911E 06	0,14510E 05	0,14510E 05	*DE*	0,30274E 01	0,98988E 00	0,98988E 00	*RM*	0,35363E 01

DWELL TIME = 0 DAYS

CHANNEL POWER
0,60700E 06

MIXED GAS OUTLET TEMPERATURE 868,

INNER FLOW RATE 0,12049E 03
OUTER FLOW RATE 0,85402E 02

TEMPERATURES

Z	TG1	TW1	TI1	TF1	TFI	TF2	TI2	TW2	TG2	TW3
0	300	474	501	599	617	600	480	462	300	308
50	330	562	602	711	737	717	576	551	358	372
100	372	675	736	850	884	861	695	660	434	455
150	425	770	847	955	995	971	797	755	522	548
200	482	853	944	1042	1087	1063	888	841	613	645
250	534	857	939	1026	1068	1049	906	868	690	719
300	587	911	997	1075	1118	1101	966	928	764	794
350	642	960	1049	1118	1162	1147	1021	983	834	866
400	695	995	1082	1143	1186	1173	1062	1027	895	930
450	742	995	1069	1121	1159	1151	1069	1045	954	979
500	780	976	1033	1076	1110	1106	1057	1043	991	1008

Z	INNER GAP	HEAT SPLIT RADIUS	OUTER GAP
0	0,10847E-01	0,23805E 01	0,15418E-01
50	0,10002E-01	0,23961E 01	0,16541E-01
100	0,88519E-02	0,24082E 01	0,17956E-01
150	0,78136E-02	0,24196E 01	0,19210E-01
200	0,68904E-02	0,24299E 01	0,20427E-01
250	0,68357E-02	0,24483E 01	0,20922E-01
300	0,62373E-02	0,24586E 01	0,21809E-01
350	0,56722E-02	0,24681E 01	0,22880E-01
400	0,52805E-02	0,24813E 01	0,23385E-01
450	0,52962E-02	0,25089E 01	0,23741E-01
500	0,55174E-02	0,25557E 01	0,23831E-01

GRAPHITE SURFACE DIMENSIONS

Z	RC0	RC1	RC2
0	0,15086E 01	0,32675E 01	0,37957E 01
50	0,15094E 01	0,32693E 01	0,37971E 01
100	0,15106E 01	0,32717E 01	0,37990E 01
150	0,15117E 01	0,32737E 01	0,38013E 01
200	0,15126E 01	0,32756E 01	0,38037E 01
250	0,15126E 01	0,32761E 01	0,38055E 01
300	0,15131E 01	0,32775E 01	0,38074E 01
350	0,15137E 01	0,32788E 01	0,38092E 01
400	0,15140E 01	0,32797E 01	0,38109E 01
450	0,15140E 01	0,32800E 01	0,38121E 01
500	0,15137E 01	0,32799E 01	0,38129E 01

PRESSURE DROPS

Z	PD(BORE)	PD(ANNULUS)
0	0,0	0,0
50	0,16039E 05	0,14596E 05
100	0,34221E 05	0,31305E 05
150	0,54538E 05	0,50292E 05
200	0,76711E 05	0,71550E 05
250	0,99536E 05	0,94419E 05
300	0,12385E 06	0,11902E 06
350	0,14950E 06	0,14530E 06
400	0,17629E 06	0,17307E 06
450	0,20370E 06	0,20195E 06
500	0,23109E 06	0,23142E 06

CORROSION DATA

	PLANAR REMOVAL			ROUGHNESS HEIGHTS		
Z	RC0	RC1	RC2	RC0	RC1	RC2
0	0,0	0,0	0,0	0,0	0,0	0,0
50	0,0	0,0	0,0	0,0	0,0	0,0
100	0,0	0,0	0,0	0,0	0,0	0,0
150	0,0	0,0	0,0	0,0	0,0	0,0
200	0,0	0,0	0,0	0,0	0,0	0,0
250	0,0	0,0	0,0	0,0	0,0	0,0
300	0,0	0,0	0,0	0,0	0,0	0,0
350	0,0	0,0	0,0	0,0	0,0	0,0
400	0,0	0,0	0,0	0,0	0,0	0,0
450	0,0	0,0	0,0	0,0	0,0	0,0
500	0,0	0,0	0,0	0,0	0,0	0,0

	HEAT TRANSFER COEFF.		AND	FRICTION FACTOR (TRANSFORMED)		
Z	RC0	RC1	RC2	RC0	RC1	RC2
0	0,22600E 00	0,12694E 00	0,41327E 00	0,39683E-02	0,70073E-02	0,69754E-02
50	0,22549E 00	0,12903E 00	0,35019E 00	0,40159E-02	0,71311E-02	0,70443E-02
100	0,22544E 00	0,13173E 00	0,30309E 00	0,40755E-02	0,72748E-02	0,71851E-02
150	0,22716E 00	0,13499E 00	0,27789E 00	0,41339E-02	0,74143E-02	0,73316E-02
200	0,22968E 00	0,13837E 00	0,25829E 00	0,41901E-02	0,75430E-02	0,74703E-02
250	0,23410E 00	0,14156E 00	0,24857E 00	0,42242E-02	0,76291E-02	0,75759E-02
300	0,23683E 00	0,14409E 00	0,23938E 00	0,42674E-02	0,77175E-02	0,76721E-02
350	0,23954E 00	0,14670E 00	0,22958E 00	0,43080E-02	0,77971E-02	0,77591E-02
400	0,24248E 00	0,14904E 00	0,22355E 00	0,43435E-02	0,78655E-02	0,78350E-02
450	0,24600E 00	0,15145E 00	0,21767E 00	0,43684E-02	0,79144E-02	0,78942E-02
500	0,24932E 00	0,15411E 00	0,20974E 00	0,43839E-02	0,79428E-02	0,79321E-02

HEATAX RESULTS

RE	0,16371E 06	0,25314E 05	0,25314E 05	*DE*	0,30171E 01	0,98090E 00	0,98090E 00	*RM*	0,35218E 01
RE	0,15830E 06	0,23661E 05	0,23661E 05	*DE*	0,30192E 01	0,98081E 00	0,98081E 00	*RM*	0,35233E 01
RE	0,15083E 06	0,21995E 05	0,21995E 05	*DE*	0,30220E 01	0,98086E 00	0,98086E 00	*RM*	0,35251E 01
RE	0,14244E 06	0,20484E 05	0,20484E 05	*DE*	0,30244E 01	0,98121E 00	0,98121E 00	*RM*	0,35251E 01
RE	0,13441E 06	0,19161E 05	0,19161E 05	*DE*	0,30269E 01	0,98192E 00	0,98192E 00	*RM*	0,35251E 01
RE	0,12832E 06	0,18173E 05	0,18173E 05	*DE*	0,30266E 01	0,98423E 00	0,98423E 00	*RM*	0,35251E 01
RE	0,12266E 06	0,17326E 05	0,17326E 05	*DE*	0,30286E 01	0,98633E 00	0,98633E 00	*RM*	0,35251E 01
RE	0,11760E 06	0,16577E 05	0,16577E 05	*DE*	0,30313E 01	0,99075E 00	0,99075E 00	*RM*	0,35251E 01
RE	0,11318E 06	0,15481E 05	0,16317E 05	*DE*	0,30334E 01	0,97096E 00	0,10234E 01	*RM*	0,35286E 01
RE	0,10967E 06	0,14297E 05	0,16372E 05	*DE*	0,30329E 01	0,93733E 00	0,10734E 01	*RM*	0,35201E 01
RE	0,10719E 06	0,13065E 05	0,16780E 05	*DE*	0,30311E 01	0,88525E 00	0,11369E 01	*RM*	0,35071E 01

DWELL TIME = 77 DAYS

CHANNEL POWER
0,58900E 06

MIXED GAS OUTLET TEMPERATURE 852,

INNER FLOW RATE 0,11909E 03

OUTER FLOW RATE 0,86548E 02

TEMPERATURES

Z	TG1	TW1	TI1	TF1	TFI	TF2	TI2	TW2	TG2	TW3
0	300	462	503	623	646	619	498	466	300	307
50	328	566	626	714	751	726	575	540	359	372
100	371	698	784	833	869	862	669	629	430	450
150	427	797	902	933	999	971	757	711	507	532
200	489	876	990	1023	1093	1065	842	792	587	616
250	543	873	972	1001	1063	1041	860	819	656	682
300	598	922	1022	1050	1112	1091	926	879	723	750
350	652	967	1068	1096	1158	1137	974	934	768	817
400	705	996	1093	1119	1176	1160	1015	978	850	877
450	751	992	1072	1094	1145	1133	1025	997	902	923
500	787	970	1030	1047	1069	1082	1017	999	939	953

Z	INNER GAP	HEAT SPLIT RADIUS	OUTER GAP
0	0,14662E-01	0,23604E 01	0,15410E-01
50	0,79467E-02	0,24079E 01	0,18810E-01
100	0,34553E-02	0,24415E 01	0,24030E-01
150	0,54559E-03	0,24535E 01	0,27971E-01
200	-0,12869E-02	0,24558E 01	0,30559E-01
250	-0,53435E-03	0,24670E 01	0,30195E-01
300	-0,11451E-02	0,24682E 01	0,30474E-01
350	-0,12286E-02	0,24732E 01	0,32187E-01
400	-0,16776E-02	0,24805E 01	0,32691E-01
450	-0,10563E-02	0,24981E 01	0,31609E-01
500	0,15028E-02	0,25274E 01	0,28599E-01

AIX-19

GRAPHITE SURFACE DIMENSIONS

GRAPHITE SURFACE DIMENSIONS

Z	RC0	RC1	RC2
0	0,15086E 01	0,32677E 01	0,37957E 01
50	0,15096E 01	0,32692E 01	0,37971E 01
100	0,15110E 01	0,32710E 01	0,37990E 01
150	0,15122E 01	0,32728E 01	0,38009E 01
200	0,15134E 01	0,32745E 01	0,38030E 01
250	0,15133E 01	0,32749E 01	0,38047E 01
300	0,15143E 01	0,32759E 01	0,38069E 01
350	0,15156E 01	0,32765E 01	0,38100E 01
400	0,15167E 01	0,32765E 01	0,38150E 01
450	0,15165E 01	0,32763E 01	0,38214E 01
500	0,15155E 01	0,32761E 01	0,38273E 01

PRESSURE DROPS

Z	PD(BORE)	PD(ANNULUS)
0	0,0	0,0
50	0,15455E 05	0,14963E 05
100	0,33339E 05	0,31857E 05
150	0,53638E 05	0,50829E 05
200	0,75856E 05	0,71843E 05
250	0,98618E 05	0,94333E 05
300	0,12275E 06	0,11857E 06
350	0,14812E 06	0,14375E 06
400	0,17489E 06	0,17068E 06
450	0,20216E 06	0,19994E 06
500	0,22899E 06	0,22940E 06

CORROSION DATA

	PLANAR REMOVAL			ROUGHNESS HEIGHTS		
Z	RC0	RC1	RC2	RC0	RC1	RC2
0	0,26138E-07	0,31123E-07	0,15280E-09	0,26138E-07	0,31123E-07	0,15280E-09
50	0,77137E-06	0,37078E-06	0,46999E-08	0,77137E-06	0,37078E-06	0,46999E-08
100	0,20182E-04	0,40914E-05	0,16543E-06	0,20182E-04	0,40914E-05	0,16543E-06
150	0,13836E-03	0,26714E-04	0,28667E-05	0,13836E-03	0,26714E-04	0,28667E-05
200	0,50193E-03	0,12680E-03	0,30938E-04	0,50193E-03	0,12680E-03	0,30938E-04
250	0,48234E-03	0,20163E-03	0,14720E-03	0,48234E-03	0,20163E-03	0,14720E-03
300	0,98179E-03	0,52229E-03	0,60514E-03	0,98179E-03	0,52229E-03	0,60514E-03
350	0,18296E-02	0,11552E-02	0,20245E-02	0,18296E-02	0,11552E-02	0,20245E-02
400	0,26382E-02	0,20882E-02	0,53885E-02	0,26382E-02	0,20882E-02	0,53885E-02
450	0,25049E-02	0,26549E-02	0,10594E-01	0,25049E-02	0,26549E-02	0,10594E-01
500	0,19051E-02	0,27247E-02	0,15718E-01	0,19051E-02	0,27247E-02	0,15718E-01

HEAT TRANSFER COEFF, AND FRICTION FACTOR (TRANSFORMED)

Z	RC0	RC1	RC2	RC0	RC1	RC2
0	0,22443E 00	0,12808E 00	0,45117E 00	0,39768E-02	0,69859E-02	0,69019E-02
50	0,22296E 00	0,13076E 00	0,34679E 00	0,40271E-02	0,71035E-02	0,70218E-02
100	0,22235E 00	0,13367E 00	0,29722E 00	0,41094E-02	0,72332E-02	0,71538E-02
150	0,22428E 00	0,13665E 00	0,27393E 00	0,41718E-02	0,74009E-02	0,73269E-02
200	0,22722E 00	0,13947E 00	0,25993E 00	0,42303E-02	0,75191E-02	0,74514E-02
250	0,23200E 00	0,14228E 00	0,25190E 00	0,42646E-02	0,75996E-02	0,75487E-02
300	0,23482E 00	0,14426E 00	0,24437E 00	0,43080E-02	0,76649E-02	0,76396E-02
350	0,23739E 00	0,14585E 00	0,23703E 00	0,43795E-02	0,77638E-02	0,77243E-02
400	0,24194E 00	0,14750E 00	0,23159E 00	0,45417E-02	0,78901E-02	0,81690E-02
450	0,24499E 00	0,14924E 00	0,24180E 00	0,45353E-02	0,80368E-02	0,93111E-02
500	0,24718E 00	0,15171E 00	0,25162E 00	0,44364E-02	0,82079E-02	0,10440E-01

H E A T A X   R E S U L T S .

RE	0,15175E 06	0,24074E 05	0,24074E 05	*DE*	0,30178E 01	0,98128E 00	0,98128E 00	*RM*	0,35217E 01
RE	0,14599E 06	0,22603E 05	0,22603E 05	*DE*	0,30199E 01	0,98108E 00	0,98108E 00	*RM*	0,35231E 01
RE	0,13859E 06	0,21079E 05	0,21079E 05	*DE*	0,30226E 01	0,98091E 00	0,98091E 00	*RM*	0,35249E 01
RE	0,13083E 06	0,19666E 05	0,19666E 05	*DE*	0,30253E 01	0,98122E 00	0,98122E 00	*RM*	0,35249E 01
RE	0,12346E 06	0,18405E 05	0,18405E 05	*DE*	0,30292E 01	0,98232E 00	0,98232E 00	*RM*	0,35249E 01
RE	0,11793E 06	0,17470E 05	0,17470E 05	*DE*	0,30287E 01	0,98498E 00	0,98498E 00	*RM*	0,35249E 01
RE	0,11275E 06	0,16651E 05	0,16651E 05	*DE*	0,30326E 01	0,98908E 00	0,98908E 00	*RM*	0,35249E 01
RE	0,10807E 06	0,15551E 05	0,16240E 05	*DE*	0,30377E 01	0,97534E 00	0,10185E 01	*RM*	0,35275E 01
RE	0,10396E 06	0,14114E 05	0,16286E 05	*DE*	0,30417E 01	0,93940E 00	0,10840E 01	*RM*	0,35174E 01
RE	0,10072E 06	0,11979E 05	0,17129E 05	*DE*	0,30413E 01	0,84634E 00	0,12102E 01	*RM*	0,34932E 01
RE	0,98488E 05	0,11823E 05	0,16558E 05	*DE*	0,30384E 01	0,87895E 00	0,12310E 01	*RM*	0,35014E 01

DWELL TIME = 231 DAYS

CHANNEL POWER
0,55100E 06

MIXED GAS OUTLET TEMPERATURE 851,

INNER FLOW RATE 0,11040E 03 | OUTER FLOW RATE 0,82310E 02

TEMPERATURES

Z	TG1	TW1	TI1	TF1	TFI	TF2	TI2	TW2	TG2	TW3
0	300	486	549	613	651	622	493	451	300	308
50	332	589	673	709	766	736	568	523	355	368
100	380	709	817	843	919	885	664	613	422	442
150	436	801	921	950	1036	1001	750	695	496	520
200	498	880	1007	1038	1130	1094	830	772	574	603
250	552	873	983	1010	1089	1060	849	801	641	666
300	607	921	1031	1057	1137	1108	908	861	707	734
350	661	957	1066	1092	1173	1147	959	914	772	800
400	714	978	1081	1106	1165	1162	997	957	832	858
450	761	978	1063	1084	1150	1133	1009	978	884	902
500	798	966	1031	1047	1099	1087	1008	986	921	935

Z	INNER GAP	HEAT SPLIT RADIUS	OUTER GAP
0	0,72306E-02	0,23972E 01	0,16746E-01
50	0,32153E-02	0,24301E 01	0,23868E-01
100	-0,46472E-03	0,24474E 01	0,31247E-01
150	-0,51410E-03	0,24534E 01	0,37326E-01
200	-0,53392E-03	0,24574E 01	0,42628E-01
250	-0,44347E-03	0,24633E 01	0,40036E-01
300	-0,53912E-03	0,24654E 01	0,40907E-01
350	-0,52740E-03	0,24732E 01	0,42730E-01
400	-0,34030E-03	0,24818E 01	0,42442E-01
450	-0,51626E-03	0,24917E 01	0,39961E-01
500	-0,96662E-03	0,25078E 01	0,35193E-01

GRAPHITE SURFACE DIMENSIONS

GRAPHITE SURFACE DIMENSIONS

Z	RC0	RC1	RC2
0	0,15089E 01	0,32675E 01	0,37957E 01
50	0,15099E 01	0,32689E 01	0,37970E 01
100	0,15113E 01	0,32708E 01	0,37988E 01
150	0,15126E 01	0,32725E 01	0,38006E 01
200	0,15146E 01	0,32740E 01	0,38027E 01
250	0,15143E 01	0,32743E 01	0,38046E 01
300	0,15163E 01	0,32748E 01	0,38074E 01
350	0,15188E 01	0,32743E 01	0,38125E 01
400	0,15209E 01	0,32729E 01	0,38219E 01
450	0,15206E 01	0,32716E 01	0,38356E 01
500	0,15192E 01	0,32712E 01	0,38505E 01

PRESSURE DROPS

Z	PD(BORE)	PD(ANNULUS)
0	0,0	0,0
50	0,13850E 05	0,13494E 05
100	0,29831E 05	0,28680E 05
150	0,47683E 05	0,45708E 05
200	0,67096E 05	0,64547E 05
250	0,87003E 05	0,84668E 05
300	0,10847E 06	0,10606E 06
350	0,13187E 06	0,12881E 06
400	0,15720E 06	0,15372E 06
450	0,18303E 06	0,18174E 06
500	0,20808E 06	0,20822E 06

CORROSION DATA

	PLANAR REMOVAL			ROUGHNESS HEIGHTS		
Z	RC0	RC1	RC2	RC0	RC1	RC2
0	0,15435E-06	0,65869E-07	0,48151E-09	0,15435E-06	0,65869E-07	0,48151E-09
50	0,37446E-05	0,81071E-06	0,13260E-07	0,37446E-05	0,81071E-06	0,13260E-07
100	0,71572E-04	0,95864E-05	0,40580E-06	0,71572E-04	0,95864E-05	0,40580E-06
150	0,43478E-03	0,64404E-04	0,68558E-05	0,43478E-03	0,64404E-04	0,68558E-05
200	0,15675E-02	0,30350E-03	0,74513E-04	0,15675E-02	0,30350E-03	0,74513E-04
250	0,14488E-02	0,49836E-03	0,35547E-03	0,14488E-02	0,49836E-03	0,35547E-03
300	0,29288E-02	0,13124E-02	0,14879E-02	0,29288E-02	0,13124E-02	0,14879E-02
350	0,50786E-02	0,29421E-02	0,49398E-02	0,50786E-02	0,29421E-02	0,49398E-02
400	0,69226E-02	0,53242E-02	0,12913E-01	0,69226E-02	0,53242E-02	0,12913E-01
450	0,67776E-02	0,69123E-02	0,25437E-01	0,67776E-02	0,69123E-02	0,25000E-01
500	0,55692E-02	0,74826E-02	0,39536E-01	0,55692E-02	0,74826E-02	0,25000E-01

	HEAT TRANSFER COEFF.		AND	FRICTION FACTOR (TRANSFORMED)		
Z	RC0	RC1	RC2	RC0	RC1	RC2
0	0,21009E 00	0,12370E 00	0,37527E 00	0,40596E-02	0,70670E-02	0,69897E-02
50	0,20934E 00	0,12596E 00	0,31325E 00	0,41135E-02	0,71802E-02	0,71029E-02
100	0,20961E 00	0,12839E 00	0,28185E 00	0,41974E-02	0,73082E-02	0,72302E-02
150	0,21169E 00	0,13105E 00	0,26311E 00	0,42598E-02	0,74757E-02	0,74019E-02
200	0,21423E 00	0,13373E 00	0,24926E 00	0,43195E-02	0,75936E-02	0,75767E-02
250	0,21884E 00	0,13621E 00	0,24274E 00	0,43539E-02	0,76749E-02	0,76236E-02
300	0,22334E 00	0,13782E 00	0,23439E 00	0,45963E-02	0,77617E-02	0,77159E-02
350	0,23589E 00	0,13943E 00	0,22394E 00	0,50082E-02	0,78887E-02	0,81053E-02
400	0,25087E 00	0,14164E 00	0,23993E 00	0,54140E-02	0,84655E-02	0,98093E-02
450	0,25231E 00	0,14458E 00	0,27266E 00	0,53786E-02	0,90411E-02	0,12688E-01
500	0,24593E 00	0,14216E 00	0,25683E 00	0,51111E-02	0,90914E-02	0,12529E-01

HEATAX RESULTS

RE	0,13939E 06	0,22867E 05	0,22867E 05	*DE*	0,30181E 01	0,98132E 00	0,98132E 00	*RM*	0,35218E 01
RE	0,13366E 06	0,21467E 05	0,21467E 05	*DE*	0,30202E 01	0,98128E 00	0,98128E 00	*RM*	0,35231E 01
RE	0,12665E 06	0,20049E 05	0,20049E 05	*DE*	0,30228E 01	0,98097E 00	0,98097E 00	*RM*	0,35231E 01
RE	0,11957E 06	0,18724E 05	0,18724E 05	*DE*	0,30259E 01	0,98143E 00	0,98143E 00	*RM*	0,35231E 01
RE	0,11283E 06	0,17551E 05	0,17551E 05	*DE*	0,30311E 01	0,98278E 00	0,98278E 00	*RM*	0,35231E 01
RE	0,10787E 06	0,16684E 05	0,16684E 05	*DE*	0,30303E 01	0,98579E 00	0,98579E 00	*RM*	0,35231E 01
RE	0,10316E 06	0,15916E 05	0,15916E 05	*DE*	0,30357E 01	0,99149E 00	0,99149E 00	*RM*	0,35231E 01
RE	0,98881E 05	0,14747E 05	0,15631E 05	*DE*	0,30422E 01	0,97396E 00	0,10323E 01	*RM*	0,35255E 01
RE	0,95043E 05	0,12725E 05	0,16208E 05	*DE*	0,30481E 01	0,89957E 00	0,11457E 01	*RM*	0,35047E 01
RE	0,91991E 05	0,12066E 05	0,15778E 05	*DE*	0,30488E 01	0,91791E 00	0,12003E 01	*RM*	0,35078E 01
RE	0,89886E 05	0,11956E 05	0,15107E 05	*DE*	0,30454E 01	0,97427E 00	0,12311E 01	*RM*	0,35218E 01

DWELL TIME = 385 DAYS

CHANNEL POWER
0,51400E 06

MIXED GAS OUTLET TEMPERATURE 851,

INNER FLOW RATE 0,10143E 03

OUTER FLOW RATE 0,78186E 02

TEMPERATURES

Z	TG1	TW1	TI1	TF1	TFI	TF2	TI2	TW2	TG2	TW3
0	300	503	577	625	676	641	498	451	300	309
50	335	603	697	716	788	752	569	520	355	369
100	385	712	827	851	942	901	663	607	421	440
150	442	801	923	950	1052	1009	744	685	494	517
200	503	876	1005	1033	1142	1098	821	760	576	597
250	557	868	977	1001	1095	1059	837	788	634	658
300	611	911	1021	1045	1140	1105	894	846	698	724
350	665	938	1049	1073	1170	1138	944	898	761	788
400	718	962	1067	1091	1184	1155	984	942	820	842
450	767	970	1059	1079	1159	1136	1002	968	872	891
500	804	965	1033	1048	1111	1095	1006	982	911	926

Z	INNER GAP	HEAT SPLIT RADIUS	OUTER GAP
0	0,54201E-02	0,24078E 01	0,22113E-01
50	-0,17019E-03	0,24362E 01	0,28371E-01
100	0,64112E-05	0,24452E 01	0,30617E-01
150	0,11145E-03	0,24523E 01	0,44144E-01
200	-0,63796E-04	0,24562E 01	0,50766E-01
250	0,40554E-04	0,24604E 01	0,47207E-01
300	-0,20673E-03	0,24628E 01	0,47961E-01
350	0,31396E-03	0,24728E 01	0,49161E-01
400	0,47897E-03	0,24790E 01	0,46100E-01
450	-0,16335E-04	0,24847E 01	0,45222E-01
500	-0,32448E-03	0,24959E 01	0,39459E-01

GRAPHITE SURFACE DIMENSIONS

Z	RC0	RC1	RC2
0	0,15091E 01	0,32675E 01	0,37958E 01
50	0,15101E 01	0,32689E 01	0,37971E 01
100	0,15114E 01	0,32707E 01	0,37987E 01
150	0,15129E 01	0,32723E 01	0,38006E 01
200	0,15156E 01	0,32736E 01	0,38026E 01
250	0,15151E 01	0,32738E 01	0,38045E 01
300	0,15179E 01	0,32738E 01	0,38079E 01
350	0,15211E 01	0,32726E 01	0,38147E 01
400	0,15240E 01	0,32699E 01	0,38278E 01
450	0,15244E 01	0,32677E 01	0,38479E 01
500	0,15227E 01	0,32667E 01	0,38719E 01

PRESSURE DROPS

Z	PD(BORE)	PD(ANNULUS)
0	0,0	0,0
50	0,12082E 05	0,12280E 05
100	0,25938E 05	0,26117E 05
150	0,41261E 05	0,41541E 05
200	0,58132E 05	0,58548E 05
250	0,75316E 05	0,76652E 05
300	0,94023E 05	0,95790E 05
350	0,11488E 06	0,11639E 06
400	0,13775E 06	0,13979E 06
450	0,16135E 06	0,16341E 06
500	0,18430E 06	0,18482E 06

CORROSION DATA

	PLANAR REMOVAL			ROUGHNESS HEIGHTS		
Z	RC0	RC1	RC2	RC0	RC1	RC2
0	0,37591E-06	0,99986E-07	0,86682E-09	0,37591E-06	0,99986E-07	0,86682E-09
50	0,79957E-05	0,11960E-05	0,22968E-07	0,79957E-05	0,11960E-05	0,22968E-07
100	0,12620E-03	0,14391E-04	0,63157E-06	0,12620E-03	0,14391E-04	0,63157E-06
150	0,72911E-03	0,95060E-04	0,10448E-04	0,72911E-03	0,95060E-04	0,10448E-04
200	0,25643E-02	0,44452E-03	0,11200E-03	0,25643E-02	0,44452E-03	0,11200E-03
250	0,23300E-02	0,73289E-03	0,52768E-03	0,23300E-02	0,73289E-03	0,52768E-03
300	0,46017E-02	0,19409E-02	0,22087E-02	0,46017E-02	0,19409E-02	0,22087E-02
350	0,75382E-02	0,43304E-02	0,73843E-02	0,75382E-02	0,43304E-02	0,73843E-02
400	0,10282E-01	0,79076E-02	0,19100E-01	0,10282E-01	0,79076E-02	0,19100E-01
450	0,10619E-01	0,10662E-01	0,38020E-01	0,10619E-01	0,10662E-01	0,25000E-01
500	0,90910E-02	0,11838E-01	0,61115E-01	0,90910E-02,	0,11838E-01	0,25000E-01

	HEAT TRANSFER COEFF.		AND	FRICTION FACTOR (TRANSFORMED)		
Z	RC0	RC1	RC2	RC0	RC1	RC2
0	0,19567E 00	0,11882E 00	0,34674E 00	0,41512E-02	0,71582E-02	0,70805E-02
50	0,19542E 00	0,12103E 00	0,29595E 00	0,42076E-02	0,72717E-02	0,71952E-02
100	0,19622E 00	0,12326E 00	0,26971E 00	0,42924E-02	0,74430E-02	0,73649E-02
150	0,19820E 00	0,12583E 00	0,25169E 00	0,43559E-02	0,75658E-02	0,74933E-02
200	0,20163E 00	0,12830E 00	0,23863E 00	0,45630E-02	0,76823E-02	0,76166E-02
250	0,20522E 00	0,13053E 00	0,23288E 00	0,45447E-02	0,77621E-02	0,77117E-02
300	0,21293E 00	0,13181E 00	0,22424E 00	0,49016E-02	0,78487E-02	0,78634E-02
350	0,23381E 00	0,13297E 00	0,21718E 00	0,55516E-02	0,81949E-02	0,85075E-02
400	0,25147E 00	0,13635E 00	0,25082E 00	0,60998E-02	0,90396E-02	0,11356E-01
450	0,25505E 00	0,14021E 00	0,25270E 00	0,61504E-02	0,98218E-02	0,12622E-01
500	0,24736E 00	0,13598E 00	0,23838E 00	0,58186E-02	0,99562E-02	0,12398E-01

HEATAX RESULTS

RE	0,12782E 06	0,21523E 05	0,21523E 05	*DE*	0,30186E 01	0,98140E 00	0,98140E 00	*RM*	0,35217E 0
RE	0,12202E 06	0,20215E 05	0,20215E 05	*DE*	0,30204E 01	0,98129E 00	0,98129E 00	*RM*	0,35231E 0
RE	0,11553E 06	0,18879E 05	0,18879E 05	*DE*	0,30229E 01	0,98121E 00	0,98121E 00	*RM*	0,35231E 0
RE	0,10905E 06	0,17654E 05	0,17654E 05	*DE*	0,30264E 01	0,98178E 00	0,98178E 00	*RM*	0,35231E 0
RE	0,10292E 06	0,16571E 05	0,16571E 05	*DE*	0,30329E 01	0,98335E 00	0,98335E 00	*RM*	0,35231E 0
RE	0,98496E 05	0,15778E 05	0,15778E 05	*DE*	0,30317E 01	0,98660E 00	0,98660E 00	*RM*	0,35231E 0
PE	0,94226E 05	0,15068E 05	0,15068E 05	*DE*	0,30382E 01	0,99357E 00	0,99357E 00	*RM*	0,35231E 0
RE	0,90317E 05	0,13938E 05	0,14837E 05	*DE*	0,30461E 01	0,97681E 00	0,10399E 01	*RM*	0,35248E 0
RE	0,86797E 05	0,11834E 05	0,15535E 05	*DE*	0,30536E 01	0,89345E 00	0,11729E 01	*RM*	0,35010E 0
RE	0,83918E 05	0,11926E 05	0,14461E 05	*DE*	0,30559E 01	0,98208E 00	0,11909E 01	*RM*	0,35209E 0
RE	0,81901E 05	0,11837E 05	0,13731E 05	*DE*	0,30526E 01	0,10610E 01	0,12308E 01	*RM*	0,35402E 0

DWELL TIME = 539 DAYS

CHANNEL POWER
0,47700E 06

MIXED GAS OUTLET TEMPERATURE 852,

INNER FLOW RATE	OUTER FLOW RATE
0,93030E 02	0,73590E 02

TEMPERATURES

Z	TG1	TW1	TI1	TF1	TFI	TF2	TI2	TW2	TG2	TW3
0	300	526	602	624	686	651	495	448	300	310
50	339	613	703	722	799	760	568	520	355	368
100	390	717	824	847	942	899	654	602	421	439
150	448	800	917	942	1047	1003	731	676	492	515
200	509	871	996	1021	1134	1089	805	749	566	592
250	562	861	965	986	1082	1045	821	775	628	651
300	615	898	1003	1025	1122	1086	877	831	690	715
350	669	927	1032	1054	1153	1120	926	882	750	776
400	722	950	1052	1074	1170	1139	966	925	808	829
450	771	967	1057	1075	1161	1135	994	959	860	880
500	811	966	1035	1050	1116	1098	1002	976	902	918

Z	INNER GAP	HEAT SPLIT RADIUS	OUTER GAP
0	0,23404E-02	0,24254E 01	0,26134E-01
50	0,15249E-03	0,24356E 01	0,31026E-01
100	0,59170E-03	0,24459E 01	0,41597E-01
150	-0,59985E-04	0,24517E 01	0,50273E-01
200	-0,60309E-03	0,24562E 01	0,58200E-01
250	-0,71440E-04	0,24595E 01	0,53394E-01
300	-0,54765E-04	0,24634E 01	0,53145E-01
350	0,25102E-03	0,24716E 01	0,54230E-01
400	0,20975E-03	0,24764E 01	0,52916E-01
450	0,44465E-03	0,24799E 01	0,48936E-01
500	0,27065E-03	0,24880E 01	0,42653E-01

GRAPHITE SURFACE DIMENSIONS

GRAPHITE SURFACE DIMENSIONS

Z	RC0	RC1	RC2
0	0,15093E 01	0,32675E 01	0,37958E 01
50	0,15102E 01	0,32689E 01	0,37971E 01
100	0,15115E 01	0,32706E 01	0,37987E 01
150	0,15132E 01	0,32721E 01	0,38005E 01
200	0,15164E 01	0,32752E 01	0,38025E 01
250	0,15158E 01	0,32753E 01	0,38045E 01
300	0,15191E 01	0,32730E 01	0,38082E 01
350	0,15230E 01	0,32711E 01	0,38163E 01
400	0,15268E 01	0,32675E 01	0,38323E 01
450	0,15280E 01	0,32642E 01	0,38587E 01
500	0,15263E 01	0,32625E 01	0,38911E 01

PRESSURE DROPS

Z	PD(BORE)	PD(ANNULUS)
0	0,0	0,0
50	0,10594E 05	0,10983E 05
100	0,22516E 05	0,23354E 05
150	0,35647E 05	0,37100E 05
200	0,50179E 05	0,52214E 05
250	0,64951E 05	0,68248E 05
300	0,81269E 05	0,85114E 05
350	0,99493E 05	0,10337E 06
400	0,11970E 06	0,12460E 06
450	0,14085E 06	0,14427E 06
500	0,16164E 06	0,16145E 06

CORROSION DATA

	PLANAR REMOVAL			ROUGHNESS HEIGHTS		
Z	RC0	RC1	RC2	RC0	RC1	RC2
0	0,83794E-06	0,12991E-06	0,12748E-08	0,83794E-06	0,12991E-06	0,12748E-08
50	0,13445E-04	0,15783E-05	0,32638E-07	0,13445E-04	0,15783E-05	0,32638E-07
100	0,18587E-03	0,18530E-04	0,85273E-06	0,18587E-03	0,18530E-04	0,85273E-06
150	0,10172E-02	0,12027E-03	0,13771E-04	0,10172E-02	0,12027E-03	0,13771E-04
200	0,34998E-02	0,55772E-03	0,14521E-03	0,34998E-02	0,55772E-03	0,14521E-03
250	0,31204E-02	0,91690E-03	0,67310E-03	0,31204E-02	0,91690E-03	0,67310E-03
300	0,59870E-02	0,24322E-02	0,28049E-02	0,59870E-02	0,24322E-02	0,28049E-02
350	0,96312E-02	0,54285E-02	0,93513E-02	0,96312E-02	0,54285E-02	0,93513E-02
400	0,13174E-01	0,99410E-02	0,24020E-01	0,13174E-01	0,99410E-02	0,24020E-01
450	0,14227E-01	0,13903E-01	0,49097E-01	0,14227E-01	0,13903E-01	0,25000E-01
500	0,12655E-01	0,15901E-01	0,80514E-01	0,12655E-01	0,15901E-01	0,25000E-01

HEAT TRANSFER COEFF, AND FRICTION FACTOR (TRANSFORMED)

Z	RC0	RC1	RC2	RC0	RC1	RC2
0	0,18175E 00	0,11347E 00	0,30669E 00	0,42481E-02	0,72658E-02	0,71892E-02
50	0,18241E 00	0,11533E 00	0,27853E 00	0,43250E-02	0,73819E-02	0,73043E-02
100	0,18340E 00	0,11756E 00	0,25407E 00	0,43921E-02	0,75538E-02	0,74768E-02
150	0,18537E 00	0,11996E 00	0,23818E 00	0,44554E-02	0,76757E-02	0,76045E-02
200	0,18962E 00	0,12225E 00	0,22586E 00	0,47620E-02	0,77912E-02	0,77268E-02
250	0,19302E 00	0,12426E 00	0,22085E 00	0,47338E-02	0,76692E-02	0,76200E-02
300	0,20579E 00	0,12528E 00	0,21217E 00	0,52477E-02	0,79552E-02	0,79110E-02
350	0,22563E 00	0,12667E 00	0,21158E 00	0,59515E-02	0,84709E-02	0,90390E-02
400	0,24595E 00	0,13321E 00	0,25147E 00	0,66559E-02	0,96931E-02	0,12495E-01
450	0,25221E 00	0,13430E 00	0,23603E 00	0,68304E-02	0,10492E-01	0,12545E-01
500	0,24607E 00	0,12900E 00	0,21535E 00	0,65143E-02	0,10685E-01	0,12263E-01

HEATAX RESULTS

RE	0,11660E 06	0,20118E 05	0,20118E 05	*DE*	0,30189E 01	0,98140E 00	0,98140E 00	*RM*	0,35218E 01
RE	0,11098E 06	0,18870E 05	0,18870E 05	*DE*	0,30206E 01	0,98122E 00	0,98122E 00	*RM*	0,35231E 01
RE	0,10496E 06	0,17628E 05	0,17628E 05	*DE*	0,30230E 01	0,98142E 00	0,98142E 00	*RM*	0,35231E 01
RE	0,99058E 05	0,16506E 05	0,16506E 05	*DE*	0,30268E 01	0,98215E 00	0,98215E 00	*RM*	0,35231E 01
RE	0,93496E 05	0,15521E 05	0,15521E 05	*DE*	0,30344E 01	0,98386E 00	0,98386E 00	*RM*	0,35231E 01
RE	0,89559E 05	0,14804E 05	0,14804E 05	*DE*	0,30329E 01	0,98736E 00	0,98736E 00	*RM*	0,35231E 01
RE	0,85705E 05	0,14155E 05	0,14155E 05	*DE*	0,30403E 01	0,99536E 00	0,99536E 00	*RM*	0,35231E 01
RE	0,82147E 05	0,12984E 05	0,14050E 05	*DE*	0,30494E 01	0,97220E 00	0,10520E 01	*RM*	0,35225E 01
RE	0,78911E 05	0,11323E 05	0,14428E 05	*DE*	0,30586E 01	0,91828E 00	0,11701E 01	*RM*	0,35054E 01
RE	0,76190E 05	0,11569E 05	0,13239E 05	*DE*	0,30631E 01	0,10356E 01	0,11851E 01	*RM*	0,35317E 01
RE	0,74257E 05	0,11591E 05	0,12396E 05	*DE*	0,30602E 01	0,11454E 01	0,12249E 01	*RM*	0,35581E 01

DWELL TIME = 693 DAYS

CHANNEL POWER
0,44000E 06

MIXED GAS OUTLET TEMPERATURE 852,

INNER FLOW RATE 0,84869E 02

OUTER FLOW RATE 0,68785E 02

TEMPERATURES

Z	TG1	TW1	TI1	TF1	TFI	TF2	TI2	TW2	TG2	TW3
0	300	539	621	636	702	666	496	450	300	310
50	342	621	710	728	806	767	569	520	356	370
100	394	719	822	842	936	894	649	597	422	440
150	452	798	909	931	1033	991	719	668	492	514
200	513	866	983	1006	1114	1071	791	738	563	589
250	565	854	951	970	1061	1026	805	762	623	645
300	618	888	986	1006	1099	1064	860	817	682	707
350	671	916	1015	1035	1129	1097	908	868	741	765
400	725	943	1039	1058	1151	1121	950	911	797	818
450	775	967	1055	1073	1157	1130	987	951	850	871
500	817	969	1037	1051	1116	1098	998	972	893	913

Z	INNER GAP	HEAT SPLIT RADIUS	OUTER GAP
0	0,28017E-03	0,24290E 01	0,29929E-01
50	0,45347E-03	0,24364E 01	0,35213E-01
100	0,57722E-03	0,24463E 01	0,45444E-01
150	-0,43367E-03	0,24526E 01	0,55856E-01
200	-0,18401E-02	0,24564E 01	0,63762E-01
250	-0,99302E-03	0,24598E 01	0,59622E-01
300	-0,94472E-03	0,24640E 01	0,58655E-01
350	-0,63373E-03	0,24710E 01	0,57933E-01
400	-0,30636E-03	0,24745E 01	0,56419E-01
450	0,24558E-03	0,24764E 01	0,52506E-01
500	0,41797E-03	0,24818E 01	0,46203E-01

GRAPHITE SURFACE DIMENSIONS

GRAPHITE SURFACE DIMENSIONS

Z	RC0	RC1	RC2
0	0,15094E 01	0,32675E 01	0,37958E 01
50	0,15103E 01	0,32689E 01	0,37971E 01
100	0,15115E 01	0,32705E 01	0,37987E 01
150	0,15134E 01	0,32718E 01	0,38005E 01
200	0,15172E 01	0,32728E 01	0,38025E 01
250	0,15164E 01	0,32728E 01	0,38045E 01
300	0,15202E 01	0,32722E 01	0,38085E 01
350	0,15247E 01	0,32699E 01	0,38177E 01
400	0,15293E 01	0,32655E 01	0,38362E 01
450	0,15316E 01	0,32611E 01	0,38683E 01
500	0,15301E 01	0,32585E 01	0,39081E 01

PRESSURE DROPS

Z	PD(BORE)	PD(ANNULUS)
0	0,0	0,0
50	0,90824E 04	0,97424E 04
100	0,19227E 05	0,20687E 05
150	0,30351E 05	0,32811E 05
200	0,42695E 05	0,46096E 05
250	0,55205E 05	0,60146E 05
300	0,69147E 05	0,74852E 05
350	0,84805E 05	0,90892E 05
400	0,10224E 06	0,10908E 06
450	0,12076E 06	0,12531E 06
500	0,13918E 06	0,13895E 06

CORROSION DATA

	PLANAR REMOVAL			ROUGHNESS HEIGHTS		
Z	RC0	RC1	RC2	RC0	RC1	RC2
0	0,15394E-05	0,16290E-06	0,17020E-08	0,15394E-05	0,16290E-06	0,17020E-08
50	0,20429E-04	0,19654E-05	0,41859E-07	0,20429E-04	0,19654E-05	0,41859E-07
100	0,24837E-03	0,22233E-04	0,10832E-05	0,24837E-03	0,22233E-04	0,10832E-05
150	0,12971E-02	0,14122E-03	0,17019E-04	0,12971E-02	0,14122E-03	0,17019E-04
200	0,43635E-02	0,65002E-03	0,17573E-03	0,43635E-02	0,65002E-03	0,17573E-03
250	0,38316E-02	0,10626E-02	0,80001E-03	0,38316E-02	0,10626E-02	0,80001E-03
300	0,71864E-02	0,28204E-02	0,33099E-02	0,71864E-02	0,28204E-02	0,33099E-02
350	0,11440E-01	0,63043E-02	0,10970E-01	0,11440E-01	0,63043E-02	0,10970E-01
400	0,15788E-01	0,11607E-01	0,28129E-01	0,15788E-01	0,11607E-01	0,25000E-01
450	0,17838E-01	0,16826E-01	0,58839E-01	0,17838E-01	0,16826E-01	0,25000E-01
500	0,16448E-01	0,19863E-01	0,97654E-01	0,16448E-01	0,19863E-01	0,25000E-01

	HEAT TRANSFER COFFF,		AID	FRICTION FACTOR (TRANSFORMED)		
Z	RC0	RC1	RC2	RC0	RC1	RC2
0	0,16843E 00	0,10753E 00	0,28278E 00	0,43506E-02	0,73906E-02	0,73120E-02
50	0,16941E 00	0,10946E 00	0,25589E 00	0,44306E-02	0,75093E-02	0,74315E-02
100	0,17064E 00	0,11155E 00	0,23758E 00	0,44981E-02	0,76823E-02	0,76063E-02
150	0,17255E 00	0,11382E 00	0,22315E 00	0,45651E-02	0,78029E-02	0,77335E-02
200	0,17714E 00	0,11591E 00	0,21216E 00	0,49383E-02	0,79172E-02	0,78543E-02
250	0,18017E 00	0,11772E 00	0,20766E 00	0,48985E-02	0,79934E-02	0,79457E-02
300	0,19499E 00	0,11850E 00	0,19935E 00	0,55147E-02	0,80787E-02	0,80356E-02
350	0,21510E 00	0,11997E 00	0,20787E 00	0,63056E-02	0,87120E-02	0,94713E-02
400	0,23509E 00	0,12703E 00	0,23489E 00	0,70995E-02	0,10101E-01	0,12654E-01
450	0,24374E 00	0,12687E 00	0,21465E 00	0,74249E-02	0,10996E-01	0,12445E-01
500	0,23991E 00	0,12115E 00	0,16771E 00	0,71666E-02	0,11238E-01	0,12145E-01

H E A T A X   R E S U L T S

RE*	0,11482E 06	0,19972E 05	0,19972E 05	*DE*	0,30187E 01	0,98156E 00	0,98156E 00	*RM*	0,35217E 01
RE*	0,10942E 06	0,18773E 05	0,18773E 05	*DE*	0,30204E 01	0,98141E 00	0,98141E 00	*RM*	0,35230E 01
RE*	0,10363E 06	0,17573E 05	0,17573E 05	*DE*	0,30228E 01	0,98161E 00	0,98161F 00	*RM*	0,35230E 01
RE*	0,97909E 05	0,16485E 05	0,16485E 05	*DE*	0,30267E 01	0,98234E 00	0,98234F 00	*RM*	0,35230E 01
RE*	0,92496E 05	0,15526E 05	0,15526E 05	*DE*	0,30347E 01	0,98410E 00	0,98410F 00	*RM*	0,35230E 01
RE*	0,88671E 05	0,14826E 05	0,14826E 05	*DE*	0,30331E 01	0,98760E 00	0,98760F 00	*RM*	0,35230E 01
RE*	0,84907E 05	0,14189E 05	0,14189E 05	*DE*	0,30408E 01	0,99597E 00	0,99597E 00	*RM*	0,35230E 01
RE*	0,81418E 05	0,12968E 05	0,14146E 05	*DE*	0,30503E 01	0,96931E 00	0,10574E 01	*RM*	0,35211E 01
RE*	0,78235E 05	0,11456E 05	0,14407E 05	*DE*	0,30602E 01	0,92865E 00	0,11670E 01	*RM*	0,35070E 01
RE*	0,75555E 05	0,11728E 05	0,13195E 05	*DE*	0,30654E 01	0,10530E 01	0,11847E 01	*RM*	0,35346E 01
RE*	0,73662E 05	0,11752E 05	0,12344E 05	*DE*	0,30626E 01	0,11695E 01	0,12284E 01	*RM*	0,35624E 01

DWELL TIME = 770 DAYS

CHANNEL POWER
0,42180E 06

MIXED GAS OUTLET TEMPERATURE 835,

INNER FLOW RATE 0,83568E 02
OUTER FLOW RATE 0,68287E 02

TEMPERATURES

Z	TG1	TW1	TI1	TF1	TFI	TF2	TI2	TW2	TG2	TW3
0	300	532	611	625	688	654	491	444	300	310
50	341	611	697	714	789	752	559	512	354	368
100	391	707	806	825	915	875	637	587	417	435
150	448	784	891	912	1010	969	705	655	485	506
200	508	850	962	985	1089	1047	773	723	554	579
250	559	838	931	950	1037	1003	787	746	617	633
300	610	870	964	983	1073	1040	840	799	669	692
350	662	897	992	1011	1102	1071	867	848	725	748
400	714	923	1015	1034	1123	1094	926	889	786	799
450	763	946	1030	1048	1129	1103	963	929	831	850
500	804	948	1014	1027	1091	1072	974	949	872	890

Z	INNER GAP	HEAT SPLIT RADIUS	OUTER GAP
0	0,35769F-03	0,24291E 01	0,29176E-01
50	0,55541F-03	0,24362E 01	0,35132E-01
100	0,70332F-03	0,24467E 01	0,45333E-01
150	-0,28757F-03	0,24532E 01	0,55712E-01
200	-0,16726E-02	0,24571E 01	0,63580E-01
250	-0,83004F-03	0,24600E 01	0,58824E-01
300	-0,75661F-03	0,24650E 01	0,57625E-01
350	-0,43263E-03	0,24721E 01	0,57071E-01
400	-0,98780F-04	0,24750E 01	0,56125E-01
450	0,46211E-03	0,24768E 01	0,52193E-01
500	0,63929E-03	0,24816E 01	0,45872E-01

GRAPHITE SURFACE DIMENSIONS

Z	RC0	RC1	RC2
0	0,15094E 01	0,32674E 01	0,37958E 01
50	0,15102E 01	0,32687E 01	0,37970E 01
100	0,15114E 01	0,32703E 01	0,37986E 01
150	0,15134E 01	0,32715E 01	0,38003E 01
200	0,15174E 01	0,32724E 01	0,38022E 01
250	0,15165E 01	0,32724E 01	0,38042E 01
300	0,15204E 01	0,32717E 01	0,38083E 01
350	0,15252E 01	0,32691E 01	0,38178E 01
400	0,15301E 01	0,32644E 01	0,38372E 01
450	0,15327E 01	0,32595E 01	0,38712E 01
500	0,15313E 01	0,32565E 01	0,39137E 01

PRESSURE DROPS

Z	PD(BORE)	PD(ANNULUS)
0	0,0	0,0
50	0,87589E 04	0,95607E 04
100	0,18520E 05	0,20268E 05
150	0,29209E 05	0,32096E 05
200	0,41089E 05	0,45023E 05
250	0,53129E 05	0,58673E 05
300	0,66601E 05	0,72925E 05
350	0,81775E 05	0,88540E 05
400	0,98691E 05	0,10607E 06
450	0,11670E 06	0,12153E 06
500	0,13466E 06	0,13438E 06

CORROSION DATA

	PLANAR REMOVAL			ROUGHNESS HEIGHTS		
Z	RC0	RC1	RC2	RC0	RC1	RC2
0	0,18191E-05	0,17624E-06	0,19100E-08	0,18191E-05	0,17624E-06	0,19100E-08
50	0,23148E-04	0,21167E-05	0,45947E-07	0,23148E-04	0,21167E-05	0,45947E-07
100	0,27275E-03	0,23634E-04	0,11774E-05	0,27275E-03	0,23634E-04	0,11774E-05
150	0,14066E-02	0,14904E-03	0,18276E-04	0,14066E-02	0,14904E-03	0,18276E-04
200	0,47006E-02	0,68420E-03	0,18713E-03	0,47006E-02	0,68420E-03	0,18713E-03
250	0,41092E-02	0,11166E-02	0,84677E-03	0,41092E-02	0,11166E-02	0,84677E-03
300	0,76447E-02	0,29635E-02	0,34940E-02	0,76447E-02	0,29635E-02	0,34940E-02
350	0,12128E-01	0,66259E-02	0,11552E-01	0,12128E-01	0,66259E-02	0,11552E-01
400	0,16784E-01	0,12216E-01	0,29608E-01	0,16784E-01	0,12216E-01	0,25000E-01
450	0,19214E-01	0,17902E-01	0,62349E-01	0,19214E-01	0,17902E-01	0,25000E-01
500	0,17886E-01	0,21317E-01	0,10387E 00	0,17886E-01	0,21317E-01	0,25000E-01

	HEAT TRANSFER COEFF,		AND	FRICTION FACTOR (TRANSFORMED)		
Z	RC0	RC1	RC2	RC0	RC1	RC2
0	0,16660E 00	0,10701E 00	0,28186E 00	0,43654E-02	0,74013E-02	0,73750E-02
50	0,16754E 00	0,10884E 00	0,25568E 00	0,44443E-02	0,75165E-02	0,74407E-02
100	0,16869E 00	0,11086E 00	0,23733E 00	0,45106E-02	0,76860E-02	0,76119E-02
150	0,17049E 00	0,11303E 00	0,22307E 00	0,45762E-02	0,78035E-02	0,77356E-02
200	0,17520E 00	0,11503E 00	0,21214E 00	0,49791E-02	0,79149E-02	0,78532E-02
250	0,17815E 00	0,11676E 00	0,20771E 00	0,49363E-02	0,79894E-02	0,79423E-02
300	0,19438E 00	0,11745E 00	0,19916E 00	0,56042E-02	0,80728E-02	0,80303E-02
350	0,21526E 00	0,11903E 00	0,20464E 00	0,64397E-02	0,87635E-02	0,96151E-02
400	0,23541E 00	0,12667E 00	0,23466E 00	0,72674E-02	0,10237E-01	0,12664E-01
450	0,24491E 00	0,12615E 00	0,21320E 00	0,76451E-02	0,11173E-01	0,12442E-01
500	0,24167E 00	0,12004E 00	0,18600E 00	0,74039E-02	0,11450E-01	0,12121E-01

APPENDIX X

EXPECTED FREQUENCY DISTRIBUTIONS OF TEMPERATURE

HISTRAND output for peak fuel and graphite temperatures of the peak rated channel (Tables 4/1, 5/1)

TNPG EXPECTED FREQUENCY DISTRIBUTION OF TFP;

EXPECTED FREQUENCY IN REGION BELOW X=	750.0	0.0
EXPECTED FREQUENCY IN INTERVAL BELOW X=	760.0	0.0
	770.0	0.0
	780.0	0.0
	790.0	0.0
	800.0	0.0
	810.0	0.0
	820.0	0.1
	830.0	0.1
	840.0	0.2
	850.0	0.4
	860.0	0.7
	870.0	1.1
	880.0	1.8
	890.0	2.6
	900.0	3.9
	910.0	5.4
	920.0	7.5
	930.0	10.0
	940.0	13.1
	950.0	16.8
	960.0	21.3
	970.0	26.6
	980.0	32.7
	990.0	39.7
	1000.0	47.8
	1010.0	57.1
	1020.0	67.9
	1030.0	80.3
	1040.0	94.9
	1050.0	111.9
	1060.0	131.8
	1070.0	154.5
	1080.0	179.8
	1090.0	206.9
	1100.0	234.2
	1110.0	259.6
	1120.0	280.7
	1130.0	295.2
	1140.0	300.9
	1150.0	296.6
	1160.0	282.4
	1170.0	259.3
	1180.0	229.5
	1190.0	195.5
	1200.0	160.4
	1210.0	126.6
	1220.0	96.2
	1230.0	70.4
	1240.0	49.5
	1250.0	33.6
	1260.0	21.9
	1270.0	13.7
	1280.0	8.3
	1290.0	4.8
	1300.0	2.7
	1310.0	1.5
	1320.0	0.8
	1330.0	0.4
	1340.0	0.2
	1350.0	0.1
EXPECTED FREQUENCY IN REGION ABOVE X=	1350.0	0.1

TNPG EXPECTED FREQUENCY DISTRIBUTION OF TW1;

EXPECTED FREQUENCY IN REGION BELOW X=	650.0	0.0
EXPECTED FREQUENCY IN INTERVAL BELOW X=	660.0	0.0
	670.0	0.0
	680.0	0.0
	690.0	0.1
	700.0	0.2
	710.0	0.5
	720.0	0.9
	730.0	1.5
	740.0	2.5
	750.0	4.0
	760.0	5.8
	770.0	8.2
	780.0	11.1
	790.0	14.5
	800.0	18.5
	810.0	23.1
	820.0	28.3
	830.0	34.4
	840.0	41.5
	850.0	49.8
	860.0	59.8
	870.0	71.8
	880.0	86.5
	890.0	104.6
	900.0	127.0
	910.0	154.3
	920.0	187.0
	930.0	224.2
	940.0	263.8
	950.0	301.9
	960.0	333.4
	970.0	353.1
	980.0	356.8
	990.0	343.0
	1000.0	312.9
	1010.0	270.4
	1020.0	221.2
	1030.0	171.1
	1040.0	125.2
	1050.0	86.5
	1060.0	56.5
	1070.0	34.8
	1080.0	20.3
	1090.0	11.1
	1100.0	5.7
	1110.0	2.8
	1120.0	1.3
	1130.0	0.5
	1140.0	0.2
	1150.0	0.1
EXPECTED FREQUENCY IN REGION ABOVE X=	1150.0	0.1

TNPG EXPECTED FREQUENCY DISTRIBUTION OF TW2;

EXPECTED FREQUENCY IN REGION BELOW X=	650.0	0.0
EXPECTED FREQUENCY IN INTERVAL BELOW X=	660.0	0.0
	670.0	0.1
	680.0	0.1
	690.0	0.3
	700.0	0.6
	710.0	1.1
	720.0	1.9
	730.0	3.0
	740.0	4.7
	750.0	6.8
	760.0	9.6
	770.0	12.8
	780.0	16.5
	790.0	20.8
	800.0	25.6
	810.0	31.2
	820.0	37.8
	830.0	45.6
	840.0	55.0
	850.0	66.2
	860.0	79.5
	870.0	95.2
	880.0	113.7
	890.0	135.4
	900.0	160.9
	910.0	190.3
	920.0	223.0
	930.0	256.9
	940.0	288.6
	950.0	314.0
	960.0	328.9
	970.0	330.5
	980.0	317.8
	990.0	292.2
	1000.0	256.9
	1010.0	216.2
	1020.0	174.3
	1030.0	134.7
	1040.0	99.8
	1050.0	70.8
	1060.0	48.1
	1070.0	31.2
	1080.0	19.3
	1090.0	11.4
	1100.0	6.3
	1110.0	3.3
	1120.0	1.7
	1130.0	0.8
	1140.0	0.3
	1150.0	0.1
EXPECTED FREQUENCY IN REGION ABOVE X=	1150.0	0.1

TNPG EXPECTED FREQUENCY DISTRIBUTION OF TW3;

EXPECTED FREQUENCY IN REGION BELOW X=	600.0	0.0
EXPECTED FREQUENCY IN INTERVAL BELOW X=	610.0	0.0
	620.0	0.0
	630.0	0.0
	640.0	0.0
	650.0	0.1
	660.0	0.2
	670.0	0.5
	680.0	1.0
	690.0	1.9
	700.0	3.5
	710.0	5.8
	720.0	8.7
	730.0	12.3
	740.0	16.4
	750.0	20.7
	760.0	25.4
	770.0	30.8
	780.0	37.4
	790.0	45.7
	800.0	56.0
	810.0	68.4
	820.0	82.8
	830.0	99.2
	840.0	118.0
	850.0	140.3
	860.0	168.0
	870.0	202.3
	880.0	242.4
	890.0	284.5
	900.0	322.4
	910.0	348.8
	920.0	358.1
	930.0	348.2
	940.0	321.0
	950.0	281.5
	960.0	235.6
	970.0	188.9
	980.0	145.6
	990.0	108.0
	1000.0	77.1
	1010.0	52.8
	1020.0	34.5
	1030.0	21.4
	1040.0	12.5
	1050.0	6.9
	1060.0	3.5
	1070.0	1.6
	1080.0	0.7
	1090.0	0.3
	1100.0	0.1
EXPECTED FREQUENCY IN REGION ABOVE X=	1100.0	0.1

REFERENCES

(1) VOICE, E.H. DRAGON PROJECT - Private communication 1973

(2) BISHOP, J.F.W. et al. TRG Memo 5135(R) December, 1969

(3) GREEN, C.H. TNPG/MTS. Int. 1807 May, 1971

(4) WALTHER, H. D.P. Report 683 1969

(5) CONWAY-JONES, A.H. RPC/M3 FIP/N(70) 118 1970

(6) SMITH, E. D.P. Report 672 October, 1969

(7) BALLARD, T.D. TNPG Tech Memo STM/417 October, 1971

(8) BALLARD, T.D. TNPG Memo No. STM/P21 103/G/01/TB/LM 7th May, 1970

(9) OLDBURY B TENDER TNPG Ref. T43 April, 1971

(10) WILLIAMS, L.G. FOIL Report No. TNPG 795 August, 1971

(11) ROSSITER, F. Temperature distribution within a fuel compact - A method of calculation - M3/PMDG/P29 November 1969

(12) RAPIER, A.C. Local temperature variations in a dispersed fuel compact - TRG Report 2062(W) 1970

(13) MAIN, F.K. Heat transfer at gas/solid interfaces AERE M1784 1966

(14) WARBURTON, C. The surface roughness of graphite and its effect on friction factor RD/B/N2219 March, 1972

(15) GREEN, C.H. Private communication TNPG 1972

(16) NIKURADSE, J. VDI Forschungsheft No. 356 1932

(17) MARTINELLI, R.C. Trans. ASME, Vol 69 P. 947 1947

(18) VAN DRIEST, E.R. Heat Transfer Fluid Mech. Inst. XII 1955

(19) KAYS, W.M. Convective heat and mass transfer - McGraw-Hill 1966

(20) WILKIE, D. M3 PMDG P9 Revision 1

(21) KAYS, W.M., LEUNG, E.Y. International Journal of Heat and Mass Transfer Vol 6, 537-557 1963

(22) BARNES, J.F., JACKSON, J.D. Journal of Mech. Eng. Sci. Vol 3, No. 4, 1961

(23) LAWN, C.J., ELLIOT, C.J. Fully developed turbulent flow through concentric annuli. Journal of Mech. Sci. Vol 14, No. 3 1972

(24) HALL, W.B. Heat transfer in channels having rough and smooth surfaces. Journal of Mech. Eng. Sci. Vol 4, No. 3 1962

(25) JACOB, M. Heat transfer. Vols I and II WILEY 1949, 1957

(26) BALLARD, T.D. A method of adapting AZIMUSTAP to allow for the temperature and time dependence of interface gap conductance. TNPG SYSTEMS TECH MEMO NO. STM/187 February, 1969

(27) BALLARD, T.D. The estimation of interface gaps in HTR fuel elements. Draft memo. TNPG SYSTEMS June, 1970

(28) TIMOSHENKO, S., GOODIER, J.N. Theory of Elasticity McGraw-Hill 1951

(29) HAIGH, R.E. A theoretical analysis of stress and strain in a Tubular Interacting HTR fuel pin RPC/PTK/N(70)/42 October, 1970

(30) ROBINSON, J.A. Private communication TNPG 1970

(31) BALLARD, T.D. HTR fuel sleeve corrosion - effect on local heat transfer. M3/PMDG/P.23 September, 1969

(32) BALLARD, T.D. Corrosion effects on heat transfer for the Mk III Tubular Interacting Fuel Pin RPC/PTK/P(70)23 November, 1970

(33) BIRCH, D. et al. I.R.D. 69-14 April, 1969

(34) HELSBY, G.H., EVERETT, M.R. Some graphite ocrrosion problems relating to helium cooled HTR's D.P. Report 566 August, 1968

(35) MERRETT, D.J., FERN, C.W. Safety aspects of HTR systems Conf. Paris 24/25th November 1971 Paper No. 10 Session 111

(36) SINCLAIR, W.S. Unpublished Data

(37) NIKURADSE, J. Laws of flow in rough pipes. VDI Forschungsheft 361 July/August 1933

(38) WHITE, L. TRG Memo 5426(W) November, 1970

(39) NICOL, A.A., MEDWELL, J.O. Journal of Mechanical Engineering Science Vol 6 No. 2 1964

(40) DIPPREY, D.F., SABERSKY, R.H. Int. J. Heat Mass Transfer Vol 6 1963

(41) WALKER, V, WHITE, L. The effect of physical property variations on heat transfer from roughened surfaces TRG Report 1933(W) 1969

(42) HOUGH, B. RPC/PTK/N(71)9 January 1971

(43) TRG REPORT 1000(R) Data and conventions for Mk III calculations

(44) CONWAY-JONES, A.H. SEAGERS, K.J. RPC/PTK/N(71)10 1971

(45) GUILD, R.S. RPC/PTK/N(70)58 December, 1970

(46) LUXMOORE, R.J. TNPG Internal Memo to T.D. Ballard

(47) GRUNDY, W. RPC/PTK/P(70)7 August, 1970

(48) ABERNATHY, F.H. The statistical aspects of nuclear reactor fuel element temperature Nu Sci. & Eng. 11 290-297 (1961)

(49) GRUNDY, W. Temperature effects of Manufacturing Tolerances - Mk III G.C.R. tubular interacting fuel. RPC/PTK/N(70)39

(50) VANDER STEEN, R.F. HISTRAND TNPG/MTS Int. 1729

(51) SINCLAIR, W.S. AZIMUSTAP 5 TNPG/MTS Int. 1795